NASA

Technical Memorandum 82071

Earth Survey Applications Division Research Report – 1980

JANUARY 1981

National Aeronautics and
Space Administration

Goddard Space Flight Center
Greenbelt, Maryland 20771

EARTH SURVEY
APPLICATIONS DIVISION
RESEARCH REPORT - 1980

EDITED BY
LLOYD CARPENTER

JANUARY 1981

GODDARD SPACE FLIGHT CENTER
GREENBELT, MARYLAND

CONTENTS

viii

EARTH SURVEY APPLICATIONS DIVISION

CODE 920

LIST OF RESEARCHERS

Vincent V. Salomonson, Chief
Ph.D., 1968, Colorado State University, Atmospheric Science

Robert D. Price, Assistant Chief
Ph.D., 1974, Catholic University, Space Science

(Gwendolyn Sharps, Secretary)

GEODYNAMICS BRANCH

Code 921

David Smith, Branch Head
Ph.D., 1966, University of London, Mathematics

(Beatrice Boccucci, Secretary)

Lloyd Carpenter, *B.S., 1951, U. of Missouri, Mathematics*
Robert Cheney, *M.S., 1974, U. of Rhode Island, Oceanography*
Steven Cohen, *Ph.D., 1973, U. of Maryland, Physics*
Theodore Felsentreger, *M.A., 1961, U. of Maryland, Mathematics*
Vincent Grano, *Ph.D., 1981, Johns Hopkins U., Physical Oceanography*
Werner Kahn, *M.S., 1955, University of Illinois, Mathematics*
Ronald Kolenkiewicz, *M.S., 1965, Catholic University, Space Science and Applied Physics*
Francis Lerch, *M.S., 1950, University of Delaware, Mathematics*
Han-Shou Liu, *Ph.D., 1963, Cornell University, Physics*
James Marsh, *M.S., 1963, West Virginia University, Physics*
David McAdoo, *Ph.D., 1976, Cornell University, Geophysics*
Patrick McClain, *M.S., 1959, Howard University., Mathematics*
Barbara Putney, *B.S., 1960 Brooklyn College, Mathematics*
David Rubincam, *Ph.D., 1973, University of Maryland, Physics*
Braulio Sanchez, *Ph.D., 1975, University of Texas, Aerospace Engineering*
Frederick Schamann, *B.S., 1967, City College of New York, Mathematics*
George Wyatt, *B.S., 1962, North Carolina State College, Mathematics*

GEOPHYSICS BRANCH

Code 922

Charles C. Schnetzler, Branch Head
Ph.D., 1962, MIT, Geochemistry

(Barbara Lueders, Secretary)

Richard J. Allenby, *Ph.D., 1952, U. of Toronto, Geophysics*
Robert Belcher, *Ph.D., 1979, U. of Texas, Geology*
Herbert Frey, *Ph.D., 1977, U. of Maryland, Astronomy*
Charles W. Kouns, *M.S., 1966, George Washington U., Geology*
Mark Labovitz, *Ph.D., 1978, Penn State U., Geostatistics*
Robert A. Langel, *Ph.D., 1973, U. of Maryland, Physics*
Paul D. Lowman, Jr., *Ph.D., 1963, U. of Colorado, Geology*
Edward Masuoka, *M.S., 1978, U. of Tennessee, Geology*
Kenneth Meehan, *Ph.D., 1978, Idaho U., Geology (resigned 11/80)*
Alicia W. Siegrist, *M.S., 1977, Penn State U., Geology*
Patrick T. Taylor, *Ph.D., 1965, Stanford U., Geophysics*
Herman H. Thomas, *Ph.D., 1973, U. of Pennsylvania, Geochemistry*
William J. Webster, Jr., *Ph.D., 1970, Case Western Reserve U., Astronomy*

Postdoctoral Associate

Charles A. Wood, *Ph.D., 1979, Brown U., Geology (resigned 9/80)*

EARTH RESOURCES BRANCH

Code 923

Robert Murphy, Acting Branch Head
Ph.D., 1969, Case Western Reserve U., Astronomy

(Robin, Mohr, Secretary)

John Barker, *Ph.D., 1967, U. Chicago, Physical Chemistry*
Thomas Brakke, *Ph.D., 1980, Kansas State U., Agronomy*
Emmett Chappelle, *M.S., 1954, U. Washington, Biochemistry*
Donald Deering, *Ph.D., 1978, Texas A&M U., Range Sciences*
Lisette Dottavio, *Ph.D., 1979, Purdue U., Forestry*
Michael Forman, *M.S., 1965, Lowell Tech. Inst., Physics*
Brent Holben, *M.S., 1975, Colorado State U., Agricultural Sciences*
James Irons, *M.S., 1978, Penn State U., Agronomy*
Daniel Kimes, *Ph.D., 1979, Colorado State U., Natural Resources*
Julie Kirchner, *M.S., 1980, Colorado State U., Remote Sensing*
Brian Markham, *M.S., 1978, Cornell U., Civil Engineering*
Ross Nelson, *M.S., 1979, Purdue U., Forestry*
John Schutt, *Ph.D., 1954, Rochester U., Physical Chemistry*
David Toll, *M.S., 1978, Colorado State U., Natural Resources*
Compton J. Tucker, *Ph.D., 1975, Colorado State U., Remote Sensing*
Steven Wharton, *M.S., 1979, Penn State U., Forestry/Computer Sciences*
Darrel Williams, *M.S., 1975, Penn State U., Forestry*
Frank Wood, *Technician*

Postdoctoral Associates

Christopher Justice, *Ph.D., 1978, U. Redding, ENG, Geography*
John Townshend, *Ph.D., 1974, U. London, ENG, Geography*

HYDROLOGICAL SCIENCES BRANCH

Code 924

Albert Rango, Branch Head
Ph.D., 1969, Colorado State University, Watershed Management

(Joyce Tippett, Secretary)

Bruce J. Blanchard, *Ph.D., 1974, U. of Oklahoma, Civil Engineering and Environmental Science*
Alfred T.C. Chang, *Ph.D., 1971, University of Maryland, Physics*
James L. Foster, *M.A., 1977, University of Maryland, Geography*
Dorothy K. Hall, *Ph.D., 1980, University of Maryland, Geomorphology*
Bevery K. Hartline, *Ph.D., 1976, University of Washington, Geophysics*
Peggy E. O'Neill, *M.A., 1979, U. of California, Santa Barbara, Geography*
James P. Ormsby, *Ph.D., 1973, Cornell University, Meteorology*
Manfred Owe, *M.S., 1979, State University of New York, Syracuse, Hydrology*
Thomas Schmugge, *Ph.D., 1965, University of California, Berkeley, Solid State Physics*

INTRODUCTION

by

Robert D. Price

The primary functions of the Earth Survey Applications Division, Applications Directorate, are to conduct basic and applied research and data analysis in order to advance scientific knowledge and understanding of physical parameters and processes inside the earth and on the earth's surface; to define techniques and systems for remotely sensing the processes and measuring the parameters of scientific and applications interest; and to develop and transfer promising operational applications techniques to the user community of earth resources monitors, managers, and decision-makers. The physical processes and parameters studied span the disciplies of: geodynamics including mantle convection, gravity field mapping, plate tectonics, and polar motion; geophysics including geology, magnetic field mapping, crustal dynamics, and geobotany; earth surface features including agricultural vegetation sciences, forestry, land use change detection, and environmental monitoring; and hydrology including watershed management, snow and ice properties, and soil moisture. Research in each of these disciplines defines the prime function of each of the four branches of the Division, the Geodynamics, Geophysics, Earth Resources, and Hydrological Sciences Branches.

The bulk of the work is supported by, and the broad objectives defined by, three programs in the Office of Space and Terrestrial Applications at NASA Headquarters: Non-Renewable Resources (geodynamics), Renewable Resources (geophysics, earth surface features, and hydrology) and AgRISTARS (agricultural vegetation sciences and soil moisture).

This document is the Third Annual Research Report of the staff of the Division. It contains descriptions of the accomplishments of the activities conducted in Fiscal Year 1980 by the many groups in the Division as they perform their primary function for the Division and progress toward the achievement of the broad programmatic objectives established by Headquarters.

In the past year the highlights of those accomplishments would be the production of the first global maps of magnetic anomalies using Magsat satellite data; utilization of GEOS-3 and Seasat altimetry data for computation of the global mean sea surface; delineation and increased understanding of the effects of topography on the interpretation of remotely-sensed data; the development of hand-held radiometer instruments and their widespread application to research and operational biomass measurements; the development and application of snowmelt runoff models to water resources management in medium- and large-sized basins; and the mapping of snow depth over wheat-growing areas, including Russia, using NIMBUS microwave data.

CHAPTER 1

GEOBOTANICAL RESEARCH

edited by

Mark L. Labovitz

OVERVIEW

Geologic mapping augmented by remote sensing technology has been conducted largely in regions of little vegetation cover. For many field geologists, vegetation represents a nuisance to be bulldozed away. However, large portions of the land surface of the earth are heavily vegetated. In areas such as portions of the eastern United States heavy vegetation not only conceals the geology, but combines with the topography to hinder movement on the ground, which consequently makes exploration for mineral resources somewhat problematic.

Motivated by the strategic resource needs of the world in general, and the U.S. in particular, research is being conducted under the auspices of the Non-Renewable Resource Branch of NASA Headquarters into (1) the information contained in vegetation about the nature and composition of the substrate and, (2) the utility of remote sensing techniques to capture this information. While geobotanical research did not begin with the present efforts, we are attempting through a series of systematic, quantitative field and laboratory studies, to reduce the anecdotal tone that characterizes much of the previous research.

This chapter reports on (1) field site research being conducted by Goddard personnel in two locations--Mineral, VA and Cotter Basin, MT; (2) laboratory and field studies supervised by Goddard personnel under a contract with Barringer Research, Inc. (Golden, CO) and Imperial College (London, England); and (3) a Landsat mapping study done by a Goddard summer faculty fellow.

The field work at Mineral, VA is a part of a larger field program to study geobotanical-remote sensing relationships in several geologically important environments. The research is directed towards testing specific hypotheses developed in previous laboratory and field studies and possesses a strong experimental design character. A site at Cotter Basin, MT has previously been demonstrated to possess a geobotanical anomaly detectable through remote sensing. However, the instrument used in prior research has very narrow bands which are impractical to use from satellites, so the present research reports on the results of using the Thematic Mapper Simulator. The research being conducted in the laboratories at Imperial College is directed towards examining the relationship between the optical properties of vegetation and certain microscopic constituents of vegetation grown in metal-rich solutions of varying concentrations. The Landsat study focussed on the potential of satellite digital data to detect and map serpentine bodies in the Piedmont of Pennsylvania, Maryland and Virginia.

A. GEOBOTANICAL TEST SITE INVESTIGATIONS

MINERAL SULFIDE DISTRICT, MINERAL, VIRGINIA

by

M.L. Labovitz, E.J. Masuoka, R. Bell, R.F. Nelson,
A.W. Siegrist, S. Wharton

OBJECTIVES

The objectives of the geobotanical test site investigations program are: (1) to determine the utility of different spectral bands for mapping the geobotanical anomaly over a known metal sulfide deposit; (2) to determine the best spatial resolution for mapping the anomaly; (3) to determine the best temporal window for mapping the anomaly; (4) to assess the reproducibility of spectral, biogeochemical and geobotanical measurements within the anomalous area over several growing seasons; and (5) to select other geobotanical anomalies, more complex than the first, on which to evaluate the general applicability of the above determinations. The geobotanical test site at Mineral, VA is the first of four test sites which we hope to examine over the period FY1980-1983.

BACKGROUND

The of vegetation type or vigor as a guide to subsurface mineral or petroleum deposits has been an accepted exploration tool for centuries. However, the possibility of using remote-sensing techniques to detect the changes in vegetation caused by nearby mineralization has just recently received attention. An increasing awareness of potential mineral and energy shortages has stimulated the development of new exploration techniques. Satellite remote sensing enables investigators to analyze large segments of the Earth's surface repeatedly at different seasons and under different conditions. Since over two-thirds of the Earth's land surface is covered with vegetation, the need to establish a research program for the development and evaluation of geobotanical exploration techniques is essential.

In May and June 1979 we started a search for a suitable initial test site. It was to be of minimum complexity and located near GSFC in order to minimize travel time and expense. Prior to this search, a list of criteria that we felt an initial test site should meet was generated.

These criteria are:

1.   Within the test site there must be an economic deposit of a mineral commodity.

2.   There should be evidence of mineralization in the soil and/or vegetation, so that conclusions can be drawn about relationships between metal stressed vegetation and its optical properties.

3.   The test site must be accessible to Goddard (within a 200 mile radius).

4.   The topographic relief should be low to avoid potential complications within the field environment (Arden and Westra, 1977; Birnie and Francica, 1979).

5.   Forested areas within the site should have continuous canopy cover.

6.   Only a few tree species should dominate the forest community.

It should be noted that for most of the factors which are affected by the above criteria we are attempting to control the experimental environment by "keeping things constant."

An initial test site was selected near Mineral, Virginia, about 80 miles southwest of Washington, DC. The site is in the Piedmont Physiographic Province (Figure 1A-1) which features low, gently rolling relief. The geology consists of schists, clastic volcanics, metamorphosed sediments, gneisses and rocks of granitic composition (Miller, 1978). The formations are of uncertain age but are believed to be in the range of late Precambrian to early Paleozoic (Geologic Map of Virginia, 1963). Geologically, the region represents a high rank greywacke environment in the definition of Kyrnine (1948) and Griffiths (1980). A summary of the characteristics of the area--known as the Mineral District--is given in Table 1A-1 and a geologic map is given in Figure 1A-2.

The Mineral District is an area approximately 5 miles wide by 7 miles long and encompasses three trends of mineralization which conform to the regional strike N 30º E (Cox, 1979). The central and western trends are base metal bearing and are composed of quartz-sericite, actinolite-chlorite, and amphibolite schists. The mineralization is often found in shear zones at or near the contact of the quartz-sericite and amphibolite schists. Mineralized zones consist of massive pyrite lenses containing lesser amounts of chalcopyrite, sphalerite, galena, pyrrhotite, and magnetite with traces of gold, silver, and arsenic in some locations (Cox, 1979; Luttrell, 1966). Deposits in this area are thought to be volcanogenic in origin as they resemble Kuroko and Besshi types of mineralization (Miller, 1978).

The Mineral District was mined at a number of locations at various times from the 1830's to the 1920's. No major mining activities have occurred since the 1920's and, so, the forested areas not in pine plantation are a minimum of 50-60 years old. This is sufficient time to develop a climax forest (Milton, 1979) which, in this location, is dominated by oaks and pines.

FY79 Field Work

In August and September of 1979, four test site locations within the Mineral District were selected. These sites were laid out as two pairs with one mineralized (M) and one non-mineralized (NM) site in each pair. The mineralized sites were located in the vicinity of two inactive mines--the Julia mine (1.25 miles southwest of Mineral, VA) and the Allah Cooper (Valcooper) mine (5.5 miles northeast of Mineral, VA). Both of these mines are on the contact of the quartz-sericite and amphibolite schists. The two non-mineralized sites were located on similar contacts. Also, each non-mineralized locality was constrained by its proximity to its mineralized counterpart so that similar conditions of soil moisture, species density and diversity were assured. Test site locations are plotted in Figure 1A-3.

The test sites were arranged so that spatial variation at a number of scales was discernable. As seen in Figure 1A-3, the four sites are arranged so that they form a grid whose perimeter lies approximately along and perpendicular to the regional strike. Thus, if test sites display different forms for the relationships among important variables or if they differ with respect to means or variances for factors under investigation, a geologic framework for interpreting these differences is available.

Grid sampling schemes are common in field sciences and are extremely efficient for data collection. Such a scheme is used in laying out individual test sites (see Figures 1A-4 and 1A-5). This sampling strategy will be used for collecting vegetative, soil and remote sensing measurements as the data collected in this manner can be easily and statistically analyzed by an analysis of variance (Fisher, 1971). The data collected in a preliminary experiment in October 1979, may serve as an illustrative example of this approach. In this experiment, vegetation samples were collected at three of the test sites--Julia, Valcooper and Sarkis--sites 1, 3 and 4 (refer to Figure 1A-3). In the context of the sampling grid given in Figure 1A-4 each grid node was a white oak (Quercus alba). Leaf samples were collected from each tree and analyzed for trace metal content. (In a previous study within the Mineral District, Leavitt (1977), found differences in the trace metal content of vegetation growing over mineralized versus non-mineralized areas were greatest in second year twigs. In the present study, however, leaves are examined because among the aerial parts of a plant they contribute the overwhelming portion of the reflected energy detected by a sensor.) One of the questions to be answered by this experiment is whether or not trace metal differences are detectable in senescing leaves from mineralized and non-mineralized regions.

A second question to be addressed is whether or not the trace metal content of a leaf is related to its position in the canopy of a tree. Such a question arises because, if we are to analyze those leaves contributing the most reflected energy to a sensor, we should be collecting samples from the top of the tree in the sun facing the direction of the sensor. This is difficult when sampling trees 35-50 feet tall. If, however, the trace metal content of a leaf is not related to its position in the canopy or if the functional relationship is simple, we may sample from more easily reached heights in the canopy. To answer this question, we used tree trimmers, extendable to 30 feet, to collect eight samples from each white oak: high and low in the canopy at compass azimuths of 30°, 120°, 210° and 300°.

To summarize, Table 1A-2 lists all the levels at which can be obtained information on the trace metal distribution in leaf samples. Figure 1A-5 diagrams the experimental design.

TABLE 1A-2 - TESTABLE PHENOMENA, FIELD EXPERIMENT FY79

Source of Variation

1. Mineralized - Non-Mineralized

2. Across and along strike--district level

3. Across and along strike--test site level

4. Across and along strike--subsites

5. Orientation (azimuth)

6. Height in canopy.

Phenomena 1 through 6 may be used to answer the two questions posed above. Question 1 will be examined in phenomena 1-4. We may test for differences in the trace metal content and model how the trace metal content changes with spatial scale. Variations in effects 5 and 6 may answer question 2 and indicate the appropriate location to sample, the variation in trace metal content and, hence, the appropriate sample size for further work.

Four hundred and nineteen leaf samples were analyzed by induced plasma spectroscopy and atomic absorption for 14 elements including the trace metals of specific interest--Zn, Pb, Cu, Cd. The results of these analyses are given in Table 1A-3.

Several conclusions and conjuctures should be noted.

1.   There does not appear to be any significant variation in the concentration of elements with orientation. This means we can drop this as a potential source of variation and reduce by a factor of 4 our sample size in future collections. (We repeated this sampling procedure in June 1980 to test the validity of the October 1979 results; analysis is not yet completed.)

2.   There is a significant decrease in the concentration of several elements (see Table 1A-3) with height in the canopy. (Nelson and Labovitz are presently investigating the functional form describing the manner in which concentrations decrease.)

3.   The tree to tree variation is masking any significance between sites or subsites. A further analysis of covariance procedure, using analyses of soil chemistry as the covariate, is being performed to determine if this tree to tree variation is due to local soil variations or genetic factors.

RECENT ACCOMPLISHMENTS

In FY80 there was one data collection in June, July, August and October, and two data collections in September. Students from the University of Maryland were employed to assist in the data collections. This system permitted rapid collection of a large amount of data. Each data collection consisted of leaf samples which were subjected to reflectance measurements and chemical analysis and was performed on the same sampling grid as the October 1979 experiment.

Reflectance measurements were accomplished using a three band hand-held radiometer (Tucker et al., 1980). Figure 1A-6 (after Tucker, 1978) shows the position of the three bands superimposed on a typical vegetation spectrum. These bands mimic Thematic Mapper (TM) bands 3, 4 and 5. TM 3 is related to the amount of chlorophyll present. TM 4 is positioned to capture information in the photographic infrared regions, where vegetation is highly reflective. TM 5 is interpreted as a measure of the amount of leaf water present in the vegetation.

Analysis of the data collected in FY80 field season should be completed in late December 1980 or early January 1981. However, preliminary results from June 1980 are given in Table 1A-4 and Figures 1A-7 and 1A-8. Before summarizing the results, we should like to stress that the trends have not yet been confirmed by analysis of data from other months, nor was the June experiment designed to compensate

for certain potential sources of bias (as was done in later months). Table 1A-4 demonstrates a significantly higher radiance in all three bands from clipped vegetation at the mineralized site (Julia) versus the non-mineralized site (Sarkis). These results are consistent with those of other researchers for spectral regions equivalent to TM 3 and TM 4 and at variance with the results of Barber and Horler (1979) for TM 5. Further, Figure 1A-7 shows a distinct trend of increasing radiance values as one moves towards the former mine shaft opening on the Julia site versus the "flat" surface described by the radiance values measured at the Sarkis site.

SIGNIFICANCE

We are rapidly achieving a position where definitive statements (definitive in a statistical sense) can be made about the relationship between the presence of mineralization and the reflectance of vegetation in a piedmont type environment. Development of exploration procedures or protocols based upon these relationships will be of great value in the reconnaissance stage of exploration for similarly vegetated metal sulfide deposits. In performing this research, we have also learned a great deal about how to sample a vegetated population and structuring data collection teams.

FUTURE EMPHASIS

In FY81 we will repeat the experiment at Mineral, VA in order to determine the reliability of FY80 test site results. A second test site similar in physiography to Mineral, VA will be chosen and monthly data collection performed. We will also expand our remote sensing data to include wide band thermal measurements testing hypotheses about stomatal dysfunction and consequent evapotranspiration changes. A summary of proposed research to cover the FY80-83 period is given in Table 1A-5.

REFERENCES AND PUBLICATIONS

Arden, D.D., Jr. and R.N. Westra, "Remote Sensing of Geobotanical Relations in Georgia: Final Report," Contract No. NAS8-30884, 96 pp., 1977.

Barber, J. and D.N.H. Horler, "Fundamental Relationships Between Plant Spectra and Geobotanical Stress Phenomena," Sixth Month Report on NASA Contract NAS5-25738, Goddard Space Flight Center, Greenbelt, Maryland, 1979.

Birnie, R.W. and J.R. Francica, Jr., "Remote Detection of Geobotanical Anomalies: A Method for Mineral Exploration," (abstract) Abstracts with Programs, Geological Society of America Annual Meeting, November 1979, San Diego, p. 389, 1979.

Cox, L.J., "Mineralogy and Petrogenesis of the Arminius Deposit, Louisa County, Virginia," Unpublished Master's Thesis, Virginia Polytechnic Institute and State University, 113 pp., 1979.

Fisher, R.A., "The Design of Experiments," 9th Ed., New York, Hafner Press, 248 pp., 1970.

Geologic Map of Virginia, 1963, Commonwealth of Virginia, Department of Conservation and Economic Development, Division of Mineral Resources, James L. Calver, Commission and State Geologist, Charlottesville, Virginia, Scale 1:500,000, 1963.

Griffiths, J.C., Personal communication, Professor Emeritus of Petrography, Department of Geosciences, The Pennsylvania State University.

Krynine, P.D., "The Megascopic Study and Field Classification of Sedimentary Rocks," Journ. of Geol., 56, 130-165, 1948.

Leavitte, S.W., "Soil-Plant Relationships to Nutrient and Non-Nutrient Metals in Louisa County, Virginia," Unpublished Master's Thesis, Department of Environmental Sciences, University of Virginia, 95 pp., 1977.

Luttrell, G.W., "Base- and Precious-Metal and Related Ore Deposits of Virginia," Mineral Resources Report 7, Virginia Division of Mineral Resources, Charlottesville, Virginia, 167 pp., 1966.

Miller, J.W., Jr., "The Ore Mineralogy of the Cofer Property, Louisa County, Virginia: A Volcanogenic Massive Sulfide Deposit," Unpublished Master's Thesis, Virginia Polytechnic Institute and State University, 89 pp., 1978.

Milton, N., Personal communication, Botanist, U.S. Geological Survey, Reston, VA., 1979.

Tucker, C.J., "An Evaluation of the First Four Landsat-D Thematic Mapper Reflective Sensors for Monitoring Vegetation: A Comparison with Other Satellite Sensor Systems, GSFC Technical Memorandum 79617, 1978.

Tucker, C.J., W.H. Jones, W.A. Kley and G.J. Sundstrom, "A Three Band Hand-Held Radiometer for Field Use," GSFC Technical Memorandum 80641, 1980.

TABLE 1A-1: Description of Mineral District Field Site

o Mineral Virginia Sulfide District - Previously Mined for Economic Concentrations
   of Pb, Zn, Cu, Fe (Young, 1956; many others)

o Anomalous Concentrations Pb, Zn, Cu, Cd, in Selected Soil Horizons and In
   Indigenous Hardwoods (Leavitt, 1977)

o Temperate Climate and Close Proximity to GSFC - Accessible Year Round and
   Inexpensive

o Low Relief - Piedmont Physiographic Province

o Canopy Cover 100% (Milton, P.C., 1979)

o Dominant Species - Oak/Pine Forest (Milton, P.C., 1979)

TABLE 1A-3:   Results1 of Hierarchial Analysis, October 1979
Sarkis Versus Julia Sites

ELEMENT	SITE	SUBSITE	TREE	ORIENTATION	HEIGHT
P	NS	NS	★★	NS	NS
K	NS	NS	★★	NS	★★
Ca	NS	NS	★★	NS	★
Mg	NS	★★	★★	NS	NS
Mn	NS	NS	★★	NS	NS
Fe	NS	NS	NS	NS	★
Cu	NS	NS	★	NS	NS
B	NS	NS	★★	NS	★★
Al	NS	NS	★★	NS	NS
Zn	NS	NS	★★	NS	★★
Sr	NS	NS	★★	NS	★★
Pb	NS	NS	★★	NS	★★
Cd	NS	NS	★★	NS	NS
Si	NS	NS	NS	NS	NS

NS = NOT SIGNIFICANT AT α = 0.05

★ = SIGNIFICANT AT   α = 0.01 TO 0.05

★★ = SIGNIFICANT AT   α = 0.01

1 BASED UPON BONFERRONI PROCEDURE FOR CONTROLLING FAMILY α LEVEL AT .05 AND .01

TABLE 1A-4: Comparison of Spectral Radiance in Bands TM3, TM4 and
TM5 of Leaves from Mineralized and Non-Mineralized Sites

BAND1 TM3 (0.63-0.69 μm)

GROUP	JULIA	SARKIS
MEAN	1.1719	1.0433
STD DEV	0.2543	0.1431
S.E.M.	0.0450	0.0261
SAMPLE SIZE	32	30
MAXIMUM	1.8000	1.4000
MINIMUM	0.8000	0.7000

STATISTICS		P VALUE	DF	
T (POOLED)	2.43	0.018	60	
F (FOR VARIANCES) LEVENE	8.80	0.263	1,	60

BAND2 TM4 (0.76-0.90 μm)

GROUP	JULIA	SARKIS
MEAN	19.2405	16.7432
STD DEV	2.6894	1.9461
S.E.M.	0.4754	0.3553
SAMPLE SIZE	32	30
MAXIMUM	25.3000	19.8000
MINIMUM	11.9000	12.0000

STATISTICS		P VALUE	DF	
T (POOLED)	4.16	0.000	60	
F (FOR VARIANCES) LEVENE	2.06	0.511	1,	60

BAND3 TM 5 (1.55-1.75 μm)

GROUP	JULIA	SARKIS
MEAN	2.5687	2.2733
STD DEV	0.4461	0.2664
S.E.M.	0.0789	0.0486
SAMPLE SIZE	32	30
MAXIMUM	4.2000	2.9000
MINIMUM	1.5000	1.8000

STATISTICS		P VALUE	DF	
T (POOLED)	3.14	0.003	60	
F (FOR VARIANCES) LEVENE	1.55	0.575	1,	60

TABLE 1A-5: Highlights of Geobotanical Research FY1980-1983

HIGHLIGHT

FY

1980 — STUDY OF TEMPORAL AND SPATIAL VARIATION IN TEST SITE AT MINERAL, VA.

1981 — VALIDATION STUDY AT MINERAL

— SELECT AND STUDY 2ND TEST SITE WITH TERRAIN SIMILAR TO THAT OF MINERAL

— EXTEND RESEARCH TO THERMAL REGION OF THE SPECTRUM

1982 — STUDY TEST SITE POSSESSING INTERMEDIATE LEVEL TERRAIN COMPLEXITY

— COLLECT DATA IN MICROWAVE REGION FOR FIRST AND SECOND LEVEL (COMPLEXITY) TEST SITES

— REPLICATE THERMAL OBSERVATION FIRST LEVEL (SITES)

1983 — VALIDATION STUDY 2ND LEVEL TEST SITE

— CHOOSE AND STUDY A THIRD TEST SITE POSSESSING HIGH LEVEL OF TOPOGRAPHIC AND BOTANICAL COMPLEXITY

— PERFORM COMPARATIVE ANALYSIS OF TEST SITES FROM THE THREE LEVELS OF COMPLEXITY
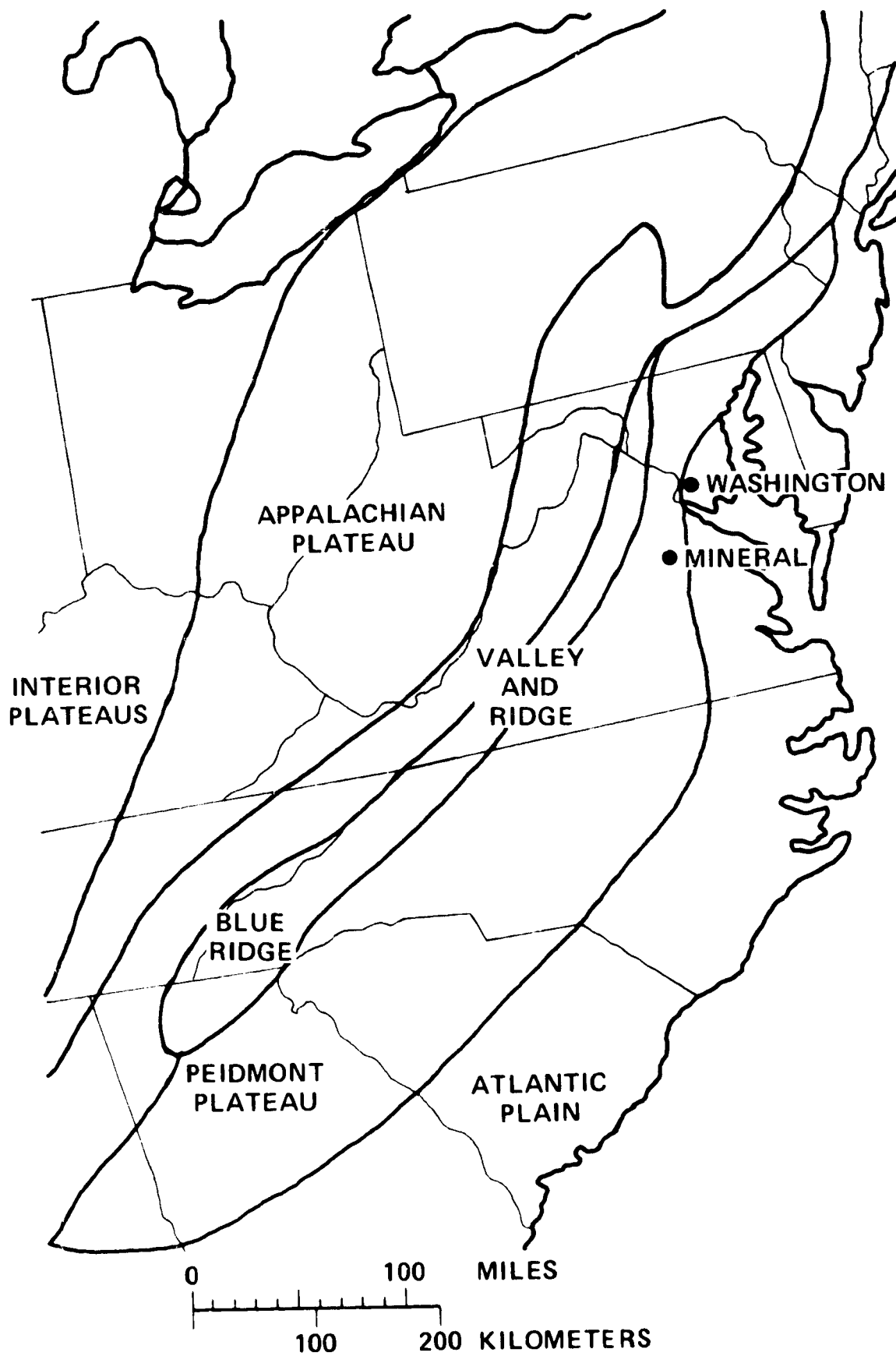
Figure lA-l: Location of Test Site

MINERAL SULFIDE DISTRICT

■ QUARTZ SERICITE SCHIST AND GNEISS

■ QUARTZ SERICITE BIOTITE SCHIST AND GNEISS

■ BIOTITE SERICITE FRAGMENTAL SCHIST

□ TRANSITIONAL AMPHIBOLITE

▦ AMPHIBOLITE

▤ BIOTITE SERICITIC AND SERICITIC QUARTZITE

□ GARNET MUSCOVITE CHLORITE SCHIST

▨ GRANODIORITE

Figure 1A-2: Geologic Map of Mineral Sulfide District

1--14
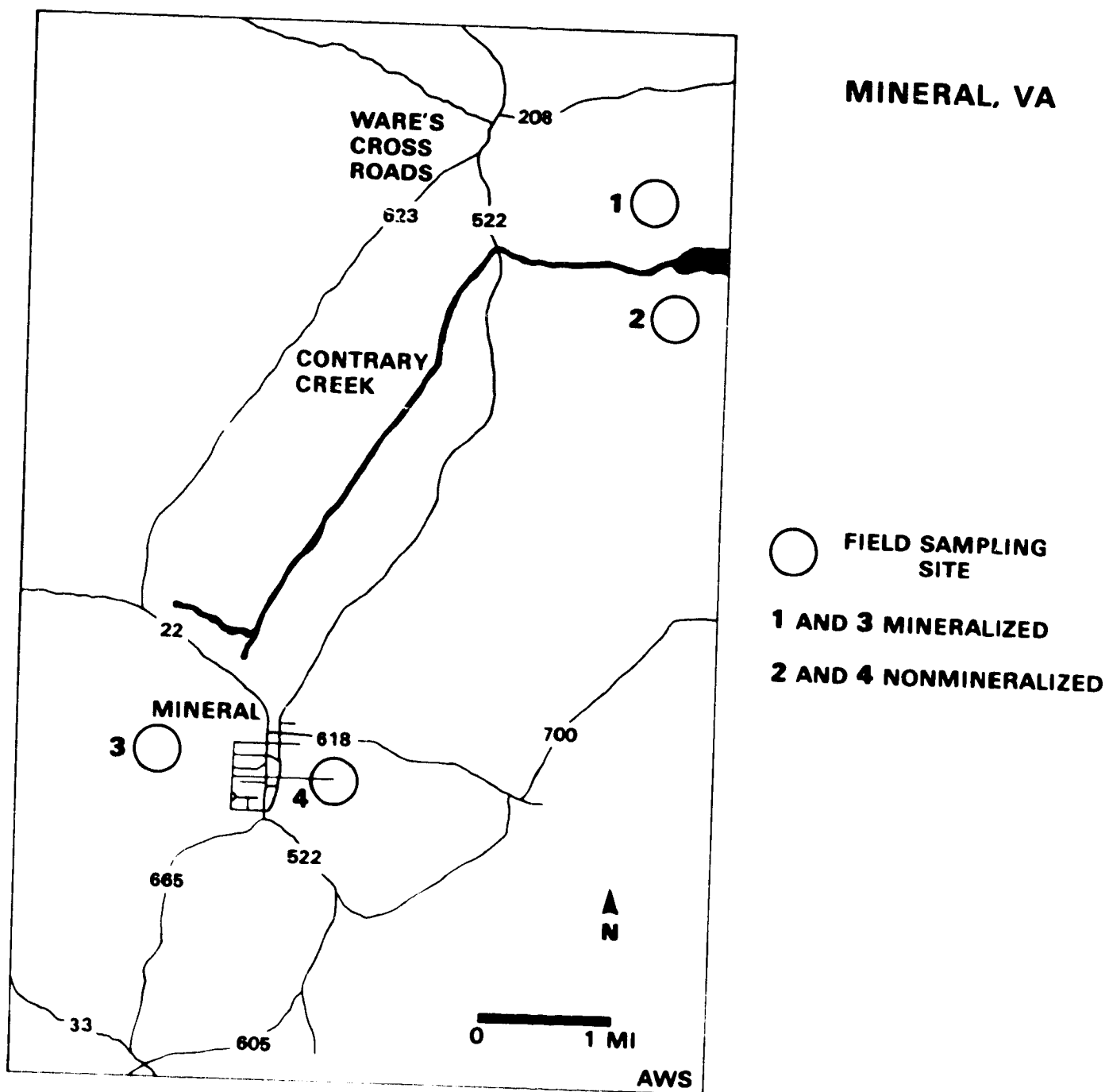
Figure 1A-3: Location of Individual Mineralized and Non-Mineralized Test Sites
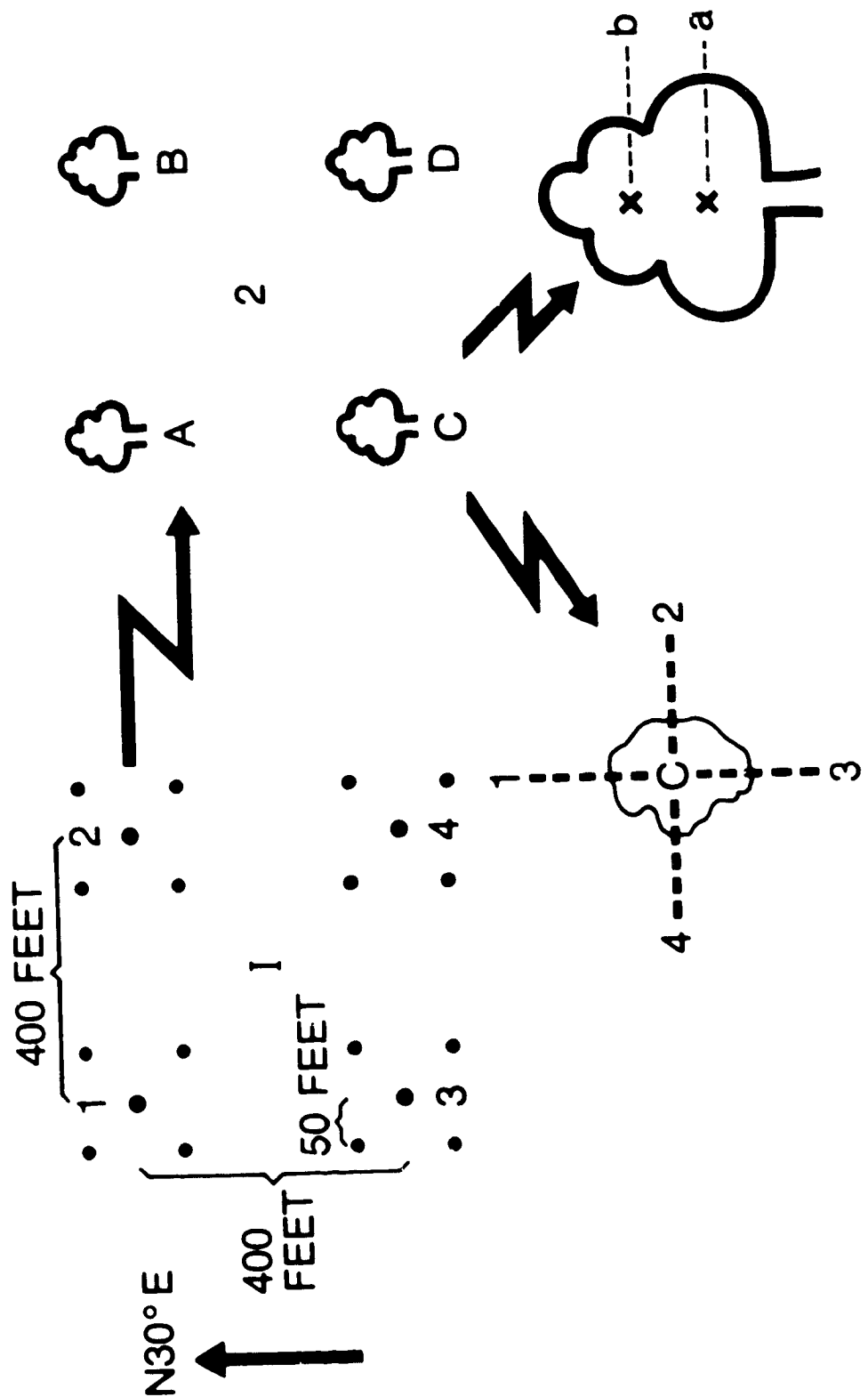
Figure 1A-4: Illustration of Elements in Hierarchial Experimental Design for Individual Test Sites
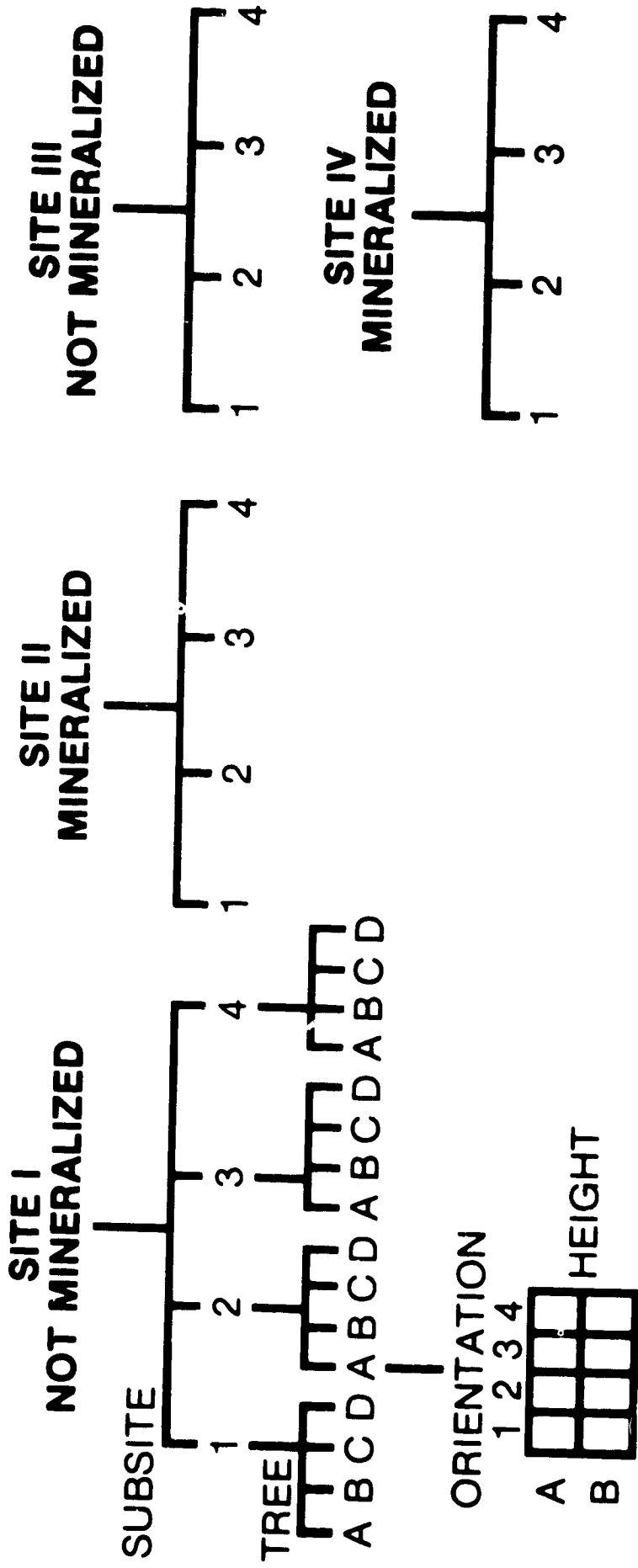
Figure 1A-5: Hierarchial Experimental Design

1 17
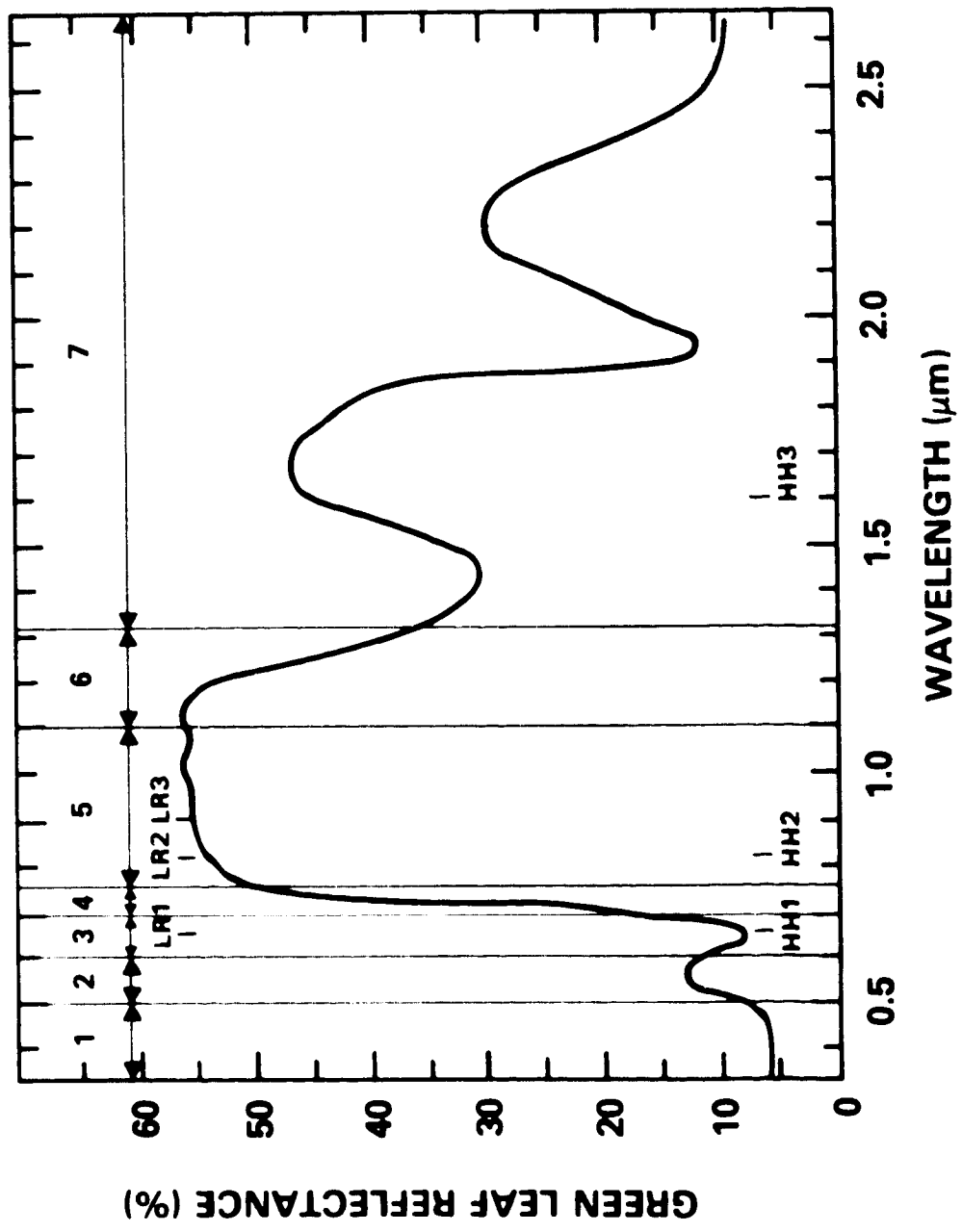
Figure 1A-6: Green Vegetation--Spectral Reflectance Relationships from 0.35-1.50 ‚m (after Tucker, 1978)

Figure 1A-7: Julia Test Site--June 1980
Radiance[1] Values from TM3 (0.63-0.69 um)
Using Three Band Hand-Held Radiometer
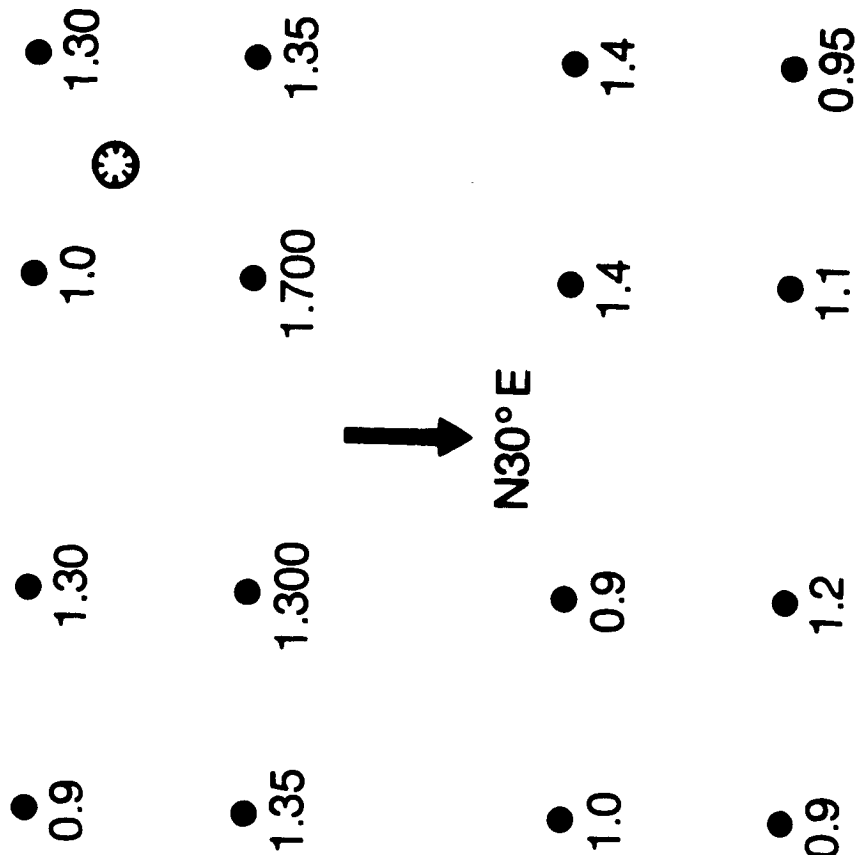
[1] VALUES ARE MEANS OF HIGH AND LOW SAMPLES
⊛ FORMER MINE SHAFT OPENING

● 1.15

● 0.95

● 1.05

● 0.95

● 1.1

● 1.10

MISSING

● DATA

● 1.05

N30° E

● 1.00

● 1.00

● 1.05

● 1.35

● 1.05

● 1.00

● 1.0

● 0.85
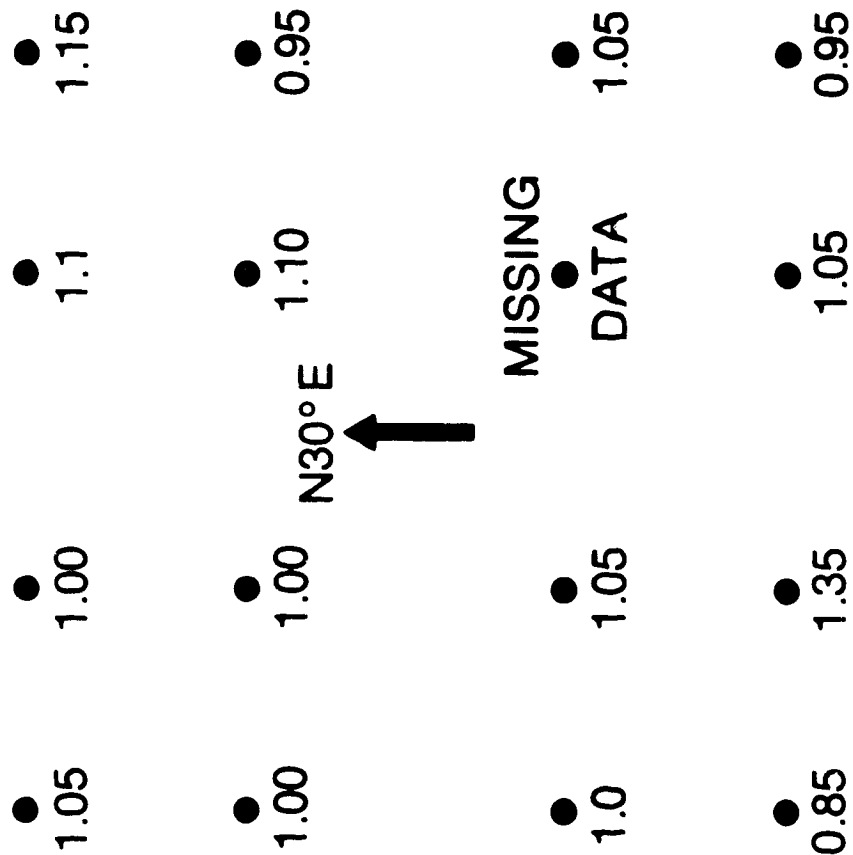
¹VALUES ARE MEANS OF HIGH AND LOW SAMPLES.

Figure 1A-8: Sarkis Test Site--June 1980
Radiance¹ Values for TM3 (0.63-0.69 μm)
Using Three Hand-Held Radiometer

B.   THEMATIC MAPPER SIMULATOR FLIGHT OVER THE

COTTER BASIN GEOBOTANICAL ANOMALY

BY

A.W. Siegrist, E. Masuoka, C.C. Schnetzler

OBJECTIVE

The next generation of land observing systems, to be inaugurated
by Landsat D in 1982, will carry an advanced scanner known as the
Thematic Mapper. This scanner will cover a broader spectral region
and have more optimally chosen bands than the presently flying
Multispectral Scanner. The objective of this study was to deter-
mine if the Thematic Mapper's spectra regions are useful to detect
geobotanical anomalous areas.

BACKGROUND

Abnormal metal concentrations in plants may stress the plants
internal constituents to the point of modifying the spectral
reflectance of the species. In both laboratory and field experi-
ments, several authors (Barker and Horler, 1979; Birnie and
Francica, 1979; Birnie and Dykstra, 1978; Canney et al., 1970;
Collins et al., 1977; Howard et al., 1971; Lyon, 1975; Press, 1974;
and Yost, 1975) have studied the optical properties of plants as
heavy metal concentrations were allowed to influence physiological
processes such as the balance between chlorophyll synthesis,
chlorophyll breakdown, growth and leaf structure. Table 1B-1 presents
the significant results of these numerous studies by plant species
observed, type of metal stress and the direction (increase or
decrease) in which reflectance values of stressed plants tend in
comparison to background plants. For example, Barber and Horler
(1979) report that Pisum sativum stressed by abnormal cadmium con-
centrations exhibit, as compared to control plants, increased
reflectance in visible wavelengths (.475, .550, .660 μm) simultan-
eously with decreased reflectance in infrared wavelengths (.850,
1.65, 2.20 μm). On studying this table, it may be stated generally
over a variety of species, metals, and experimental conditions that
metal stressed plants, in comparison to background plants, exhibit
increased reflectance values at visible wavelengths and decreased
values at near infrared wavelengths (1.0-2.5 μm regions). Results
at visible wavelengths are explained by depressed total leaf
chlorophyll concentrations per unit leaf fresh weight. Results
at near infrared wavelengths, provided by Barber and Horler (1979)
only in the 1.5-2.0 μm region, may be associated with changes in
leaf structure which increase the internal scattering or trans-
mittance of leaves.

Collins et al. (1977) surveyed conifer forests covering copper sulfide bodies in an area of Lewis and Clark County, Montana known as Cotter Basin. Visible and near infrared (.45-1.00 μm) reflected radiance data were collected by an airborne, 500-band, high resolution (0.0015 μm bandwidth) spectroradiometer. Using this instrument anomalous spectral reflectivity properties were detected in the conifers. Specifically, the reflectance spectrum over the mineralized zone shifted towards shorter, blue wavelengths in the 0.70-0.78 μm region.

The present study was undertaken in order to determine whether a spectral anomaly is demonstrable with Thematic Mapper Simulator (TMS) data over the same site as the vegetation-spectral anomaly demonstrated by Collins et al. (1977) with the narrow-band spectroradiometer. From the results published by other workers and presented in Table 1B-1, it is expected that an anomalous site should exhibit increased reflectance values in visible wavelengths and decreased values in infrared wavelengths in comparison to a background site.

RECENT ACCOMPLISHMENTS

Thematic Mapper Simulator (TMS) data were collected over the Cotter Basin, Montana, test site on August 29, 1979 by a NC130B aircraft flown at an altitude of approximately 3 km (10,000 ft). The scanner has an active scan angle of 100 degrees and a spatial resolution of 2.5 milliradians. Each pixel is approximately 7.5 meters on a side. The TMS simultaneously records dispersed electromagnetic radiation in eight discrete channels, the seven Thematic Mapper channels, plus a band in the 1.0 to 1.3 μm region.

"Anomalous" and "background" sites were outlined within the TMS data by referring closely to Collins' vegetation-spectral anomaly as well as to the soil geochemistry anomaly as given by Collins. Initially, the anomalous site was selected entirely within Collins' vegetation-spectral anomaly (which was within the soil geochemistry anomaly) and is referred to hereafter as the small anomaly. The background is located outside of both Collins' vegetation-spectral anomaly and the soil geochemistry anomaly, located at approximately the same angle from flight line nadir and on similar topography as the anomalous site. Each contain about 500 pixels and covers a ground area approximately 160 meters on a side. From the means and standard deviations of each site, for each band, t-values were calculated and tested to determine if significant statistical differences exist between the mean reflectance values of the anomalous and background sites in the various spectral channels. The means, standard deviations and t-values are given in Table 2. Negative t-values indicate that reflectance values from an anomalous site are higher than values from a background site, positive t-values indicate that reflectance values from an anomalous site are lower than a background and NS indicates that

the reflectance values are not significantly different from one
another. As can be seen from Table 1B-2, all but the 1.0-1.3 μm band
showed significant differences between the small anomalous and
background sites. The increased reflectance of the small anomaly
over the background sites in visible wavelengths is consistent
with previously published results (refer to Table 1B-1) whereas
increased reflectance in near infrared wavelengths is not.

Having produced results which were only partly consistent with
other studies, larger sites were chosen. The large anomaly test
site incorporates the Collins vegetation-spectral anomaly area
plus the soil geochemistry anomaly. The large background site was
chosen outside of both of these but at approximately the same
distance from flight line nadir and on similar topography. Each
of these sites contains approximately 2000 pixels and covers a
ground area of approximately 345 meters on a side. Results of
the t-value test on larger sites were somewhat different. TMS 1
was still statistically different, but in an opposite sense; like-
wise TMS 4. The thermal band, TMS 8, show no statistical difference.
The other five bands show the same direction and general statis-
tical difference as for the small test sites--that is, the reflec-
tance values for the anomaly are greater than those for the back-
ground over both visible and near infrared wavelength regions.

Fearing the possibility of autocorrelation between observations
biasing the t-values, every 10th line and every 10th pixel were
sampled from the large sites (thus, only about 20 pixels/site
were used instead of 2000) for TMS channels 3, 4, 5, and 6 and
t-values were recalculated. The results are generally the same
as for the total test sites for all channels except TMS 4, in
which case, there was no significant difference between the anomaly
mean reflectance and the background mean reflectance.

Finally, it was suspected that perhaps the large anomaly site
included excessively high reflectance pixels attributable to
small test pits and/or road surfaces, not related to the problem
of vegetation-spectral anomaly versus background. Therefore, the
large sites were modified to exclude the excessively high outliers;
again the results for the three bands were generally the same,
except t-values were even higher, but TMS channel 4 results were
not significant.

To summarize, TMS channel 1 gave mixed results--both tests were
statistically significant but in opposite directions. TMS channels
2 and 3 gave statistically significant results which were consis-
tent with a fairly large body of laboratory, field and aircraft
data. TMS channel 4 had mixed statistically significant results
in two tests and two "not significant" results in the special
autocorrelation and outlier tests. The previous laboratory, field
and aircraft results are mixed for this spectral region--in some
cases showing small increases and in others small decreases. There

is essentially no other data with which to compare our results for channel 5, which showed significant variations in 3 of the 4 tests. Both channels 6 and 7 consistently show statistically higher reflectance in the anomalous sites compared with the background sites, contrary to the small amount of laboratory data available. The thermal channel, TMS 8, shows mixed results on the two tests-- a small but significant t-value, and a non-significant value. The data also suggest that anomalous sites have a "richer texture," or greater variation in reflectance (as shown by the standard deviations in Table 1B-2) than the background sites.

SIGNIFICANCE

This study suggests that the Thematic Mapper can be used to detect geobotanical anomalies. In particular, it indicates that the near infrared regions, especially the 1.55-1.75 µm region, could be the most sensitive region to measurements of stress related changes in vegetation spectra. There is also the suggestion that the degree of variation in reflectance may be indicative of stress in plants.

FUTURE EMPHASIS

During the next few months, several aspects of this data will be examined further. We will try to examine the non-geochemically related, "natural," variation in vegetation spectra in the region, again trying to hold known parameter change, such as topography and scan angle variation, to a minimum. Also, we will expand the attempt to remove autocorrelation to all eight bands. If the basic conclusions do not change as a result of this further analysis, Barber and Horler will be asked to repeat their initial laboratory analysis which indicated that near infrared reflectance should decrease with increased metal content, an effect opposite to that which we observe at Cotter Basin.

REFERENCES

Barber, J. and D.N.H. Horler, "Fundamental Relationships Between Plant Spectra and Geobotanical Stress Phenomena," Sixth Month Report on NASA Contract NAS 5-25738, GSFC, Greenbelt, MD 20771, 1979.

Birnie, R.W. and J.D. Dykstra, "Application of Remote Sensing to Reconnaissance Geologic Mapping and Mineral Exploration," Proc. 12th Int. Symp. on Remote Sensing of the Environment, April 20-26, Manila, 1978.

Birnie, R.W. and J.R. Francica, Jr., "Remote Detection of Geobotanical
    Anomalies: A Method for Mineral Exploration," (Abstract):
    Abstracts with Programs, G.S.A. Annual Meeting, November,
    San Diego, p. 389, 1979.

Canney, F.C., S. Wenderoth and E. Yost, "Relationship Between
    Vegetation Spectra and Soil Geochemistry-New Data from Catheart
    Mountain, Main," Third Annual Earth Resources Program Rev.,
    v. 1, Geology and Geography, Houston, TX, NASA/JSC, 18.1-189,
    1970.

Collins, W.E., G.L. Raines and F.C. Canney, "Airborne Spectro-
    radiometer Discrimination of Vegetation Anomalies over Sulfide
    Mineralization-A Remote Sensing Technique," G.S.A. Abstracts
    with Programs, v. 9, no. 7, 932-933, 1977.

Howard, J.A., R.D. Watson and T.D. Hessin, "Spectral Reflectance
    Properties of Pinus Ponderosa in Relation to Copper Content
    of the Soil-Malachite Mine, Jefferson County, CO.," Proc.
    7th Symp. Remote Sensing of Envir., Univ. Michigan, 285-297,
    1971.

Lyon, R.J.P., "Correlation Between Ground Metal Analysis, Vegetation
    Reflectance and ERTS Brightness Over a Molybdenum Skarn
    Deposit, Pine Nut Mountains, Western Nevada," Proc. 10th
    Int. Symp. Remote Sensing of Invir., Univ. Michigan, 1031-
    1041, 1975.

Press, N.P., "Remote Sensing to Detect the Toxic Effects of Metals
    on Vegetation for Mineral Exploration," Proc. 9th Int. Symp.
    Remote Sensing of Envir., Univ. Michigan., 2027-2038, 1974.

Yost, E., "Multispectral Color Photography for Mineral Exploration
    by the Remote Sensing of Biogeochemical Anomalies," NASA-CR-
    144-11 N77-10606, 147 pp., 1975.

TABLE 1B-1: Summary of Previous Spectral Analysis of Metal Stressed Vegetation

SPECIES	METAL	WAVELENGTH (μm)	REFERENCES
PISUM SATIVUM	Cd Cu Pb Zn		BARBER & HORLER (1979)
QUERCUS ROBUR	Cu As		BARBER & HORLER (1979)
DOUGLAS FIR	Cu		BIRNIE & FRANCICA (1979)
LODGEPOLE PINE	Cu Mo		BIRNIE & DYKSTRA (1978)
PICEA RUBENS	Cu Mo		CANNEY & OTHERS (1970)
ABIES BALSAMEA	Cu Mo		CANNEY & OTHERS (1970)
CONIFERS	Cu SULFATES		COLLINS & OTHERS (1977)
PINUS PONDEROSA	Cu		HOWARD & OTHERS (1971)
PINUS MONOPHYLLA	Mo		LYON (1975)
JUNIPERUS UTAHENSIS	Mo		LYON (1975)
QUERCUS SP	Pb Zn		PRESS (1974)
PINUS PONDEROSA	Cu		YOST (1975)
JUNIPERUS SP	Cu		
QUERCUS SP	Cu		

KEY: ↑ INCREASED REFLECTANCE WITH INCREASED METAL CONTENT ↓ DECREASED REFLECTANCE WITH INCREASED METAL CONTENT

1-26

TABLE 1B-2:   MEAN, STANDARD DEVIATION AND T-VALUES OF TMS BANDS

TMS BAND #	(µm)	Small Anomaly*		Small Background*		Large Anomaly*		Large Background		Calculated t-values Small Back-ground vs. Anomaly	Calculated t-values Large Back-ground vs. Anomaly
		$\bar{x}$	σ	$\bar{x}$	σ	$\bar{x}$	σ	$\bar{x}$	σ		
1	0.45- .52	98.1	26.7	89.4	5.8	88.5	5.0	89.5	4.1	- 7.22	+ 6.91
2	0.52- .60	68.3	28.0	59.0	6.4	58.7	5.7	56.1	5.2	- 7.37	-15.31
3	0.63- .69	40.8	24.2	32.3	6.0	32.0	4.9	30.2	4.2	- 7.44	-13.04
4	0.76- .90	54.7	12.5	58.1	10.1	57.0	11.2	56.2	10.1	+ 4.60	- 2.43
5	1.00-1.30	61.9	15.2	61.6	12.1	64.5	14.8	57.8	11.4	N.S.	-16.50
6	1.55-1.75	47.2	19.6	36.8	9.0	43.1	11.5	31.5	7.3	-10.33	-38.90
7	2.08-2.35	55.7	12.4	49.0	5.9	53.8	5.8	50.9	5.5	-11.12	-14.34
8	10.4 -12.5	37.9	13.0	36.4	9.5	38.8	9.4	38.5	7.4	- 2.10	N.S.

*Number of pixels in small anomaly and background sites: Bands 1,2,7,8 = 513
                                                            Bands 3,4,5,6 = 468

+Number of pixels in large anomaly and background sites: Bands 1,2,7,8 = 1989
                                                            Bands 3,4,5,6 = 2100

C. FUNDAMENTAL RELATIONSHIPS BETWEEN PLANT SPECTRA

AND GEOBOTANICAL STRESS PHENOMENA

by

E. Masuoka

OBJECTIVE

As part of an integrated program of fundamental and applied research in geobotanical exploration, NASA is sponsoring research at Imperial College (London, England) to study the optical and physiological responses of plants grown under conditions of metal stress. This approach will provide important fundamental information about the spectral properties of plants growing in metal-rich solutions, which can be used in the planning and interpretation of remote sensing field studies.

Current research conducted at Imperial College is directed toward investigating three potential signatures of metal stressed vegetation: a shift of the chlorophyll absorption edge to shorter wavelengths (Collins et al., 1977 and Chang and Collins, 1980) (see Figure 1C-1); increased reflectance in the visible wavelengths (Horler et al., 1980 and Canney et al., 1970); and increased canopy temperatures (Canney et al., 1972 and Horler et al., 1980).

BACKGROUND

Peas, soybeans, and sunflowers were grown in aerated hydroponic solutions containing nutrients and varying amounts of copper, lead, cadmium or zinc. Measurements of reflectance at wavelengths characteristic of the first six Thematic Mapper (TM) bands (see Table 1C-1), measurements of thermal emissivity and measurements of the dimensions of roots and shoots were recorded throughout the experiments.

A separate study of oaks (Quercus rober) growing on mine tailings at a copper-arsenic mine was undertaken to determine if the laboratory results concerning heavy metal stress and reflectance could be duplicated at a field site.

RECENT ACCOMPLISHMENTS

Experimental results indicate that the increase in reflectance in the visible wavelengths noted in the leaves of metal stressed vegetation is associated with the destruction of chlorophyll or the inhibition of chlorophyll synthesis. The experiments also revealed that not all plants exhibit higher reflectance calues under metal stress. Of special interest were the oaks which showed no change in the visible bands, but a significant decrease in reflectance in two of the infrared bands, 0.8 and 1.65 µm. Work in the red region

of the spectrum, from 0.675 to 0.725 μm strongly suggests that the 'red shift' of Chang and Collins (1980) is due to a reduction in the total chlorophyll in the leaf (Horler et al., 1980).

Results from experiments which measured the effects of heavy metal stress on plant canopy temperatures, show that plants growing in a solution containing 200 ppm copper or 200 ppm cadmium were $1^{O}C$ warmer than controls. However, experimental results also revealed that metal stress is impossible to detect when plants are in a state of water stress. Under water stress the canopy temperature of both metal stressed plants and controls rose 3.5^{O} (Horler et al., 1980).

SIGNIFICANCE

Results of the reflectance experiments suggest that if reflectance measurements are to be used to detect geobotanical anomalies, the researcher must have an intimate knowledge of the normal reflectance values of each major plant species in the survey area, because there is no general relationship between reflectance and metal stress which holds for all species. Results of experiments studying the 'red shift' suggest that the development of highly sophisticated sensors to detect changes in the proportions of different chlorophyll pigments is unnecessary because the 'red shift' is due primarily to a decrease in total chlorophyll. Results from the thermal experiments are significant because they suggest that the best time to look for geobotanical anomalies with thermal remote sensing is during periods of ample rainfall.

FUTURE EMPHASIS

In the future the work at Imperial College will center on examining the effects of climatic and edaphic variables, i.e., ambient light, humidity, temperature, soil pH, etc., which may complicate the extrapolation of laboratory results to the field. These experiments will be carried out in field plots, where anomalous soil conditions will be created by mixing mine wastes containing copper, lead, and zinc into uncontaminated soil, and in a forest in North Wales, which is growing on a massive porphory copper deposit.

REFERENCES

Canney, F.C., T.D. Hessin and W.G. Burge, "Analysis of Thermal Patterns of Geochemically Stressed Trees at Catheart Mountain, Maine," 4th Annual Earth Resources Program Review, NASA, Houston, Texas, p. 57-1, 1972.

Change, S. H. and W. Collins, "Toxic Effects of Heavy Metals on Plants," Abstracts of 6th Annual Pecora Symp., Sioux Falls, South Dakota, April 1980.

Collins, W., G.L. Raines and F.C. Canney, "Airborne Spectroradiometer
    Discrimination of Vegetation Anomalies over Sulphide Mineraliza-
    tion-A Remote Sensing Technique," Geol. Soc. Amer., Annual
    Meeting, Seattle, Washington., Abstracts with Programs, 932-
    933, 1977.

Horler, D.N.H., J. Barber and A.R. Barringer, "Effects of Heavy
    Metals on the Absorbance and Reflectance Spectra of Plants,"
    Int. J. Remote Sensing 1 (2), in press, 1980.

Horler, D.N.H., J. Barber and A.R. Barringer, "Effects of Cadmium
    and Copper Treatments and Water Stress on the Thermal Emission
    from Peas (Pisum sativum L.): Controlled Environment Experi-
    ments," Remote Sensing of Environ., in press, 1980.
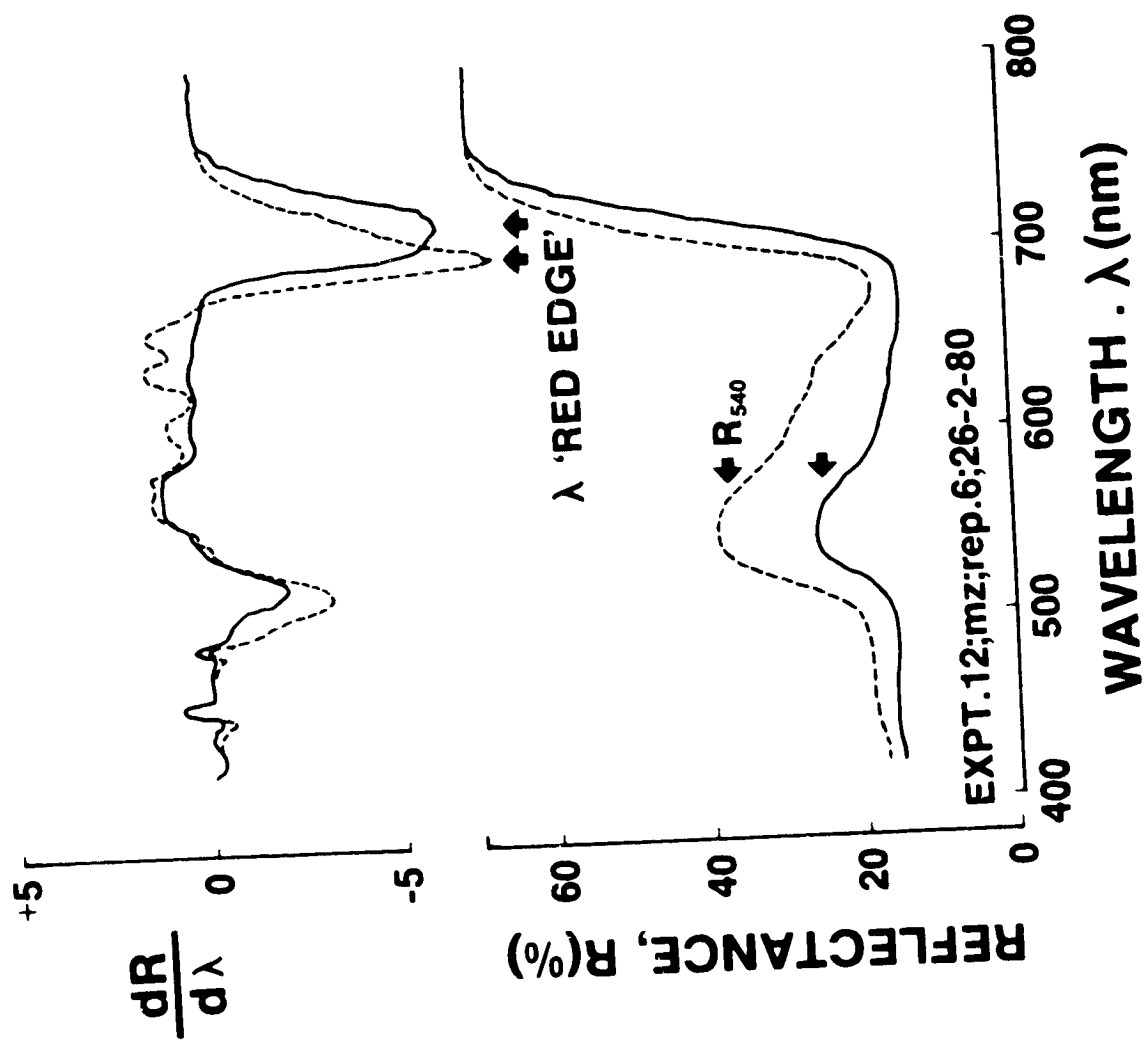
Figure 1C-1: Reflectance and first derivative reflectance spectra of two maize leaves. Solid line: control plant, not metal-treated. Dashed line: treated with 200 mg.l-1 Cu in the nutrient solution. λ red edge is defined using the derivative spectra and shows a clear effect of metal treatment.

Table 1C-1: WAVELENGTHS AT WHICH REFLECTANCE MEASUREMENTS WERE MADE IN LABORATORY STUDIES OF METAL STRESSED VEGETATION

THEMATIC MAPPER BAND	WAVELENGTH MEASURED	SIGNIFICANCE
1	0.475 μm	Approximately the blue reflectance minimum corresponding to the chlorophyll absorption peak
2	0.550 μm	The green reflectance peak
3	0.660 μm	The reflectance minimum corresponding to the red chlorophyll absorption peak
4	0.850 μm	Representative of the very high near infrared reflectance 'plateau'
5	1.65 μm	Reflectance peaks between the main water-absorption bands
6	2.20 μm	

D.   EXPERIMENTAL APPLICATION OF LANDSAT TO

GEOBOTANICAL PROSPECTING OF SERPENTINE OUTCROPS IN THE

CENTRAL APPALACHIAN PIEDMONT OF NORTH AMERICA

by

Howard W. Mielke*

OBJECTIVE

The purpose of this research is to test the use of the Landsat as
a tool for geobotanical prospecting of serpentine outcrops.

BACKGROUND

Geobotanical prospecting is the branch of earth sciences which
employs field observation of the distribution of vegetation as a
tool for locating mineral deposits. One example of geobotanical
prospecting was the staking of claims and purchasing of land having
potential chromium deposits in the Appalachian Piedmont of the
eastern United States during the nineteenth century. These chromium
deposits, associated with sites having serpentine outcrops, could
be easily distinguished from sites containing other rock types by
their vegetation. One of the most productive chromium mines was
located within a large Maryland serpentine outcrop called Soldiers
Delight.

This serpentine outcrop currently supports a stunted tree-flora
with an open canopy that is dominated by Virginia Pine (Pinus
virginiana), Post Oak (Quercus stellata) and Blackjack Oak (Quercus
marilandica). In contrast, the neighboring ultramafic and schist
rock outcrops support a robust tree-flora with a closed canopy
consisting of a variety of species and dominated by Chestnut Oak
(Quercus prinus) and White Oak (Quercus alba). Prospecting for
potential chromium deposits was a matter of search for the atypical
scrubby and open canopied tree-flora among lands supporting agri-
cultural production or dense deciduous forests.

The overal study site extends along the Appalachian Piedmont from
southeastern Pennsylvania through Maryland to northern Virginia
and covered an area of 13137 km^2 (5072 mi^2). The Pennsylvania and
Maryland sector of the study, an area of 7778 km^2 (3003 mi^2),
includes serpentine outcrops with their well documented occurrences
of serpentine mineral deposits. The Virginia sector, an area of
5359 km^2 (2069 mi^2), was included because the presence of serpentine
outcrops there has not been as well documented as in the sector
north of the Potomac. The inclusion of both regions with documented
serpentine outcrops as well as an adjacent area provided a means of
evaluating the methodology and application of Landsat as a tool for
geobotanical prospecting.

RECENT ACCOMPLISHMENTS

Four Landsat passes, in February, April, July and October were analyzed on Goddard's AOIPS system. It was initially assumed that early spring, late fall or winter, when deciduous trees are leaf-less, were the times of year when conifer sites could be most easily distinguished from deciduous leaf-bearing trees. However, analysis of the CCT's revealed that the best time of the year for distinguishing coniferous sites from deciduous sites was in summer (mid-July) when all vegetation was in full leaf. At that time, sun angles are highest, the image is brightest and produces greatest contrast giving maximum resolution. Subtle vegetation differences are most easily observed from Landsat at the height of the growing season. Also, because of the brightness of the summer scene, image enhancement (subroutines which increase contrast) was not required. This is an advantage because each transformation of the image tends to degrade some aspect of its quality.

Two well studied and documented serpentine bodies were chosen as training sites--Soldiers Delight, northwest of Baltimore and Nottingham Park in the State Line District of Pennsylvania. Using the serpentine multispectral signature, a total of 159 sites with 50 pixels or more were identified in the study area (Figure 1D-1). A subset of 41 of these sites were chosen for on site visit (numbered sites on Figure 1), and a further subset (23) were subjected to soil chemistry analysis and tree identification and measurement. Of these 23 sampled sites, eight had many chemical and vegetation features similar to the training sites. Thus the overall success rate was eight out of 23 samples or about a 35 percent success rate in identifying serpentine sites. However, the distribution of successfully identified sites was not even over the overall study area. North of the Potomac River eight of 12, or 67 per-cent, of the sampled sites had soil chemical features which linked them with serpentine outcrops while south of the Potomac none of the 11 sampled sites were, in fact, serpentine. This apparently is because north of the Potomac the broad leaf deciduous forest dominates, but south of the Potomac the natural vegetation is dominated by needle leaf evergreen coniferous species. In the study sites north of the Potomac, a multispectral signature based on conifers facilitated discrimination of anomalous vegetation when compared to the background vegetation. However, south of the Potomac the target sites were indistinguishable from the natural background vegetation.

SIGNIFICANCE

While the study demonstrated that south of the Potomac another multi-spectral signature should be developed, on the 7778 km^2 (3003 mi^2) sector north of the Potomac this study established the effectiveness of the multispectral imaging satellite as a tool for quickly and accurately locating mineral sensitive vegetation communities over vast areas of land.

FUTURE EMPHASIS

No expansion of this work on serpentine is planned for the near future. A study of the use of geobotanical analysis of satellite data for general geologic mapping in the Appalachian area is being planned.

PUBLICATION

Mielke, H.W., "Experimental Application of Landsat to Geobotanical Prospecting of Serpentine Outcrops in the Central Appalachian Piedmont of North America," GSFC Technical Memorandum 80741, July 1980.
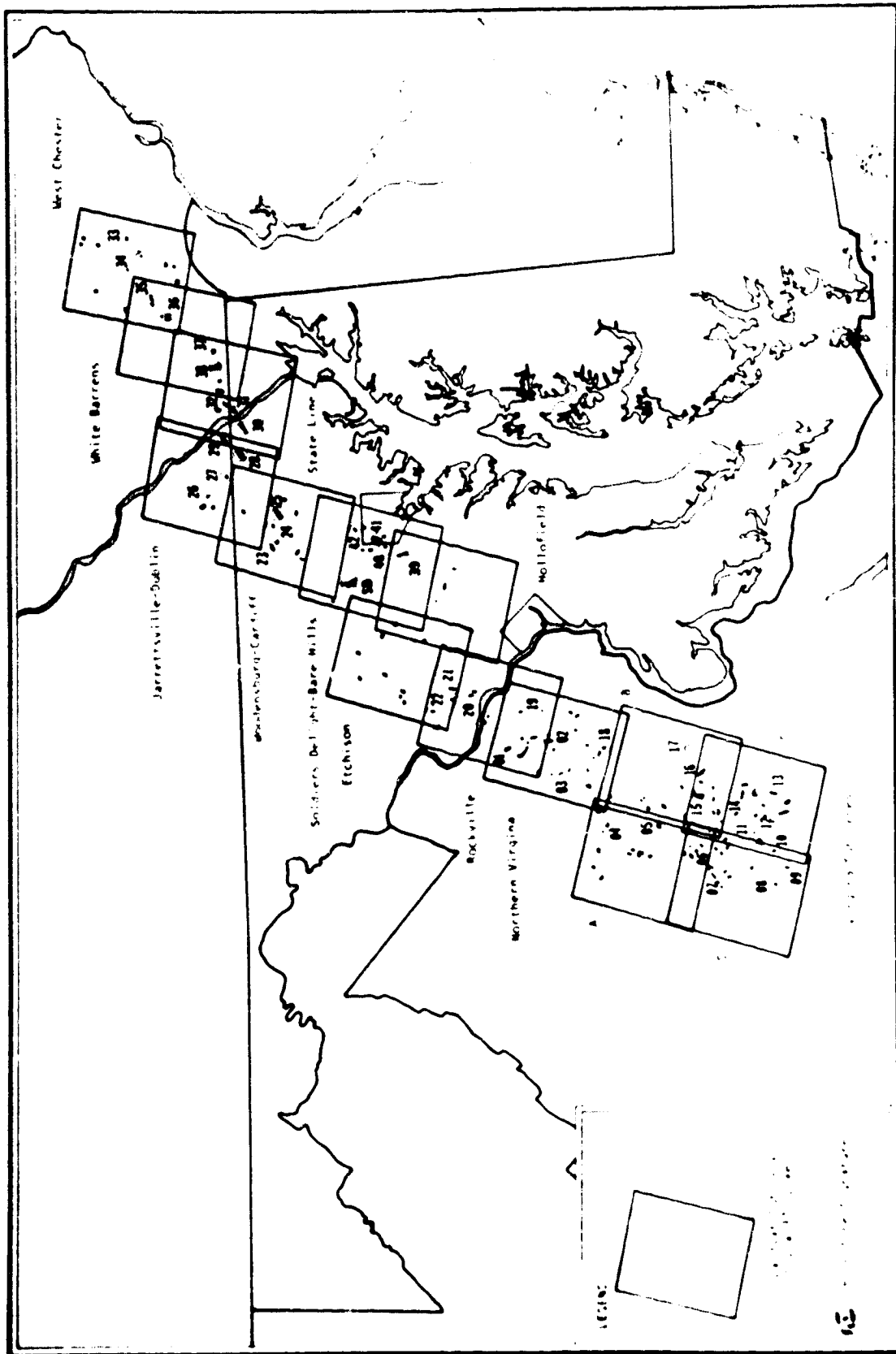
Figure 1D-1: Study Site, Showing Serpentine Bodies Mapped and Distribution of the Field Sites Actually Visited

CHAPTER 2

MAGNETIC FIELD MODELING

edited by

R.A. Langel

OVERVIEW

The objective of the magnetic field modeling program is twofold:

o   To develop techniques for determining accurate, up-to-date models of the earth's main magnetic field and its secular variation.

o   To develop methods for obtaining, verifying and representing crustal geopotential fields so that these data can be used for developing broad-scale models of the composition, structure and evolution of the earth's crust.

A key to research in geomagnetism is the ability to represent magnetic fields from sources internal to the earth in terms of mathematical functions and/or maps which are easily reproducible and in a form usable for modeling studies. Our primary data source is from satellite-borne magnetometers (POGO in the past and Magsat currently), supplemented by data from geomagnetic observatories, aircraft, ship and land surveys, and repeat stations. The internal geomagnetic field has a natural division into fields from the core of the earth and fields from the earth's crust. The mantle should not be a significant source of magnetic field because its temperatures are mainly above the Curie isotherm, thus eliminating rock magnetism, because the internal circulation of conducting material is believed to be slow compared to that of the core, and because the material circulated is of lower conductivity than that in the core. Thus modeling divides itself naturally into modeling of the core field with spherical harmonic functional representations and modeling of the crustal field with maps and equivalent source functions.

The object of modeling of the core field is, first, to maintain a useful representation of the time-varying field for purposes of navigation, magnetospheric physics and background removal in the study of crustal and magnetospheric fields; and second, to serve as a source of information regarding processes in the earth's core.

While modeling of the core field is an old, established discipline of geomagnetism and is pursued by several groups around the world, in many respects it is still in a rudimentary stage of development. No existing techniques are useful for extrapolation of the field more than one or two years into the future with acceptable accuracy, which means that we do not understand the mechanism for geomagnetic secular variation, nor do we even know how to model it properly. Recent research seems to indicate that some of the changes formerly attributed to changes of the internal field are in reality due to changing currents in the earth's magnetosphere, a phenomena not yet well modeled in itself. In addition, measurements from magnetic observatories, although accurate in themselves to within about fifty gamma or better, have not been capable of representation by global models any better than an rms of several hundred gamma.

Research is thus directed toward the general problems of accurate modeling of the core field of the earth and its long term or secular variation.

The object of modeling the crustal field is to provide a tool, or tools, to the solid earth geophysicist and geologist for regional scale crustal modeling. Because crustal fields at satellite altitude are very small (0-20 gamma) in the presence of the core field (20,000-50,000 gamma) and magnetospheric fields (0-2000 gamma), detection and representation of such fields is first of all a problem of extracting the signal from the background "noise" of the other fields and then developing appropriate mathematical representations of the resulting fields, such as equivalent source models. A good beginning has been made in solution of these problems and some useful results will be presented in the following sections.

Because data from the Magsat spacecraft became available during 1980, a large portion of the work reported has to do with processing and analysis of that data. This includes exciting new results in modeling both core and crustal fields. An overview of the Magsat program is contained in the July-September 1980 issue of The Johns Hopkins APL Technical Digest (volume 1, no. 3).

A. PROCESSING OF THE MAGSAT DATA

by

R.A. Langel and J.H. Berbert

OBJECTIVE

The objective is to prepare the Magsat data for analysis and to distribute that data to investigators.

BACKGROUND

Magsat is a spacecraft dedicated to measuring the magnetic field near the earth. It was launched at 1416 UT on October 30, 1979 and re-entered the earth's atmosphere at 0720 UT on June 11, 1980. Data acquisition began on November 2, 1979 and continued until a few hours prior to re-entry. Two instruments provided the field measurements. A cesium vapor magnetometer measured the magnitude of the field (scalar field) to an accuracy of about +1 gamma and a fluxgate magnetometer measured the components of the field to about +3 gamma. On-board star cameras, sun sensor and a pitch gyro were utilized to measure the attitude of the spacecraft to an accuracy of a few tens of arc seconds. Because the star cameras were located on the main body of the spacecraft while the sun sensor was located at the end of a boom, with the vector magnetometer, an optical attitude transfer system (ATS) was incorporated to relate the location of the end of the boom relative to the star cameras.

CALIBRATION OF VECTOR DATA

Because fluxgate magnetometers are subject to drift, a procedure was devised to utilize the scalar data to redetermine the calibration parameters of the fluxgate magnetometer (Lancaster et al., 1980).

The procedure has been applied successfully. In doing so it was observed that the fluxgate calibration parameters were indeed changing with time. As a result, the calibration parameters have been recomputed at four day intervals. An additional complication was caused by the partial failure of the scalar magnetometer. This magnetometer actually contains two sensors, designated A and B, which can operate either together or singly. Beginning in early December, only sensor A was utilized, except for selected days when both sensors were turned on. The single sensor calibrations differ slightly from the combined sensor calibrations. The reason for this is still under investigation.

Figure 2A-1 illustrates the quality of the results. Calibration parameters were derived utilizing data from November 22, 1979. Those parameters were then utilized to reduce selected data from other days. For each of those days the field magnitude computed from the fluxgate magnetometer was compared to that measured by the cesium magnetometer. The mean rms and maximum difference are plotted. It is apparent that the calibration from November 22 data becomes less accurate as the time of the data differs more and more from November 22. The symbols plotted to indicate maximum differences are A, B or C depending on whether scalar sensor A, B or both were operable. On November 22 both sensors were operating. Examination of the curve for mean differences shows that when only sensor A was operating the mean difference increased. This is indicative of the differences in calibration as a function of the mode of operation of the scalar instrument.

ATTITUDE OF THE VECTOR COMPONENTS

Although the relative alignments of the ATS, sun sensor and star cameras were carefully measured prior to launch, it became apparent that one or more of these shifted during launch and that some shifts were occurring during flight. The Attitude Determination and Control Section at GSFC were able to compute the relative realignments in a very satisfactory manner but there is no information in the attitude data itself to determine the new absolute alignment. To resolve this problem we took advantage of the fact that the spacecraft is rotating relative to the earth and that, therefore, any magnetic field bias caused by an attitude bias which is constant or nearly so, in the spacecraft, or measurement, coordinate system, is rotating with respect to the earth's fixed geomagnetic field. Accordingly, the software for deriving the spherical harmonic representation of the earth's main field was modified to also derive attitude biases. The results were successful to within about 20 arc seconds and were utilized to make the final adjustments necessary for the Magsat fine attitude data.

PROCESSING OF THE DATA

Decommutated data is furnished by the Information Processing Division in three forms:

(1) The magnetometer data on DECOM tape;

(2) Intermediate accuracy attitude data; and

(3) Final accuracy (FINE) attitude data.

We in Code 900 then subject the data to a two-stage preparation process prior to sending it to the investigators. In the first step only intermediate accuracy attitude data is available. The

results of this step are to eliminate most of the spurious data, to verify the times assigned to the data, to eliminate duplicate data and to put the data in an accessible, time ordered, format. In the second step a further check is performed to eliminate outlying (spurious) data points and to apply the fine attitude solution. The data is then forwarded to the National Space Science Data Center for distribution to investigators.

As of this writing (12/15/80), of the 223 days of data acquired, we have processed 180 days through step one and 17 days through step two.

REFERENCES AND PUBLICATIONS

Lancaster, E.R., T. Jennings, M. Morrissey and R.A. Langel, "Magsat Vector Magnetometer Calibration Using Magsat Geomagnetic Field Measurements," GSFC Technical Memorandum 82046, November 1980.

Figure 2A-1

STATISTICS FOR CALIBRATION OF NOVEMBER 22, 1979

2-6
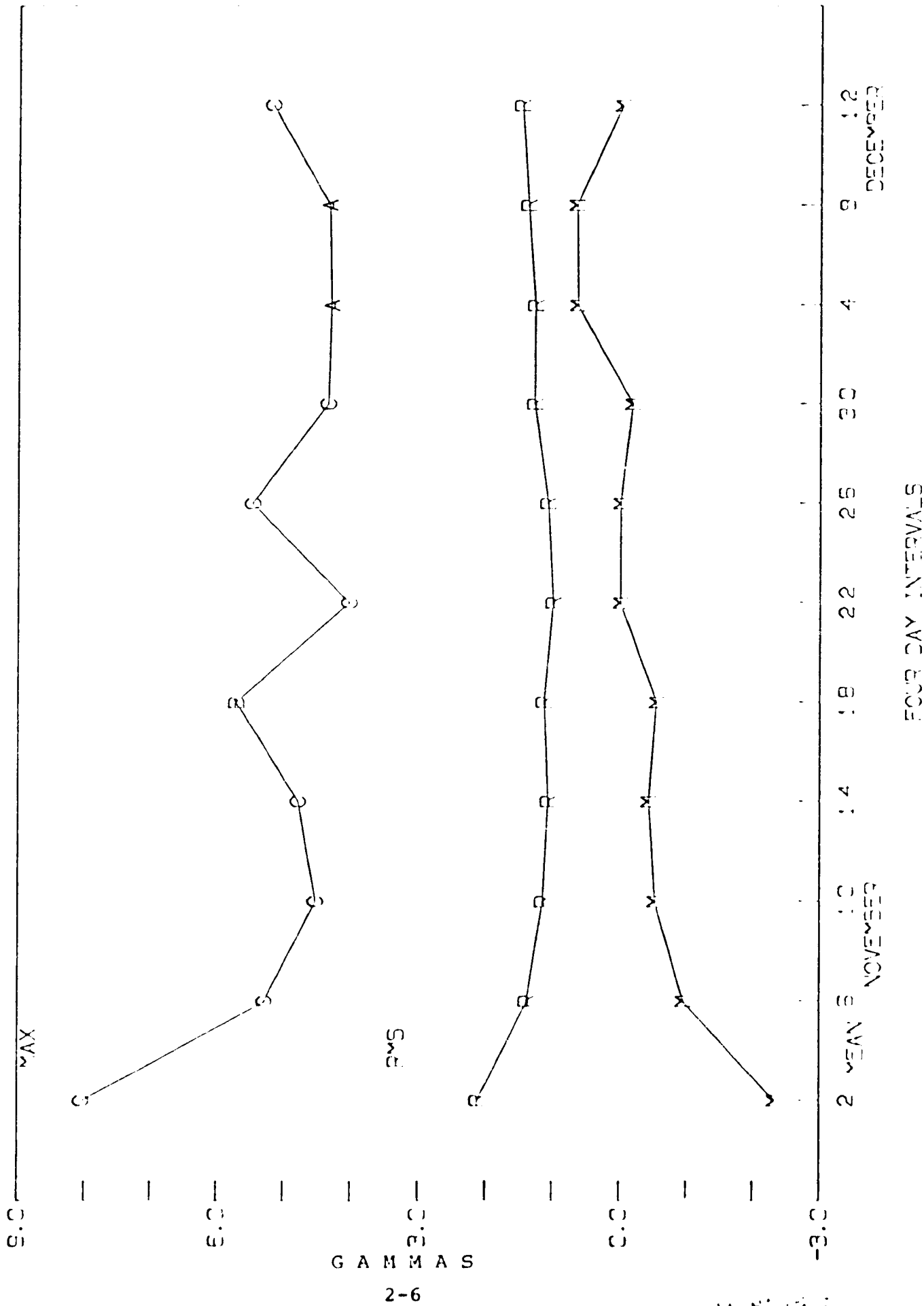
B. SPHERICAL HARMONIC MODELS OF THE CORE FIELD

by

R.A. Langel, G.D. Mead and R.H. Estes

OBJECTIVES

The objectives of developing spherical harmonic models of the
earth's main or core field are to provide a current, accurate
representation of that field and its secular variation for all
applications; to provide a research tool for study of the earth's
deep interior, and to enable background removal of the core field
in the determination of crustal fields.

BACKGROUND

Until Magsat was launched in October 1979, our basic data set
was from the POGO satellites. This has been supplemented by
data from magnetic observatories, repeat stations, shipborne and
aircraft surveys, and land surveys. Magsat successfully acquired
data from November 2, 1979 to June 11, 1980. During past years
GSFC has published a series of models based on the POGO and sur-
face data which have become the standard for the rest of the
scientific community. However, some basic problems in repre-
sentation accuracy still remain, both for the main field and for
its secular variation. These problems include accounting for the
large residuals in the land-based data and the seeming inability
to accurately predict secular variation for any appreciable time
into the future. Some progress was noted in these areas in last
years report and additional progress has been made in 1980.

RECENT ACCOMPLISHMENTS

Magsat Models

With the acquisition of vector data from the Magsat spacecraft
it became possible to derive an accurate up-to-date model of the
main field. The first such derivation, denoted MGST(3/80),
(Langel et al., 1980a) utilized vector data accurate to only 20
arc-minutes but a subsequent model, denoted MGST(6/80), (Langel
et al., 1980b) utilized data accurate to 20 arc-seconds. These
models were of degree and order thirteen and made no attempt to
model the secular variation.

MGST(6/80) is regarded as the most accurate model of its kind ever derived. This model utilized data from November 5-6, 1979 and fit that data with root-mean-square deviations of 8.2, 6.9, 7.6 and 7.4 nT for the scalar magnitude, B_r, B_θ, and B_ϕ, respectively. Table 2B-1 contains the resulting coefficients. The model includes the three first-order coefficients of the external field. Comparison with averaged Dst indicates that zero Dst corresponds with 25 nT of horizontal field from external sources. When compared with earlier models, the earth's dipole moment continues to decrease at a rate of about 26 nT/yr, as shown in Figure 2B-1.

In response to a request from Dr. Edward Benton of the University of Colorado (a Magsat Investigator), we also derived models of degree/order 5, 7, 9, 11, 14 and 17. These will be utilized in trying to pin down accurate low degree and order (i.e., ≤ 8) terms which can be projected to the core/mantle boundary.

Stern and Bredekamp (1975) showed that field models derived from scalar data only (e.g., POGO) are likely to have systematic errors in certain series of spherical harmonics, which they called "Backus" series after George Backus who did the pioneering work leading to the results of Stern and Bredekamp. These systematic coefficient errors have little effect on the scalar field computed from the model but can result in large discrepancies in field direction, i.e., in the component data. Magsat furnished an opportunity to test and demonstrate this effect (Stern et al., 1980). Since MGST(6/80) utilized vector data they systematic errors should not be present. Another model was created utilizing Magsat scalar data only. Examination of the coefficients indeed showed systematic errors of the type predicted by Stern and Bredekamp (1975). Further, a plot of the component differences showed large systematic errors in the model derived only from scalar data. Figure 2B-2 shows these errors in the vertical component.

Models with Magsat and Pre-Magsat Data

Utilizing software changes reported last year together with the correlative data reported last year, preliminary models for the epoch 1960-1980 have been developed. These models incorporate our latest efforts in attempting to understand and represent the secular variation.

The data utilized includes: (1) Magsat data from November 5-6, 1979; (2) our standard selection of POGO data; (3) data from 167 magnetic observatories selected for best geographic coverage; (4) selected repeat station data in derivative form; (5) marine magnetic data selected from regions where other surface data are sparse. The marine data were low-pass filtered to minimize the contribution of crustal anomalies. Aeromagnetic data were not used because we are encountering difficulty in assessing its accuracy.

Last year we reported on a new technique intended to account for the presence of crustal anomaly fields in the observatory data. Such fields can be substantial, tens to hundreds of gammas, and almost certainly are the cause of the high residuals of observatory data to past field models. The following excerpt from last years report summarizes this technique:

"Annual means from a world-wide network of magnetic observatories represent the most useful data set for determining the secular variation of the internal field. The incorporation of annual means data into a main internal core field model for a particular epoch, however, suffers from the fact that the magnetic field measured at the observatory is the vector sum of the main internal field and a contribution due to local crustal magnetization,

$$\bar{B} = \bar{B}_i + \bar{B}_c$$

where $\bar{B}_c$ may change appreciably over the distance of a few kilometers. While $\bar{B}_i$ varies with time, however, $\bar{B}_c$ remains constant. Thus models of secular variation based on time derivatives of annual means observations, i.e.,

$$\dot{\bar{B}} = \dot{\bar{B}}_i$$

are not influenced by the local anomalous field.

GSFC has developed a field modeling technique which solves for the main internal field and its secular variation simultaneously, using both annual means and other data types (satellite, marine, airborne, survey). The annual means data is accommodated by solving for the local observatory bias, $\bar{B}_c$, at each observatory. This allows the data to properly distribute its influence among the secular variation and constant parameters of the model in a least squares sense. The local biases, $\bar{B}_c$, which are estimated along with the field model, provide some physical measure of the local anomaly field."

Availability of Magsat data has enhanced the solution for observatory "anomaly" field by providing an independent vector data set at an altitude where the effects of such fields are small. Table 2B-2 summarizes the "anomalies" found at various observatories utilizing this technique.

In order to represent the secular variation of the earth's field the solution often includes not only the spherical harmonic coefficients but also their first and, sometimes, second derivatives. A problem then encountered is that the representation of secular variation rapidly deteriorates outside the time interval of the data. This deterioration increases in severity as the derivatives used increases from first to second. We found, however, that, when the solution for observatory "anomalies" is included, the secular variation does not deteriorate nearly as rapidly. Furthermore, when third time derivatives were included the predictive capability was improved rather than made worse. This is illustrated by two field models of degree and order thirteen in constant and first derivative terms, five in second derivative terms and four in third derivative terms. Both of these models were derived utilizing data from the POGO spacecraft and data from 167 magnetic observatories. However, model A included solution for the observatory anomalies whereas model B did not. The observatory data utilized extended through 1977 for most observatories with a small amount of data in 1978. The predictive capability of these models was compared by computing residuals of Magsat data to each, as shown in Table 2B-3. Clearly model A is the better predictor.

Based on these results it was decided to proceed further with models incorporating station anomaly solutions and third derivatives of the spherical harmonic coefficients. As of now we have not suffi- cient evidence to determine an optimum degree and order for the spherical harmonic coefficients and their derivatives. Spectral and statistical significance studies of those parameters are now underway. Meanwhile, we have utilized 13th degree and order for the constant and first derivative terms, sixth degree and order for the second derivative terms and fifth degree and order for the third derivative terms. Two such models were derived. PMAG(7/80) utilized observatory, repeat, POGO and selected marine data from 1960 through 1980. This model is regarded as our "best pre-Magsat" model. GSFC(9/80) results from the addition of Magsat data to the data utilized in PMAG(7/80). Table 2B-4 summarizes the statistics relevant to these models and, for comparison, the recently published (Barker and Barraclough, 1980) model used in the British and U.S. Naval 1980 World Magnetic Charts, WC80, the model (Peddie and Fabiano, 1976) utilized in the USGS 1975 world charts, and the MGST(6/80) model. From the Table we note:

1. The GSFC(9/80) model represents the Magsat data almost as well as does MGST(6/80) even though GSFC(9/80) is applicable for 20 years while MGST(6/80) is for a single epoch.

2. PMAG(7/80) represents Magsat data substantially better than other pre-Magsat models.

3. Both PMAG(7/80) and GSFC(9/80) represent the POGO data better then either WC80 or ACW75.

It is not really fair to compare the representation of surface data between models since some models include solution for the observatory anomaly fields.

Figure 2B-3 shows how these procedures allow accurate representation of observatory data during the time span of the data utilized in the model. The data plotted is for the observatory at Amberley. The three measured components, yearly averages, are plotted with X, Y, Z symbols. The predicted field from GSFC(9/80), taking the observatory anomaly solution into account, is represented by the numerals 1, 2, 3 connected with solid lines. The solid lines represent the measured field very well for 1960.5-1975.5 but increasingly diverge for years prior to 1960. This is typical for prediction outside the range of data included in the spherical harmonic derivation. For some observatories the divergence is much greater than for Amberley while for some it is not as large. The predictive capability of GSFC(9/80) seems to be acceptable back to about 1955 or 1956, a range of 4-5 years outside the data span of the model.

FUTURE EMPHASIS

It is now necessary to thoroughly evaluate the new technique used in these models. Further, we must develop a quantitative measure for deciding on the proper degree and order of the spherical harmonics and their derivatives. One problem that is apparent is that when using derivatives of the harmonic coefficients, any prediction must eventually diverge because the number of derivatives that can be meaningfully determined is not enough for the series to converge, even asymptotically. Another area which needs attention is the possible inclusion of aeromagnetic data. This will require a thorough evaluation of the quality of the data and the development of a method for removing anomaly fields from the data.

REFERENCES

Barker, F.S. and D.R. Barraclough, "World Magnetic Chart Model for 1980," EÐS Trans. Am. Geophys. Un., 61, 453, 1980.

Langel, R.A., R.H. Estes, G.D. Mead, E.B. Fabiano and E.R. Lancaster, "Initial Geomagnetic Field Model from Magsat," NASA TM 80679, April 1980a.

Langel, R.A., R.H. Estes, G.D. Mead, E.B. Fabiano and E.R. Lancaster, "Initial Geomagnetic Field Model from Magsat Vector Data," Geophys. Res. Lett., 7, 793-796, 1980b.

Peddie, N.W. and E.B. Fabiano, "A Model of the Geomagnetic Field for 1975," J. Geophys. Res., 81, 2359-2542, 1976.

Stern, D.P. and J.H. Bredekamp, "Error Enhancement in Geomagnetic Field Models Derived from a Scalar Data," J. Geophys. Res., 80, 1776-1787, 1975.

Stern, D.P., R.A. Langel and G.D. Mead, "Backus Effect Observed by Magsat," Geophys. Res. Lett., 7, 941-944, 1980.

Table 2B-1

The MGST(6/80) field model. All coefficients in nT.
Mean radius of the Earth = 6371.2
Mean epoch is 1979.85.

INTERNAL COEFFICIENTS

n	m	g_n^m	h_n^m	n	m	g_n^m	h_n^m	n	m	g_n^m	h_n^m
1	0	-29989.6		8	0	18.4		11	5	-0.4	0.6
1	1	-1958.6	5608.1	8	1	6.8	6.9	11	6	-0.3	-0.1
2	0	-1994.8		8	2	-0.1	-17.9	11	7	1.7	-2.4
2	1	3027.2	-2127.3	8	3	-10.8	4.0	11	8	1.8	-0.3
2	2	1661.6	-196.1	8	5	-7.0	-22.3	11	9	-0.6	-1.4
3	0	1279.9		8	5	4.3	9.2	11	10	2.1	-1.6
3	1	-2179.8	-334.4	8	6	2.7	16.1	11	11	3.5	0.6
3	2	1251.4	270.7	8	7	6.3	-13.1	12	0	-1.6	
3	3	833.0	-251.1	8	8	-1.2	-14.8	12	1	0.4	0.6
4	0	938.3		9	0	5.6		12	2	-0.1	0.6
4	1	782.5	211.6	9	1	10.4	-21.1	12	3	-0.1	2.3
4	2	398.4	-256.7	9	2	1.1	15.2	12	4	0.6	-1.5
4	3	-419.2	52.0	9	3	-12.6	8.9	12	5	0.5	0.5
4	4	199.3	-297.6	9	4	9.5	-4.8	12	6	-0.6	0.2
5	0	-217.4		9	5	-3.3	-6.5	12	7	-0.4	-0.4
5	1	357.6	45.2	9	6	-1.3	9.0	12	8	0.1	0.0
5	2	261.0	149.4	9	7	6.8	9.5	12	9	-0.4	0.0
5	3	-73.9	-150.3	9	8	1.4	-5.9	12	10	-0.2	-1.5
5	4	-162.0	-78.1	9	9	-5.1	2.1	12	11	0.7	0.3
5	5	-48.3	91.8	10	0	-3.3		12	12	0.0	0.7
6	0	48.3		10	1	-3.5	1.4	13	0	0.0	
6	1	65.2	-14.5	10	2	2.5	0.4	13	1	-0.5	-0.4
6	2	41.4	93.4	10	3	-5.3	2.6	13	2	0.3	0.4
6	3	-192.2	70.6	10	4	-2.1	5.6	13	3	-0.7	1.6
6	4	3.5	-42.9	10	5	4.6	-4.2	13	4	0.0	0.0
6	5	13.7	-2.4	10	6	3.1	-0.4	13	5	1.2	-0.6
6	6	-107.6	16.9	10	7	0.6	-1.3	13	6	-0.4	-0.1
7	0	71.7		10	8	1.8	3.5	13	7	0.4	0.8
7	1	-59.0	-82.4	10	9	2.8	-0.5	13	8	-0.6	0.2
7	2	1.6	-27.5	10	10	-0.5	-6.2	13	9	0.2	0.8
7	3	20.5	-4.9	11	0	2.4		13	10	0.1	0.5
7	4	-12.6	16.1	11	1	-1.3	0.7	13	11	0.4	-0.1
7	5	0.6	18.1	11	2	-1.9	1.7	13	12	-0.4	0.0
7	6	10.6	-22.9	11	3	2.2	-1.1	13	13	0.0	-0.1
7	7	-2.0	-9.9	11	4	0.1	-2.7				

EXTERNAL COEFFICIENTS

n	m	$\bar{g}_n^m$	$\bar{h}_n^m$
1	0	20.4	
1	1	-0.6	-0.4

TABLE 2B-2:   OBSERVATORY ANOMALIES

STATION	LAT.	LONG.	ALT.	ANOMALY BIAS			BEGINNING TIME	ENDING TIME
				X	Y	Z		
				NORTH	EAST	DOWN		
ADDIS ABABA	9.03	38.76	2.44	489.5	15.1	148.6	1960.5	1970.5
AGINCOURT	43.78	-79.27	0.18	-45.7	175.7	-140.4	1960.5	1969.1
ALERT	82.50	-62.50	0.06	5.7	34.6	-143.2	1961.9	1974.5
ALIBAG	18.64	72.87	0.01	-80.2	463.7	669.0	1960.5	1973.5
ALMA ATA	43.25	76.92	1.30	125.9	42.2	-152.1	1963.5	1976.5
ALMERIA	36.85	-2.46	0.06	-6.0	8.6	22.2	1960.5	1976.5
AMBERLEY	-43.15	172.72	0.04	-44.0	-16.8	70.1	1960.5	1976.5
ANNAMALAINAGAR	11.37	79.68	0.0	219.5	-80.4	-174.6	1960.5	1974.5
APIA	-13.81	-171.78	0.0	-86.9	208.1	-1017.2	1960.5	1976.5
AQUILA	42.38	13.32	0.63	-8.4	42.2	9.5	1960.5	1976.5
ARGENTINE ISLND	-65.24	-64.26	0.01	69.3	-83.5	512.8	1960.5	1967.5
BAKER LAKE	64.33	-96.03	0.04	149.0	-41.9	-103.8	1960.5	1968.5
	64.33	-96.03	0.04	219.4	-109.7	-114.3	1969.5	1976.5
BANGUI	4.44	18.56	0.44	-85.6	42.0	95.0	1960.3	1968.5
	4.44	18.56	0.44	-119.3	36.6	107.3	1969.5	1974.5
BARROW	71.30	-156.75	0.0	23.9	-66.1	-32.0	1960.5	1977.5
BELSK	51.84	20.79	0.18	96.5	153.5	314.0	1960.5	1976.5
BEREZNAYKI	49.82	73.08	0.0	-423.8	14.7	338.9	1965.5	1976.5
BINZA	-4.27	15.37	0.0	-144.4	-118.0	-177.5	1960.5	1966.5
BJORNOYA	74.50	19.20	0.08	-107.6	40.7	37.8	1960.5	1964.5
	74.50	19.20	0.08	-119.9	54.6	2.5	1965.5	1969.5
	74.50	19.20	0.08	-122.1	47.1	28.0	1970.5	1972.5
BOULDER	40.14	-105.24	1.65	-52.5	53.5	-160.3	1964.5	1977.5
BYRD	-80.02	-119.52	1.52	-24.2	37.5	-147.2	1962.5	1968.3
CASTLE ROCK	37.24	-122.13	0.46	-128.6	-16.5	5.7	1970.5	1974.5
CHA PA	22.35	103.83	1.55	-119.6	-90.5	-2.9	1960.5	1975.5
CHAMBON FORET	48.02	2.26	0.15	-79.7	-24.5	119.0	1960.5	1975.5
CHELYUSKIN	77.72	104.28	0.01	-49.7	-95.0	-80.1	1960.5	1976.5
COIMBRA	40.22	-8.42	0.10	-5.4	-22.8	48.0	1960.5	1976.5
COLLEGE	64.86	-147.84	0.09	-17.2	-60.7	-107.3	1960.5	1977.5
DALLAS	32.99	-96.75	0.21	-15.1	23.8	-73.5	1964.5	1974.5
DIKSON	73.55	80.57	0.02	-114.5	-140.0	-278.3	1960.5	1962.5
	73.55	80.57	0.02	-104.5	-147.6	-248.6	1963.5	1976.5
DOMBAS	62.07	9.12	0.66	-93.7	-79.0	-234.8	1960.5	1974.5
DOURBES	50.10	4.59	0.23	-7.7	-16.8	98.4	1960.5	1976.5
DUMONT DURVILLE	-66.66	140.01	0.04	-172.8	-389.2	-2687.6	1960.5	1972.5
	-66.66	140.01	0.04	-1 2.0	-419.3	-2852.9	1973.5	1975.5
DUSHETI	42.09	44.70	0.98	-238.4	4.8	-82.7	1960.5	1976.5
DYMER	50.72	30.30	0.18	-26.6	90.1	117.9	1964.5	1976.5
FORT CHURCHILL	58.77	-94.10	0.04	-140.2	46.8	-255.8	1965.5	1976.5
FREDERICKSBURG	38.21	-77.37	0.07	28.1	-69.7	120.5	1960.5	1977.5
FUQUENE	5.47	-73.74	2.54	14.4	-88.7	215.8	1960.5	1974.5
FURSTNFELDBRUCK	48.17	11.28	0.57	-31.2	-5.9	14.9	1960.5	1976.5
GNANGARA	-31.78	115.95	0.06	-51.0	-127.8	122.5	1960.5	1976.5
GODHAVN	69.24	-53.52	0.01	207.6	-257.3	469.0	1960.5	1973.5
GORNOTAYEZHNAYA	43.68	132.17	0.30	-13.3	-23.5	-37.8	1960.5	1976.5
GREAT WHALE R	55.27	-77.78	0.02	258.3	113.5	-58.9	1966.5	1975.5
GROCKA	44.63	20.77	0.23	-40.0	-48.9	-51.1	1960.5	1976.5
GUAM	13.58	144.87	0.04	174.9	104.3	-2.7	1960.5	1977.5
HALLEY BAY	-75.52	-26.68	0.03	-26.3	400.2	-7.4	1960.5	1966.5
HARTLAND	51.00	-4.48	0.09	-54.6	7.0	64.2	1960.5	1976.5
HEL	54.61	18.81	0.0	31.8	-157.2	-73.6	1960.5	1968.5
HERMANUS	-34.42	19.22	0.03	-17.6	24.0	-5.7	1960.5	1975.5
HONOLULU	21.32	-158.00	0.0	-174.4	112.9	-304.6	1961.5	1977.5
HUANCAYO	-12.04	-75.34	3.31	90.3	48.5	246.8	1960.5	1976.5
HYDERABAD	17.41	78.55	0.50	352.2	109.6	457.0	1965.5	1976.5

2-14

STATION	LAT.	LONG.	ALT.	ANOMALY BIAS			BEGINNING TIME	ENDING TIME
				X NORTH	Y EAST	Z DOWN		
ISTANBL KNDILLI	41.06	29.06	0.13	171.5	121.7	1.9	1960.5	1975.5
KAKIOKA	36.23	140.19	0.03	-1.5	0.5	-89.8	1960.5	1964.5
	36.23	140.19	0.03	-6.8	3.1	-64.3	1965.5	1976.5
KELES	41.42	69.20	0.45	-215.5	-43.4	-12.4	1960.5	1963.5
KERGUELEN	-49.35	70.20	0.05	177.2	206.1	633.0	1960.5	1975.5
KIEV	50.72	30.30	0.18	-70.4	187.7	129.9	1960.5	1963.5
KLYUCHI	55.03	82.90	0.0	159.1	-88.2	6.3	1967.5	1976.5
KRASNAYA PAKHRA	55.48	37.31	0.20	108.3	-12.8	243.5	1960.5	1976.5
KSARA	33.82	35.89	0.92	-67.1	67.4	-77.7	1960.5	1970.5
LEIRVOGUR	64.18	-21.70	0.01	-299.9	594.9	-482.9	1960.5	1975.5
LERWICK	60.13	-1.18	0.08	-137.3	169.3	37.7	1960.5	1976.5
LOGRONO	42.46	-2.51	0.44	-2.3	0.6	56.4	1960.5	1976.5
LOPARSKOYE	68.25	33.08	0.21	90.1	337.4	-481.6	1961.5	1976.5
LOURENCO MARQES	-25.92	32.58	0.05	328.5	34.2	-159.6	1960.5	1971.5
LOVO	59.35	17.83	0.02	35.2	0.9	7.5	1960.5	1976.5
LUANDA BELAS	-8.92	13.17	0.05	193.0	-6.4	50.0	1960.5	1974.5
LUNPING	25.00	121.17	0.10	16.0	-34.6	79.9	1965.8	1974.5
LVOV	49.90	23.75	0.33	128.9	125.3	153.7	1960.5	1976.5
LWIRO	-2.25	28.80	1.68	246.5	130.7	19.6	1960.5	1970.5
M BOUR	14.39	-16.96	0.01	143.0	-48.4	78.8	1960.5	1971.5
MACQUARIE ISLND	-54.50	158.95	0.0	236.3	-7.3	309.5	1960.5	1976.5
MAGADAN	60.12	151.02	0.0	-1365.2	346.4	1273.7	1960.5	1966.5
MAURITIUS	-20.09	57.55	0.05	475.5	-201.8	-441.5	1960.5	1965.5
MAWSON	-67.60	62.88	0.0	16.7	25.0	197.7	1960.5	1976.5
MEANOOK	54.62	-113.33	0.68	67.9	8.3	-160.3	1960.5	1975.5
MEMAMBETSU	43.91	144.19	0.04	-239.3	133.1	77.2	1960.5	1976.5
MIRNYY	-66.55	93.02	0.02	-135.1	50.2	-428.5	1960.5	1976.5
MISALLAT	29.52	30.89	0.12	-90.1	73.8	123.4	1960.6	1973.5
MOCA	3.34	8.66	1.35	-102.6	1.4	151.6	1960.5	1971.5
MOLODEZHNAYA	-67.67	45.85	0.0	-40.6	-95.5	-207.4	1965.5	1976.5
MOULD BAY	76.20	-119.40	0.15	-22.4	5.0	-40.7	1962.8	1976.5
MUNTINLUPA	14.38	121.01	0.06	-64.2	-183.9	19.1	1960.5	1975.5
NAIROBI	-1.33	36.81	1.67	47.4	62.0	-46.1	1964.5	1976.5
NARSSARSSUAQ	61.10	-45.20	0.0	-373.2	273.1	575.5	1968.9	1973.5
NEWPORT	48.26	-117.12	0.78	-71.3	110.2	-129.2	1966.6	1977.5
NIEMEGK	52.07	12.67	0.08	-41.3	0.1	-68.0	1960.5	1975.5
NOVOLAZAREVSKAY	-70.77	11.83	0.0	-310.9	72.4	194.6	1961.5	1976.5
NURMIJARVI	60.51	24.65	0.11	271.1	-98.3	107.2	1960.5	1975.5
OTTAWA	45.40	-75.55	0.76	104.7	-143.0	184.7	1968.7	1974.5
PANAGYURISHTE	42.52	24.18	0.56	-197.1	-167.7	-182.1	1960.5	1975.5
PARAMARIBO	5.81	-55.22	0.08	-25.1	-32.2	-1.5	1960.5	1974.5
PARATUNKA	52.90	158.43	0.11	-356.5	225.1	271.6	1969.5	1976.5
PATRONY	52.17	104.45	0.54	0.8	46.8	-79.2	1960.5	1976.5
PILAR	-31.67	-63.83	0.34	77.2	-10.6	42.3	1960.8	1974.5
PLAISANCE	-20.43	57.67	0.0	0.0	0.0	790.0	1966.5	1976.5
PLESHENITZI	54.50	27.88	0.20	264.9	166.4	-104.9	1962.5	1967.5
	54.50	27.88	0.20	269.4	148.3	-119.6	1968.5	1976.5
PODKAM TUNGUSKA	61.60	90.00	0.0	28.9	54.2	-293.3	1969.5	1975.5
PORT MORESBY	-9.41	147.15	0.08	-40.2	59.8	163.4	1960.5	1975.5
PRUHONICE	49.99	14.55	0.33	-51.4	25.4	-69.2	1960.5	1971.5
QUETTA	30.19	66.95	1.75	-3.0	52.8	-36.4	1960.5	1967.5
	30.19	66.95	1.75	-11.3	50.7	-54.6	1968.5	1975.5
QUIACA	-22.10	-65.61	3.45	88.5	-54.4	160.9	1960.5	1974.5
RESOLUTE BAY	74.70	-94.90	0.02	36.7	30.1	72.0	1960.5	1975.5
ROBURENT	44.30	7.89	0.82	76.5	48.6	117.7	1964.8	1965.5
	44.30	7.89	0.82	66.0	-56.3	143.9	1966.5	1968.5
	44.30	7.89	0.82	81.3	59.1	89.1	1969.5	1973.5
RUDE SKOV	55.84	12.46	0.05	19.1	-5.5	-33.4	1960.5	1976.5

TABLE 2B-2: OBSERVATORY ANOMALIES (cont'd)

STATION	LAT.	LONG.	ALT.	ANOMALY BIAS			BEGINNING TIME	ENDING TIME
				X	Y	Z		
				NORTH	EAST	DOWN		
SABHAWALA	30.36	77.80	0.68	-15.2	-27.8	63.0	1964.5	1973.5
SAN JUAN	18.38	-66.12	0.10	61.0	33.5	220.6	1960.5	1964.5
	18.12	-66.15	0.40	-139.3	182.0	213.6	1965.5	1977.5
SAN MIGUEL	37.77	-25.65	0.18	684.7	421.2	1711.4	1960.5	1976.5
SANAE	-70.30	-2.37	0.05	-51.4	-19.1	28.6	1962.7	1970.5
	-70.30	-2.37	0.05	-90.7	-72.7	-5.8	1971.7	1975.5
SCOTT BASE	-77.85	166.78	0.0	-2276.1	-936.6	-3766.9	1960.8	1976.5
SIMOSATO	33.58	135.94	0.06	-44.6	29.4	20.9	1960.5	1975.5
SITKA	57.06	-135.33	0.02	-11.6	-14.5	-82.9	1960.5	1977.5
SODANKYLA	67.37	26.63	0.18	-164.6	-104.3	-578.9	1960.5	1975.5
SOUTH POLE	-89.99	-13.32	2.80	-1342.7	-3469.6	79.8	1960.5	1971.5
ST JOHN S	47.59	-52.68	0.0	9.0	26.5	-2.1	1968.8	1976.5
STEKOLINIY	60.12	151.02	0.0	-289.9	-742.5	52.5	1966.5	1976.5
STEPANOVKA	46.78	30.88	0.14	-123.1	-698.5	68.1	1960.5	1976.5
SYOWA BASE	-69.01	39.59	0.0	-24.3	-82.9	-14.7	1960.6	1968.5
TAHITI	-17.57	-149.58	0.0	-633.1	-1078.3	297.7	1966.2	1972.5
	-17.57	-149.58	0.0	-675.8	-691.5	-209.7	1973.5	1973.5
TAMANRASSET	22.79	5.53	1.38	126.4	-208.8	-78.8	1960.5	1970.5
TANANARIVE	-18.92	47.50	1.38	371.9	0.2	-447.3	1960.5	1974.5
TATUOCA	-1.20	-48.51	0.0	31.4	-177.5	89.7	1960.5	1971.5
TEHRAN	35.74	51.38	1.36	-114.1	13.9	-192.2	1960.5	1970.5
TENERIFE	28.48	-16.28	0.31	-470.4	87.5	-1051.2	1960.5	1975.5
TEOLOYUCAN	19.75	-99.18	2.28	-124.0	3.0	-11.9	1960.5	1970.5
	19.75	-99.18	2.28	-67.0	38.1	-98.7	1971.5	1975.5
THULE II	77.48	-69.17	0.06	-55.9	104.9	13.3	1960.5	1973.5
TIHANY	46.90	17.89	0.19	-16.6	-16.6	-27.7	1960.5	1976.5
TIKSI	71.58	129.00	0.04	-112.2	-159.0	-134.0	1960.5	1967.5
	71.58	129.00	0.04	-86.1	-164.1	-86.0	1970.5	1976.5
TOMSK	56.47	84.93	0.11	-21.7	-64.5	-239.8	1960.5	1969.5
TOOLANGI	-37.53	145.47	0.46	-48.9	-22.6	42.6	1960.5	1976.5
TRELEW	-43.25	-65.32	0.03	170.9	5.0	25.8	1960.5	1970.5
TRIVANDRUM	8.48	76.95	0.30	215.3	99.0	79.5	1960.5	1964.5
	8.48	76.95	0.30	255.0	195.2	73.0	1965.5	1974.5
TSUMEB	-19.22	17.70	0.0	-5.9	-60.0	63.0	1964.8	1975.5
TUCSON	32.25	-110.83	0.77	-116.1	-67.1	167.1	1960.5	1977.5
UELEN	66.16	-169.84	0.01	-104.6	25.1	-117.4	1960.5	1976.5
TROMSO	69.66	18.95	0.12	55.5	-402.0	197.6	1960.5	1971.5
ULAN BATOR	47.85	107.05	0.0	-69.2	-17.3	-95.2	1966.5	1975.5
VALENTIA	51.93	-10.25	0.01	118.3	-56.1	25.4	1960.5	1976.5
VANNOVSKAYA	37.95	58.11	0.57	171.5	93.4	58.8	1960.5	1974.5
VASSOURAS	-22.40	-43.65	0.50	44.5	-126.5	-71.9	1960.5	1973.5
VICTORIA	48.52	-123.42	0.18	-17.6	-6.6	-328.2	1960.5	1976.5
VOSTOK	-78.45	106.87	3.50	-17.9	129.6	111.0	1960.5	1976.5
VOYEYKOVO	59.95	30.70	0.07	64.8	23.2	-261.6	1960.5	1976.5
VYSOKAY DUBRAVA	56.73	61.07	0.29	-291.6	-123.5	-521.4	1960.5	1966.5
	56.73	61.07	0.29	-297.5	-112.0	-432.8	1967.5	1976.5
WILKES	-66.25	110.58	0.01	619.2	-296.5	29.4	1960.5	1966.5
WINGST	53.74	9.07	0.05	44.4	46.1	-54.7	1960.5	1976.5
YAKUTSK	62.02	129.72	0.10	40.5	-1184.3	113.7	1960.5	1975.5
YANGI-BAZAR	41.33	69.62	0.81	-301.6	61.0	-96.3	1964.5	1976.5
YUZHNO SAKHALSK	46.95	142.72	0.07	36.0	-165.6	-151.3	1960.5	1969.5
	46.95	142.72	0.07	-84.3	-48.7	116.8	1970.5	1976.5
ZAYMISHCHE	55.83	48.85	0.08	-294.5	-315.7	-240.2	1960.0	1977.0

TABLE 2B-3

| | | MODEL | |
DATE TYPE	STATISTIC	$\underline{A}$	$\underline{B}$
Magsat:			
	rms	88.1	246.0
Scalar	mean	-37.5	41.9
	std. Dev.	79.6	242.4
	rms	72.9	322.9
X-component	mean	-40.2	-7.5
	std. Dev.	60.8	322.8
	rms	56.6	444.3
Y-component	mean	0.6	-3.2
	std. Dev.	56.6	444.3
	rms	96.1	598.9
Z-component	mean	-10.2	8.9
	std. Dev.	95.5	598.8

TABLE 2B-4

MODEL

DATA TYPE	STATISTIC TYPE	MGST(6/80)	AvIC75	WC80	PMAG(7/80)	GSFC(9/80)
Magsat:						
scalar	r.m.s.	8.2	138.9	118.7	82.2	10.1*
	mean	0.1	60.0	-20.6	-2.4	-1.6
	std. dev.	8.2	125.2	116.9	78.5	10.0
X-component	r.m.s.	21.7	93.5	91.6	67.4	22.3
	mean	-1.2	3.8	-21.9	-33.0	-2.2
	std. dev.	21.7	93.4	88.9	58.8	22.1
Y-component	r.m.s.	22.7	88.6	60.6	61.1	23.3
	mean	1.5	1.6	1.1	0.5	1.4
	std. dev.	22.7	88.6	60.5	61.1	23.3
Z-component	r.m.s.	8.2	153.7	125.4	94.0	10.3
	mean	-2.1	-25.3	-31.4	-13.1	-1.7
	std. dev.	7.9	151.6	121.4	92.9	10.1
POGO:						
scalar	r.m.s.	--	69.8	121.6	6.7	6.9
	mean	--	43.8	21.3	37.7	-0.15
	std. dev.	--	54.4	119.8	3.5	6.9
Observatory:						
X-component	r.m.s.	--	285.0	135.7	37.6**	39.9**
	mean	--	-18.0	-1.3	18.7	5.6
	std. dev.	--	284.0	135.7	-0.06	39.6
Y-component	r.m.s.	--	350.0	139.6	18.7	19.3
	mean	--	-42.0	32.3	16.5	0.4
	std. dev.	--	347.0	135.8	-0.05	19.3
Z-component	r.m.s.	--	499.0	219.7	16.5	15.2
	mean	--	-23.0	1.1	26.9	-0.11
	std. dev.	--	498.0	219.7	0.52	15.2

*Magsat residuals to GSFC(9/80-1) were taken including the MGST(6/80) external terms with GSFC(9/80-1) because the Magsat data used to derive GSFC(9/80-1) was corrected for that external field.

**PMAG(7/80) and GSFC(9/80-1) include estimates of observatory "anomalies" which are taken into account when computing residuals.
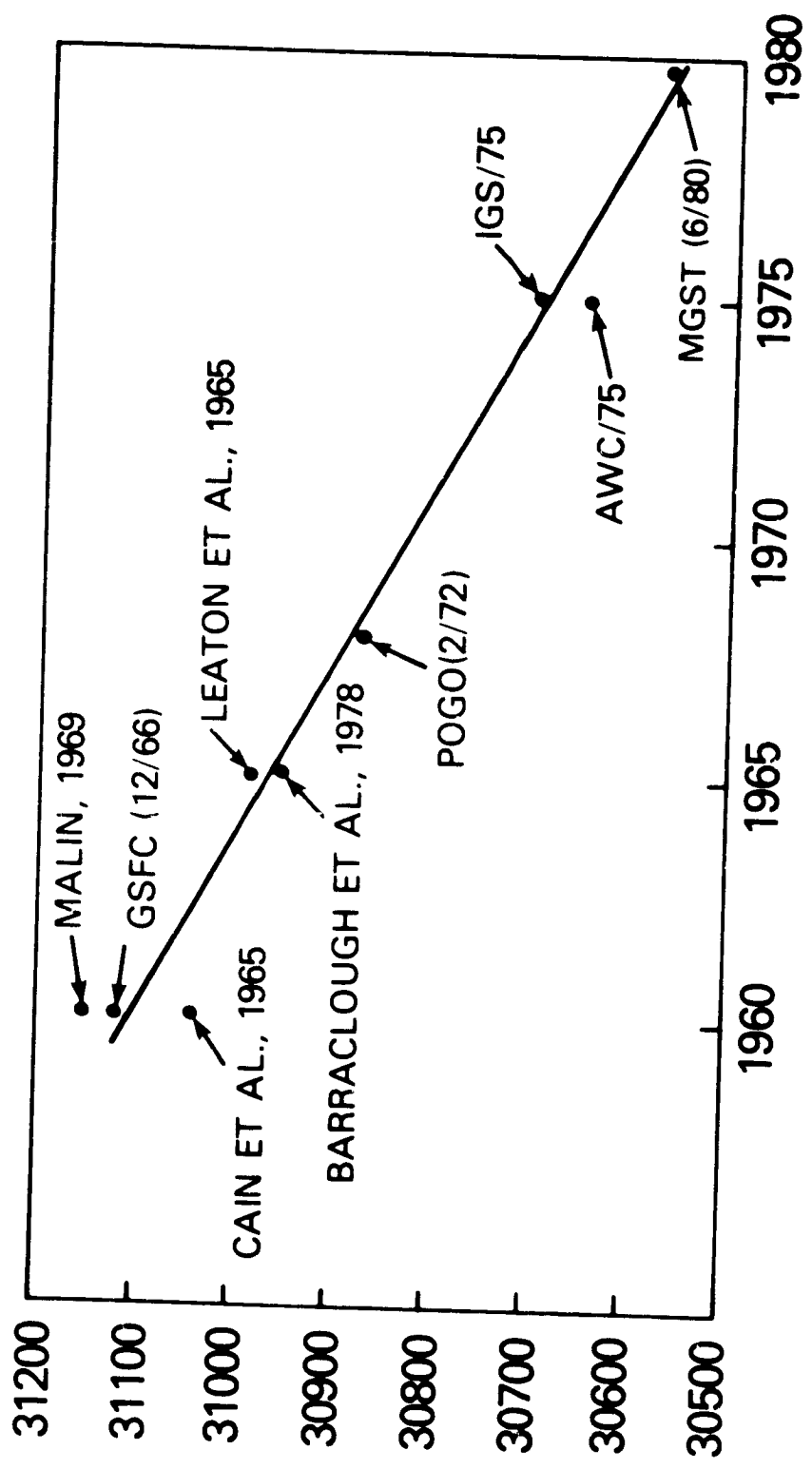
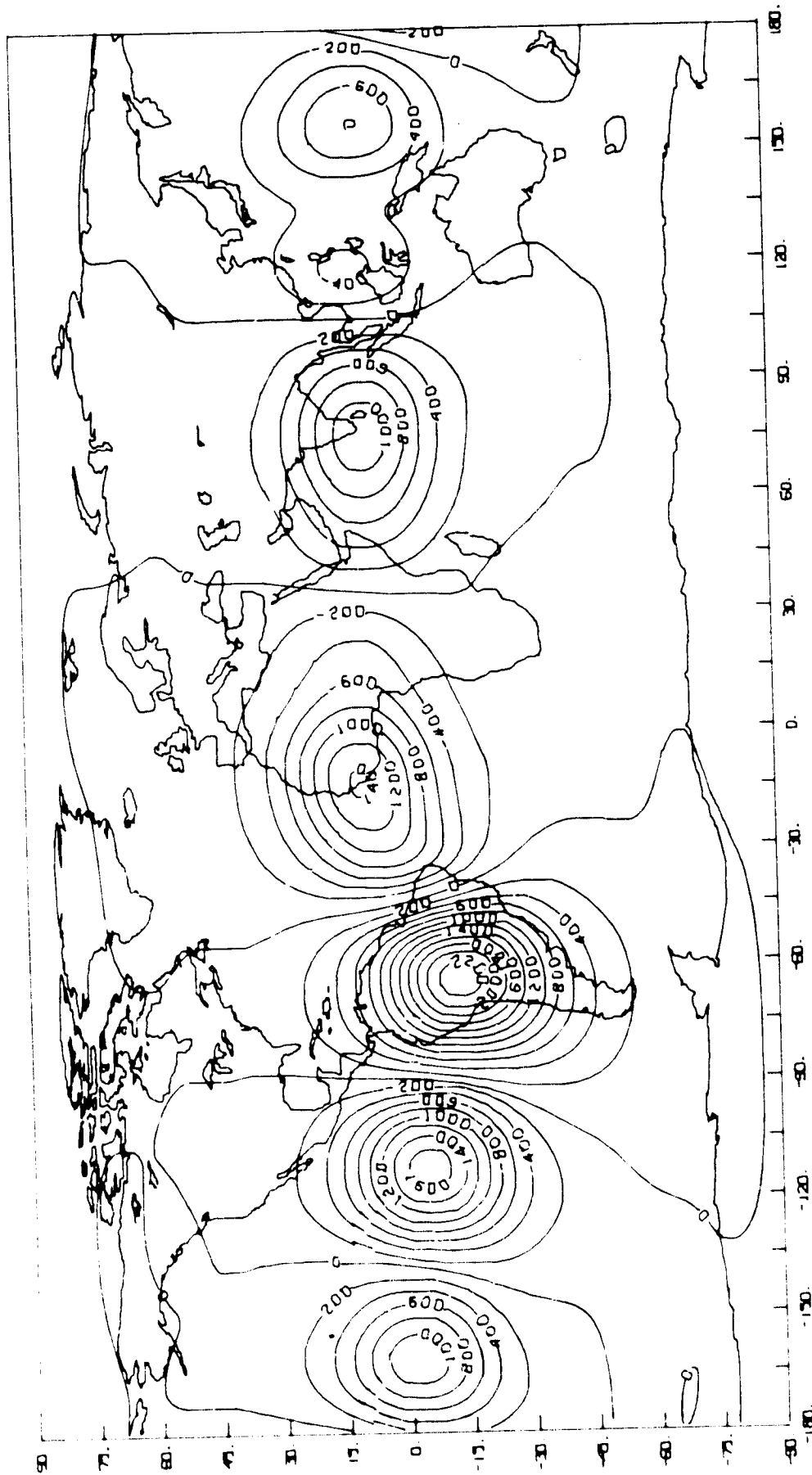STRENGTH OF CENTERED DIPOLE

Figure 2B-1

Figure 2B-2: Difference In Vertical Component Between Two Models Derived From Magsat Data. One Model Utilized Scalar Data Only, The Other Included Vector Data.
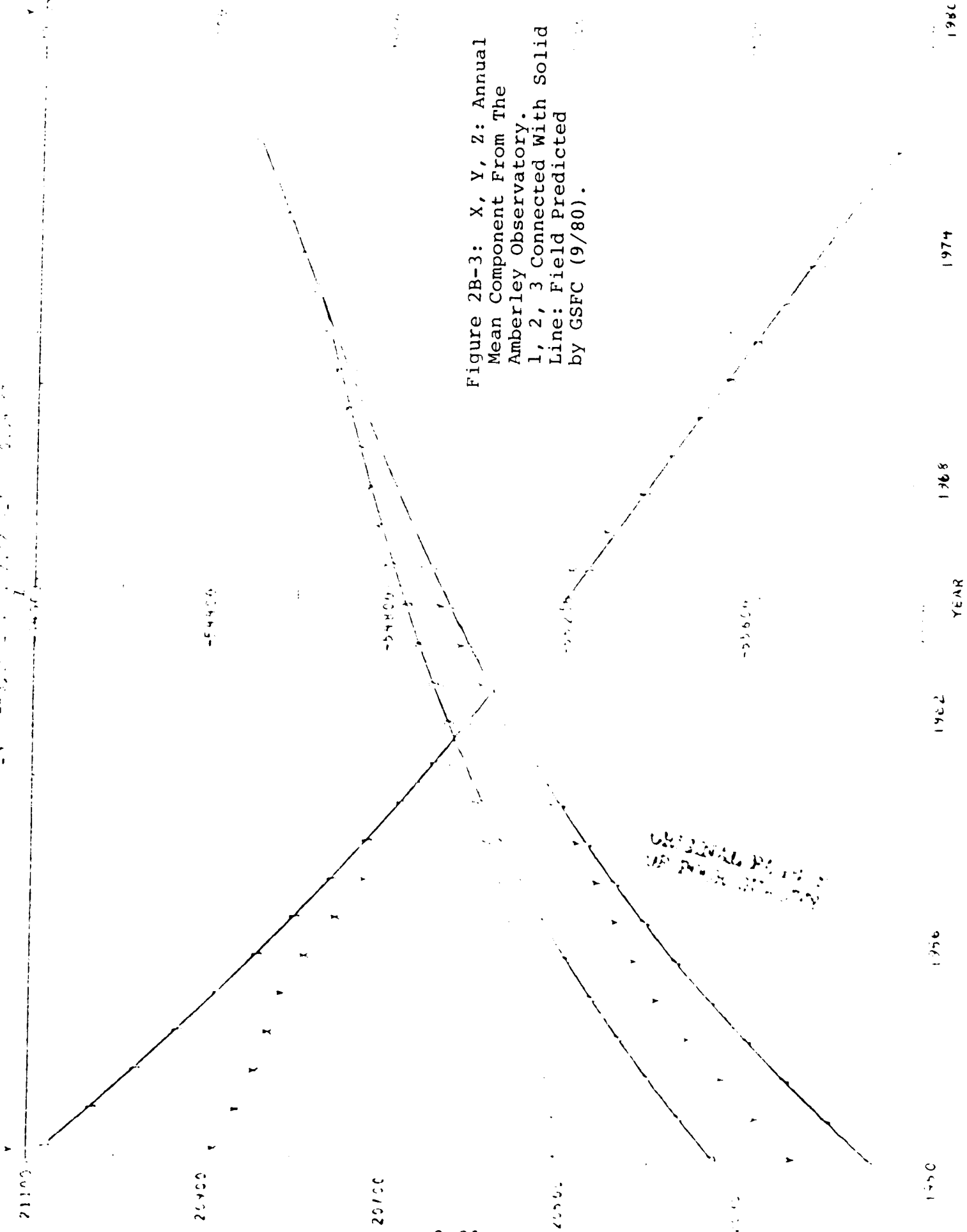
2-20

Figure 2B-3: X, Y, Z: Annual Mean Component From The Amberley Observatory. 1, 2, 3 Connected With Solid Line: Field Predicted by GSFC (9/80).

C. MAGNETIC ANOMALY REPRESENTATION AND INTERPRETATION

by

R.A. Langel

OBJECTIVE

Fields from crustal anomalies are of small magnitude relative to
the main field of the earth and to many magnetospheric fields.
The objective of this effort is to carefully separate the fields
from these three sources in order to isolate the crustal fields
and to represent them in a manner suitable for analysis by geo-
physicists modeling the structure, composition and evolution of
the crust.

BACKGROUND

Anomalous magnetic fields at satellite altitude represent a small
(0-20 nT) field in the presence of larger core (30,000-50,000 nT)
and external (0-1,000 nT) fields. Isolation of the anomaly field
from the core field depends upon the assumption that the geomag-
netic power spectrum can be broken into a longer wavelength portion
from the core and a shorter wavelength portion from the crust
(Cain et al., 1974; McLeod and Coleman, 1980). The core field is
then represented by a spherical harmonic analysis of appropriate
degree and order. This procedure is valid except in the region
where the two contributions are almost equal. This appears to be
at or near degree and order thirteen. Further research is needed
for a more definitive determination of the best degree and order
field model to utilize. External fields at low latitudes, except
for the equatorial electrojet, are also mainly of longer wave-
length than the anomalous fields and their main effects are
filterable. At high latitudes external fields often have the
same spectral characteristics as anomaly fields and are not
easily separated by filtering techniques. Successful techniques
involving visual inspection of all data remaining after an initial
computer screening have been successfully applied to high latitude
data, as reported in the reports of the previous two years. Some
of these results have now been published by Langel et al. (1980).

After the anomaly field has been isolated it is necessary to reduce
it to a constant altitude and at the same time provide a mathemat-
ical representation which can be reproduced at different altitudes
and on different projections. This is accomplished with the equi-
valent source program described two years ago and applied to data
between +50° in last years report.

The application of these techniques to Australia, mentioned in last years report, has now been published (Mayhew et al., 1980).

RECENT ACCOMPLISHMENTS

Equivalent Source Representation

The equivalent source map from POGO data has now been extended to all latitudes. A global map is presented in Figure 2C-1. These contour plots are free from the effects of altitude variations from location to location and have most of the noise filtered out. There is, however, an obvious mismatch of the high and low latitude portions at $+50^{\circ}$ and at -50° latitude. This is because there is an ambiguity in zero level in both data sets which cannot be resolved.

Regional Studies

The effort to model Greenland reported on last year has resulted in the first draft of a paper. This work is cooperative with Dr. Leif Thorning of the Geological Survey of Greenland.

Magsat Results

Sufficient scalar data is now available from Magsat to begin the isolation of magnetic anomalies. As shown in Figures 2C-2 and 2C-3 the early Magsat data verifies the previous POGO results. On these figures the underlying anomaly map is derived from POGO data, the dark line is the sub-satellite track for one orbit of Magsat, and the plot at the top of the figure is the anomalous field from Magsat determined by subtracting a thirteenth degree and order model (MGST(3/80)) from the Magsat scalar data. The corresponding anomalies are numbered for ease of identification. The two data sets are in close agreement.

Utilizing the techniques developed over the past few years with POGO data, we then derived the scalar magnetic anomaly map shown in Figure 2C-4. With only a few exceptions, this map confirms the existence of the major anomalies already known from the POGO data. This is important in view of the fact that the anomaly field is small compared to core and external fields. The detection of near identical anomalies in two independent data sources is a strong indicator of their reality.

Comparison of Figure 2C-4 with the comparable POGO map shows more than agreement, however. The Magsat map shows significantly better resolution. For example, the positive anomaly over the Michigan Basin is now clearly seen and the trend connecting it with the high over Oklahoma shows that the contours of trend on the POGO map were in error.

The data used to derive Figure 2C-4 was from the early portion of the mission. Because the altitudes decreased steadily, future maps will utilize data from lower altitudes. This is expected to substantially improve the resolution. Figure 2C-5 gives an indication of how resolution increases as altitude decreases. The anomaly map is from POGO data. The solid line shows a common track location for OGO-4 and Magsat. The scalar residual fields from the two spacecraft are shown on the right. The OGO-4 altitude was 414-420 km whereas the Magsat data, acquired the day prior to re-entry, are at 187-191 km. Examination of the plots show clearly the existence of anomalous fields in the Magsat data which are only hinted at in the POGO data.

Magsat has also acquired vector data. Analysis of the data is considerably more time consuming than for scalar data and no anomaly maps have been prepared. Figure 2C-6 shows one full orbit of data. The plots are of residuals to a thirteenth degree and order field model. Anomalous fields are clearly present in the scalar data at the top. In the X and Y components, external fields are present as indicated by the fluctuating residuals near the poles. Two anomalies, however, are clearly present in the vector data. In the center of the plot at about 5-10° north latitude is a low in scalar field and a corresponding low in the X and Z components. This is the Bangui or Central African anomaly. Just to the north of Bangui, at about 60°N latitude (at 4:42:39 UT) is another low in scalar field with corresponding lows evident in the X and Z component. This anomaly is over northern Scandanavia.

Thus it is clear that anomalous features will be detectable in the vector data.

FUTURE EMPHASIS

As noted, the joining of the high and low latitude data sets in Figure 2C-2 is not entirely satisfactory. Future work includes selecting an overlapping data set to seek to smoothly join all parts of the map.

The zero level of the data continues to be ambiguous and certain biases are known to exist in the resulting maps. Work is needed to understand more precisely the severity of this problem and to minimize its impact on interpretation of the maps.

The above problem areas apply to Magsat as well as to POGO. In addition, the remainder of the scalar data will be utilized to make a final map, as well as maps of the polar regions, and we will attempt to extend our techniques to the utilization of vector data in the derivation of anomaly maps.

Equivalent source representations will be derived using Magsat data but this will await the completion of selection of the best data and derivation of averaged maps.

REFERENCES AND PUBLICATIONS

Cain, J.C., W.M. Davis and R.D. Regan, "An N=22 Model of the Geo-magnetic Field," abstract, EOS Trans. Am. Geophys. Un., 56, 1108, 1974.

McLeod, M.G. and P.J. Coleman, Jr., "Spatial Power Spectra of the Crustal Geomagnetic Field and Core Geomagnetic Field," Physics of the Earth and Planetary Interiors, 23, 5-19, 1980.

Langel, R.A., R.L. Coles and M.A. Mayhew, "Comparisons of Magnetic Anomalies of Lithospheric Origin Measured by Satellite and Airborne Magnetometers over Western Canada," Can. Jour. Earth Sci., 17, 876-887, 1980.

Mayhew, M.A., B.D. Johnson and R.A. Langel, "An Equivalent Source Model of the Satellite-Altitude Magnetic Anomaly Field over Australia, Earth and Planetary Sci. Lett., 51, 189-198, 1980.
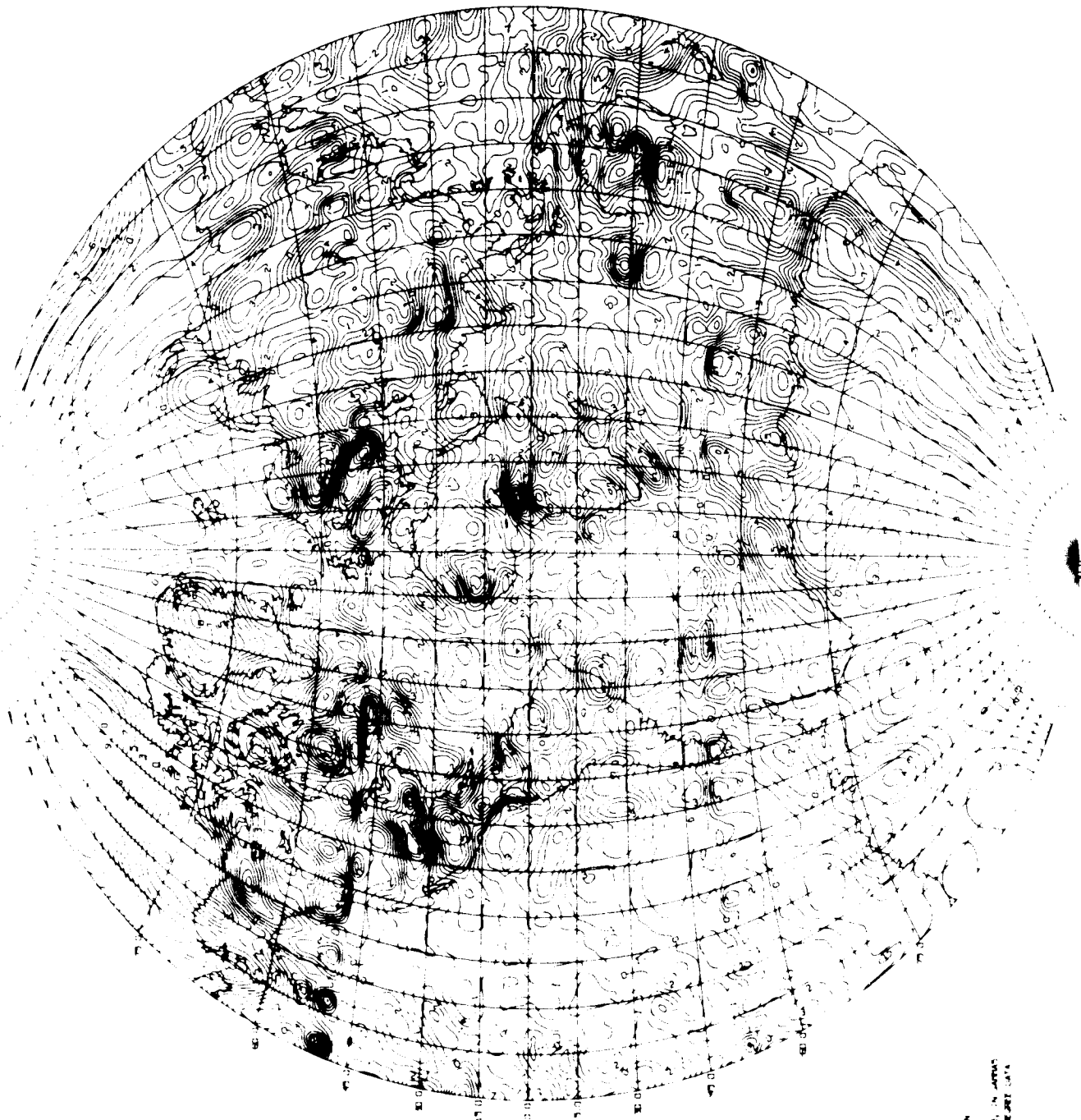
Figure 2C-1: Crustal Anomaly Map Reduced to 500 km Altitude, Derived from POGO Data

2-26

Figure 2C-2: Comparison of Magsat and POGO Anomaly
              Data at Low Latitudes
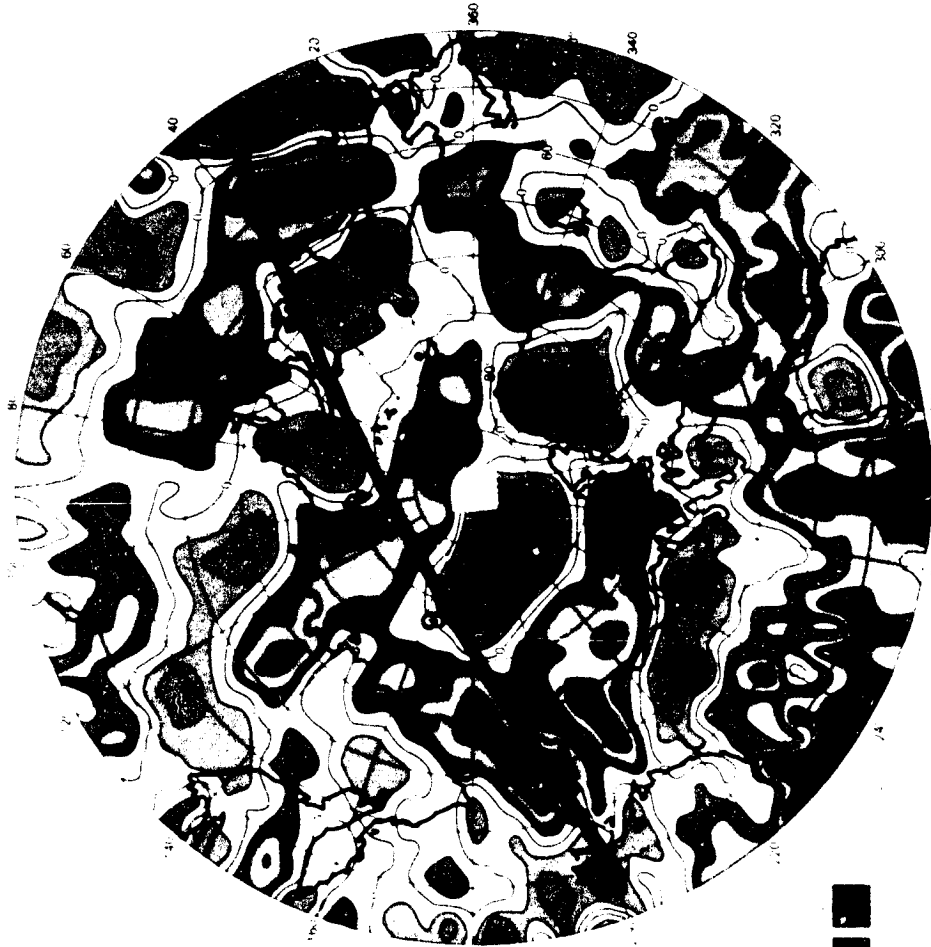
Figure 2C-3: Comparison of Magsat and POGO Anomaly Data at Northern High Latitudes
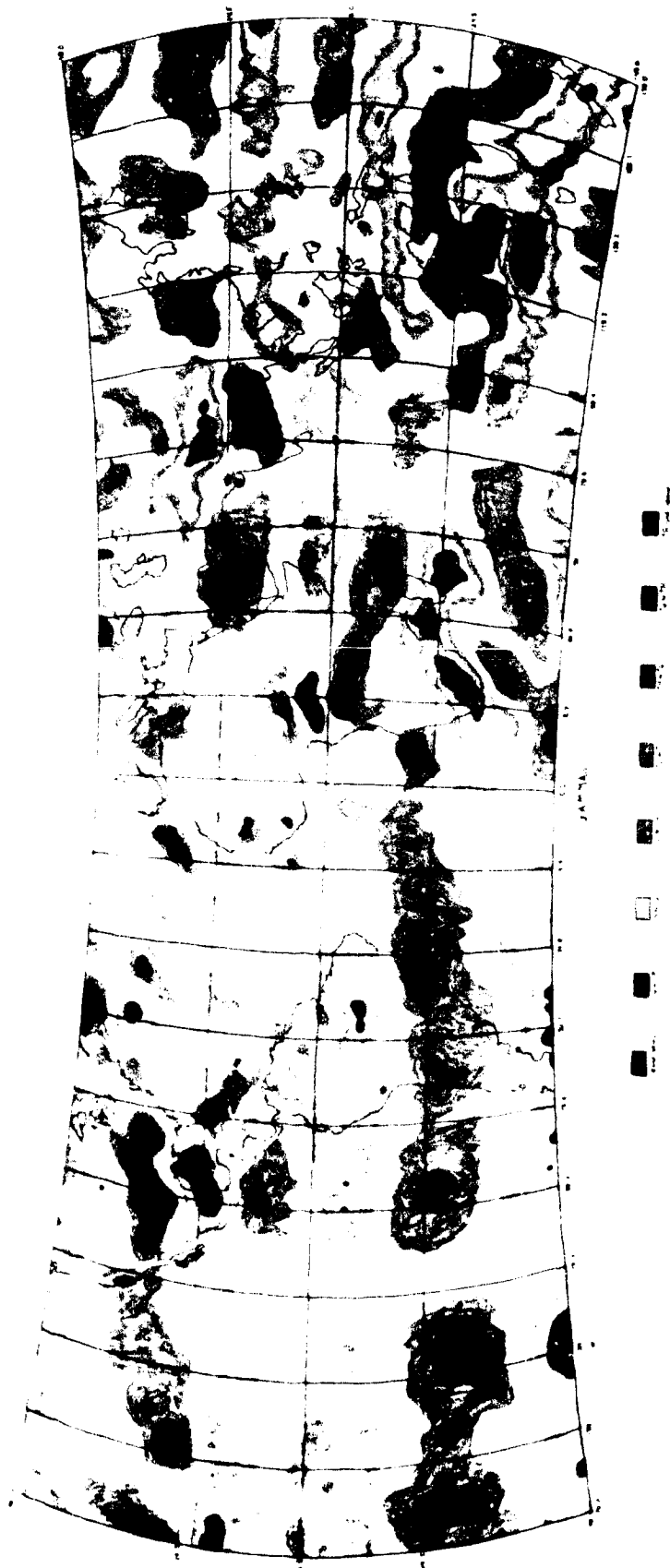
Figure 2C-4: Average Scalar Anomaly Map from Magsat Data

Figure 2C-5

CRUSTAL RESEARCH
ORBITAL POTENTIAL FIELD ANALYSIS
COMPARISON BETWEEN MAGSAT AND POGO DATA

ANOMALY MAP AT 500 KM DERIVED FROM POGO DATA
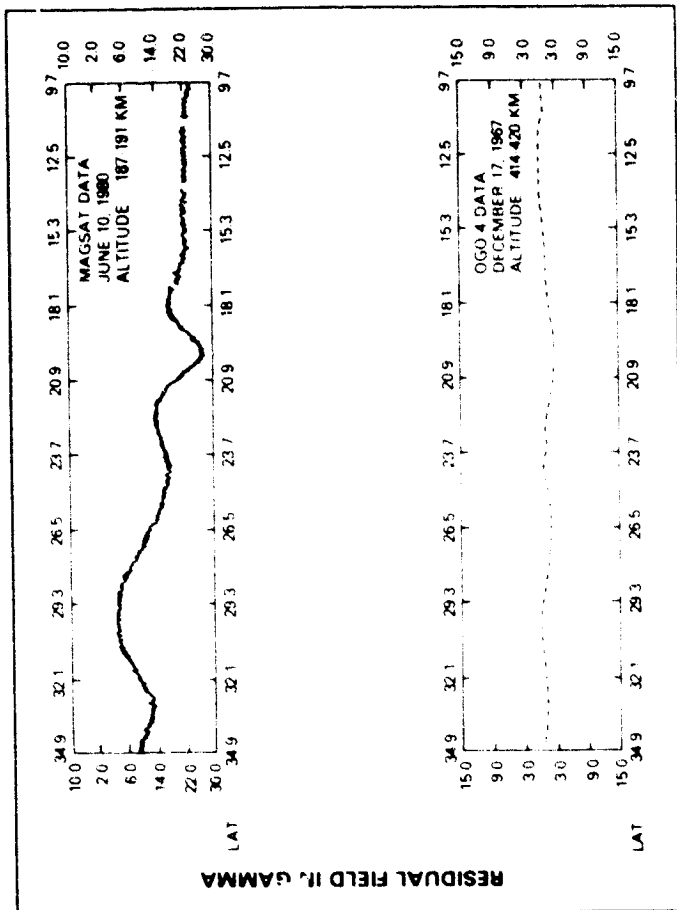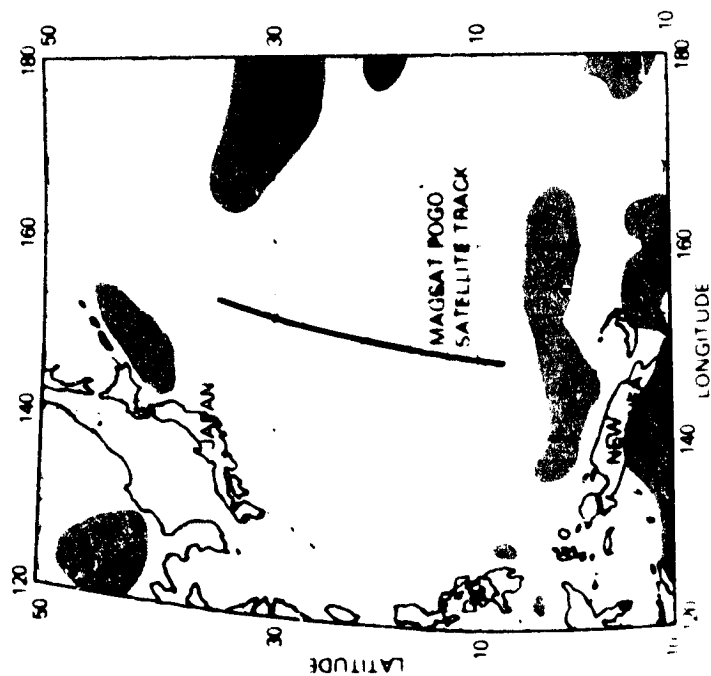
MAGSATS LOWER ALTITUDE MAKES
ANOMALY DETECTION POSSIBLE

Figure 2C-6

MAGSAT LATITUDE PLOT

NOVEMBER 5, 1979

LAT	0.00	60.00	60.00	0.00	60.00	60.00	0.00
TIME	42750	44239	45815	51407	52943	54550
LONG	-169.8	30.3	14.5	-1.7	-161.5	-177.3
ALT	395.8	355.6	425.5	534.0	575.5	508.7

DELTA-B

DELTA-X

DELTA-Y

DELTA-Z

2-31
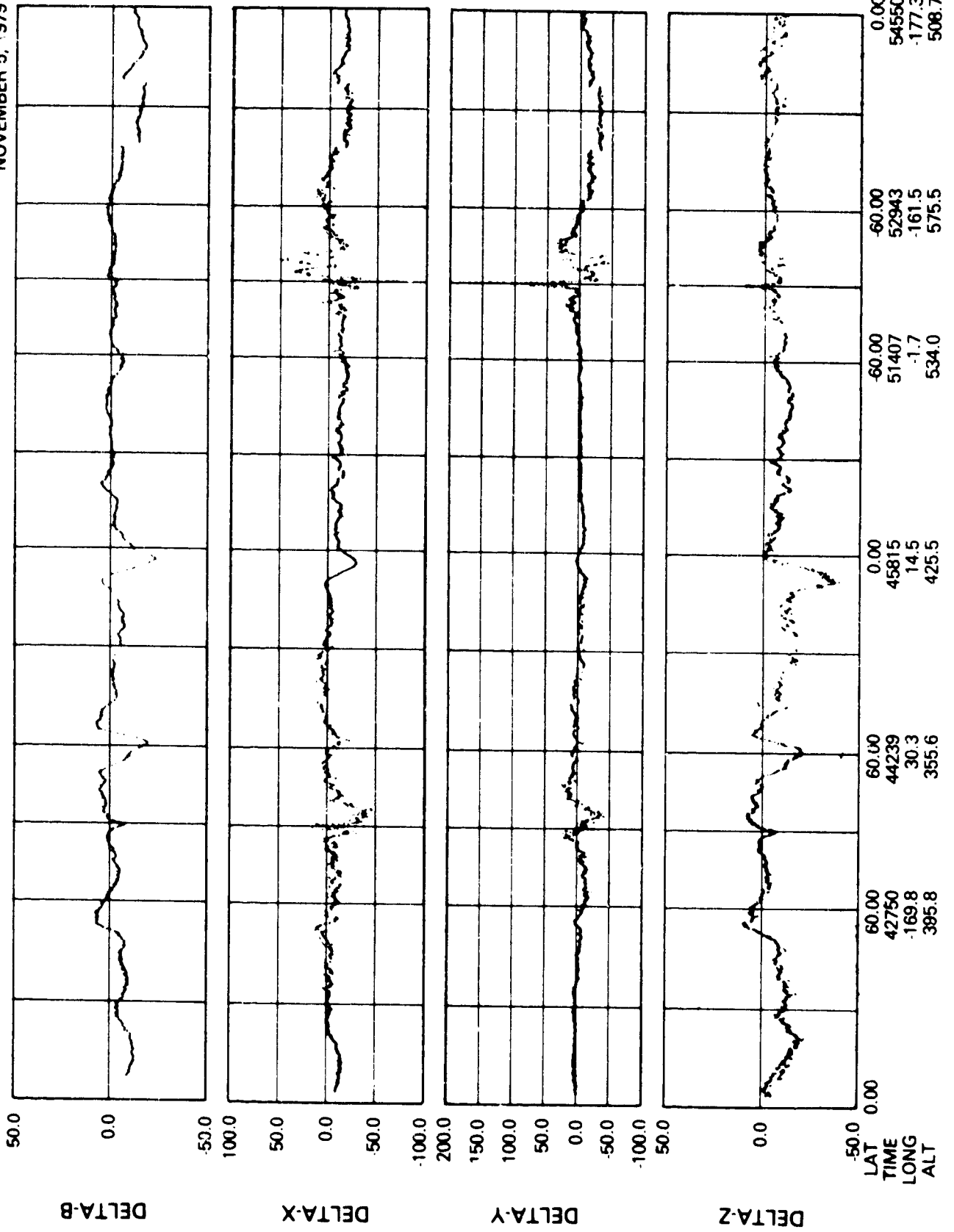
D. PRELIMINARY MODELING OF MAGSAT ANOMALY DATA

by

P.T. Taylor

OBJECTIVES

As part of the Magsat data analysis program an effort is being
made to ascertain the amount and nature of geological informa-
tion encoded in these low-level magnetic component data. After
the initial Magsat profiles became available it was decided to
initiate a preliminary model study over a well documented
geological/geophysical feature.

BACKGROUND

Both aircraft and satellites have recorded the presence of a
large negative magnetic anomaly located in west-central Afric
(Figure 2D-1); geographically this feature covers part of the
Central African Republic and Republic of the Congo. This anomaly
has been named dor the large city situated near its center,
Bangui.

Previous studies of this magnetic anomaly have been carried out
(Regan and Marsh, 1980) using the POGO series of satellites.
Magsat also recorded the Bangui anomaly during its lifetime in
orbit. In order to understand more fully the nature of this
magnetic field anomaly measured by Magsat, we constructed a
relatively simple computer model to represent this feature. The
anomaly model program SPHERE (von Frese et al., 1980) was used in
this effort. The model parameters were selected by using the
Geological Map of the Central African Republic as a guide
(Mestrand, 1964; Figure 2D-1).

The model anomaly profiles were computed at an elevation of
450 km, regional field was 33,000 nT, inclination was -10° (up)
and declination was 8° (west) and a magnetization of 0.01 cgsu
was used; the magnetic field anomaly parameters were computed
by removing the POGO2/72, within SPHERE, from the total field
data. The dimensions of the anomalous body were taken as 1000 km,
777 km and 29.5 km thick at a depth of 0.5 km. The body was tilted
or skewed some 26° counter clockwise off an east-west axis with the
southwest corner acting as a pivot point. The program SPHERE
calculates a two-dimensional anomalous magnetic field for the
following: total field (B; Figure 2D-2; north-south component (X);
east-west component (Y) and vertical component (Z). From these
contoured model anomaly data (Figure 2D-2) profiles were extracted
and compared with the same four components observed during a
Magsat orbit (Figure 2D-3). These observed data were adjusted to
a main field datum which produced the best agreement between
model and profiles. A small change in magnetization of the
body would produce the same effect. In any case, the magnetic

2-32

anomaly-matching procedures are relative, lacking an absolute datum. The main purpose or goal in anomaly-model field matching techniques is to duplicate the shape of the anomaly, the anomaly levels can be adjusted by varying magnetization or field.

RESULTS

With the exception of the east-west (ΔY) component (Figure 2D-3) the match between the model and observations is quite good. The contour map of the anomalous east-west magnetic component (ΔY) indicates the smallest anomalous field variations. The maximum absolute anomaly amplitude variation for ΔY is 20 nT as compared to: ΔX, 32; ΔZ, 32; and ΔB, 27 nT. This surprisingly close agreement could indicate several important geological implications. The main source for this magnetic anomaly is due to induced magnetization and not remanence. If our value of magnetization is correct, then the caustive body could have as much as 5% magnetite (Lindsley et al., 1966). Since the ΔY is the smallest variable field component, small deviations from the model would tend to be amplified. Alternatively, there may be an east-west component of remanence superimposed and nearly opposite in direction with the inducing field.

FUTURE EMPHASIS

In view of the promising results from our initial efforts to model the Bangui anomaly it is likely that other geological structures will be amenable to mathematical representation. At present, an effort is underway to model Magsat data over the Arctic Basin. The primary aspect of this study will be the evaluation of tne Magsat data with regard to potential economic resource.

REFERENCES

Lindsley, D. H., G. E. Andreason and J. R. Balsley, "Magnetic Properties of Rocks and Minerals," in S. P. Clark, ed., Handbook of Physical Constants, Geol. Soc. of America, Memoir 97, 543-553, 1966.

Regan, R. and B. Marsh, "The Bangui Anomaly," in press, 1980.

von Frese, R. R. B., W. J. Hinze, L. W. Braile and A. J. Luca, "Spherical Earth Gravity and Magnetic Anomaly Modeling by Gauss-Legendre Quadrature Integration," Dept. of Geosciences, Purdue Univ., W. Lafayette, IN, 116 p., Prepared under NASA/GSFC Contract NAS 5-25030, 1980.
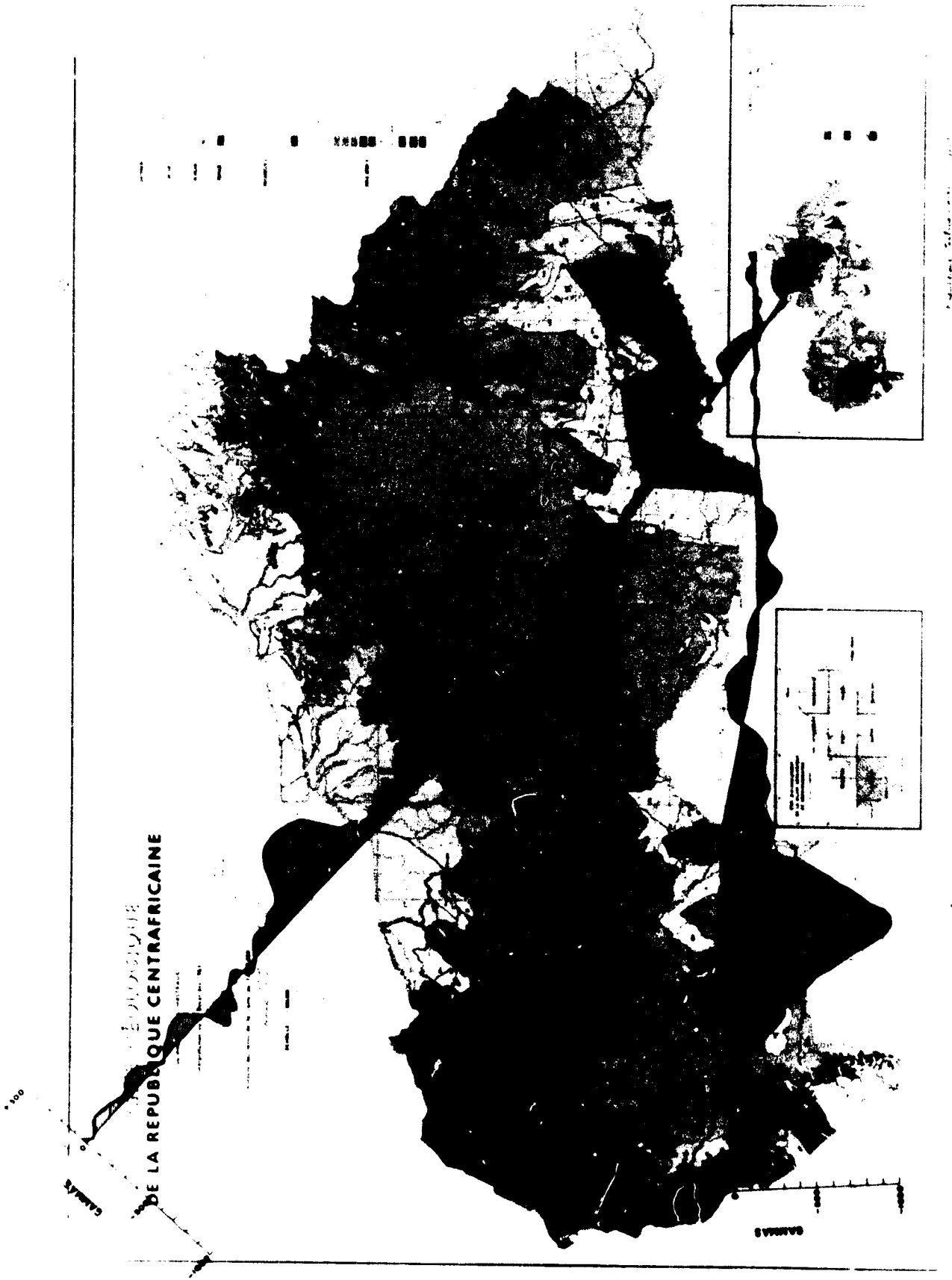
Figure 2D-1: Geological Map of the Central African Republic (Mestrand, 1964) with two project MAGNET aeromagnetic profiles superimposed

2-34
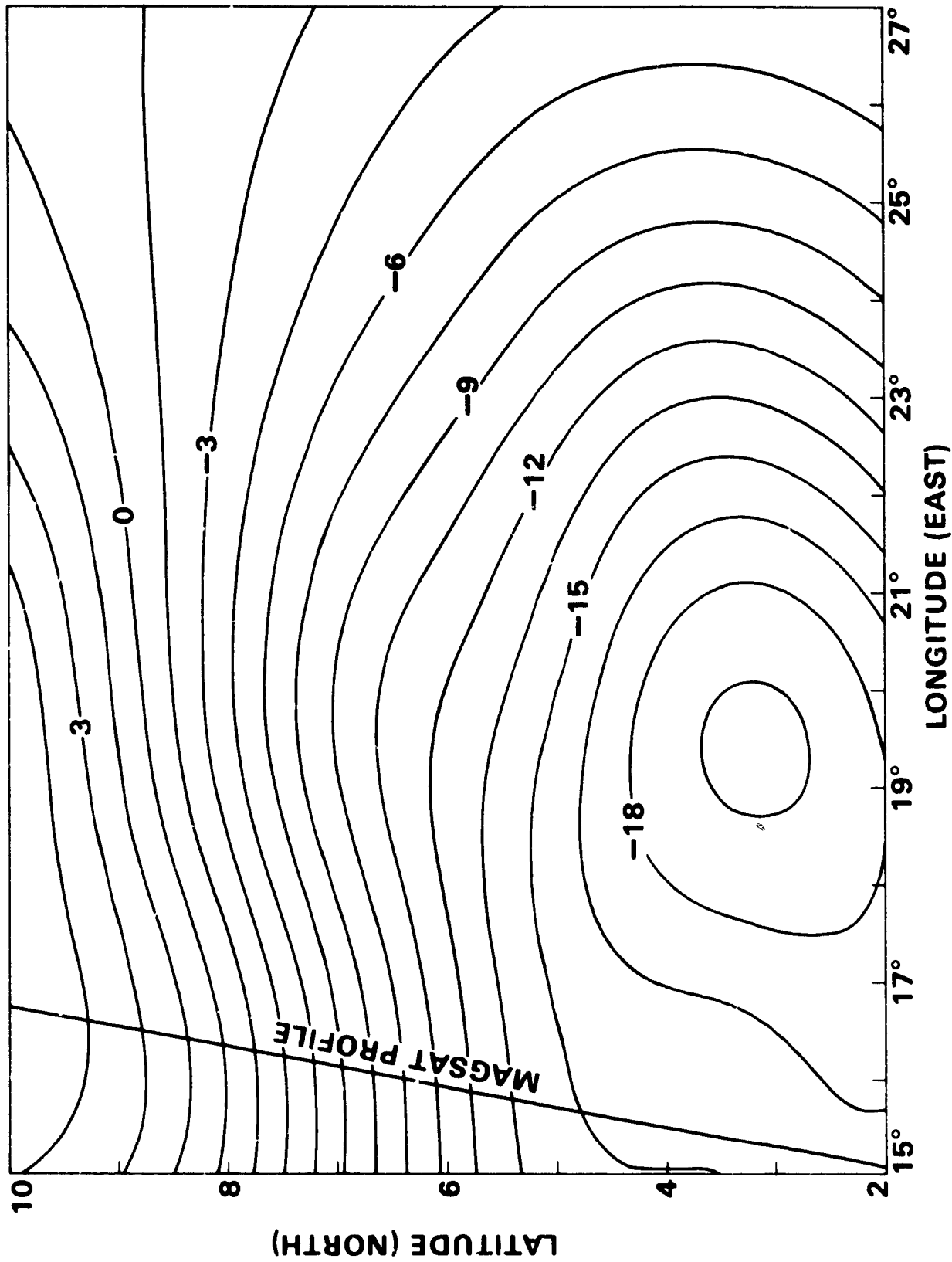
Figure 2D-3: Skewed Prism Model of the Bangui Anomaly for the Total Field Component (B) Computed at 450 km Altitude. Orbit of Magsat Profile is Superimposed on the Field Anomaly.

Figure 2D-3: Plots of Magsat Profile Data (Solid Line) and Profiles from Model Anomalies (Dashed). Amplitude Scale is Relative but Latitude Scale is Constant.

2-36

CHAPTER 3

CRUSTAL STUDIES

edited by

H.H. Thomas

OVERVIEW

Crustal studies using satellite geopotential field data are an aid
to understanding subsurface geology and tectonics. Techniques,
once established for satellite data, will constrain models of the
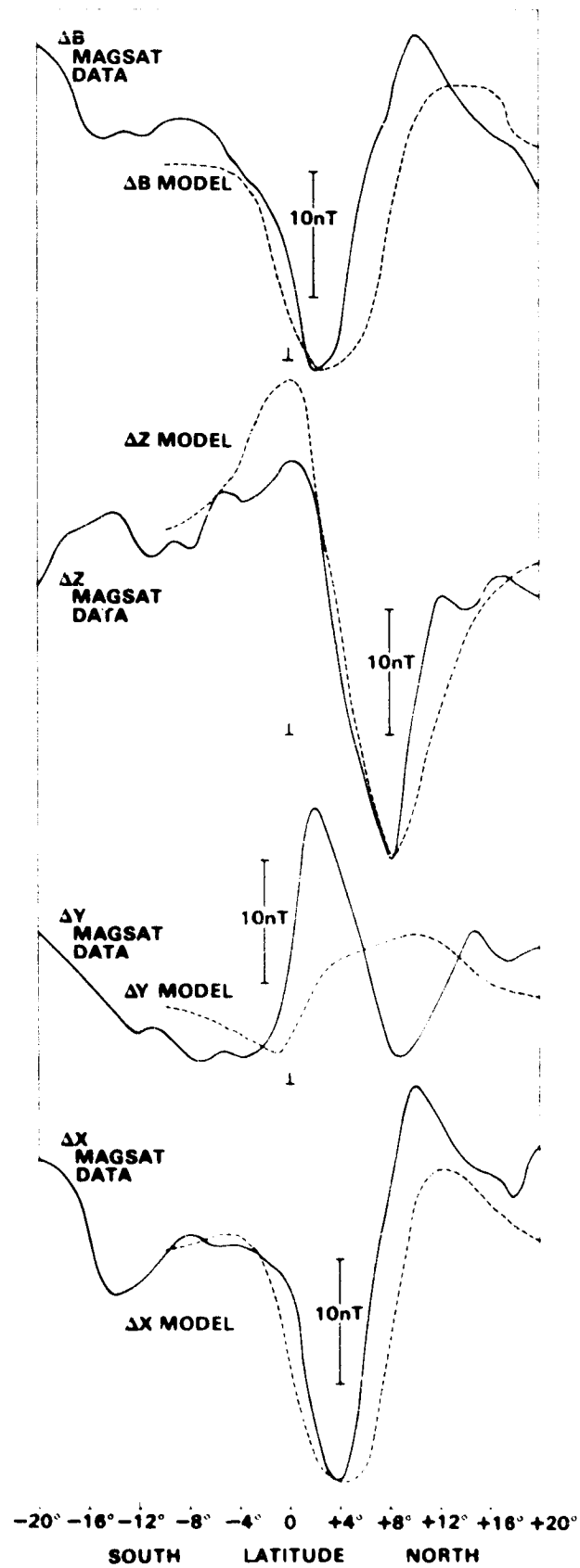evolution and state of the earth's lithosphere as well as provide
compositional data necessary for resource studies.

Geophysical models are generally compromises among several data
inputs; the solutions are normally non-unique, so the greater the
number of constraints the better the model. It is not, however,
feasible to sample the earth's crust in a very fine grid; generali-
zations on the earth's composition and structure are necessary to
study the earth's problems in an expeditious and economic manner.

Comparative planetology approaches have long been the basis for
speculations on the earth's interior and evolution. We are
especially interested in the earth's differentiation and rediffer-
entiations because:

    a. Differentiation of the earth produced the crust, that part
of the solid earth that is most accessible to us.

    b. The crust is generally thought to contain most of the
earth's mineral resources.

    c. Much of our satellite geopotential anomaly data is compatible
with sources in the crust.

Catalogs of terrestrial and extraterrestrial land forms and struc-
tures will eventually give data sets where the effects of varying
planetary size, thermal activity and atmospheric compositions on
tectonic processes can be determined. Comparisons between terres-
trial and martian pseudocraters are examples of data which give
information on volatiles and volcanics of terrestrial planets.

The science of interpretation of satellite potential field data is still very young. Basic information is required on the stability of geopotential anomalies through time and geologic activity. We must ask ourselves to what extent are geopotential anomalies created/destroyed/preserved during major periods of plate tectonic activity.

Crustal thickness (depth to Moho) data are necessary for the interpretation and correlation of magnetization with thickness of the upper and lower crust. Although gravity anomalies are not restricted to the crust, crustal thickness is one of the first parameters to be considered in their modeling. Good correlation between crustal thickness and apparent magnetization contrast is found for the United States.

Comprehensive geophysical modeling of a large satellite magnetic anomaly in Kentucky continues with the analysis of a new Tennessee Valley Authority aeromagnetic survey. Denser flight lines in the survey allow the construction of a three-dimensional geophysical model.

A. COMPARATIVE PLANETOLOGY/CRUSTAL REDIFFERENTIATION

by

Paul D. Lowman, Jr.

OBJECTIVE

To investigate the chemical redifferentiation of the primordial crust of the Earth.

BACKGROUND

Granite or granite gneisses dominate the terrestrial crust in most Precambrian shield areas, to the point that continents are frequently characterized as "granite" in contrast to the basalt of oceanic crust. On the other hand, granite (chemically speaking) is very scarce on the Moon, even if we include the KREEP composition breccias, and apparently equally scarce on Mars. It has been proposed (Lowman, 1976, 1977, 1978) that a major reason for the abundance of granites on Earth is that they result primarily from "redifferentiation" of an originally intermediate composition crust with bulk composition equivalent to andesite (Figures 3A-1, 3A-2). Redifferentiation is probably a composite process, including partial melting, metasomatism, and high-grade metamorphism, whose ultimate result on the Earth has been production of a vertically-zoned crust consisting of granitic rocks in the upper levels and granulites (high-grade metamorphic rocks depleted in water and lithophile elements) in lower levels. Redifferentiation has happened repeatedly in the Earth's continental crust because of the high level of tectonic and igneous activity accompanying the planet's continuing crustal evolution. The Moon, however, essentially stopped evolving about 3 billion years ago with the eruption of the last mare basalts. Mars evolved somewhat further, but did not reach the stage of full plate tectonic activity involving repeated heating and reworking of the crust. The scarcity of granites on the Moon and Mars is thus the result of their arrested crustal development.

Redifferentiation of the Earth's crust is relevant to GSFC programs for several reasons. One is that it has permitted construction of a generalized crustal model with implications for the interpretation of satellite magnetic data, since such interpretation involves assumptions about the lower continental crust. Another is that redifferentiation may be expressed as radiometric age provinces, such as the Grenville province, which could in principle affect

satellite magnetic anomaly patterns since both radiometric ages and magnetic properties of crustal segments can be strongly affected by the thermal events responsible for redifferentiation. Finally, redifferentiation has undoubtedly affected the distribution of metallic mineral deposits, and must thus be considered in planning orbital resource surveys.

RECENT ACCOMPLISHMENTS

As outlined in RTOP 677-45-01, it was proposed to continue studies of redifferentiation by several approaches, including synthesis of data on structure of the continental crust from investigations such as the COCORP seismic reflection profiling, literature searches on the subject of high-grade metamorphism and anatexis, and field studies of critical Precambrian areas. Two areas picked for investigation were the Baltimore gneiss domes, thought to represent upper crust diapiric granites formed by redifferentiation, and the Lewisian rocks of northwest Scotland, thought to represent the residual granulite lower crust. During the summer of 1980, a six-day field reconnaissance was made in the Scourie-Laxford Bridge area of Scotland, with the following results.

The area investigated was part of the Archean foreland northwest of the Moine thrust (Figures 3A-3, 3A-4). This is a rugged but low-lying area of Archean rock exposed along the northwest coast of Scotland (Figure 3A-5) and known, from geophysical evidence, to underlie much of the thrust. The area is well-exposed, both along the coast (Figure 3A-6) and inland, permitting rapid mapping of the gross structure and lithology. Findings of the mapping can be discussed under two headings, with reference to the map: the Scourian complex and the Laxfordian complex.

The Scourian Complex

Rocks of the Scourie area (Figures 3A-6, 3A-7) are strikingly different from those of most Precambrian igneous and metamorphic terrains in several characteristics:

1. There are almost no granites, granite pegmatites, or granite-bearing migmatites.

2. There are very few schists, reflecting a general scarcity of platy minerals (in particular biotite).

3. The rock is relatively undeformed, with few faults.

4. There is little if any mineralization or hydrothermal alteration.

3-4

The Scourian complex in this area was found to consist of about 1000 meters of granulitic gneisses (probably much more, since seismic data show the Moho to be at a depth of 26 km). In detail, the section is made up of interlayered felsic and mafic layers, with felsic rocks about 80% by volume of the total. Major minerals of the felsic rocks are plagioclase, quartz, and pyroxene or amphibole (chiefly pyroxene). The mafic members, generally layers or lenses, include pyroxene, amphibole, and feldspar. Structurally, the Scourian granulites at the type locality are relatively simple, dipping more or less uniformly to the northwest at shallow angles generally less than 35°. Occasional small isoclinal folds, locally referred to as "intrafolial" folds, occur, but the amount of deformation visible in the area covered (essentially a 5 kilometer traverse across strike) is surprisingly slight. It should be mentioned that published literature on the area, such as the papers by Watson (1965), Bowes (1969), and others, make it clear that the lithologic and structural characteristics described above are reasonably typical of the Scourian granulites all along the Scottish coast.

The Laxfordian Complex

The Laxfordian rocks, just northeast of the Scourian complex (Figure 3A-4), contrast with the Scourian in every way. First, they are much more strongly deformed, as indicated by the steeper dips (90° in some places). Secondly, they are lithologically very different (Figure 3A-8), consisting of amphibolites, granitic gneisses, biotite schists, migmatites, and discrete granite intrusions (locally known as the "Laxford granite sheets"). In brief, they are typical of many Precambrian amphibolite facies assemblages.

There is general agreement on the relationships between the Scourian and Laxfordian complexes. The Scourian rocks are granulite facies gneisses, characterized by extremely low water and lithophile element (K, Rb, Na) contents, resulting from the high temperature and pressure of the metamorphism. The Laxfordian rocks, which are lithologically and structurally gradational with the Scourian complex, are widely believed to have been formed by retrograde metamorphism of the Scourian granulites. This retrograde metamorphism, probably accompanying the intrusion of the Laxford granite sheets and many minor granite and granite pegmatite bodies, re-introduced the water and lithophile elements driven out in the granulite facies metamorphism. These events occurred at roughly 2.9 billion years and 1.7 to 2.2 billion years ago, according to radiometric studies.

Comparison with Crustal Models

From the viewpoint of comparative planetology, a major result of this work is the finding that the Scourian complex closely matches the generalized model for the lower crust proposed by Lowman (1976): ".....the metamorphic equivalents (probably granulite facies) of.... a complexly interlayered series of andesites and subordinate basalts, locally intruded by coeval diorites and granodiorites." The lower crust in this model "would be depleted in alkalis and SiO_2, so that an average composition of around 55% SiO_2 would be expected."

The pre-metamorphic nature of the Scourian rocks is not agreed upon completely, but the consensus is that they were formed by granulite facies metamorphism of pyroclastic rocks of andesitic composition, with some basalt. The work of Sheraton (1970) provides the strongest support for this concept; he analyzed some 254 granulites from an area just south of Scourie, finding an average SiO_2 content of 61%. The Scourian rocks thus closely resemble the lower crust in Lowman's model, and the high temperatures and pressures involved in their metamorphism are of course independent evidence that they were at one time deep in the continental crust.

From the viewpoint of crustal modeling, the Scourian and Laxfordian complexes are of interest because they correspond closely to a generalized crustal model proposed by Smithson (1978) on the basis of COCORP reflection profiling in North America and other evidence. Smithson proposed that the lower continental crust in non-orogenic areas consists of intermediate composition metamorphic rocks, with low dips, of supracrustal origin. This model is strikingly similar in composition, structure, and probable pre-metamorphic lithology, to the Scourian granulite gneisses (Figure 3A-9). Smithson further proposed that the upper crust (in crystalline terrains) consists largely of amphibolite facies gneisses, migmatites, and schists, strongly deformed by the intrusion of granites. This description is similar to that of the Laxfordian complex, although these rocks are obviously now at the same crustal level as the Scourian granu-lites. In general, it is safe to say that the geology of the Scourie-Laxford Bridge area suggests that Smithson's model may be valid for large areas of continental crust.

A preliminary review of the recent literature on the nature of the lower continental crust indicates that the models proposed by Smithson and by Lowman resemble those of other authors (e.g., Mueller, 1977). The features of several such models have therefore been combined in a preliminary composite cross section (Figure 3A-10) for non-orogenic continental crust in granite-greenstone terranes. This proposed model differs sharply from the formerly popular view

that continental crust had two major layers, an upper granitic one and a lower gabbroic or amphibolitic one. The new model consists instead of a thick sequence of originally supracrustal metamorphic rocks of intermediate SiO_2 content, except for the very base of the crust where the abundance of mafic rocks increases considerably. Its vertically-zoned composition is largely the result of redifferentiation, which has depleted the lower crust in water and lithophile elements during the generation of granite magmas and diapiric intrusions that intruded the upper crust.

SIGNIFICANCE

The Archean rocks of the Scourie-Laxford Bridge area were clearly once part of the lower continental crust, now uplifted and exposed. These rocks have been shown to resemble, in structure, composition, and pre-metamorphic orgin, models of the lower continental crust derived independently from comparative planetology and reflection seismology, thus giving strong support to such models. Scientifically, part of the significance of this finding is that these crustal models appear to contradict formation of continental crust by lateral accretion of eugeosynclines. Such an origin would result in highly deformed rocks intruded by granitic batholiths, quite different from the Scourie complex. Geophysically, results of this study imply that models for the lower crust involve dry, intermediate composition rocks of granulite facies, rather than the amphibolites or gabbros formerly popular.

FUTURE EMPHASIS

The data from Scourie are still under study; future investigations should include petrographic analysis and measurement of various geophysical parameters. Further field studies should be made of granulites in North America to see if they resemble those of Scotland. Alternate funding must be sought, since a proposal to carry out investigations of this sort was rejected by NASA Headquarters.
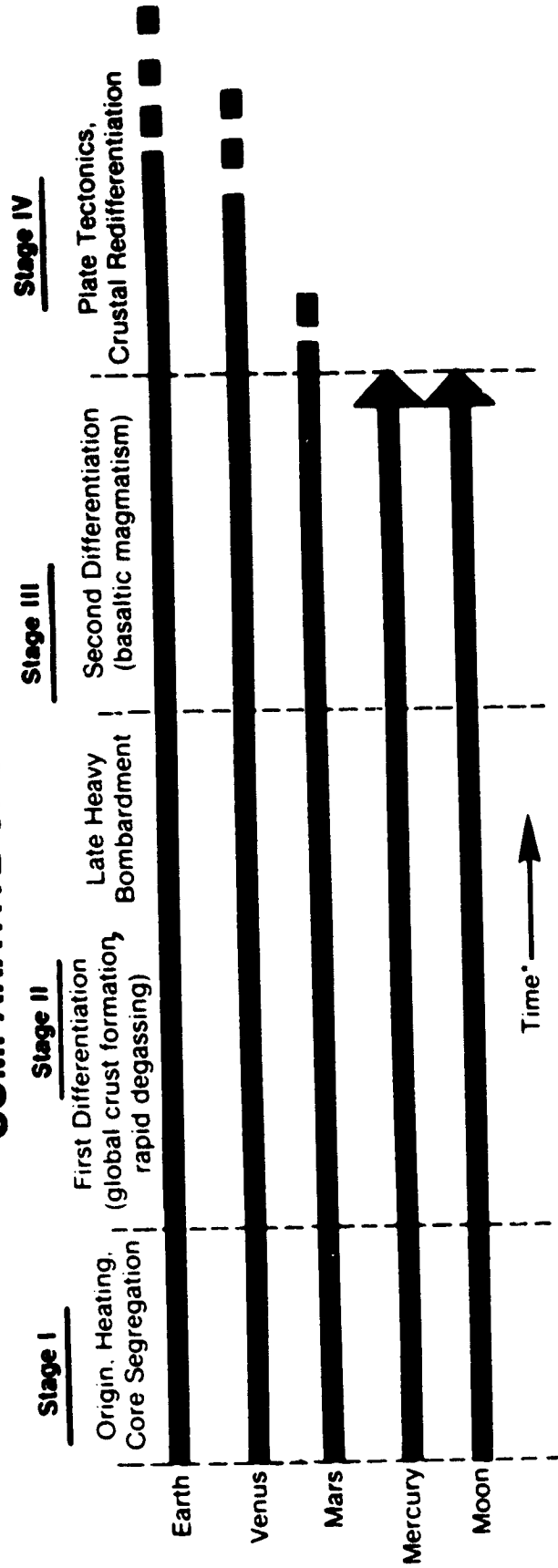
REFERENCES

Bowes, D. R., The Lewisian of Northwest Highlands of Scotland, in North Atlantic: Geology and Continental Drift, Am. Assoc. Pet. Geology. Memoir 12, 1082 p.

Lowman, P. D., Jr., Crustal Evolution in Silicate Planets: Implicacations for the Origin of Continents, J. Geology, 84, 1-26, 1976.

Lowman, P. D., Jr., Comparative Planetology and the Origin of Continents, in Comparative Planetology, C. Ponnamperuma, ed., Academic Press, New York, 275 p., 1977.

Lowman, P. D., Jr., Crustal Evolution in Silicate Planets, Naturwissenschaften, 65, 117-124, 1978.

Mueller, S., A New Model of the Continental Crust, in The Earth's Crust, J. G. Heacock, ed., Am. Geophys. Union, Washington, DC, 754 p., 1977.

Sheraton, J. W., The Origin of the Lewisian Gneisses of Northwest Scotland, with Particular Reference to the Drumbeg Area, Sutherland, Earth. Planet. Sci. Lett., 8, 301-310, 1970.

Smithson, S. B., Modeling Continental Crust: Structural and Chemical Constraints, Geophys. Res. Lett., 5, 749-752, 1978.

Watson, J., Lewisian, Chap. 2 in The Geology of Scotland, G. Y. Crag, ed., Archon Books, Hambden, Connecticut, 556 p., 1965.

Figure 3A-1: Diagram Showing Comparative Stages of Crustal Evolution in Silicate Planets; Note "Crustal Redifferentiation" in Stage IV (from Lowman, 1978).

PETROLOGIC EVOLUTION OF CONTINENTAL CRUST

PROCESSES

Sedimentation, Metamorphism,
Mantle-derived Vulcanism

Redifferentiation
a) Consuming plate boundary
b) Continental/plate interiors

Beginning of Plate Tectonic Processes
(~3 – 2.5 b.y.)
ago

Second Differentiation
(4 – 3 ? b.y.)

Impact Fracturing
(~4 b.y.)
ago

First Differentiation
(4.6 – ~4 b.y.)

Origin of Earth
(4.6 b.y.)
ago

TIME

ROCKS

Phanerozoic supracrustal rocks
(sedimentary, metamorphic, igneous)

a) Orogenic Batholiths, Volcanoes
(granites, granodiorites, diorites,
gabbros, plus volcanic equivalents)

b) Diapiric Remobilization Intrusions
(granite gneiss, sodic anorthosites,
residual granulites in lower crust)

Basic, Ultrabasic Rocks
(basalts, komatiites)

Global Intermediate Crust
(andesites, calcic anorthosites, basalts)
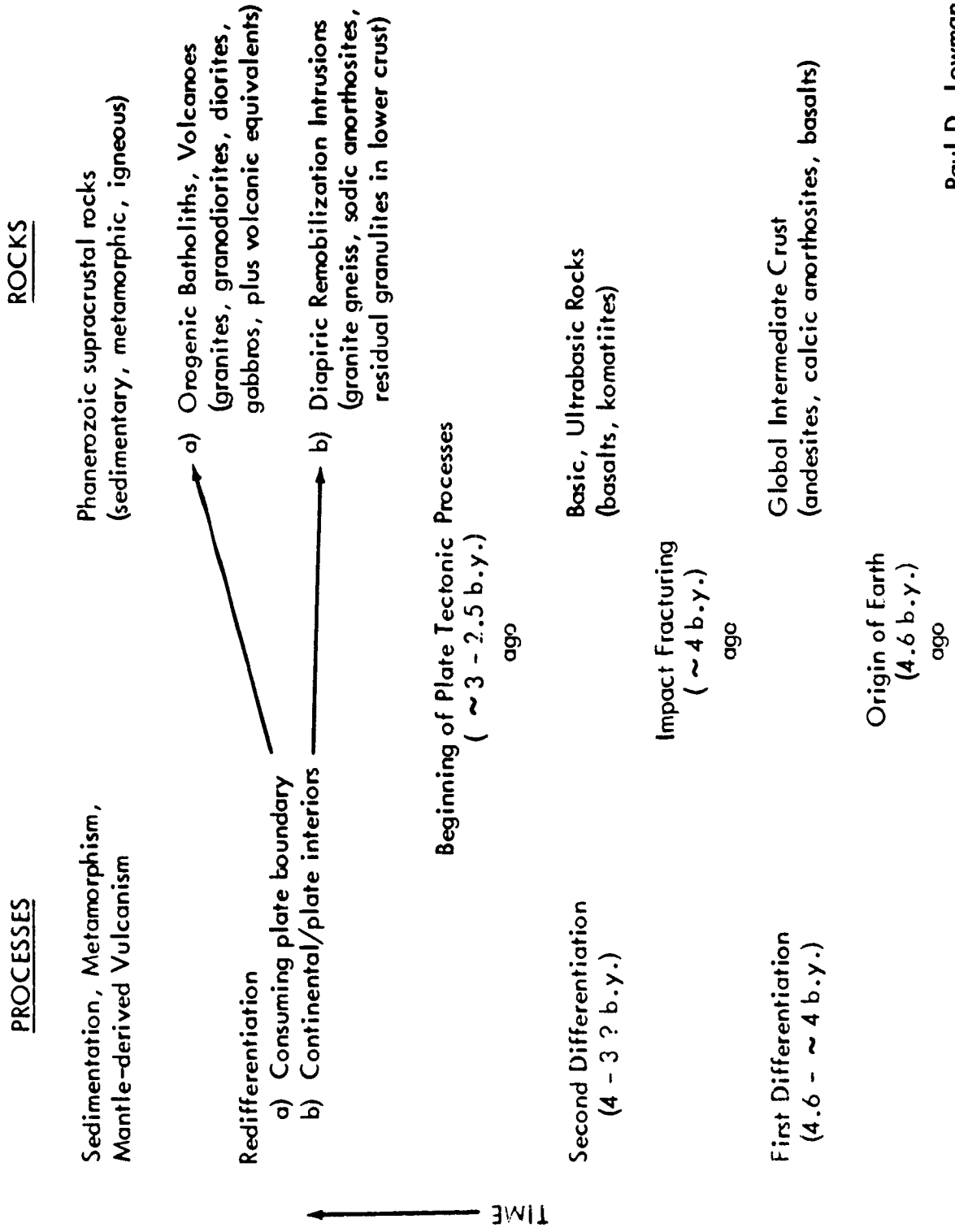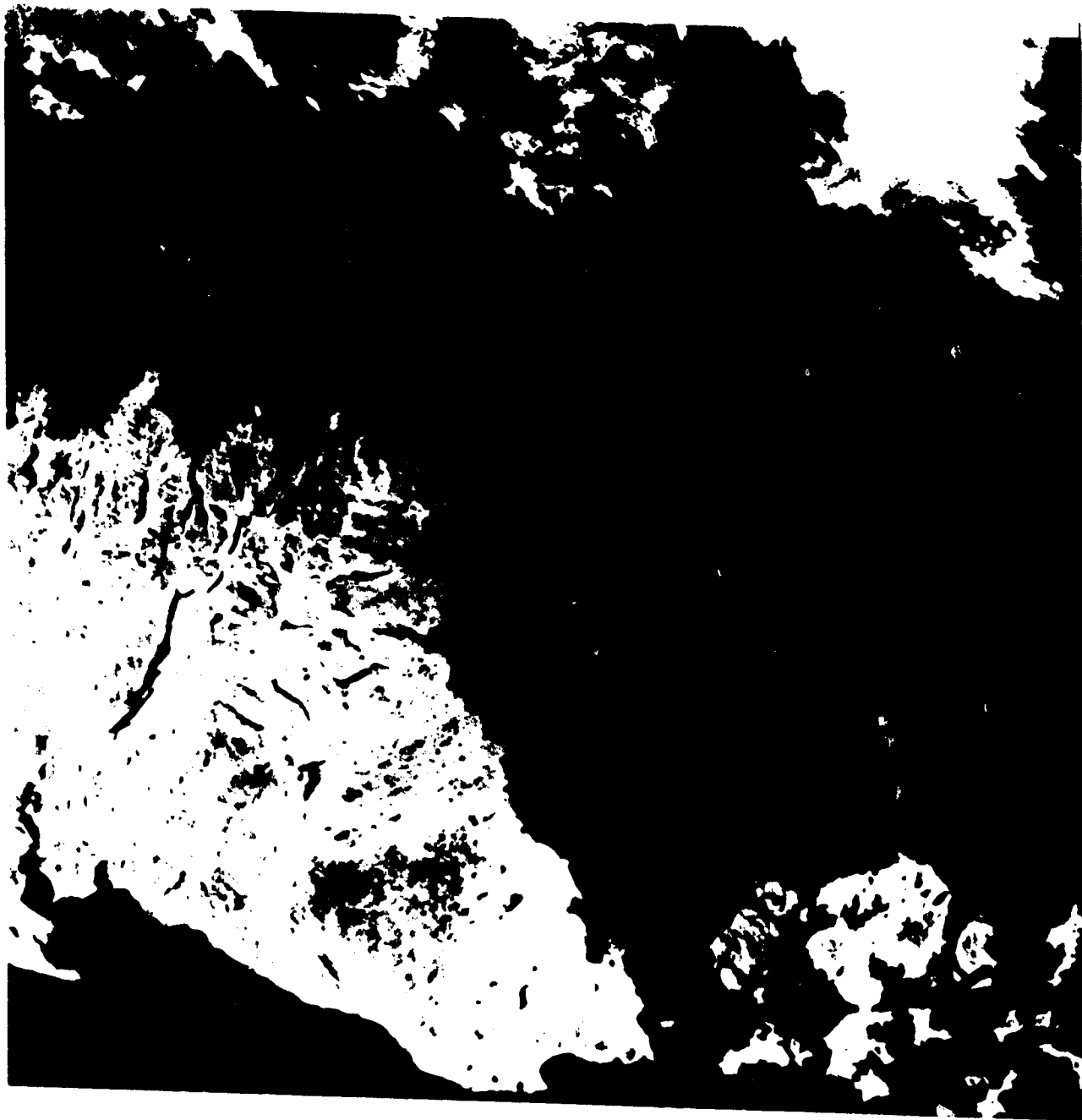
Paul D. Lowman

Figure 3A-2: Diagram of Petrologic Evolution of Terrestrial Continental
Crust; Note "Redifferentiation" After Beginning of Plate
Tectonic Processes (from Lowman, 1978).

C-2

Figure 3A-3: Landsat View of Northern Scotland; Scourie-Laxford Bridge
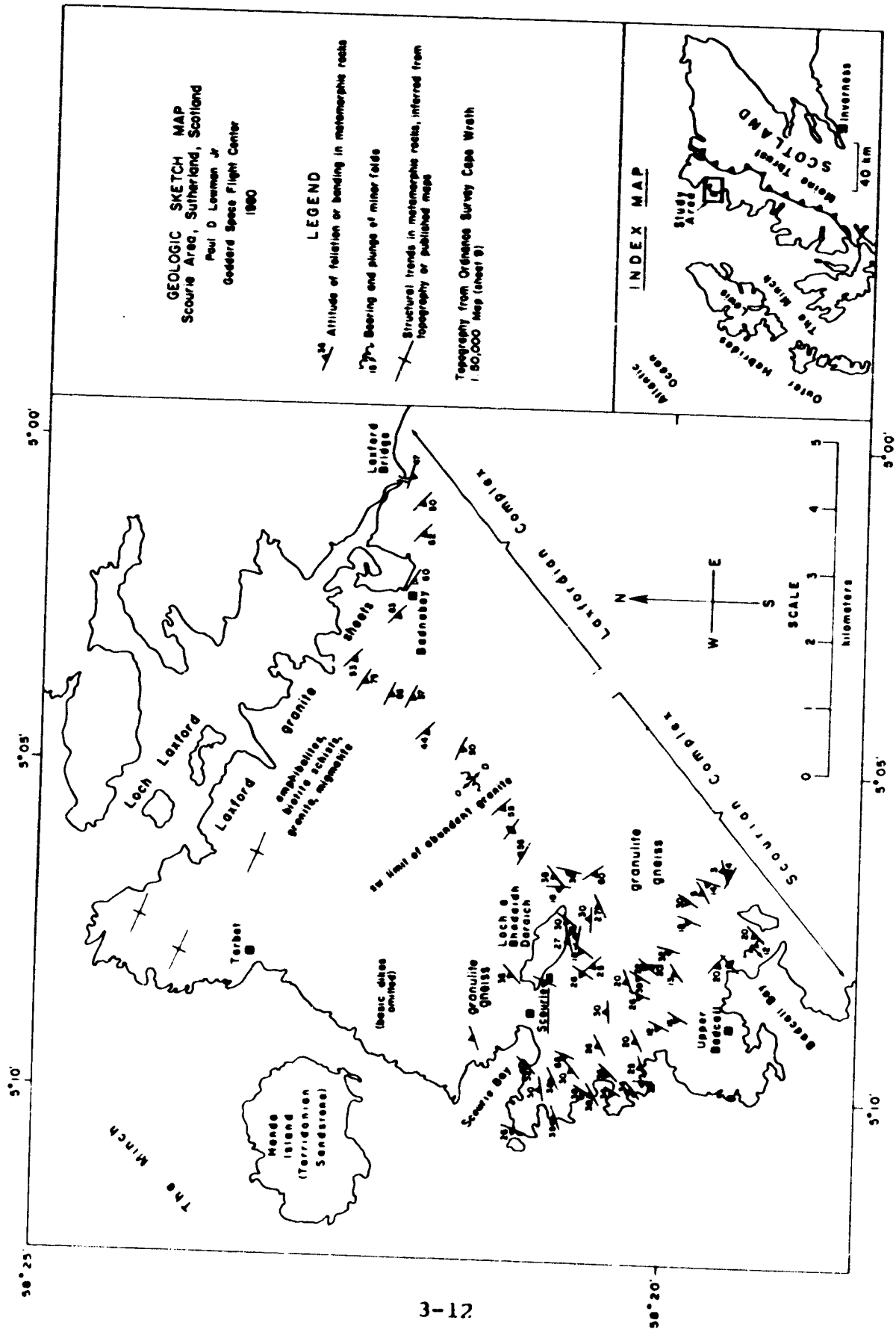Area at Bottom center. See Index Map in Figure 4. Landsat
Image Number 2194-10491.

Figure 3A-4: Geologic Sketch Map of Scourie-Laxford Bridge Area, Scotland.

Figure 3A-5: Photo Showing Archean Foreland, Underlain by Scourian Granulites; View From Point About 2 km SE of Scourie, Looking to East. Mountains on Horizon are Front of Moine Overthrust (Figure 3A-4).

Figure 3A-6: Exposure of Scourie Granulites on Coast 2 km SW of Village of Scourie, at Outlet of Loch a' Mhill Dheirg. Seagull (Circled) Gives Scale. Rocks Dip About 25° Away From Viewer; Bottom of Photo is Horizontal.

Figure 3A-7: Close up of Scourie Granulites; Compass at Left Gives Scale. Foliation Dips About 25°; View is Down Dip. Note General Lack of Obvious Deformation.

3-15

Figure 3A-8: Laxford Granite Sheets (Left) Intruding Laxfordian Amphibolites Near Badnabay.
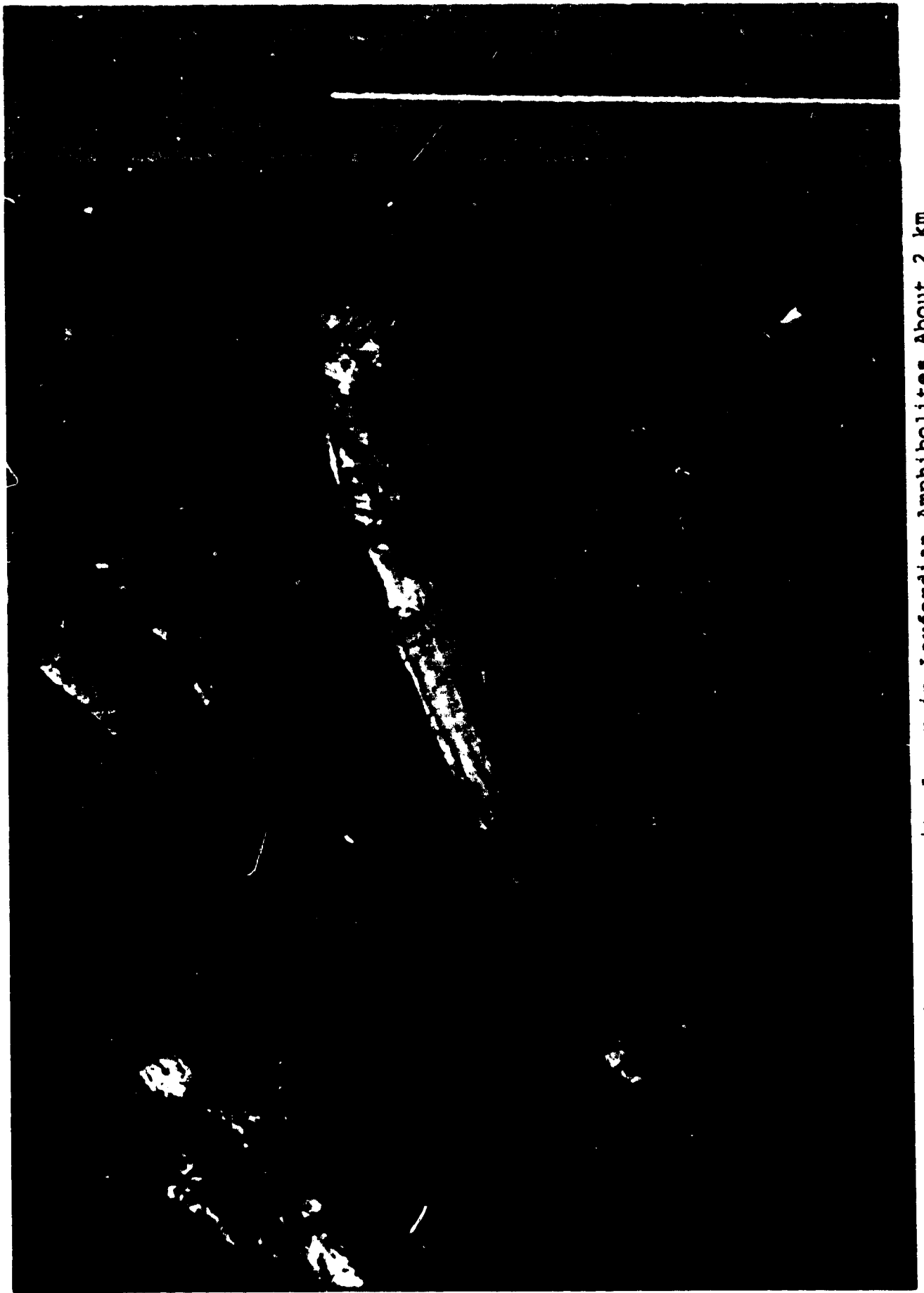
Figure 3A-9: Metaquartzite Layer in Laxfordian Amphibolites About 2 km West of Badnabay, on A894 Road. Sedimentary Nature Indicates Supracrustal Origin of Pre-Metamorphic Rocks in Area.

MODEL FOR CONTINENTAL CRUST
(Non-orogenic region; granite/greenstone terrain)

surface

Greenschist Facies — Metabasalts intruded by diapiric granites and post-diapirism high-K igneous granites; intensely folded

Amphibolite Facies — Metavolcanics, metasediments, injection migmatites

Granulite   Facies — Metavolcanics, minor metasediments; intermediate bulk SiO_2 content; anatectic migmatites; minor anorthosite

Possible amphibolite layer locally

Abundance of interlayered mafic volcanics increasing with depth; some eclogitic layers and lenses; generally low dips with minor recumbent folds

Chiefly mafic metavolcanics, granulite or eclogite facies; minor felsic layers

MOHOROVICIC DISCONTINUITY   35 km depth

Spinel peridotite, minor eclogite

(Right margin vertical axes: Increasing Si,K,Rb,U ↑ ; Increasing Fe, Mg ↓ ; Increasing degree of deformation ↑)
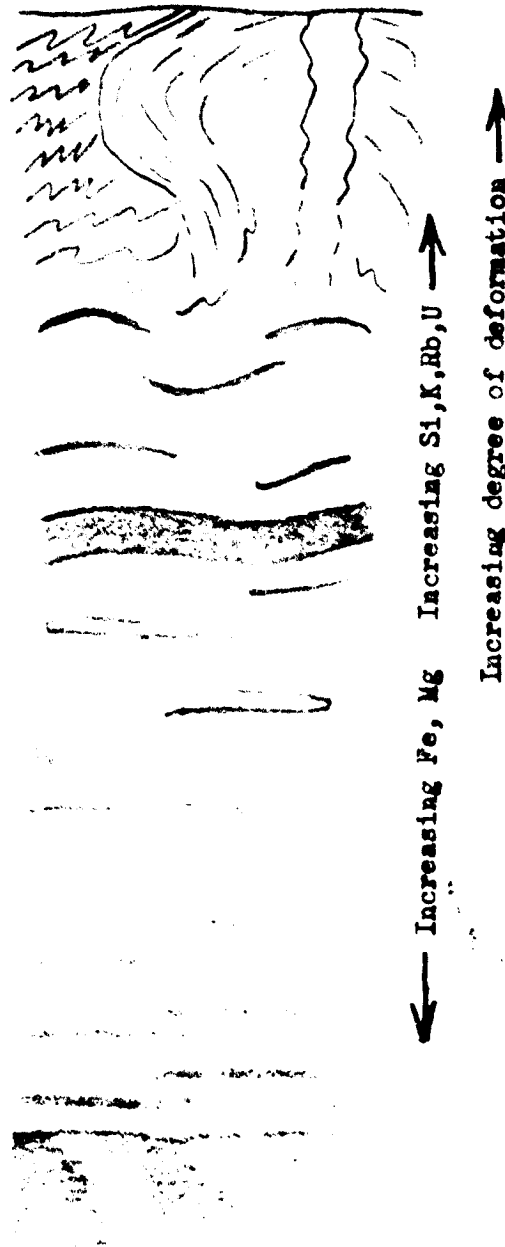
Paul D. Lowman Jr.
Goddard Space Flight Center
1980

Figure 3A-10:   Proposed Composite Crustal Model for Non-Orogenic Regions Under Granite-Greenstone Terrain.

B. COMPARATIVE PLANETOLOGY: EARTH-LIKE VOLCANIC STRUCTURES ON MARS

by

H. Frey

OBJECTIVES

The objectives of this work are to map the global distribution of martian pseudocraters and examine variations in their properties compared with known Icelandic analogs.

BACKGROUND

We previously reported the discovery of martian analogs of Icelandic pseudocraters (Frey et al., 1979). Found first in the Cydonia region of the northern plains of Mars, these small mound-like structures average under 1 km in diameter. They are extremely numerous in Cydonia, with over 900 having been counted in the original discovery mosaic. Most have subdued central pits at their summits; these pits typically have diameters of half the basal diameters of the mound. Their morphologic characteristics as well as their distribution and number led us to conclude that these features were similar to Icelandic pseudocraters, formed where lava flows come into contact with wet or marshy ground. A steam explosion cools and lifts the lava, producing the characteristic mound-like structure with a central vent. On Mars it is more reasonable to invoke ice as the volatile material. Therefore the distribution of these features may be an important clue to the distribution of (lava and) ice at or near the martian surface at the time the pseudocraters formed.

RECENT ACCOMPLISHMENTS

Theoretical studies by Rocha and Frey (unpublished) demonstrate that ice is a suitable medium for producing the necessary steam explosion required for the formation of martian pseudocraters. The additional thermal energy required to volatize ice is still much less than the thermal energy available from a typical lava flow, even at 750°C. Furthermore, the calculations suggest that in general larger pseudocraters will result from thicker lava flows, which agrees with observations in the Lake Myvatn region of Iceland. Finally, CO_2 ice is also a suitable volatile because its lower melting temperature means greater pressure is available at a given temperature. That is, it is even easier to form these structures from CO_2 ice than from water ice.

Our mapping of the distribution of pseudocraters on Mars has concentrated in the northern plains and near the volcanic units around the large Hellas impact structure. We have examined every available image with sufficient resolution to show structures less than 0.5 km across (range from spacecraft ≳ 2500 km), some 4000 images to date. We have found the pseudocraters in the Cydonia region to be much more numerous than previously thought, and distributed over a variety of terrain types. Dense fields some 300 km east of the original discovery area have pseudocraters without central pits as well as those with this characteristic feature. While most Icelandic pseudocraters near the type locality of Lake Myvatn do have central pits, those located elsewhere in Iceland often do not. A very extensive field of martian pseudocraters, both with and without pits, was found in volcanic terrain near Hellas. Other regions in which these structures have been located include southwest Elysium and Arcadia.

Properties vary among the recognized fields. For example, in Cydonia the average pseudocrater diameter we measured was 800 m. The Hellas pseudocraters, seen at similar resolution, cluster around 600 m diameter. The density of the Hellas structures is also generally higher than that found in Cydonia.

FUTURE EMPHASIS

We are examining the stratigraphic relations between pseudocraters and the various terrains on which they have been located, in order to develop a better understanding of their origin. We are also cataloging the variations in observed properties of these features. We expect to publish maps displaying these data and to continue our examination of the more recent Viking Orbiter imagery now available.

REFERENCES

Frey, H., B.L. Lowry and S.A. Chase, "Pseudocraters on Mars," J. Geophys. Res., 84, 8075-8086, and GSFC Technical Memorandum 80279, 1979.

C. SATELLITE GEOPOTENTIAL ANOMALIES AND

CONTINENTAL RECONSTRUCTIONS

by

H. Frey, R.A. Langel, G.D. Mead

OBJECTIVE

The objective of this work is to investigate the nature and
distribution of satellite-derived magnetic and gravity anomalies
for past reconstructions of the continents in order to study the
permanence of crustal geopotential anomalies since the breakup
of Pangaea.

BACKGROUND

Previous study of POGO magnetic anomaly data has revealed numerous
anomalies over continental regions, whose origin is most likely in
the lithosphere. We and others recognize some continuity of
anomalies across the now-rifted continental margins of South
America and Africa (Frey, 1979; Frey et al., 1979). Likewise,
Langel (1979) noted continuity of a large positive magnetic
anomaly across the Australian-Antarctica rifted margin. To inves-
tigate the reality of these features and their relation to litho-
spheric structures dating from before the breakup of Pangaea, we
undertook development of software on the AOIPS Image 100 interactive
computer that would allow reconstruction of the continents and dis-
play of geopotential and geological data for arbitrary continental
positions.

RECENT ACCOMPLISHMENTS

We have developed the capability of plotting continental outlines
from latitude-longitude data sets of arbitrary scale, and have
written the necessary software to move these continents to arbi-
trary positions popular in the literature for both Gondwanaland
and Laurasia. On these repositioned continents we have plotted the
contoured values of 2 x 2° gridded magnetic anomalies (from POGO
data) and gravity data (from GEM 10B, degree and order coefficients
13-30). Examples of each of these for Gondwanaland only are shown
in Figures 3C-1 and 3C-2. Similar plots exist for Laurasia.

In general there is much better agreement or continuity of anomalies across now-rifted margins for the magnetic data than for the gravity data (compare Figures 1 and 2). This has a reasonable explanation in that the source of the gravity anomalies, unlike the source of the magnetic anomalies, is not necessarily restricted to the crust or even the lithosphere. Mantle contributions to the observed gravity signatures are to be expected at the degree and order used here. Such mantle sources should be present-day inhomogeneities, not structures persisting for 180 million years.

By contrast most magnetic anomalies in the POGO data set used here probably are crustal in origin, and may be related to structures that have persisted since Pangaea. Although these anomalies have not been reduced to the pole, there is a striking degree of continuity or match-up of anomalies in these reconstructions. The strong Bangui negative anomaly in equatorial Africa and the positive anomaly to the south both have their counterparts in South America. Much farther south, twin negative anomalies trend in the same direction in South Africa and South America. The weak positive at the tip of South America may be related to the positive located over the Mozambique Ridge. Likewise a strong belt of contiguous positive anomalies runs through eastern India, Antarctica and southern Australia.

Similar matchups occur in the magnetic anomalies associated with the northern continents. Especially striking are the large positives in West Africa and the central United States, and a belt of strong negatives running from Scandanavia through Greenland and into Baffin Island. A similar band of positive anomalies runs north of these negatives, linking northern Scandanavia, Greenland and Canada in their reconstructed positions.

These results suggest that many of the large magnetic anomalies observed in the POGO data are related to crustal structures that data from before the breakup of Pangaea.

FUTURE EMPHASIS

To refine these observations we will, in the future, digitize and incorporate into the interactive system continental shelf outlines for more precise positioning of the continents. We are working on producing a set of POGO data reduced to the pole in order to more accurately locate the anomalies. Study is underway to develop a gravity anomaly field that better reflects crust and lithospheric structure than does the present model. We will incorporate GEM 10C into this effort, and also plan to update the magnetic anomaly data file with newly acquired Magsat data.

REFERENCES

Frey, H., "Global Geophysics and Geology: Correlations of Satellite-Derived Gravity and Magnetic Anomalies with Rifts and Sutures," _E⊕S Trans. Am. Geophys. Un._, _60_, 398, (abstract), 1979.

Frey, H.V., R.A. Langel and G.D. Mead, "Global Magnetic Anomalies: Implications for Plate Tectonics," IAGA Bull. No. 43, Program and Abstracts from XVII General Assembly, p. 167, 1979.

Langel, R.A., 'Near Earth Satellite Magnetic Measurements: A Prelude to Magsat," _E⊕S Trans. Am. Geophys. Un._, _60_, 667, 1979.

POGO MAGNETIC ANOMALIES
PANGAEA RECONSTRUCTION

RESIDUAL ANOMALIES
(CORE FIELD REMOVED)
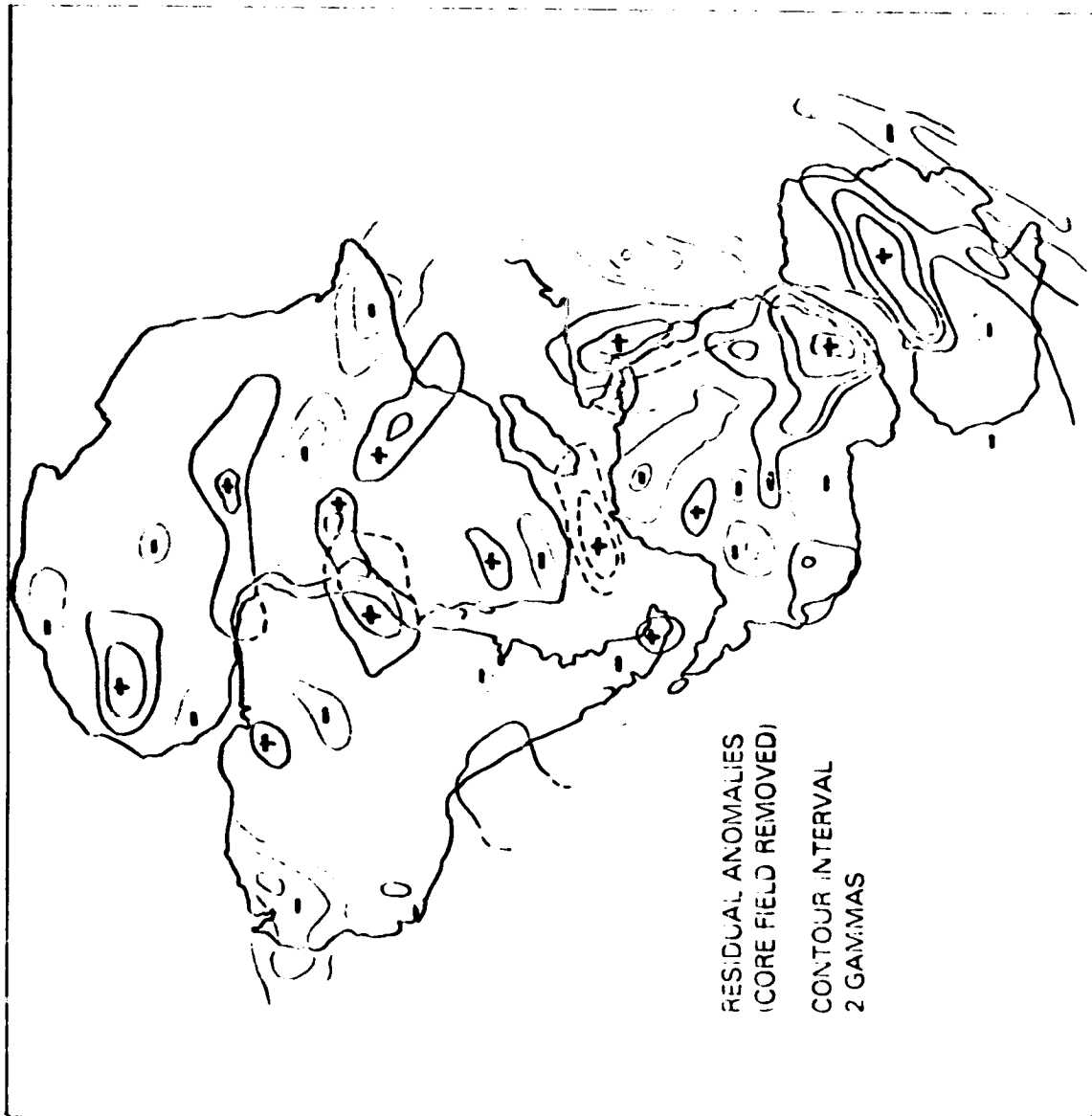
CONTOUR INTERVAL
2 GAMMAS

GONDWANALAND

Figure 3C-1: POGO Magnetic Anomalies for Gondwanaland. Anomalies are Contoured at 2 Gamma Intervals and Represent the Residuals After Removal of a Degree and Order 13 Core Field. Positive Anomalies (+) Shown as Darker Lines; Negative Anomalies (-) Appear Lighter.

Figure 3C-2: GEM-10B Free-Air Gravity Anomalies From Coefficients of Degree and Order 13-30. Positive (+) Anomalies and Negative (-) Anomalies Shown Have Much Less Continuity Across Rifted Margins Than Do Magnetic Anomalies.

D. **CRUSTAL MODELING - YEARLY REPORT**

UNITED STATES CRUSTAL STRUCTURE

by

R. J. Allenby

OBJECTIVES

The objective of this effort is to develop maps of crustal thick-
ness and top of mantle velocity (P_n) for the conterminous United
States and then investigate the relationships of anomalous map
areas with long wavelength magnetic and gravity anomalies
detected from satellites.

BACKGROUND

The success of interpreting satellite geophysical data, particu-
larly magnetic, is in part dependent on the accuracy of the
crustal thickness model used. Near surface magnetic anomalies
are a function of crustal composition and thickness. Across
regions of similar rock magnetic properties, thicker crust will
exhibit higher magnetic values. This will be true down to the
Curie isotherm or, as proposed by Wasilewski et al. (1979), the
top of the Upper Mantle (the seismic Moho discontinuity), below
which boundaries rocks lose their magnetic properites. Gravity
anomalies, on the other hand, are not constrained by any depth
barriers.

RECENT ACCOMPLISHMENTS

A survey was completed of all available seismic refraction lines
in the conterminous United States and neighboring Canada and
Mexico that penetrate the Mohorovicic (Moho) discontinuity
separating the base of the crust and the top of the upper
mantle (Allenby, 1980). Refraction profiles were indexed to
their literature data sources (74 in all, including multiple
analysis on some lines). The final report contains maps of
crustal thickness and top-of-mantle velocity. A preliminary
comparison of crustal thickness and POGO satellite equivalent
bulk magnetization anomalies (Langel, 1979) suggests good
agreement between western U.S. negative magnetic anomalies and
anomalously thin crust in areas like the Columbia - Snake River
Plateau and the Basin and Range Province (this correlation is
undoubtedly enhanced by the decreased depth of the Curie
isotherm caused by increased heat flow resulting from the shallow-
ness of the upper mantle). Other areas show little correlation,
for example, the large Kentucky magnetic anomaly appears to be
underlain by a crust of nearly uniform thickness.

FUTURE EMPHASIS

Continued work on understanding U.S. crustal structure and composition is planned using all available geophysical data.

REFERENCES AND PUBLICATIONS

Allenby, R. J., United States Crustal Structure and Satellite Magnetic Anomalies, NASA Technical Memorandum 81990, Goddard Space Flight Center, 27 pp, 1980.

Langel, R. A., Near-earth Satellite Magnetic Field Measurements: A Prelude to Magsat, EOS, 60, 667-668, 1979.

Wasilewski, P. J., Thomas, H. H. and Mayhew, M. A., The Moho as a Magnetic Boundary, Geophys. Res. Ltrs., 6, 541-544, 1979.

E. THE KENTUCKY ANOMALY, CONTINUED

by

H.H. Thomas, M.A. Mayhew, P.J. Wasilewski

OBJECTIVE

The objective of studying the Kentucky satellite magnetic anomaly
is to develop as comprehensive a magnetic, geophysical and geologic
model of the region as is possible in order to provide a basis for
understanding the sources of satellite anomalies along with their
associated mineralogy and tectonics.

BACKGROUND

We reported (Mayhew et al., ESAD Research Report, 1980) the
completion of a first step in the geophysical analysis of the
Kentucky Anomaly. In summary, a 2-dimensional geophysical model
suggests that an intrusion of mantle mafic material during a
Precambrian rifting event is responsible for the satellite magnetic
anomaly.

RECENT ACCOMPLISHMENTS

Recently released aeromagnetic maps from a Tennessee Valley
Authority survey show a clearly outlined anomalous area approxi-
mately 100 km to the west of the modeled central Kentucky anomaly
and a smaller, less intense area to the east of the modeled anomaly;
somewhat better resolution was attained by the TVA survey over
existing surveys due to a higher density of flight lines.

A 3-dimensional model of the central Kentucky anomaly, using existing
geophysical and the new aeromagnetic data, is very similar to the
2-dimensional model previously reported. The modeled body, although
providing an excellent match to the local gravity and aeromagnetics,
accounts for only 20% of the magnetism at satellite altitudes;
upward continuation of all of the regional aeromagnetic anoamlies
does, however, provide a good fit to the POGO and Magsat anomalies

Comprehensive modeling of all of the regional aeromagnetic anomalies
would be a normal next step, but a lack of seismic data inhibits
such modeling for the present. A request has been made for a COCORP
study of the region; the line required will be long and expensive
and probably won't be implemented for a couple of years. Until
COCORP data becomes available, we will make use of data from small
seismic surveys as they become available.

Magsat data, particularly the vector and low altitude data offer the best hope for a better understanding of the regional picture.

FUTURE EMPHASIS

Emphasis in the immediate future will be directed at analyzing drill cores from critical areas in the Kentucky-Tennessee region. Magnetic and mineralogic data for these cores will give information on origins and relationships between magnetic properties and regional tectonics. In the same vein, relationships will be established between rocks responsible for magnetic anomalies and the abundant sulfide ores in the region.

CHAPTER 4

CRUSTAL DEFORMATION

edited by

S.C. Cohen

OVERVIEW

Improving the understanding of global and regional scale motions of the crust and the occurrence of earthquake are the inter-related goals of research efforts in crustal deformations and earthquakes. Crustal deformations are important as the surface expressions of fundamental geodynamic processes. They can provide information on stresses within the earth, the interior rheology, and subsurface structure. Within the context of tectonic plate theory they play key roles in deducing relative plate motions, studying the driving mechanics for these motions, and assessing plate rigidity. The understanding of crustal deformations also plays a potentially important role in explaining polar motion and in interpreting gravity and magnetic fields and heat flow. On a regional scale crustal deformations can provide information on the accumulation of strain in earthquake-prone areas. Geodetic measurements of such deformation are potentially useful for long-range earthquake forecasting; in addition, the detection of other anomalous crustal movements could contribute to shorter term earthquake predictions. The monitoring of post-seismic crustal motions can also be expected to yield important information on earthquake mechanisms, postseismic stress re-distribution, and lithosphere and asthenospheric rheology and structure. Fundamental theoretical and computational studies of both earthquakes and other processes that deform the earth's surface are necessary to provide a framework for interpreting geodetic measurements and for modeling the underlying physical processes.

The research efforts of the Earth Survey Applications Division include the Crustal Dynamics Project involving the measurement and interpretation of time-dependent baseline distances and directions among numerous sites located within the United States and worldwide. The Division's activities also include a program of fundamental analytic and computational studies, mission simulations, and supportive geologic field studies. The articles in this section describe many of the research activities pursue in 1980 both in the Crustal Dynamics Project and the basic research program.

A. INTERCONTINENTAL BASELINES FROM LAGEOS

by

D.E. Smith

OBJECTIVE

The long-range objective of this study is the determination of motions of the major tectonic plates from an analysis of laser tracking of the Lageos spacecraft. The short term objective is the development and demonstration of techniques for the analysis of laser tracking data to provide intersite baselines accurate to a few centimeters.

BACKGROUND

The Lageos laser tracking data is analyzed in approximately monthly segments (30 to 35 days). An orbit is fitted to the tracking data for each of these periods beginning at launch (May 1976) and extending until April 1979. These 36 orbital arcs have been grouped according to calendar year; eight in 1976, twelve each in 1977 and 1978, and four in 1979. The eight orbital arcs in 1976 were then analyzed simultaneously in a large least squares solution for station coordinates, polar motion, corrections to Universal Time, tidal parameters, and other parameters associated with the spacecraft and its orbit. This analysis procedure was repeated for the data in 1977, 1978 and 1979. The gravity field used in this investigation was a special one developed from an analysis of all the Lageos tracking data from launch through 1978. This field was derived by permitting the adjustment of a number of geopotential coefficients in the expansion of the earth's gravity field in a combined analysis of all the data for the period just mentioned. The process was iterative in that initially some 64 coefficients were allowed to adjust but the results showed that there was no justification in solving for over half these terms. Ultimately, a set of approximately 25 coefficients were adjusted and the field used in this analysis was composed of these 25 coefficients together with those from GEM 10 out to degree and order 20.

The parameters of particular interest in the individual yearly solutions were the tracking station coordinates and, to a lesser degree, the station heights. The latitude and longitudes could not easily be compared in the different yearly solutions because polar motion and Universal Time were adjusted and all the station coordinates except one longitude were adjusted. The baselines between the stations, however, are not affected by the adjustment of these other parameters.

RECENT ACCOMPLISHMENTS

Inspection of the solutions for each of the yearly groups of data
showed only five stations appeared in all four solutions and of
these, one station, Natal Brazil appeared to have major problems.
The baselines between the four other stations: Greenbelt, MD;
San Diego, CA; Arequipa, Peru; and Orroral, Australia are shown
in Table 4A-1. Further, an error in some of the data in 1976
from the Arequipa and Orroral stations was identified and
consequently the results involving these stations for that
period are shown in Table 4A-1 in parentheses. (These data are
presently being corrected and the solution re-determined).

The four San Diego to Greenbelt baselines show consistency in
Table 4A-1 at about the ten centimeter level. The lasers at
these two sites are the best NASA systems with ranging accuracies
of a few centimeters accuracy. The trend indicated in these
baselines is probably not significant since the formal uncertainty
in each baseline is several centimeters. However, the projected
change in this baseline is about +1.6 cm/yr based on plate
tectonic models for the relative motion of the Pacific and
North America. From the perspective of data quantity and
reliability the next best tracking station (in this group) is
probably Arequipa. Its accuracy is probably 10 cm in satellite
range measurements and the three reliable baseline determinations
to Greenbelt tend to confirm its good quality. No significant
change in this line is expected from geophysical considerations
and the three laser results indicate good precision. The San Diego
to Arequipa laser line does not show the same consistency as the
two lines from Greenbelt but the variation is probably consistent
with the standard deviations. All the lines to Orroral show larger
spread than any of the others and consequently there may be some
data problems at this site. However, it should be remembered
that there is never any simultaneous observation of Lageos from
Orroral with any of the other three stations and hence the Orroral
position has been determined almost exclusively from the orbit
dynamics and will be very dependent on the accuracy of the
gravity field model. In addition, it should be noted that in 1978
San Diego was operating during July and August only and that there
were no data from Orroral at this time. In Table 4A-2, the
solutions for the station heights are shown. The four values for
Greenbelt show a spread of about 20 cm and San Diego shows a
spread of 29 cm indicating that the height determinations are
not as accurate as the baselines even for the best stations.
For Arequipa and Orroral the range over three values is 24 cm
and 34 cm, respectively. It is interesting to note, however,
that the best station, Greenbelt, has the best height consistency
and generally gives better baselines to other stations.

SIGNIFICANCE

The preliminary solutions obtained for selected baselines show precisions of about 5 cm between the best laser stations and about 10 cm in the height precision. These results are approaching the level of accuracy (precision) that can be useful geophysically. Improvements in the laser systems to the 1 or 2 centimeter level coupled with the development of an improved gravity field model for Lageos (in preparation) should give about 2 cm in baseline length and about 5 cm in station height using the methods described here. It is also very probable that other analysis techniques designed for specific baselines or stations could give a further improvement over this general all-pourpose type solution.

TABLE 4A-1. LASER BASELINES 1976-79

	GREENBELT SAN DIEGO	GREENBELT AREQUIPA	SAN DIEGO AREQUIPA	GREENBELT ORRORAL	AREQUIPA ORRORAL	SAN DIEGO ORRORAL
	3606114.28m	(5928019.33m)	(6878047.60m)	(12108540.28m)	(10787498.18m)	(10514918.46m)
MAY-DEC '76	4.29	9.54	8.17	0.07	8.26	8.97
JAN-DEC '77	4.32	9.51	8.17	0.01	8.57	8.41
JAN-DEC '78	4.34	9.55	8.30	0.17	9.18	8.83
APRIL 1979						

TABLE 4A-2. LASER STATIONS HEIGHTS

	GREENBELT MD	SAN DIEGO CA	AREQUIPA PERU	ORRORAL AUSTRALIA
MAY-DEC 1976	15.26m	984.81m	(2484.70m)	(941.99m)
JAN-DEC 1977	15.05	985.10	2484.94	941.67
JAN-DEC 1978	15.24	984.92	2484.94	941.56
APRIL 1979	15.06	985.09	2485.18	941.90

B. CRUSTAL DYNAMICS PROJECT: OBSERVING PROGRAM FOR HIGHLY MOBILE SYSTEMS

by

H. Frey

OBJECTIVE

The objective of this effort is to develop a program of deployment of highly mobile VLBI and SLR systems for the measurement of crustal deformation and strain accumulation along plate boundaries and in regions of high seismic activity.

BACKGROUND

The Crustal Dynamics Project was created by NASA for the purpose of applying space technology to the precise measurement of geodetic parameters useful for determining (a) regional deformation and strain accumulation in the western United States, (b) contemporary plate motion, (c) the internal deformation of major oceanic and continental plates, (d) the rotational dynamics of the Earth, and (e) the motions and deformation occurring in regions of high earthquake activity. The space techniques available to the Project are Very Long Baseline Interferometry (VLBI) and Satellite Laser Ranging (SLR), both of which are capable of providing extremely high precision baseline determinations, between pairs of stations. Observing systems available to the Project consist of fixed, movable and highly mobile systems. Proposed observing sites for these systems number over 200, as described previously (Lowman et al., 1979; Earth Survey Applications Division Research Report - January 1980, page 3-3). Budgetary constraints limit the number of available highly mobile systems and their deployment; weather further constrains the observations with SLR facilities.

RECENT ACCOMPLISHMENTS

A detailed program for the deployment of highly mobile VLBI and SLR observing systems has been devised, taking into account (a) the number of such systems and their ability to move between chosen sites, (b) the period of time required on site to obtain the necessary data, (c) the availability of supporting base stations against which the highly mobile systems work, (d) the scientific priority of the science objectives of the Crustal Dynamics Project, (d) the probability of obtaining permission to visit foreign sites, (f) the expected rate of motions along various baselines, (g) the number of baselines needed to define that motion, (h) the recommendations and supporting programs of other cooperating government

and non-government organizations, and (i) current guidelines for new systems expected to be available during the lifetime of the Project (1981-1986). The plan is documented as NASA/GSFC TM 82029, "Crustal Dynamics Project Observing Plan for Highly Mobile Systems, 1981-1986." It describes the month-by-month deployment of highly mobile radio antenna and laser ranging systems. A brief outline of the 1981 program is described below.

The small 4 m highly mobile VLBI system will make four observing campaigns of approximately 5 sites each in 1981. Three of these will be in southern California, at sites designed to be the end points of baselines crossing the San Andreas and other faults of the active boundary between the North American and Pacific plates. This system works in concert with base stations at Owens Valley Radio Observatory and Goldstone. Measurements are planned from JPL, Pearblossom, Palos Verdes, La Jolla and Presidio, from which previous VLBI measurements have been made. New observing sites scheduled for occupation include Pinon Flats, Yuma, Monument Pk. (a laser base station), Santa Paula, Vandenberg AFB, Gorman, Anderson Peak and Pt. Reyes in the California part of the program. In the western United States, Flagstaff, Vernal, Boulder and Duckwater/Ely will be occupied to determine baselines stretching across the Basin and Range into the more stable interior of the North American plate. These locations are shown in Figures 4B-1 and 4B-2.

The Transportable Laser Ranging System (TLRS) will visit 8 sites in 1981. Four of these will be in California, including the VLBI base stations at Goldstone and OVRO. This "mutual occupation" of several sites by both kinds of systems is an important continuing intercomparison of the techniques scheduled to continue throughout the Project. The TLRS will also observe from Vandenberg and Yuma, then move into the western United States to occupy Bear Lake, Vernal, Trinidad and Flagstaff. These sites are shown, along with laser ranging base stations, on Figure 4B-3.

FUTURE EMPHASIS

In 1982 the highly mobile system program calls for reoccupation of these same sites but also the addtion of a number of new sites. These are described in detail in the above referenced document. In general the program expands to include TLRS sites in Baja California, Easter Island and the west coast of South America. Additional sites in California will be occupied by the mobile VLBI. In the 1983-1986 time frame new highly mobile systems become available, and in addition to reoccupation of already visited sites, campaigns in Alaska, central North America and the Caribbea. e scheduled.

REFERENCES

Frey, H., "Crustal Dynamics Project Observing Plan for Highly
    Mobile Systems, 1981-1986," NASA GSFC Technical Memorandum
    82029, 1980.

Lowman, P.D., Jr., R.J. Allenby and H.V. Frey, "Proposed Satellite
    Laser Ranging and Very Long Baseline Interferometry Sites for
    Crustal Dynamics Investigations," NASA/GSFC Technical Memorandum
    80563, 1979.
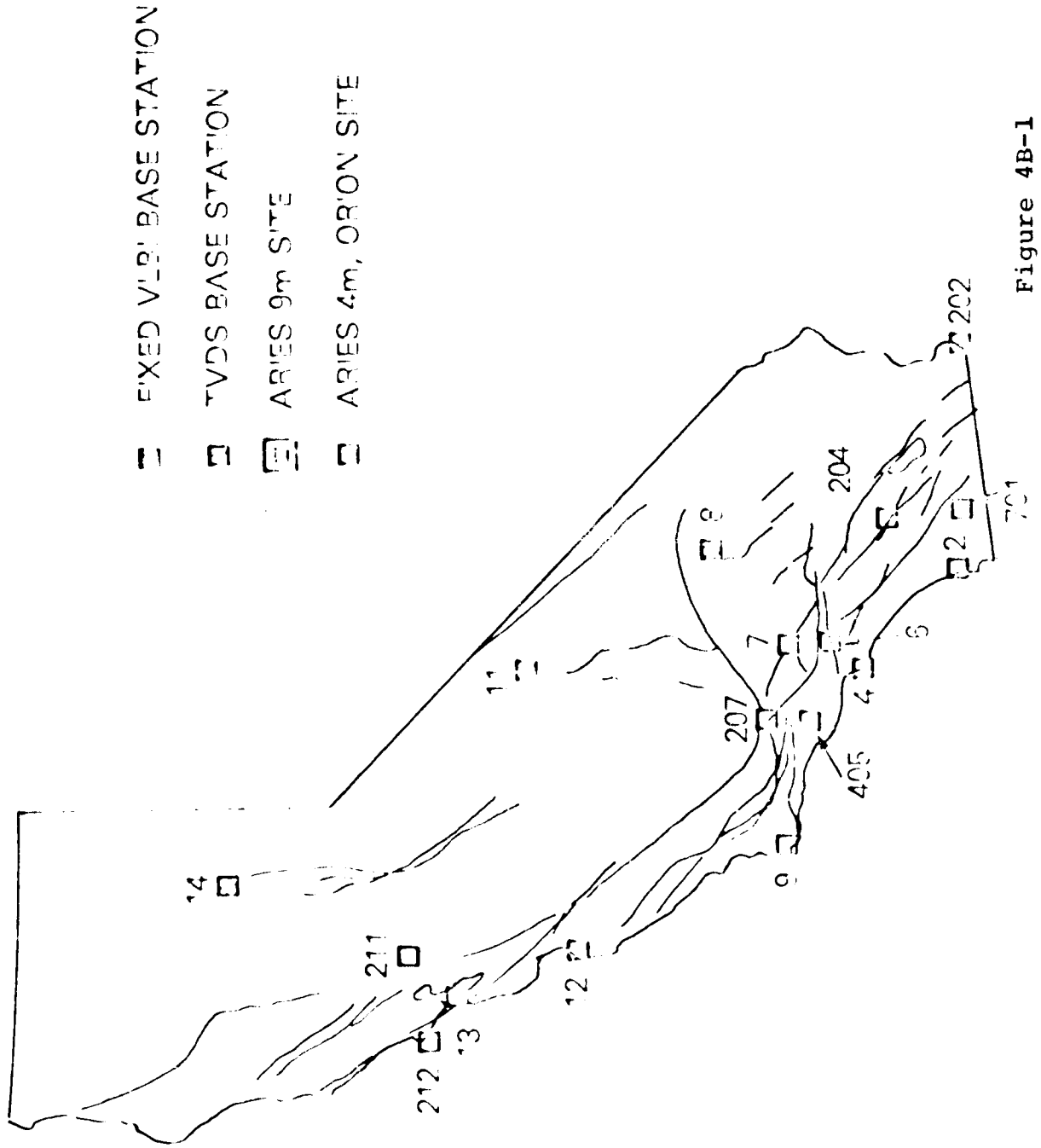
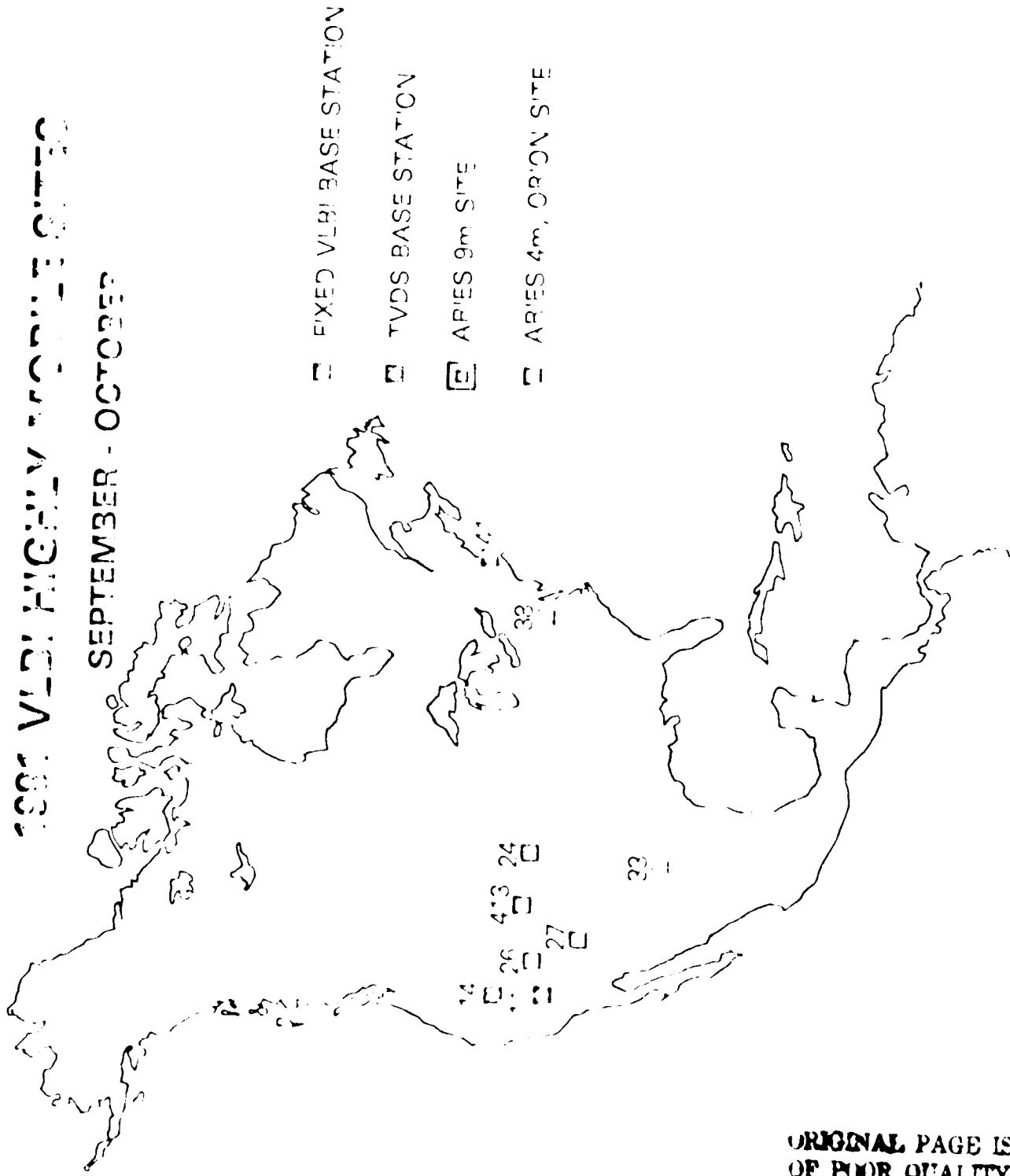1991 V_B HIGHWAY VEHICLE SITES
FEBRUARY, MAY, JULY

☐ FIXED V_B BASE STATION

☐ TVDS BASE STATION

☒ ARIES 9m SITE

☐ ARIES 4m, ORION SITE

Figure 4B-1

1981 VLBI HIGHLY MOBILE SITES

SEPTEMBER - OCTOBER

☐ FIXED VLBI BASE STATION

☐ TVDS BASE STATION

☐ ARIES 9m SITE

☐ ARIES 4m OBS'N SITE

Figure 4B-2

1981 SLR MONTHLY MOBILE SITES
MARCH - JUNE, SEPTEMBER - DECEMBER

△ FIXED LASER BASE STATION
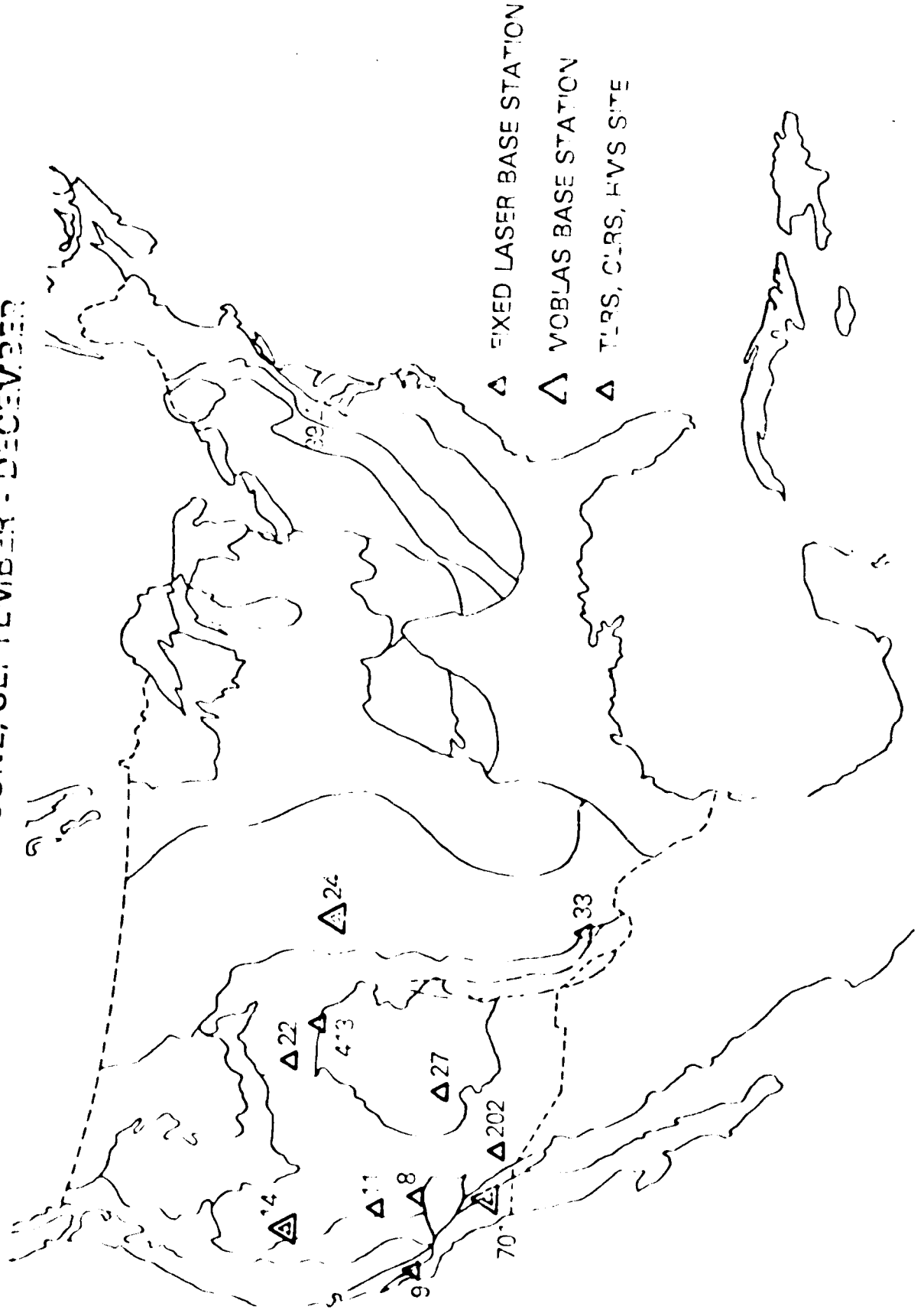
△ MOBLAS BASE STATION

△ TLRS, CLRS, HVS SITE

Figure 4B-3

C. GLOBAL TECTONIC ACTIVITY MAP

by

P.D. Lowman, Jr.

OBJECTIVES

The objectives of the global tectonic activity map were, first, to provide an objective and reasonably complete representation of geologic features active now or within the last million years, second, to provide a tectonic activity representation suitable for comparison with maps of identical scale and projection as part of the geophysical atlas reported last year, and third, to provide a tool for planning VLBI and laser measurements as part of the Crustal Dynamics Project.

BACKGROUND

Plate maps are ubiquitous in the geological literature of the last decade. However, regardless of the correctness of plate tectonic theory, these maps are of little use for interpretation of satellite geophysical data or for planning precise geodetic measurements. The main reason for this is simply that these maps are in general intended to illustrate a particular theory, and since the theory is now acknowledged to be an oversimplification, the maps are similarly oversimplified. For this reason, a compilation of geological features active within the last one million years was begun in 1977, and published in preliminary form in the geophysical atlas (Lowman and Frey, 1979).

RECENT ACCOMPLISHMENTS

The tectonic activity map was presented to a geologic hazards symposium at the 26th International Geologic Congress in Paris in July 1980, and is in press for the proceedings of that symposium. The map has been used by other writers for various purposes, with the author's permission, and hundreds of copies have been sent out in answer to mail requests. It served as a base map for the NASA OSTA "Application of Space Technology to Crustal Dynamics and Earthquake Research," 1979.

The latest up date of these tectonic activity maps are shown in Figures 4C-1, 4C-2 and 4C-3.

SIGNIFICANCE

The tectonic activity map fills a cartographic gap between conventional geologic maps and maps showing historically active features (volcanoes or earthquake-generating faults). Furthermore, it brings out a number of neglected scientific problems or phenomena, including the following.

1.   The map demonstrates that contrary to orthodox theory, the earth's crust cannot be described in terms of "a small number of well-defined plates" as called for by LePichon and his colleagues in the standard plate tectonics text. This is more obvious in southern Asia north of the Himalayas, an area cut by so many active faults that it is impossible to define meaningful micro-plates. Authorities on the area, such as Molnar and Tapponnier, have in fact found slip-line field theory necessary to describe the deformation of this region.

2.   The wide extent of diffuse plate boundaries is demonstrated, particularly in North America, Europe, and Asia. These boundaries are generally neglected in most treatments of plate tectonics and related topics. Discussions of the San Andreas fault, for example, generally consider the east block to be part of the North American plate, but as the map shows, the San Andreas is just the beginning of the plate boundary zone.

3.   The symmetrical structure of many fold belts is shown; examples include the Andes, Alps, and Zagros Mountains. This symmetry, expressed as opposing thrusts, is well-known in the pre-plate tectonics literature, but is neglected in plate theory.

4.   The wide distribution of volcanoes on the upper blocks of continent-continent convergence zones is shown clearly. This phenomenon has not received nearly as much attention as has the volcanism of ocean-continent subduction zones. The question of heat sources for this vulcanism deserves study.

5.   The apparent structural unity of the Himalayan-Alpine chain is puzzling. It is not at all clear why, for example, a unified zone of overthrusting should extend along the north front of the Pamirs-Zagros-Carpathians-Alps if this chain is the result of the interaction of independently-moving micro-plates. This is another structural relationship not shown on conventional plate maps.

6.   The map combines the measured plate velocities at spreading centers compiled by Minster and Jordan with a detailed tectonic representation. This permits easier understanding of the relation between spreading rates, seismicity, and vulcanism. The general decrease in spreading rate northward along the Mid-Atlantic Ridge is an interesting demonstration of the rotational nature of plate movement.

FUTURE EMPHASIS

Work has begun on a complete revision of the tectonic activity map. The new edition will provide better representation of the Antarctic on the equatorial projection, and will show continental margins as opposed to coastlines. It is planned to digitize the data to be plotted.

REFERENCES

Lowman, P. D., Jr., and Frey, H. V., A Geophysical Atlas for
    Interpretation of Satellite-Derived Data, NASA Technical
    Memorandum 79722, 54 p., 1979.

Lowman, P. D., Jr., A Global Tectonic Activity Map, in press,
    Bulletin of the International Association of Engineering
    Geology.

Lowman, P. D., Jr., The Evolution of Geological Space Photography,
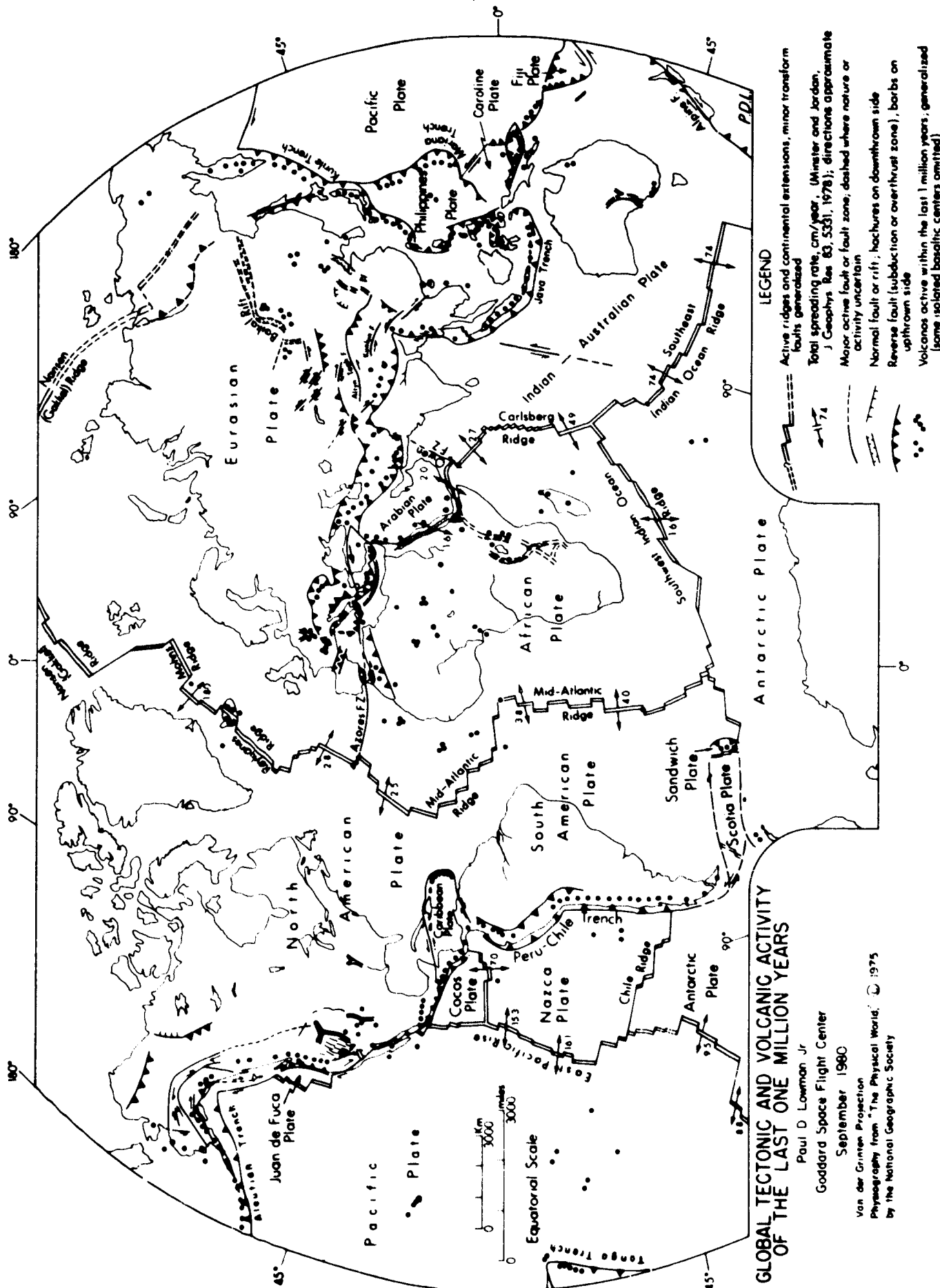   Chapter 4 in Remote Sensing in Geology, B. S. Siegal and
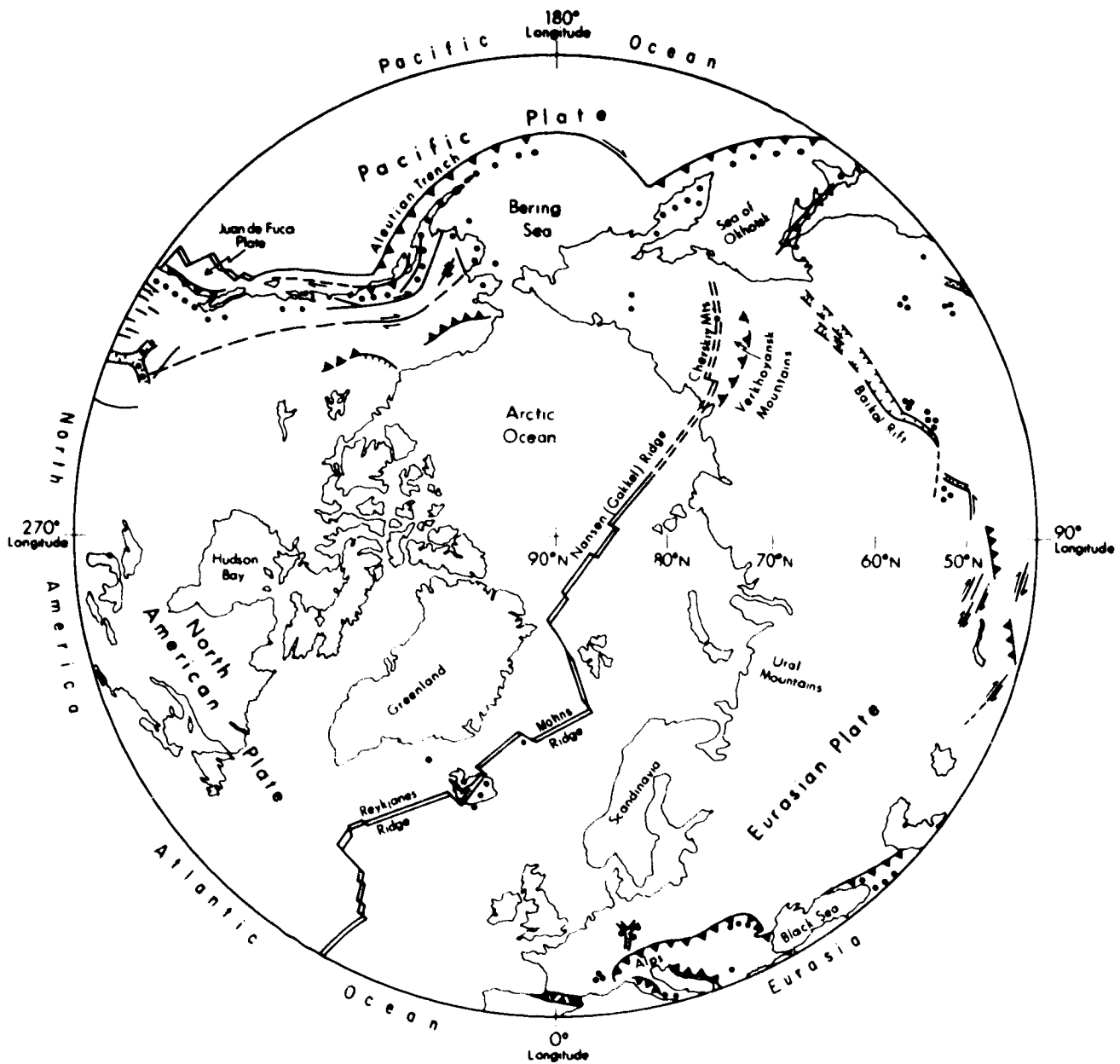   A. R. Gillespie, editors, John Wiley, New York, 702 p., 1980.
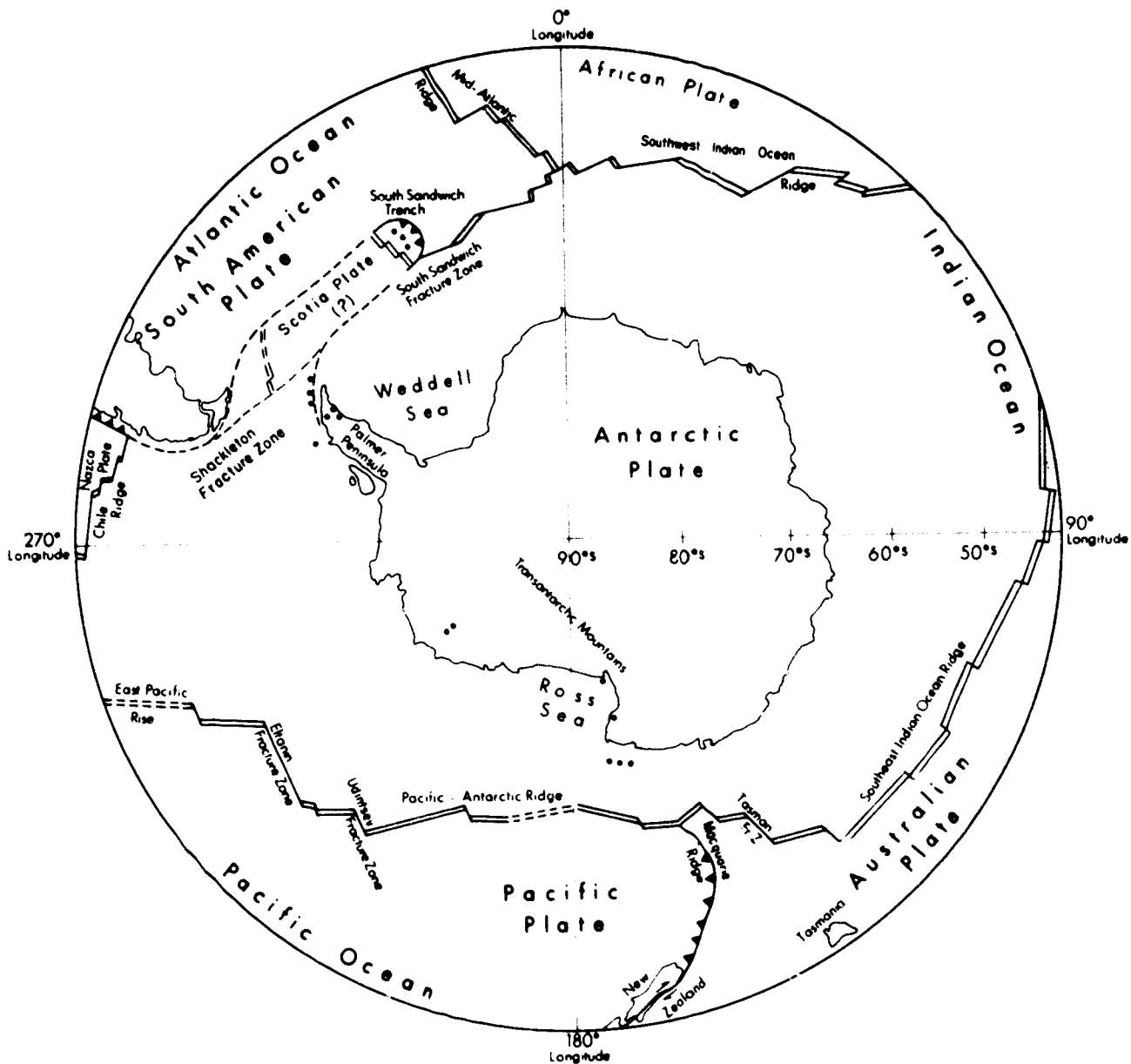
Figure 4C-1: Tectonic Activity Map, Centered on Equator

TECTONIC AND VOLCANIC ACTIVITY OF THE
ARCTIC REGIONS
(Last one million years)
Goddard Space Flight Center
1980
Paul D Lowman Jr

Orthographic
Projection Covering
Latitudes 40° to 90° North

Polar Scale

1100 Km (10⁸)
680 Miles
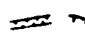
Active ridges and continental extensions,
minor transform faults generalized

Major active fault or fault zone, dashed
where nature or activity uncertain

Normal fault or rift hachures on
downthrown side

Reverse fault (subduction or overthrust
zone), barbs on upthrown side

Volcanoes active within the last
1 million years, generalized (some
isolated basaltic centers omitted)

Map labels:
Pacific Ocean
Pacific Plate
Aleutian Trench
Juan de Fuca Plate
Bering Sea
Sea of Okhotsk
Cherskiy Mtn
Verkhoyansk Mountains
Baikal Rift
Arctic Ocean
Nansen (Gakkel) Ridge
Ural Mountains
North American Plate
Hudson Bay
Greenland
Mohns Ridge
Scandinavia
Eurasian Plate
Reykjanes Ridge
North America
Atlantic Ocean
Alps
Black Sea
Eurasia

180° Longitude
270° Longitude
90° Longitude
0° Longitude
90°N 80°N 70°N 60°N 50°N

Figure 4C-2: Tectonic Activity Map, Centered on North Pole

4-16

TECTONIC AND VOLCANIC ACTIVITY OF THE
ANTARCTIC REGIONS
(Last one million years)
Goddard Space Flight Center
1980
Paul D Lowman Jr

Figure 4C-3: Tectonic Activity Map, Centered on South Pole

D. POSTSEISMIC CRUSTAL DEFORMATION

by

S.C. Cohen

OBJECTIVES

The postseismic crustal deformation study centers on the development of models of the time-dependent displacements, strains and stresses associated with earthquakes and postseismic rebound. The research objectives are the elucidation of the mechanisms for crustal deformation and the development of an improved understanding of regional and global geodynamic processes.

BACKGROUND

If the earth exhibited only elastic behavior in response to an applied stress and if slip occurred along a fault only at the time of an earthquake there would be no time-dependent postseismic effects. The displacements, strains and stresses would be governed by the elastic rebound occurring at the time of the earthquake and there would be no further adjustments. However, the earth behaves as an elastic body only on the time scale of an earthquake. Or a somewhat longer time scale flow occurs at certain depths within the interior. In particular the conditions in the upper layers of the mantle including the asthenosphere and lower lithosphere are such that creep should occur in response to an applied stress. This time dependent softening and flow of sub-crustal layers of the earth couples back to the more brittle and elastic surface resulting in geodetically significant time-dependent surface deformation. The details of the deformation depend on the rheological laws governing the rock creep, the geometry of the fault and the applied stress field. The model discussed below incorporates these fundamental controlling properties into an analytic and numeric description of how the earth deforms over time.

RECENT ACCOMPLISHMENTS

A numerical model of postseismic deformation associated with a shallow strike-slip source such as the San Andreas Fault is currently under development. The model represents the earth as a three-layer medium. The upper layer represents the brittle elastic portion of the lithosphere. Present in this layer is a vertical plane across which slip occurs at the time of an earthquake. The second layer extends from the bottom of the upper lithosphere to the top of the asthenosphere. The model takes the dilational or volumetric behavior of this layer to be elastic. The deviatoric or shear response is viscoelastic. The viscoelastic model is a three element solid consisting of an elastic element with rigidity, μ_a in series with a parallel combination of elastic (rigidity, μ_b) and viscous (viscosity, η) elements. The significance of this model is that it accounts for both instanteous, transient, and long term behavior of the viscoelastic layer. Specifically for a suddenly applied stress such as an earthquake, the substance is elastic with rigidity, μ_a. For slowly applied stress it is also elastic

but with a smaller rigidity, $\dfrac{\mu_a \mu_b}{\mu_a + \mu_b}$. This means the substance

can permanently support a portion of a suddenly applied stress
but creeps for partial relaxation. The third layer, the asthenos-
phere begins at the bottom of the lithosphere. Its dilational
rheology is elastic and deviatoric rheology is viscoelastic, the
viscoelasticity taking the form of a seris combination of elastic
(rigidity, μ') and viscous (viscosity, η') elements.

The numerical analysis is carried out using finite element
techniques. To date a two-dimension vertical cross section has
been used in the calculations with the displacements occurring
orthogonal to this plane. For the results discussed below the
following parameters have been used: upper lithosphere depth:
0-20 km, fault depth: 0-20 km, lower lithosphere depth: 20-75 km,
asthenosphere depth: 75-400 km, elastic and viscous parameters:

$$\mu=\mu_a=\frac{\mu_b}{4}=\mu'=5.10^{11} \text{ dyne/cm}, \eta=\eta'=5.10^{19} \text{ poise, fault slip} =\pm50 \text{ cm}.$$

The computed surface displacements are shown in Figure
4D-1. At the fault the coseismic displacement is 50 cm and there
is not postseismic displacement. At 100 km the coseismic
displacement is 7.5 cm and the postseismic adjustment adds another
6.5 cm of which somewhat more than 2/3 is due to asthenospheric
flow but a significant portion is also due to lower lithosphere
creep. At 500 cm, the coseismic displacement is only about 1 cm
but the postseismic creep contributes another 7 to 8 cm. In this
latter case it takes about 85 years to achieve 90% of the post-
seismic deformation whereas at 100 km it requires about 40 years.
These results depend on the assumed viscoelastic properties and
source geometry. An important implication is that it is not
necessary for the asthenosphere to be very close to the surface
to get appreciable postseismic readjustment following a shallow
earthquake. In fact the lower lithosphere creep may also produce
substantial surface deformation.

FUTURE EMPHASIS

Models of postseismic deformation have evolved in concept and
development to the point where it may now be possible to begin
making meaningful comparisons with observations. Since
long term geodetic data is most readily available for thrust
earthquakes it will be necessary to extend the present strike-
slip work to that case. In addition important questions concerning
the significance of nonlinear stress strain-rate, creep laws and
the existence of low rigidity fault zone materials must be
investigated. Finally, full three-dimensional models should
be constructed.

REFERENCES AND PUBLICATIONS

Cohen, S.C., "Postseismic Viscoelastic Surface Deformation and
     Stress 1," J. Geophys. Res., 85, 3131-3150, 1980.

Cohen, S.C., "Postseismic Viscoelastic Surface Deformation and
     Stress 2," J. Geophys. Res., 85, 3151-3158, 1980.

Cohen, S.C., "Relationships Among the Slopes of Lines Derived from
     Various Data Analysis Techniques and the Associated
     Correlation Coefficient," NASA TM 80733, 1980

Cohen, S.C., "Regional Analysis of Earthquake Occurrence and Seismic Energy Release," NASA TM 81994, 1980.

Figure 4D-1. Postseismic Displacements Versus Distance From Fault

4-21
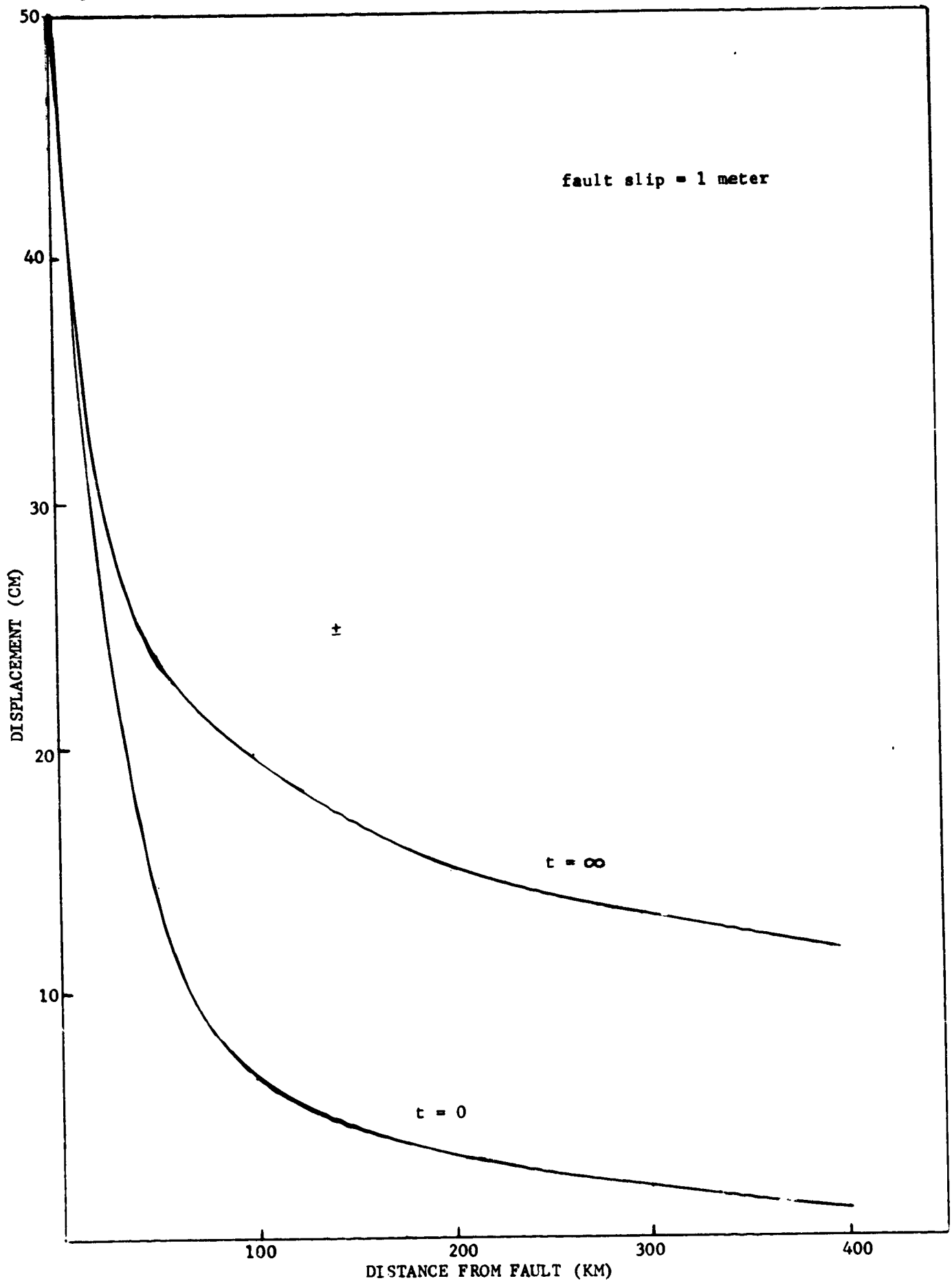
E.   MANTLE CONVECTION AND SUBCRUSTAL STRESSES UNDER THE
                         UNITED STATES

                              by

                         Han-Shou Liu

OBJECTIVES

Runcorn has developed a theory of mantle convection and pointed
out the significance of the subcrustal stress fields as inferred
from the geoid. By applying the laminar viscous flow model of
the earth mantle developed by Runcorn, Liu has endeavored to find
a band pass of harmonics from the satellite and surface gravity
data in the geopotential which would provide stress conditions
for the development of geodynamical features in Africa, Asia and
Australia. These stress conditions are due to mantle convection.
It is well known that the peculiarities of the geological and
geophysical features in the western United States are very
prominent. Therefore, it is desirable to apply these ideas and
methods to investigate the tectonic, metallogenic and seismological
provinces in the United States and shown how many of their
features are in accordance with crustal deformation associated
with stresses due to mantle convection.

BACKGROUND

One of the most convincing surface expressions of mantle plumes is
in the western United States. According to the mantle plume
hypotheses, the rising mantle convection currents are supposedly
concentrated in the mantle plume beneath the Yellowstone Park
region. A theoretical model of mantle plume is shown in Figure
4E-1. At the top of the plume, the flow becomes horizontal and
outward from the center of the plume forming the asthenosphere, a
layer of low viscosity near the top of the mantle. The velocity of
the radial flow in the asthenosphere must be zero above the center
of a radially symmetrical plume, increasing outward to a maximum
at a radial distance similar to the radius of the plume. At great
distances from the plume the velocity of the radial flow decreases
asymptotically to zero. The unknown viscosity and density variations
within the plume and probable variations in the plume radius with
depth and in the asthenosphere thickness with the distance from the
plume make it impossible to construct any accurate and reliable
flow model. However, one may assume that the horizontal component
of the mantle flow in the asthenosphere is purely radical with zero
velocity above the center of the plume and inversely proportional
to the radial distance at great distances from the plume and with
one maxima at an intermediate distance.

The horizontal radial flow near the top of a mantle plume exerts
stresses on the lower lithosphere. The velocity of this flow is a
function of the distance from the center of the plume. The radial
stress in the crust will be tensional over the plume but compressional
outside the plume, while the tangential stress is tensional throughout
the whole region of the radial flow (see Figure 4E-1). If both

radial and tengential stresses are tensional, as above the plume, the surface deformation will be related to normal faults. High volcanic acitvity is expected but only small earthquakes will occur because of the low tensile strength of crustal rocks. When the radial stress is compressional and the tangential stress is tensional, as in areas outside of the plume, the ground deformation will be largely associated with strike slip faults. Volcanic activity is expected to be low; but large earthquakes will occur because of the relatively great shear strength of crustal rocks.

RECENT ACCOMPLISHMENTS

A fundamental question about the hypotheses of mantle convection plume is the observation of mantle convection pattern under the United States. Can one establish a flow pattern or stress field by observational methods under the crust of the United States which can fulfill the above criteria? The convection generated stress field as inferred from gravity data (Figure 4E-2) seems to provide evidence for such hypotheses of mantle plume.

SIGNIFICANCE

The subcrustal stresses in the interior of the United States are large enough to cause isolated zones of persistent and potentially hazardous seismicity. Seismicity in the western and eastern United States may be influenced by the presence of subcrustal stress concentration in the unhealed fault systems. From a dynamic point of view, areas of stress concentration in the crust can be identified if the subcrustal stress fields and fault systems in a particular region are known. This can be done by applying stress analyses and photoelastic experiments.

The secular strain change ellipses for seven strainmeter sites in the western United States are shown in Figure 4E-3. These secular strain change ellipses are consistent with maximum extension in a northwest-scutheasterly direction. The similarity of ellipse orientation at seven sites may not be fortuitous, it may indicate a coherent strain field caused by the upwelling mantle convection cell under the western United States. Maximum extension at sites from Number 1 to Number 6 seems to represent the tangential tension outside the mantle plume. But maximum extension at Number 7 appears to be related to the radial tension over the upwelling convection cell.

The tectonic model of the Pacific plate moving northwest relative to the North American plate implies that the regional stress in California should be simple shear across the fault plane of the San Andreas striking N45°W. This is equivalently equal components of north-south compression and east-west tension. However, strain accumulation at seven sites in southern California from 1972 to 1978 obtained by seismologists has shown a remarkable consistent uniaxial north-south contraction of about 0.3 per part per million per year, the expected east-west tension is absent. Why does the component of the east-west extension disappear, in opposition to the associated considerable stresses, to form such a state of uniaxial north-south contraction? The results of satellite determination of subcrustal stresses (Figure 4E-4) has shown that the subcrustal stress field under the San Andreas fault in California is in the

S45°W direction or equivalently equal parts of north-south contraction and east-west compression. Therefore, the measured uniaxial north-south contraction could be formed by the superposition of two stress systems, the north-south contraction and east-west tension associated with the Pacific-North American plate boundary plus the north-south contraction and east-west compression of the subcrustal stress system caused by mantle convection. In this case, the north-south components of the stresses from both stress systems would provide the necessary contraction and the east-west component of compression from the convection generated stress field just cancels the east-west extension associated with the drift of the Pacific plate. If this interpretation is correct, the remarkable upwelling convection cell under the western United States (see Figure 4E-2) may have profound influence on the state of stress along the San Andreas fault in California.

FUTURE EMPHASIS

The concept of ultimate mantle control, via zones of crustal weakness, on the distribution of ore deposits will be verified by satellite gravity data. A geodynamical basis for the future exploration of mineral deposits will be found and this can probably be attained by considering the known ore deposits in the context of their tectonic settings influenced by the mantle disturbance persisting through long periods of geological time.

REFERENCES AND PUBLICATIONS

Liu, H.S., 1980. "Mantle Convection and Subcrustal Stresses under the United States," _Modern Geology_, 7, 81-93.
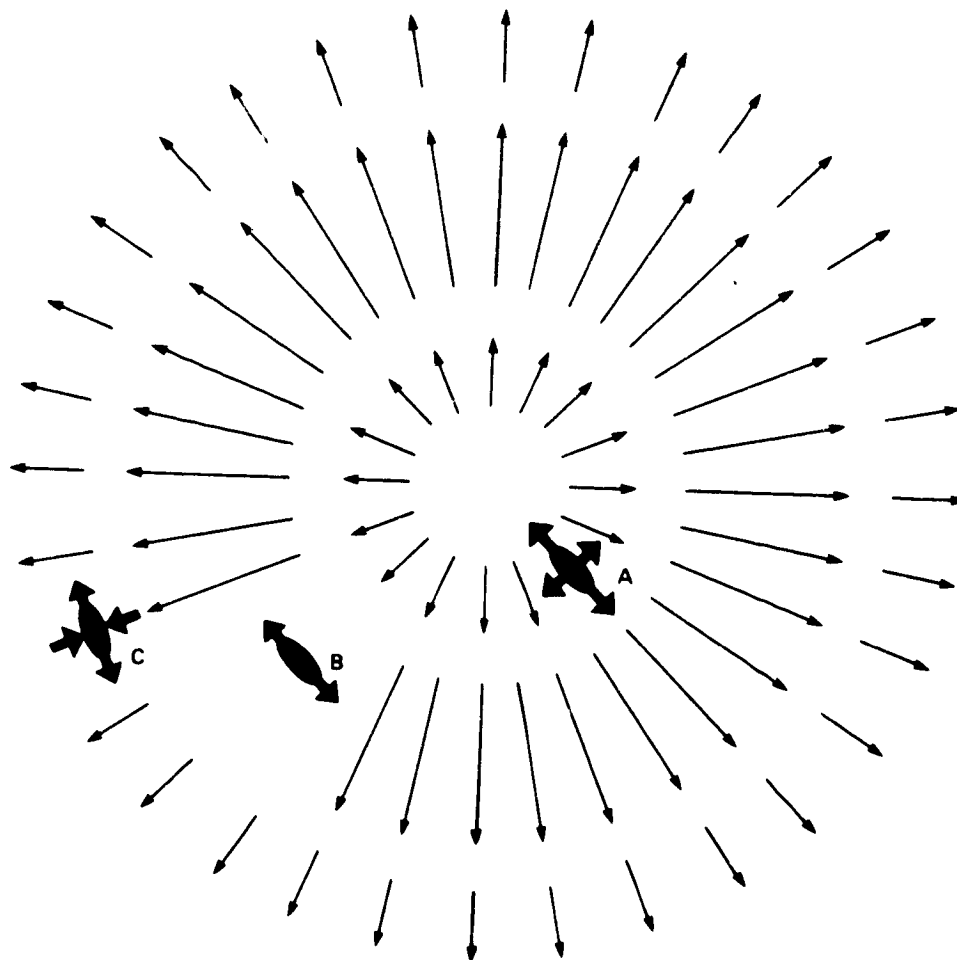
A. RADIAL AND TANGENTIAL TENSION
B. TANGENTIAL TENSION ONLY
C. RADIAL COMPRESSION AND TANGENTIAL TENSION

Figure 4E-1.   Radial and tangential tension and radial
compression in the crust caused by the
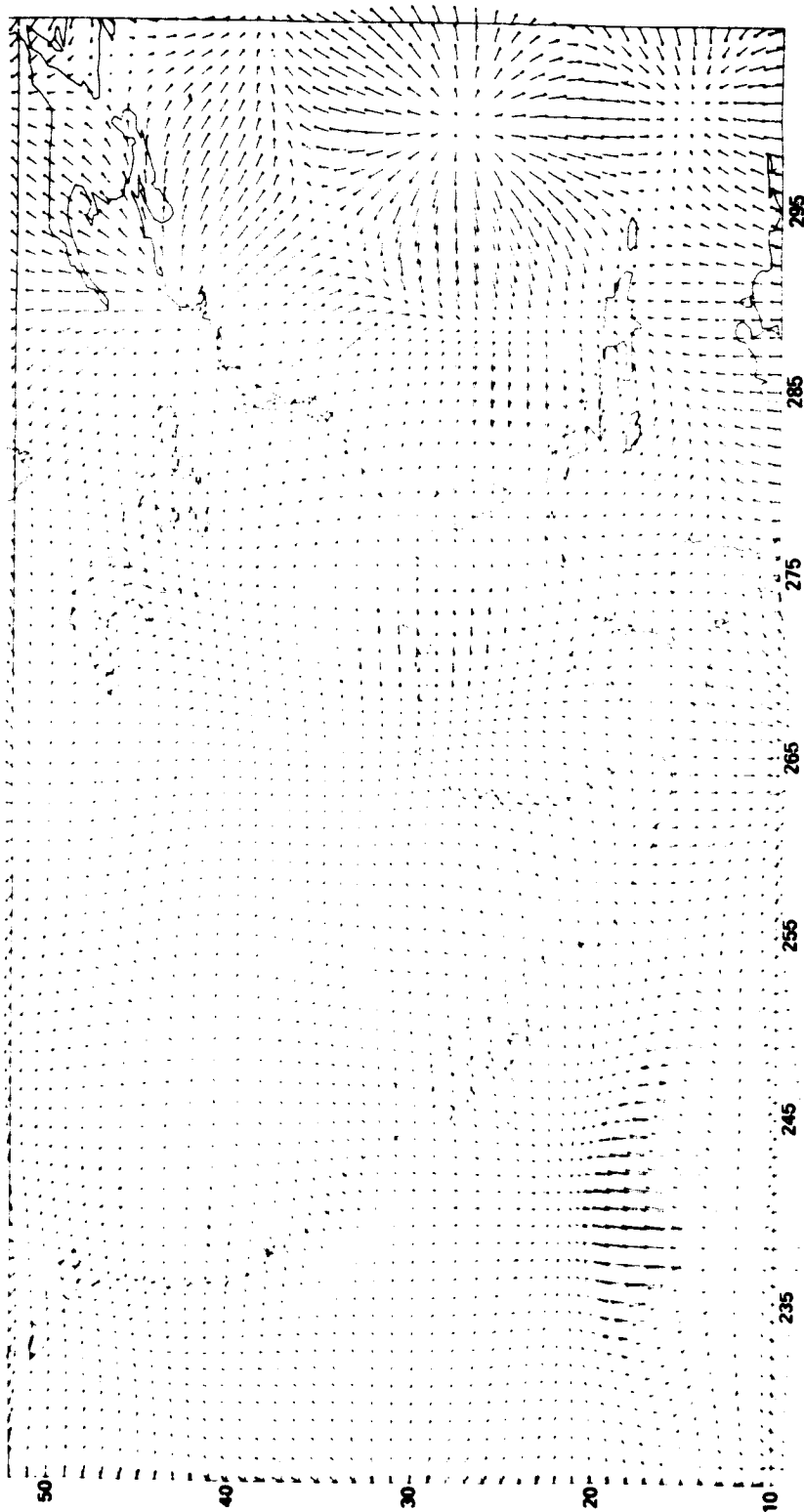upwelling mantle convection plume.

4-25

Figure 4E-2. Convection generated subcrustal stress fields under the United States inferred from the band pass of harmonics $(13 \leq n \leq 25)$ in the Geopotential.

Figure 4-3. Convection generated subcrustal stress fields and secular strain change ellipses from strainmeter data. 1. Stone Canyon Geophysical Observatory, California (Bufe, et al., 1973), 2. Parkfield-Cholame Network, California (Cherry and Savage, 1972), 3. Scotty's Junction, Nevada (Kumamoto, 1973), 4. Sleeping Mountain, Nevada (Kumamoto, 1973), 5. Round Mountain, Nevada (Malone, 1972), 6. Nuclear Test Sites, Nevada (Smith and Kind, 1972; Thompson and Burke, 1973), 7. Salt Lake City, Utah (Anderson, 1972).
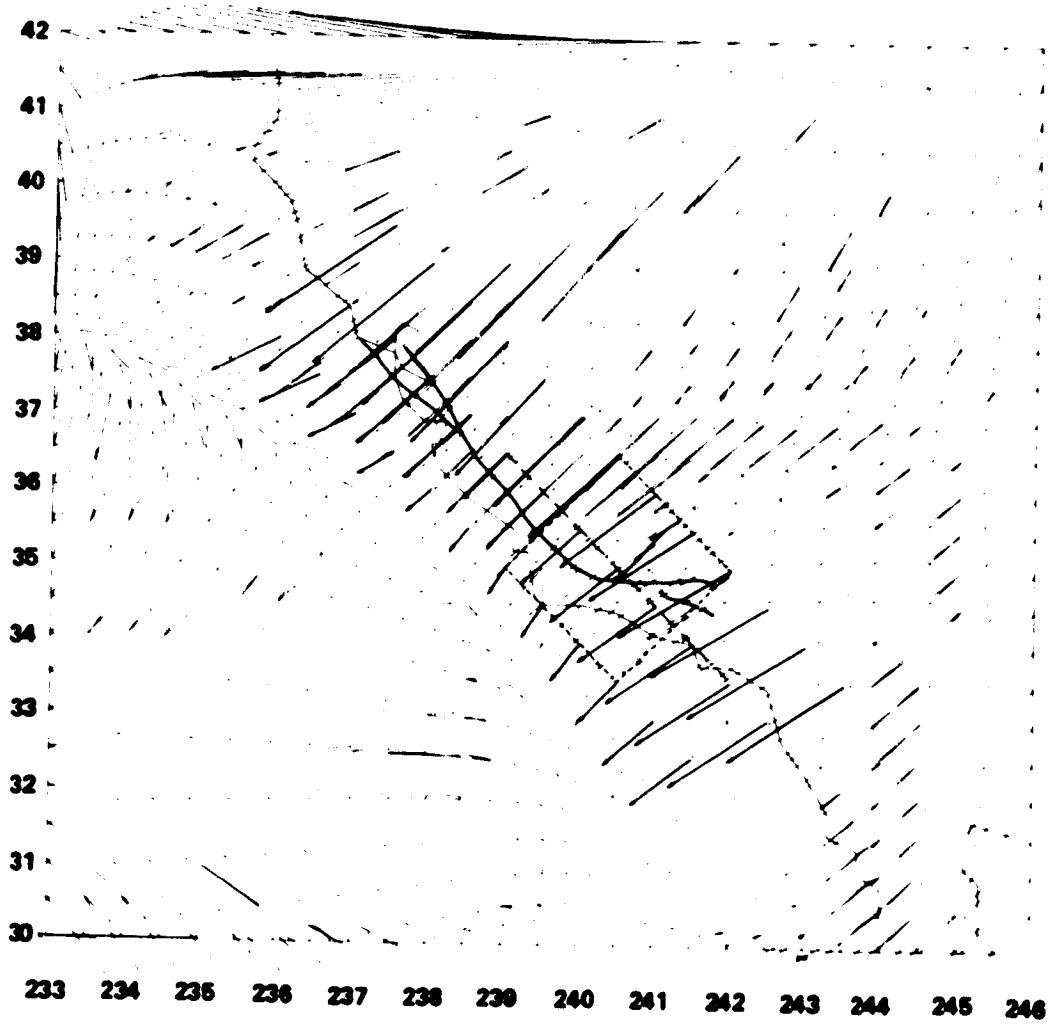
Figure 4E -4. Compressional stress field due to mantle convection
under the San Andreas fault systems.

F. CRUSTAL STRUCTURE AND DYNAMICS OF SOUTHEASTERN U.S.

by

R.J. Allenby and M.A. Mayhew

OBJECTIVES

The primary objective of this effort is to develop structural and tectonic models of the southeastern United States through a synthesis and re-interpretation of seismic, gravity, and magnetic data.

BACKGROUND

A knowledge of the thickness, composition and dynamic stability of the Earth's crust is critical to locating geodetic sites for NASA's crustal dynamics project, interpreting and modeling gravity and magnetic satellite data. We are initiating such a crustal study in the southeastern U.S. by re-interpreting deep refraction data obtained by the 1965 East Coast Onshore-Offshore Experiment (ECOOE), a cooperative effort that involved 11 participating institutes and obtained over 1100 records from a shot and station array covering portions of Maryland, Virginia, West Virginia, North Carolina, South Carolina, Georgia, Tennessee and Kentucky.

The accuracy of the initial interpretation of these results by James et al., 1968, was reduced by his assumption of a simple, one layer crust above the Moho--an assumption we now know to be erroneous. Since then a substantial body of new refraction data has been collected, improved velocity models based on surface wave dispersion studies have been constructed, and long wavelength satellite gravity and magnetic results have become available. We propose to carry out a limited synthesis of these data, something that has not hitherto been done.

RECENT ACCOMPLISHMENTS

A computer program for inverting P_n phase travel times to a 2-layer crustal thickness model using a modified time-term approach is operational, and some initial results using a selection of ECOOE data have been obtained.

The program performs an initial weeding of the shot-station pair travel term data, eliminates redundant site locations, then performs a least squares inversion by a standard method which gives a solution for upper and lower crustal thicknesses (two parameters per site) which minimizes the sum of squared travel time residuals for an assumed pair of crustal velicities. Mantle velocity is taken to be 8.10 km/sec., given by a straight line fit to the regional travel time graph. An initial program has been extensively modified to reduce computer core requirements and permit inclusion of all available data for the region in the analysis.

The methodology leads to stable solutions for crustal layer thicknesses which are reasonable and systematic for certain assumed velocity pairs. Selection of a final model will be based on statistical criteria, and on comparisons with regional gravity data and results of individual seismic lines.

Present efforts are directed toward supplementing the ECOOE data with P_n data from earthquakes, and toward developing software for computer plotting of results and for gridding, contouring, and modeling gravity data.

A regional structure/density model will permit construction of static stress models, and will form a basis for modeling crustal magnetization using Magsat data.

FUTURE EMPHASIS

Because of funding limitations, activity on this project will be considerably reduced and will concentrate on the area of the original ECOOE survey. Ground based and satellite geophysical data peripheral to the ECOOE area will be incorporated into the model as time and funds permit.

REFERENCES AND PUBLICATIONS

James, D.E., T.J. Smith and J.S. Steinhart, "Crustal Structure of the Middle Atlantic States," Jour. Geophys. Res., 73, 1983-2007, 1968.

Hales, A.L., "The East Coast Onshore-Offshore Experiment, I. The First Arrival Phases," Air Force Office of Scientific Research, Contract AF49(638)-1542, March 1967,

CHAPTER 5

GRAVITY FIELD MODEL DEVELOPMENT

edited by

W.D. Kahn

OVERVIEW

Knowledge of the earth's gravity field is fundamental to understanding the dynamics of the earth. For solid earth physics, knowledge of the variations in the gravity field provides information on the earth's physical properties and geodynamic processes and places constraints on the internal structure of the earth. In oceanography, knowledge of departure of the actual sea surface from a unique equipotential surface of the earth's gravity field (the geoid) can reveal information on oceanic circulation. In addition, other areas which benefit from knowledge of the earth's gravity field are satellite orbit determination and classical geodesy.

This chapter describes: (1) a special investigation on the cause of the force which causes a decrease in the semimajor axis of the Lageos satellite's orbit and to model it in the Geodyn program; (2) current and future capabilities of the Geodyn program are discussed. In particular, work to be performed for using this program as the analysis tool in support of the Gravsat mission, and (3) the successful development of a specialized gravity field model which has improved the accuracy of Seasat-1 orbits. Such improvement in the Seasat-1 orbits will result in more effective utilization of Seasat altimetry by the user community.

A.   UNEXPLAINED LAGEOS PERTURBATIONS

by

D.P. Rubincam

OBJECTIVE

The purpose of this work is to find the cause of the force which is decreasing the semimajor axis of Lageos' orbit, and to model it in the Geodyn program.

BACKGROUND

The semimajor axis of Lageos' orbit is decreasing at the rate of 1.1 mm day^{-1} (see Fig. 5A-1) due to an unknown force. It is important to understand and model this force so that Lageos can be used to make high precision measurements of plate motion and other geophysical phenomena.

Last year atmospheric drag from a combination of neutral and charged particles was singled out as the probable cause of the orbital decay. This conclusion was based on two factors. The first was that there may be substantial quantities of neutral helium at Lageos' altitude, which helps explain the drag on Lageos and the "helium problem" of accounting for the escape of helium from the earth's atmosphere. The second factor was that the observed rate of orbital decay fell within the limits of uncertainty of the rate predicted by various theories of charged particle drag. However, the charged particle drag calculation depended strongly on the charged particle number density at Lageos' altitude, and the voltage on Lageos, as well as the theory used. Since these were not well known or well understood, the calculation was not very satisfactory.

RECENT ACCOMPLISHMENTS

Recent work has focused on reducing these uncertainties in the calculation of charged particle drag on Lageos.

The charged particle number density at Lageos' altitude is now reliably known, it is about 2×10^9 particles m^{-3}, and consists mostly of hydrogen ions (Chappell, et al., 1979).

Charged particle drag on small charged spheres has been measured in the laboratory by Knetchtel and Pitts (1964). Their experiments give an empirical equation relating the drag to the charge particle number density and the voltage on the satellite. This approach removes the need to rely on the theories of charged particle drag, all of which disagree with each other.

The new charged particle drag calculation using this new information shows that it accounts for at least 61 percent of the observed drag. And since neutral hydrogen accounts for about another 10 percent, at least 71 percent of the observed orbital decay can be atributed to atmospheric drag from a combination of neutral and

charged particles. If it explains this much of the decay, then this mechanism probably accounts for all of the decay. This is because the estimate of charged particle drag may be slightly conservative, and because neutral helium may be a significant source of drag.

In summary, it appears that the unknown force acting on Lageos is in fact atmospheric drag from a combination of charged and neutral particles. A detailed discussion is reported in Rubincam (1980a, 1980b). A similar conclusion was reached by Afonso et al. (1980).

SIGNIFICANCE

The atmospheric drag force can be modeled as a force with a constant magnitude and a direction opposite to that of the satellite's velocity vector. It has, in fact, been so modeled in the Geodyn orbit determination program. This will allow other smaller perturbations to be looked for, such as those due to general relativity, as well as permit accurate geophysical investigations to be done with Lageos.

FUTURE EMPHASIS

Future work will focus on the continued monitoring of the decrease in the semimajor axis of Lageos' orbit, and possibly smaller perturbations coming from other sources, such as general relativity.

REFERENCES AND PUBLICATIONS

Afonso, G., F. Barlier, C. Berger, and F. Mignard, "Effet du Freinage Atmospherique et de la trainee electrique Sur la Trajectoire du Satellite Lageos," C.R. Acad. Sc. Paris, 290B, 445-448, 1980.

Chappell, C.R., K.K. Harris, and G.W. Sharp, "A Study of the Influence of Magnetic Activity on the Location of the Plasmapause as Measured by OGO 5, J. Geophys. Res., 75, 50-56, 1970.

Knetchtel, E.D., and W.C. Pitts, "Experimental Investigation of Electric Drag on Satellites," AIAA J., 2, 1148-1151, 1964.

Rubincam, D.P., "Atmospheric Drag as the Cause of the Secular Decrease in the Semimajor Axis of Lageos' Orbit," Geophys. Res. Let., 7, 468-470, 1980.

Rubincam, D.P., "On the Secular Decrease in the Semimajor Axis of Lageos' Orbit," NASA TM 80734, Goddard Space Flight Center, Greenbelt, MD 20771, July 1980. (Submitted to Celestial Mechanics).

Samir, U., "Large Space Vehicles-Platforms for Second Generation in-situ Wake Observations," J. Astronaut. Sci., 20, 347-369 1973.

Samir, U., L.H. Brace, and H.C. Brinton, "About the Influence of Electron Temperature and Relative Ionic Composition on Ion Depletion in the Wake of the AE-C Satellite, Geophys. Res. Let., 6, 101-104, 1979.

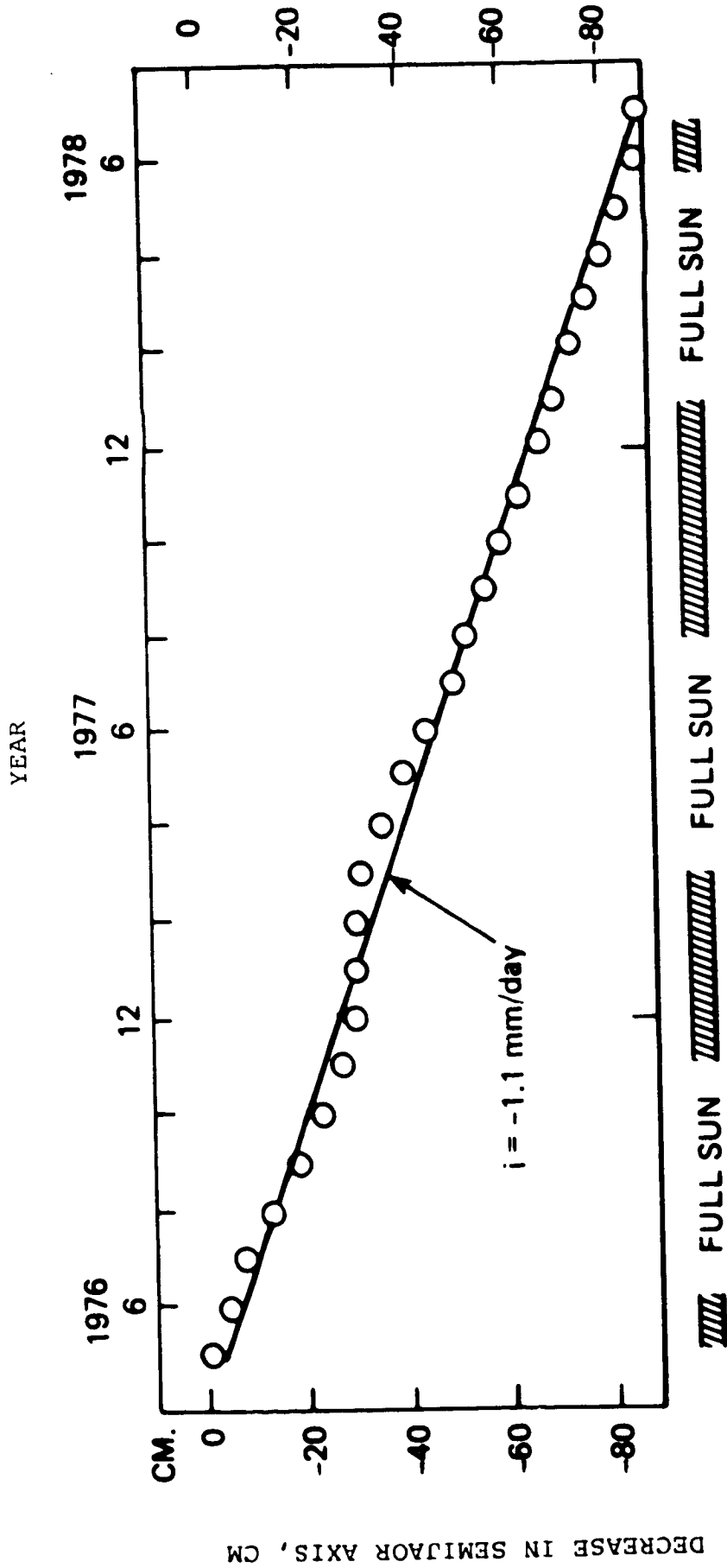FIG. 5A-1. The secular decrease in the semimajor axis.

i = -1.1 mm/day

FULL SUN   FULL SUN   FULL SUN   FULL SUN

YEAR

DECREASE IN SEMIJAOR AXIS, CM

5-4

B. GEODYN PROGRAM SYSTEMS DEVELOPMENT

by

B.H. Putney

OBJECTIVES

The purpose of the Geodyn Orbit Determination and Parameter Estimation Program is to recover geodetic and geophysical parameters from satellite data in a state-of-the-art manner.

BACKGROUND

In 1971 the Noname and Geostar programs were combined to form the Geodyn program. The philosophy of the development has been to mold the program very carefully to maintain computer efficiency and good program structure, appropriate orbit and earth modeling, precise satellite measurement modeling, efficient numerical procedures and careful benchmarking. This care has paid off in the production of several GEM's (Goddard Earth Model) precise station locations, improved tidal, GM, and polar motion values, consistent baseline determinations. Careful usage and modeling using laser, altimeter and other satellite data from the GEOS satellites, BE-C, Starlette, Lageos and Seasat satellites as well as many others has allowed these accomplishments.

RECENT ACCOMPLISHMENTS AND SIGNIFICANCE

The Seasat operational orbits were determined this year. The new time-dependent drag coefficients proved to be very useful. A new data type, altimeter crossovers, was introduced.

The Crustal Dynamics work has required Geodyn to handle many thousands of observations routinely. Since there are so many observations, sampling residual printout has become an important option.

In support of Gravsat and the Gravsat simulation, many changes had to be made to Geodyn and many more will have to be incorporated in the future. We needed dynamic allocation of gravity anomalies, surface densities and a new parameterization "geoid heights." A new Global Positioning System (GPS) data type has been introduced. Provision needed to be made for blocks less than 1° in the localized gravity parameterization. An analysis of internal numerical procedures such as stepsize and critical angle was required. In addition, a checksum for the gravity parameterization was needed by the analysts. A preliminary report entitled, "Techniques for Reduction of Computer Requirements for Gravsat Normal Equation Generation," was generated.

In the general area of modeling, the Jacchia 77 model has been implemented as well as a revised, solid-earth tidal model and general relativity model. The program now integrates in coordinate or ephemeris time instead of atomic time so that relativity can be properly modeled.

A software package is being developed to create normal equations from observational equations. This additional flexibility will be very important for future production work. Another important area has been the rewriting of Geodyn for a vector or parallel processor. Meetings are being held to plain this future activity.

One major version GDYN8006 has been released this year. Documentation in the mathematical and user guid areas has been updated for Geodyn and documentation of the Table Update Program has been created. GSFC has actively supported Geodyn users at JPL, Ohio State University and the Netherlands. Conversion of Geodyn to the Fortran Q compiler has given preliminary CPU reduction of more than 30%.

In the software development, we have tried to be responsive to the current needs. Geodyn is a very complex program, consequently, all modifications are difficult. As we handle so many observation data types and complex earth models any modification in one area causes problems to the other areas. At times, the modifications seem to come slowly and with limited resources, progress is even more difficult. Despite these problems, the program has performed well.

FUTURE EMPHASIS

With the anticipation of the Gravsat mission large local gravity type parameter solutions require many modifications to Geodyn. The local representations of gravity anomalies, surface densities and geoid heights must be made computer efficient. The order that these parameters are stored in core becomes very critical from a software point of view. The current numerical techniques for computing the accelerations from these parameters is not adequate. The resultant step function needs to be smoothed for accurate orbit determination. Since these are local representations, it is probable that the entire earth need not be used at each integration step. This approximation needs to be introduced as an option. This local property suggests using banded matrices for the parameter estimation. In addition, blocks smaller than one degree must be accomodated. The accuracies required in these solutions, will require close examination of other program approximations.

It is now desirable to allow the square root matrix inversion technique as an option in the Geodyn system. Both the Keplerian and nonsingular elements need to be included in the partitioned normal equations. A restart or continuation capability within a single arc would allow arcs to be created in pieces just as the normal equations allow the solutions to be produced in reasonable subsets.

By mid-1982, the 360/95 is scheduled to be phased out. This computer has been the most heavily utilized computer of the Geodynamics Branch and because of the phase out and other future requirements, the Geodyn program needs to be studied for the conversion to a vector or parallel processor. Part of this study should be a document, containing the current modes of operation in the branch and how the CPU and I/O is useful in each case. The Boole and Babbage Analyzer is very useful for these analyses. The subroutines of the program that are used the most can be identified for further study and it can be determined which sections of the program can benefit from the redesign.

It is also required that a document be written outlining the planned approach for the conversion, containing milestones, manpower required, and identifying areas requiring further investigations. The important Gravsat modifications need to be identified and implemented.

C. IMPROVED GRAVITY MODEL FOR SEASAT

by

F.J. Lerch

OBJECTIVE

The objective is to improve the gravity field model of the earth to reduce orbit error on Seasat for more effective use of the spacecraft altimetry. Seasat altimetry (± 10 cm) requires precise knowledge of the radial position of the satellite for oceanographic applications (e.g., tides and ocean circulation).

BACKGROUND

Seasat orbits have been computed independently by both NSWC (Malyevac and Colquitt, 1980) and GSFC for applicatons with altimetry in the Seasat project. Comparison of these orbits (Marsh and Williamson, 1980), have shown that their differences in radial position correspond through power spectral analysis to errors in the gravity field. The GSFC orbits were based upon a gravity field (Lerch, et al., 1979) that employed data from the GEM models and only ground tracking data (laser and S-Band) from Seasat which excluded the altimeter data. Since comparison with altimeter data (Table 5C-2) indicated that the GSFC orbits could be improved, a new gravity field model employing Seasat altimetry in the solution was derived. Although altimetry may be used to derive the gravity field the Seasat project requires that the orbits for the experimenters be derived directly from ground tracking data only (laser and S-Band). Orbits being tested below conform to this requirement. The gravity models developed are specialized fields designed specifically to improve the Seasat orbits and are not intended for generalized usage with other satellites.

RECENT ACCOMPLISHMENTS

The development of the new gravity model, PGS-S4 (Lerch, et al., 1980), where altimetry data has recently been added is based upon an extension of the previous Seasat gravity models PGS-S1, S2, and S3 (Lerch, et al., 1979). The data employed for these models is shown in Table 5C-1. Laser and S-Band data from Seasat was spread over a 3-month lifetime on the spacecraft altimetry. Harmonic analysis (Kaula, 1966) was performed to select the gravitational terms in the models which are important for Seasat orbits. Orbital position perturbations were computed using Kaula's rule for the size of the coefficients and results are presented in Figure 5C-1 for harmonics through degree and order 36. Perturbations above the solid black line, practically all greater than 10 cm, were included in the adjustment of the gravity field. Although the recovery of the coefficients is based upon the total position perturbations of Figure 5C-1, which are mostly due to the alongtrack component, it is the radial component which is needed for accurate reduction of the satellite altimetry.

TABLE 5C-1. DATA EMPLOYED MODELS FOR SEASAT

PGS-S1 DATA = GEM 9 + SEASAT LASER

PGS-S2 DATA = GEM 9 + SEASAT (LASER + S-BAND)

PGS-S3 DATA = PGS-S2 + GLOBAL GRAVIMETRY AND ALTIMETRY (GEOS-3)

PGS-S4 DATA = PGS-S3 + SEASAT ALTIMETRY

GEM 9 DATA

Type	No. of Obs.	No. of Satellites	No. of Arcs	Harmonics Complete
optical	150,000	24	287	16 x 16
electronic	477,000	11	97	16 x 16
laser	213,000	9	127	22 x 22

SEASAT DATA

laser	16,5000	1	8	30 x 30
S-Band	5,±00	±	8	30 x 30

TABLES 5C-2. ORBIT ANALYSIS EMPLOYING A GLOBAL COVERAGE COVERAGE OF ALTIMETER CROSSOVERS ON SEASAT

MODEL	CROSSOVER RESIDUALS	ORBIT ERROR
PGS-S1	3.0 m	2.1 m
PGS-S2	2.5	1.8
PGS-S3	1.9	1.3
PGS-S4	1.2	0.8
NSWC	1.45	1.0

5-9

FIGURE 5C-1. PERTURBATIONS FROM SEASAT FOR HARMONICS THROUGH 36 X 36

(UNITS ARE CM)

••• > 999 CM

HARMONICS ABOVE SOLID LINE INCLUDED IN SOLUTION

5-10

Radial perturbations (Lerch, et al., 1979), being significantly smaller than the total perturbation, are modeled down to a few centimeters in the adjusted set of harmonic coefficients.

In PGS-S1 and S2 the solution is based upon satellite data only and the harmonics, solid through 30 x 30, are not completely separate (ill-conditioned) in a normal least squares adjustment, where only noise is minimized in the residuals. Tp achieve separability (that is a solution for all the harmonics) least squares collocation (Moritz, 1978) was employed where both noise and signal are minimized collectively. The analysis for this method of solution is given in the above referenced report for Seasat. However, in the case of PGS-S3 where GEOS-3 altimetry and surface gravity data are combined with PGS-S2, the normal least squares method gives a well-conditioned solution (GEM 10B plus Seasat data). As with GEOS-3 orbits this latter type of solution (PGS-S3) gave better radial positions for the Seasat orbits. PGS-S4 was formed by adding Seasat altimeter data to PGS-S3, where the altimetry provides direct observations for the satellite dynamical height perturbations.

Seasat altimetry data was employed to estimate the accuracy of the radial position of Seasat orbits with use of the different gravity models. This technique is based upon the condition that at the crossover point of two altimeter tracks the difference in the altimeter measurements is equal to the difference in the radial position of the orbits. The difference in these two quantities is called the crossover residual which should be zero expect for errors in the orbits and small effects from altimeter noise or sea state changes. Here it will be assumed that the residuals are due to errors in each of the two crossing orbits. A global set of 8000 altimeter crossover points were taken over a 12-day period of Seasat altimetary. The rms of the crossover residuals were computed and are given in Table 5C-2, where it is seen that the PGS-S4 model gives the best results with orbit errors of less than one meter.

SIGNIFICANCE

Orbit errors on Seasat have been reduced from 3m with GEM 9 (Lerch, et al., 1979) to 0.8 m with PGS-S4. For the first time, as based upon the altimeter crossover results of Table 5C-2, the GSFC orbits show improvement over the NSWC orbits. GSFC orbits are dynamically computed over 3-day arcs whereas NSWC orbits are computed over two-revolution arcs.

FUTURE EMPHASIS

It is desirable to reduce the orbit error on Seasat to an accuracy of better than 10 cm for altimeter application. NSWC is planning to improve their Seasat orbits with their Doppler tracking system. In PGS-S4 only 8 days of Seasat altimetry was employed as a test case and it is planned to use altimeter data in a new solution to cover the 3-month lifetime period.

REFERENCES AND PUBLICATIONS

Kaula, W., Theory of Satellite Geodesy, Blaisdell Publishing Company, Waltham, Massachusetts, 1966.

Lerch, F.J., S.M. Klosko, R.E. Laubscher, and C.A. Wagner, "Gravity Model Improvement Using GEOS-3 (GEM 9 and 10)," J. Geophys. Res., July 31, 1979; and GSFC X-921-77-246, 1977.

Lerch, F.J., C.A. Wagner, S.M. Klosko, R.P. Belott, R.E. Laubscher, and W.A. Taylor, "Gravity Model Improvement Using GEOS-3 Altiemtry (GEM 10A and 10B)," presented at the Spring Meeting of the American Geophysical Union, Miami, Florida, April 1978.

Lerch, F.J., J.G. Marsh, "Gravity Model Improvement for Seasat," presented at the Spring American Geophysical Union Meeting, Washington, DC May 1979.

Lerch, F.J., J.G. Marsh, S.M. Klosko, and R.G. Williamson, "Gravity Model Improvement for Seasat," J. Geophys. Res., in publication.

Malyevac, C.W., and E.S. Colquitt, "NSWC Doppler Computed Seasat-1 Orbits," Journal of the Astronautical Sciences, October-December 1980.

Marsh, J.G. and R.G. Williamson, "Precision Orbit Analyses in Support of the Seasat Altimeter Experiment," The Journal of the Astronautical Sciences, October-December 1980.

Moritz, H., "Least Squares Collocation," Review of Geophysics and Space Physics, Vol. 10, No. 3, August 1978.

CHAPTER 6

GLOBAL EARTH DYNAMICS

edited by

D.P. Rubincam

OVERVIEW

The physics of the earth may be studied in a global sense as
well as in a regional sense. In some cases, the entire earth
participates in geophysical phenomena,compelling a global
viewpoint; an example is polar motion. In other cases, global
studies provide a perspective on the physics of the earth which
regional studies cannot; an example is the study of the earth's
external gravity field in relation to tectonically active areas.

The association of the Earth Survey Applications Division with
satellite orbit determination has emphasized the analysis of
satellite-derived data which give information on the earth's
global structure and dynamics. In this chapter, the results of
studies of the satellite-derived gravity field and polar motion
are presented. These studies range from the earth's internal
density structure to mantle convection to the track of the pole.

A. CONVECTION GENERATED STRESS FIELD AND INTRA-PLATE VOLCANISM

by

Han-Shou Liu

OBJECTIVES

Although most of the earth's volcanism occurs at or adjacent to plate boundaries, volcanic activity has occurred within plates, which cannot be associated with plate margin processes. The objective of this investigation is to determine the distribution of the intra-plate Cenozoic volcanism and how it is related to the convection generated tension stress field in the lithosphere.

The products of Cenozoic volcanism are widely spread in both oceanic and continental areas. In the ocean regions, our knowledge is limited. Further complexity arises as many of the islands lie on or near crustal structures associated with spreading and subduction plate boundaries and cannot be defined as intra-plate volcanism, we shall concentrate on the discussion of continental volcanism in the Western United States, Australia, Asia and Africa.

BACKGROUND

The subcrustal basalt magma is quite incapable of breaking through to surface under its own power, unless wide open fissures are available to it as channels along which it can rise. This raises the question of how such abyssal fissures, of whose existence there can be no doubt, have their origin.

Basaltic volcanism is a feature common to most rifts. In basaltic fissure eruptions, the fact that the emission of magmatic materials begins immediately when the fissure is opened, indicates that this opening takes place from below and works its way upwards, and that the magma penetrates into the fissure almost instantaneously. It thus follows that the tensional forces which cause the formation of fissures originate at the lower surface of the earth's crust. The reason for such tensional forces must thus be sought, not in the crust itself, but in its substratum. In this subcrustal zone, displacements of material can apparently occur which cause sufficiently strong tension in the overlying crust to overcome the tensile strength of the crustal material

In principle, four different types of movement in the substratum may cause tension in the overlying crust. These types of movements are illustrated in Fig. 6a-1. The first is an accelerating, horizontally directed current, which is transmitted by friction to the overlying crust and causes tension in the direction of flow. Secondly, if an ascending current splits into bilateral or centrifugal branches, these will obviously exert tensional force upon the overlying crust. Thirdly, horizontal and parallel currents of differing velocities will set up torsional forces in the crust, which will give rise to the opening of fractures lying obliquely to the direction of flow. Fourthly, a uniform but diverging current may likewise cause tensional fractures, which in this case will be parallel to the direction of flow.

Fissures which are formed in the lower parts of the earth's crust cannot remain open and gaping, since the crustal materials are plastic under high pressure and so the fissure will soon close up again. When the fissure originates at the base of the crust, or even below it, in the substratum, and penetrates upwards, the intruding magma not only keeps the fissure open, but wides it further by virtue of its own hydrostatic pressure. It is a necessary condition for the formation of all these abyssal fissures that the tensional forces should be able to overcome the tensile strength of the material concerned within a shorter period than its relaxation time, whether it should be subcrustal magma (with a relaxation time of thousands of years), or crustal rocks.

RECENT ACCOMPLISHMENTS

We have applied the gravity data to calculate the global stresses due to mantle convection. Maps of these stresses are shown in Figs. 6A-2 - 6A-6. In general, divergent arrows indicate tensional stresses due to the upwelling mantle flows and convergent arrows represent compressional stresses resulting fom the downwelling mantle flows. The tensional stress field in Figs. 6A-2 - 6A-6 consists of the four-basic stress patterns as shown in Fig. 6A-1.

SIGNIFICANCE

Convection generated stresses in the lithosphere are inferable from the high degree harmonics of the geopotential. Hot spots on the earth's surface, marked by anomalous volcanism, could be surface expressions or flaws of stress concentration in tension caused by the hotter upwelling mantle convection currents. Widespread Cenozoic intra-plate volcanism in Africa, Asia, Australia and the Western United States is almost exclusively restricted to areas of the convection generated tensional stress field. This non-random distribution indicates that during Cenozoic the convection generated stresses in the lithosphere have exerted a control on the locations of these volcanic areas. In this case intraplate volcanism would be associated with tensional tectonics. The absence of volcanism in the convection generated compressional stress regimes implies that the environment of compression in the lithosphere is unfavorable for basalt magmas to migrate from the asthenosphere to the surface of the earth. Based on the results of this study, it seems reasonable to suggest that the convection generated subcrustal tensional stress field as inferred from the satellite and surface gravity data may be the genesis of the Cenozoic intra-plate volcanism.

FUTURE EMPHASIS

Obtaining a global distribution of stresses would be a great achievement of science Unfortunately, stresses in the earth are elusive variables which are difficult to obtain for even one point in the crust. Stress measurement techniques often yield conflicting evidence concerning the state of stress in the crust. Because stress measurements are costly, they are scarce. For example, great efforts have failed to achieve the goal to develop a map for atl east ' small portion of the earth showing the state of stress.

At present there is a lack of experimental information on the natue of thermal convection in the asthenosphere and on the question of whether the lithospheric stress field is accompanied by mantle convection. However, there appears to be a number of geological phenomena in which convection generated stresses are postulated to take place. A new look at these geodynamical processes should be taken. The global distribution of the Cenozoic intra-plate volcanism in which tensional stress field has been documented suggests that intra-plate volcanics are not immune to this stress process.

In the difficult problem of convection generated stress fields, it seems better to start from the case where we have the most important information (satellite and surface gravity data) and to argue from it to the real problems in geophysics and geology, rather than to allow techniques and preconceptions in fluid mechanics to influence thinking about the mantle convection flow. In this way, we may be able to develop systematic stress fields, step-by-step, with critical guidance, and draw them together into a unified pattern.

REFERENCES AND PUBLICATIONS

Liu, H.S., 1980, "Convection Generated Stress Field and Intra-Plate Volcanism," Tectonophysics, 65, 225-244.

(a) Accelerating:
    tensional fissures ⊥

(b) Bilaterally opposed:
    tensional graben

(c) Unequal parallel:
    feather fissures

(d) Diverging:
    tensional fissures ||
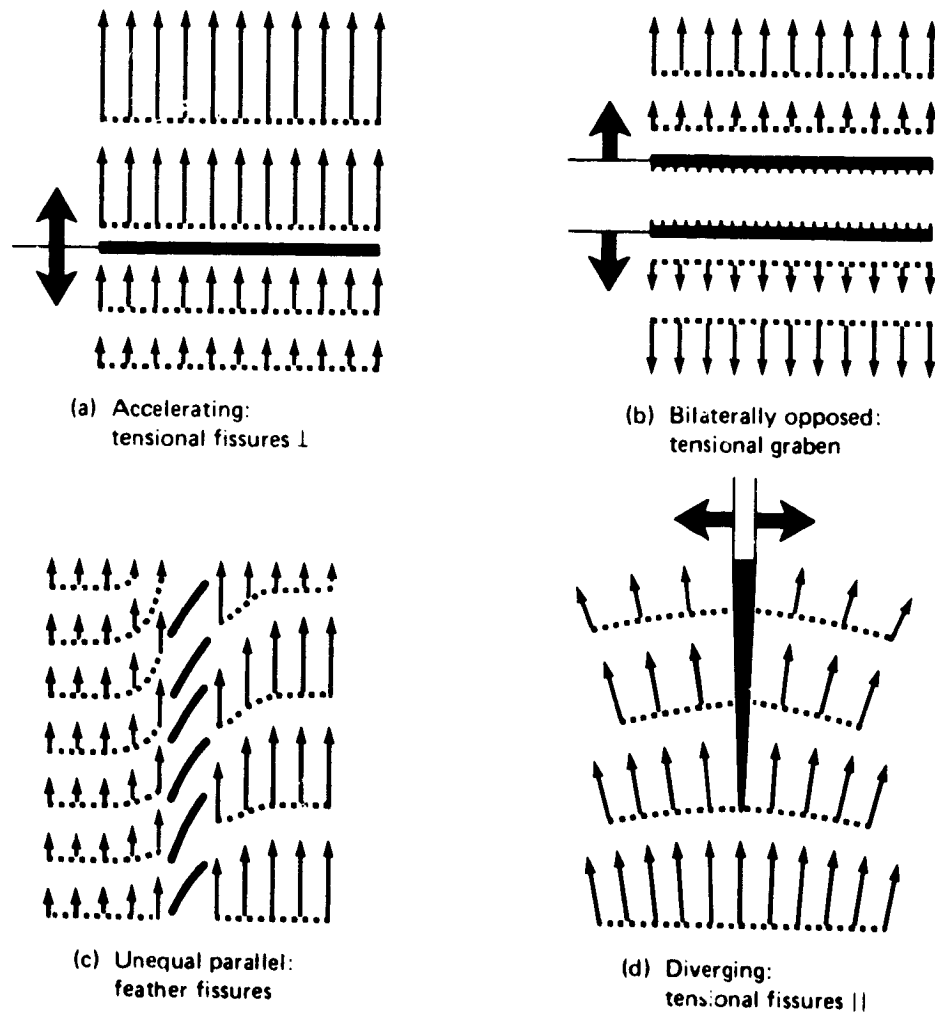
Fig. 6A-1.   Subcrustal stresses and formation of tensional fissures.
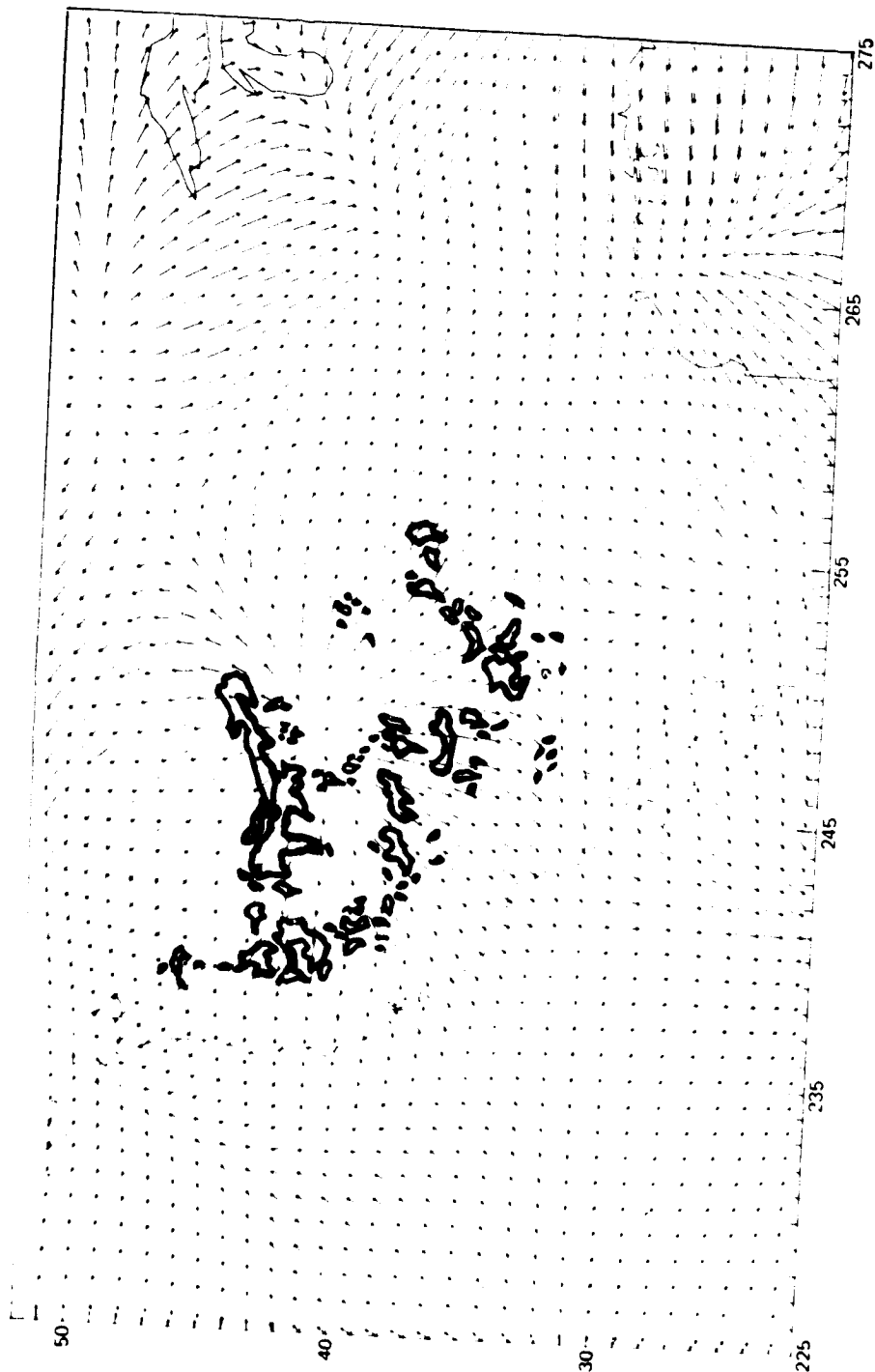
Fig. 6A-2. Convection generated stress field and Cenozoic volcanism (<7 Ma B.P.) in the Western United States. Volcanic features derived from Geological Map of the United States (King and Beikman, 1974).
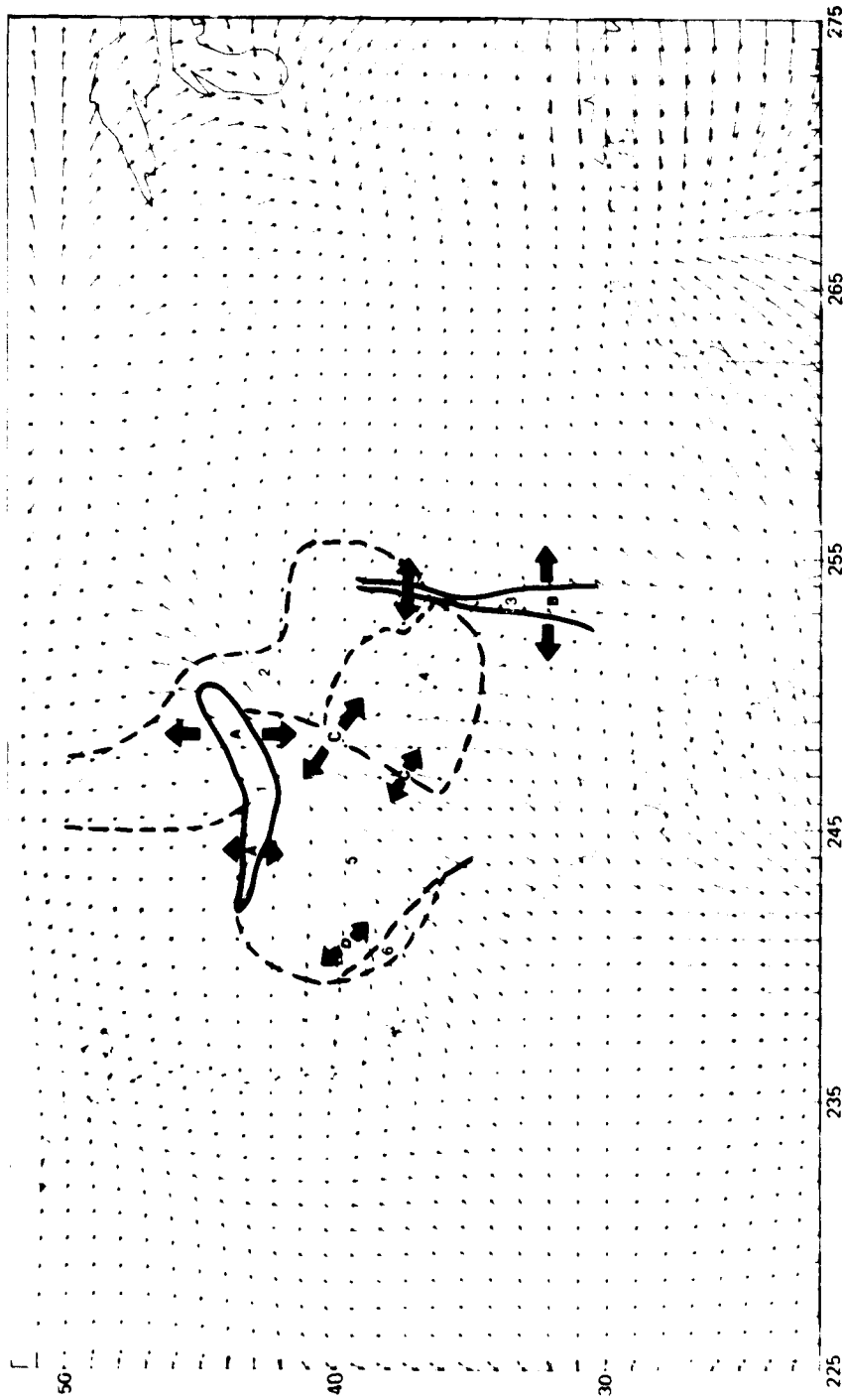
Fig. 6A-3. Convection generated stress field in the United States agrees well with the stress directions inferred from seismic focal mechanism studies. 1 = Snake River Plain; 2 = Rocky Mountains; 3 = Rio Grande Graben; 4 = Colorado Plateau; 5 = Basin and Range; 6 = Sierra Nevada. Heavy arrows derived from seismic data (Smith and Sbar, 1974).

Fig. 6A-4. Convection generated stress field and Cenozoic volcanism in Australia. (Sources of volcanic features: references in text).
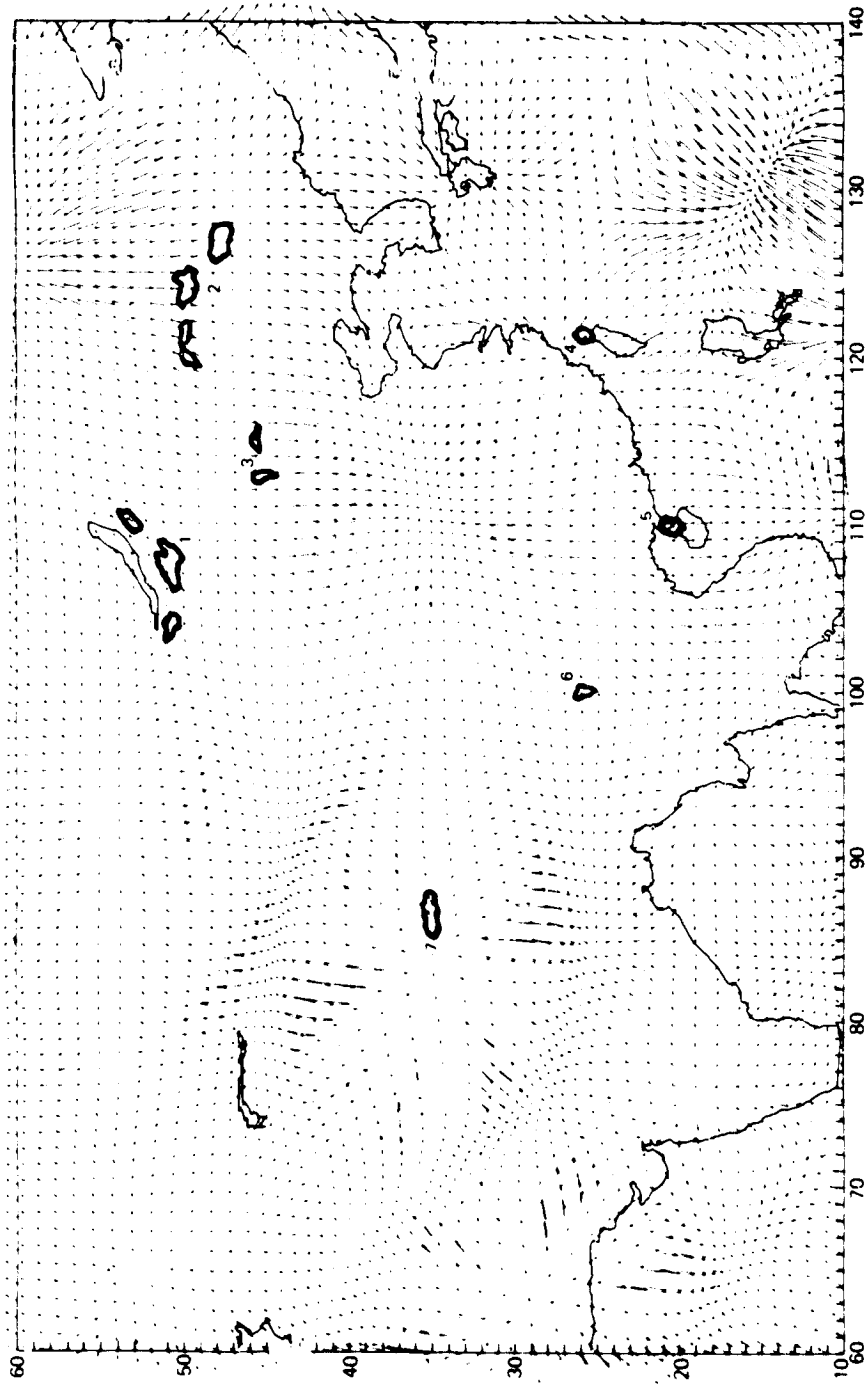
Fig. 6A-5. Cenozoic volcanism and convection generated stress field in Asia. 1 = Baikal; 2 = Heilungkang; 3 = Inner Mongolia; 4 = Taiwan; 5 = Hainan; 6 = Yunnan; 7 = Tibet. (Sources of volcanic features: references in text and the Tectonic Map of China, 1974).
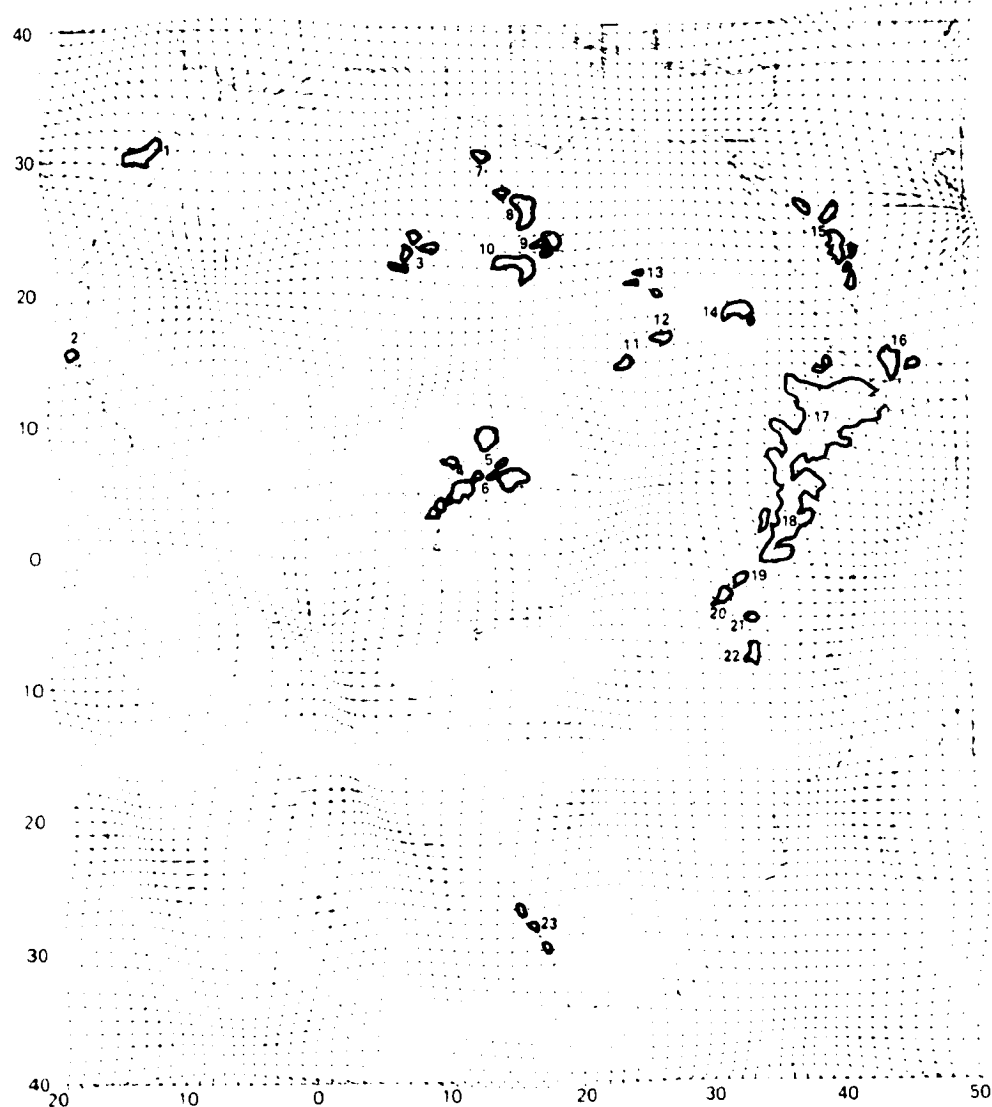
Fig. 6A-6.   Cenozoic volcanism and convection generated stress field
in Africa. 1 = Canary Islands; 2 = Dakar; 3 = Hoggar; 4 = Jos; 5 = Biu;
6 = Cameroon line; 7 = Tripolotania; 8 = J. Haruj; 9 = Eghei;
10 = Tibesti; 11 = J. Marra; 12 = Meidob; 13 - J. Uweinat; 14 = Bayuda;
15 = West Arabia; 16 = South Arabia and Aden; 17 = Ethiopia; 18 =
East African Rift· 19 = Birunga; 20 = Kivu; 21 = Igwisi; 22 = Rungwe;
23 = Southwest Africa.   (Sources of volcanic features: references in
text and the International Tectonic Map of Africa, 1968).

B.   GEOID ANOMALIES OVER SUBDUCTION ZONES

by

D.C. McAdoo

OBJECTIVES

The objective of this study is the determination of density structure associated with major subduction zones. Longer term objectives include: (i) elucidation of mechanisms by which apparent mass excesses--at subduction zones--are supported or compensated; (ii) estimation of the strength/rheology of the tongue of subducting lithosphere and the surrounding mantle.

BACKGROUND

From examination of low resolution global gravity maps it is evident that mass excesses occur near subduction zones. Theoretical studies suggest that relatively low temperatures should persist in lithospheric slabs as they subduct and, as a result, that positive density anomalies arise within the slab. To date, this study has focused on defining these apparent mass excesses in various regions and determining the extent to which they may be attributed to density anomalies within the slab. Earthquake hypocenter distributions (Benioff zones) are used to constrain the position of the slab model. Precise estimates of the intermediate wavelength (1000-4000 km) component of the geoptential are crucial to this study. GEOS-3 and Seasat altimetry provide such estimates--other measurement systems generally do not. This work is described more fully in McAdoo (1980).

As indicated below the positive density anomalies which have been inferred in this study for particular descending slabs are generally less--by varying degrees--than those predicted by a reasonable thermal conduction model. These low values of inferred density anomaly can be explained as the result of a particular "regional compensation" (Griggs, 1972) of anomalous mass in slabs. The exact nature and mechanism of this compensation are not presently understood, but are being actively investigated. In all likelihood this mechanism of compensation is intimately related to the overall dynamic interaction of slabs with their surroundings and to the processes driving major plate motions.

RECENT ACCOMPLISHMENTS

Work (McAdoo, 1980) has been completed on subduction zones of the southwest Pacific. Results include estimates of the averaged anomalous mass per unit area for the New Hebrides and Tonga-Kermadec slabs of 3.2×10^5 and 1.0×10^5 gm cm^{-2}, respectively. A good agreement was found between the marine geoid obtained from direct, (altimetric) observations and the geoid computed from the regional model (see an example in Fig. 6B-1). It was necessary in this work to model the geoidal effect arising from a substantial age (or thickness) difference between the young thermal lithsophere behind

arc and the normal oceanic lithosphere seaward of the trench. This study has now been extended to the region of the Aleutian/ Alaskan island arc. Early results indicate that the portion of the Aleutian slab west of 170°W longitude is subject to a partial (~30%) regional compensation. On the other hand the New Hebrides and Tonga-Kermadec slabs were found to have an apparent regional compensation of ~10% and 65% respectively. These percentages depend of course upon the particular choice of reference model for slab thermal history. An observed geoid (mean sea surface) and a model geoid for the Aleutian region have been computed.

This computed geoid is preliminary. It is derived using a slab model (anomalous mass per area which increases from 0 near surface to 9.5×10^5 gm cm^{-2} at 200 km depth) and a model of the mass void associated with the actual trench. The Aleutian Basin admittedly has a complex history; however, it can be interpreted as having an effective sea floor age which is slightly less than that seaward of the arc according to the thermal rejuvenation hypotheseis of Langseth, et al., (1980). This study indicates that in the western Aleutian arc the mass void of the trench proper does not noticeably compensate positive mass anomalies within the slab, and that gravitationally apparent density anomalies in the slab are concentrated at depth, perhaps extending to greater depths than the seismically defined Benioff zone.

SIGNIFICANCE

This study provides estimates of mass anomalies associated with various subducting slabs. These estimates can be used to gain understanding of mechanisms providing support or compensation of descending slabs and ultimately of mechanisms driving major motions.

FUTURE EMPHASIS

Estimates of density structure for subduction zones of the western Pacific will be obtained. This particular work awaits forthcoming results on regional hypocenter distributions. Heat flow findings are to be more fully used. In the longer term, thermo-mechanical models of subduction processes will be developed and applied.

REFERENCES AND PUBLICATIONS

Griggs, D.E., "The Sinking Lithosphere and Focal Mechanisms of Deep Earthquakes," in The Nature of the Solid Earth, E.C. Robertson (editor), McGraw Hill, New York, p. 361, 1972.

Langseth, M.G., M.A. Hobart and K. Horai, "Heat Flow in the Bering Sea," J. Geophys. Res., V. 85, p. 3740, 1980.

McAdoo, D.C., "Geoid Anomalies in the Vicinity of Subduction Zones," J. Geophys. Res., in press, also NASA/GSFC TM 80678, 1980.
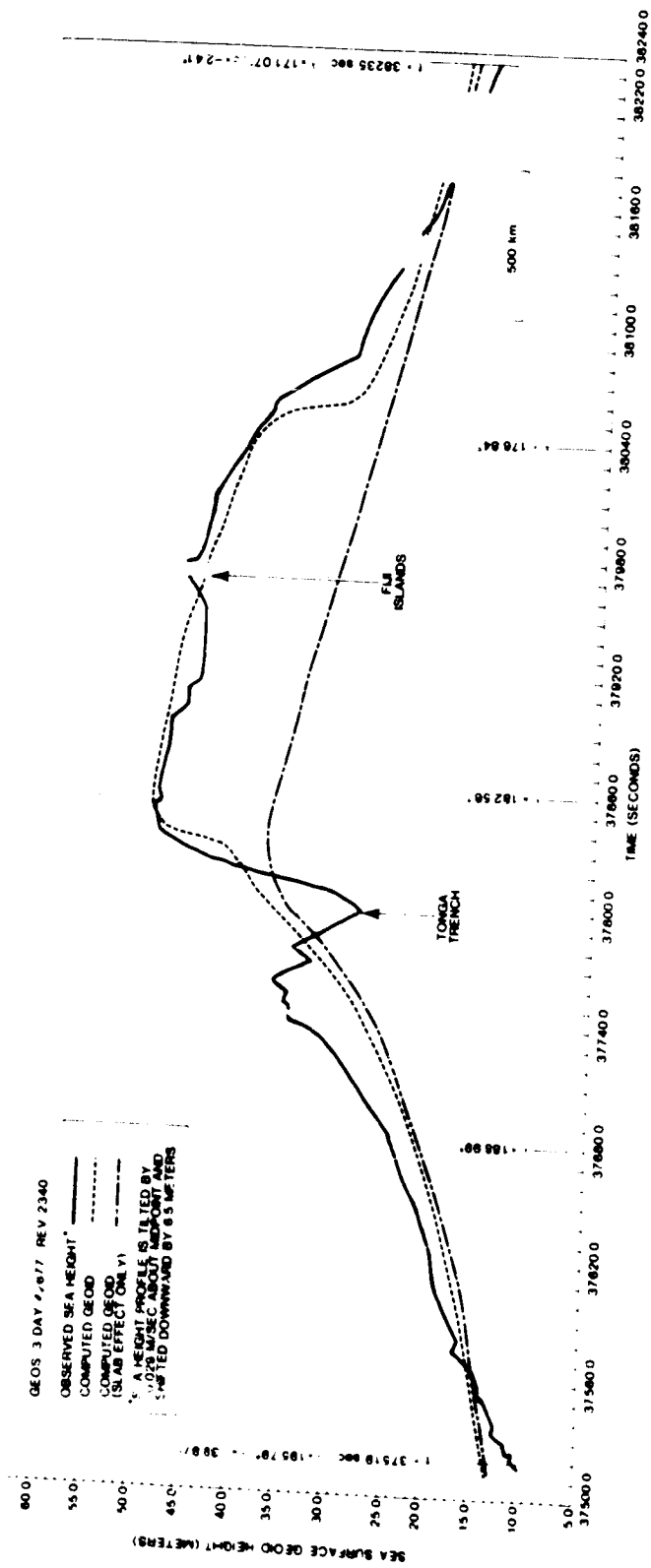
Figure 6B-1. Comparison of model results with an individual GEOS altimeter high profile. Dashed line represents a superposition of geoid heights from the slab model and heights from the thermal lithsophere model. See McAdoo (1980).

6-13

C. INFORMATION THEORY DENSITY DISTRIBUTION

by

D.P. Rubincam

OBJECTIVE

The purpose of this work is to make a rational inference as to the earth's internal density distribution and relate it to the tectonics of the earth.

BACKGROUND

A basin problem in geophysics is how to make inferences about the state of the earth's interior based on incomplete data. In this case the data is the spherical harmonic coefficients of the earth's gravity field. The lateral gravity field is generated by the earth's lateral density distribution. However, an infinite number of different density distributions will give rise to the observed gravity field. The problem is to choose the "most likely" lateral density distribution out of the infinite possibilities.

A rational inference method called ITI, Information Theory Inference (also called MEM, Maximum Entropy Method) has been applied to the problem of the lateral density distribution. A discussion of ITI may be found in Rubincam (1979). Briefly, ITI assigns probabilities to each of the possible density distributions. The probabilities are chosen so as to maximize Claude E. Shannon's information measure, subject to the constraints of the data. The density distributions are then weighted by probability and summed to obtain the "most likely" density distribution. This is in practice identical to the statistical mechanics approach of J. Willard Gibbs. The only change in the approach is to make information theory its basis, rather than entropy. This gives the approach more power and makes it applicable to problems outside of statistical mechanics.

The ITI lateral density distribution has been derived from the GEM 10B gravity field using Maxwell-Boltzmann statistics. It assumes that the spherically symmetric part of the density distribution (which we will call the radial density distribution) is known. For this the parametric earth model density distribution of Dziewonski, et al. (1975) has been used. In practice it makes little difference what radial density distribuiton is used, since it has been shown that the ITI lateral densitu distribution is very insensitive to changes in the radial density distribution. The derivation also assumes that the lateral density perturbation is small compared to the radial density distribution. This is a good assumption, since the lateral changes in density seldom exceed 1 percent of the radial density.

A computer program has been written to display teh ITI lateral density distribution in various ways, in order to observe correlations between density and tectonics. This program allowa crustal model (and hence the crustal gravity field) to be stripped off if desired, and ITI algorithm applied to the remaining gravity signal. Two crustal models have been used: an isostatically compensated crust with a compensatio depth of 30 km, and an isostatically uncompensated crust 30 km thick.

The ITI lateral density distribution at the earth's surface, with the topography flattened to the surface and no crust stripped off, is very similar to the GEM 10B gravity anomaly map. It shows mass excesses at the trenches, oceanic ridges, and hot spots (but not in all cases). It shows mass deficiencies at the abyssal plains (again not in all cases), and at the glacially depressed regions of the continents.

RECENT ACCOMPLISHMENTS

One recent accomplishment is to examine the ITI density anomalies near linear tectonic features, especially trenches and oceanic ridges. The technique used was to determine the great circle connecting two arbitrary points near the linear features. Then cross-sections through the upper mantle were taken between the two points, with each cross-section running perpendicular to the great circle. After much experimentation this appears to be the best approach for examining how the ITI density distribution varies along and across a linear tectonic feature.

An example of such a cross-section is shown in Figs. 6C-1 and 6C-2. It is for the region near the bend in the Peru-Chile Trench. Figure 6C-1 shows the positions of the great circle and the cross-section. Figure 6C-2 shows the relative density in the cross-section. Relative density is defined as the lateral density anomaly divided by the radial density distribiton. The isostatically compensated crustal model has been stripped off.

Another recent result is the completion of the paper (Rubincam, 1980) on inverting grid coordinates to find latitude and longitude in the van der Grinten projection.

SIGNIFICANCE

The cross-sections of the trenches examined generally show high density, as expected from the gravity field and plate tectonics. However, the visual evidence for the sense of plate motion is so far equivocal; Fig. 6C-2, for example shows little to indicate a dense downgoing slab. More data should be added to the ITI algorithm to sharpen the density picture.

The ITI density distribtion under the Mid-Atlantic Ridge shows a region of high density after the isostatic crust is removed. This is at variance with plate tecotnics, which states that low density material should be rising under the ridge. The disagreement is likely due to the crustal model. An isostatically compensated crust with compensation depth of 30 km probably poorly models the oceanic ridges. This indicates that better models are needed.

FUTURE EMPHASIS

The future emphasis will be on: continued examination of the ITI density distribution near linear tectonic features; the comparison of the ITI results with what is known about these features from other geophysical data, such as seismic data; the knotty problem of extending ITI to include seismic data; and better models of the crust.

REFERENCES

Dziewonski, A.M., A.L. Hales and E.R. Lapwood, "Parametrically Simple Earth Models Consistent with Experimental Data," Physics of the Earth and Planetary Interiors, 10, 12-48, 1975.

Rubincam, D.P., "Information Theory and the Earth's Density Distribution--Revised Edition," NASA-GSFC TM 80586, August 1979.

Rubincam, D.P., "Inverting x,y Gride Coordinates to Obtain Latitude and Longitude in the van der Grinten Projection," NASA-GSFC TM 81998, August 1980.
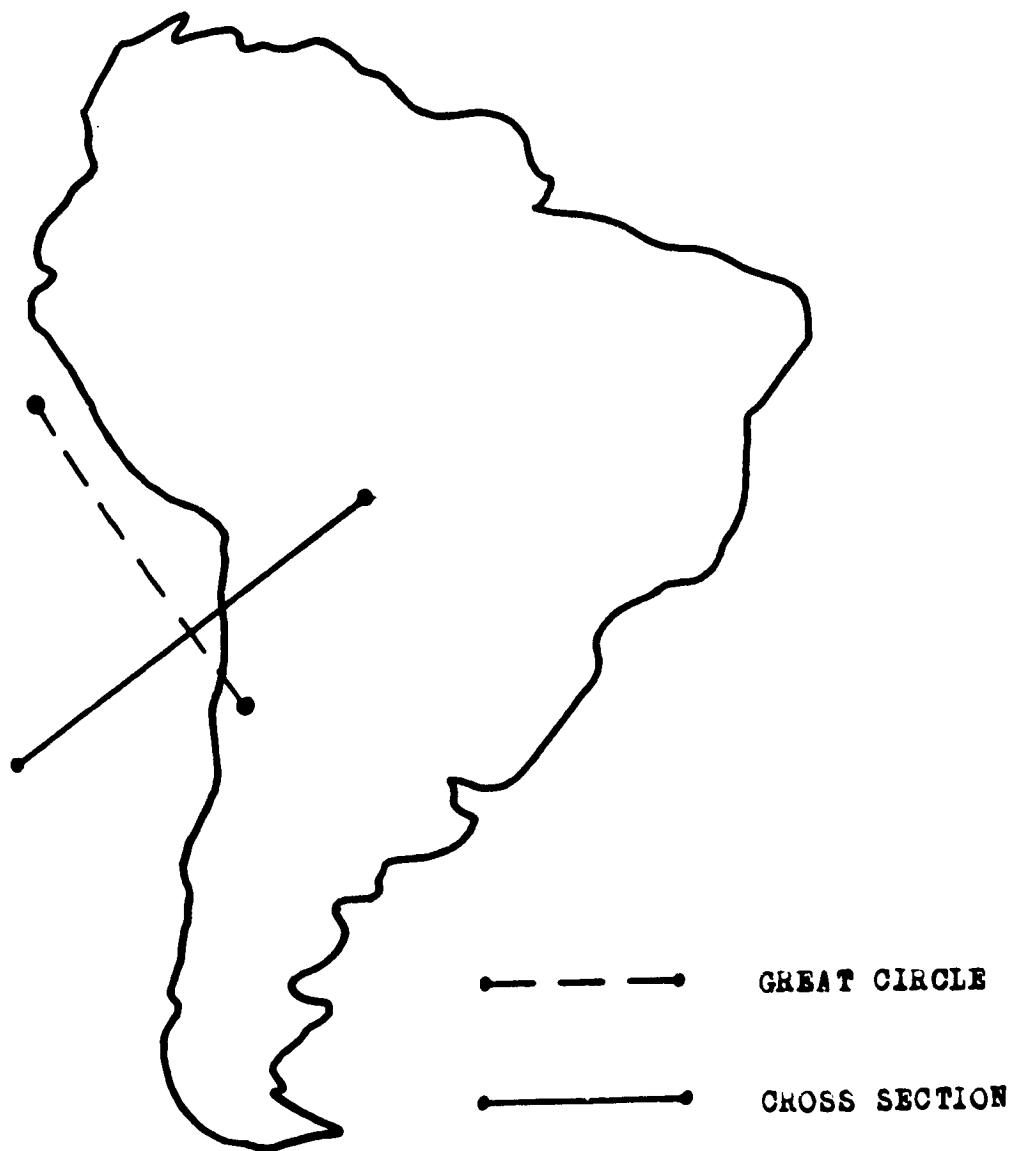
GREAT CIRCLE

CROSS SECTION

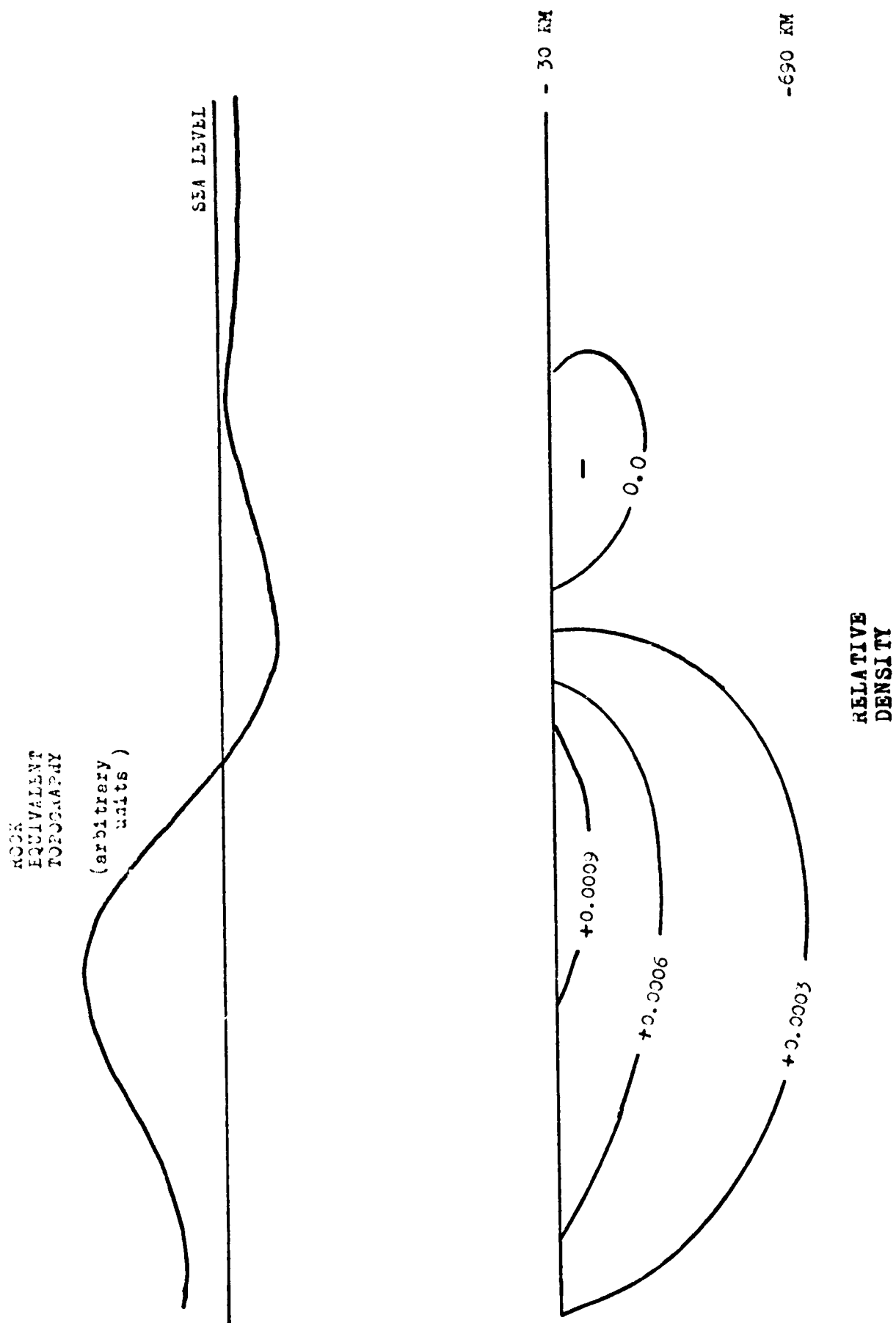Fig. 6C-1. Position of cross-section of Peru-Chile Trench.

Fig. 6C-2.   Relative density under Peru-Chile Trench.

D. LATERAL DENSITY VARIATIONS IN ELASTIC EARTH MODELS FROM AN EXTENDED MINIMUM ENERGY APPROACH

by

B. V. Sanchez

OBJECTIVES

The external gravitational potential of the earth can be expressed in spherical harmonics and its components determined by analysis of satellite data. Such an analysis indicates the presence of lateral variations of density in the earth's interior. However, it is not possible to define uniquely what these lateral density variations are by inverting only the gravity data.

The objective of this investigation was to determine the lateral density variations by means of static earth-tide theory in a modified form, imposing the condition of minimum strain and non-hydrostatic gravitational potential energy in the mantle and crust.

BACKGROUND

The question of lateral density variations and the internal stresses they produce has implications with respect to the possible existence of mantle convection within the earth. Kaula (1963) used modified static earth-tide theory to estimate the minimum shear stresses induced by the internal density anomalies and concluded that the stresses are probably excessive.

Lambeck (1976) has pointed out that the nonhydrostatic gravity field implies the existence of free potential energy within the earth and that there must be a capacity for rearrangements of mass toward distributions of lower energy (assuming no new energy generation and no kinematic constraints). A study by Rubincam (1979) indicates that the maximum nonhydrostatic gravitational potential energy in the mantle and crust is of the same order of magnitude as Kaula's estimate for the minimum shear strain energy.

RECENT ACCOMPLISHMENTS

Modified static earth-tide theory was used to determine the interior density anomalies. The lateral density variations were expressed in spherical harmonics, the parameters which define the anomalies were determined by imposing the condition of minimum strain and non-hydrostatic gravitational potential energy in the mantle and crust. The solution was constrained to satisfy the external boundary conditions provided by the gravitational potential; the surface topography was included in the problem as a loading surface density distribuiton.

The solution of the problem required the numerical integration of the equations of motion governing the vibration of an elastic body as well as the Poisson's equation for the gravitational potential. The static solution was obtained by setting the frequency equal to zero.

The transformation of Alterman, et al. (1959) was used to
obtain a set of six ordinary differential equations from the
original partial differential equqtions. The set of ordinary
differential equations was then cast into a transition matrix
form to facilitate the application of a least-squares minimi-
zation procedure. The elastic and nonhydrostatic gravitational
potential energies were expressed also in matrix form.

The nominal values for the earth's density and elastic para-
meters were obtained from the M_3 model of Landisman, et al.
(1965), these values are given in table form and a cubic spline
interpolation was used to obtain their values as functions of
the earth's radius. The spherical harmonic expansion used for
the topography is the equivalent rock set given by Balmino, et al.
(1973). The expansion used for the gravitational potential is
the Goddard Earth Model 6 by Lerch, et al. (1974) with the
hydrostatic components of the second and fourth degree zonals
subtracted out.

The interior density perturbations are determined for three
separate cases:

i)   minimization of the shear strain energy

ii)   minimization of the gravitational potential energy

iii)   minimization of the sum of the two.

The density perturbation field was obtained for each degree and
order up to degree and order eight. Table 6D-1 gives the global
energy magnitudes for each case.

The surfaces of equal density perturbation evaluated at the sur-
face of the earth are shown in figures 6D-1 and 6D-2 for two of
the cases; figures 6D-3 and 6D-4 present the surfaces of equal
radial displacement at the earth's surface; figures 6D-5 and
6D-6 show the surfaces of equal density perturbation evaluated
on an equatorial cross-section of the earth.

SIGNIFICANCE

The magnitudes of the density perturbations and dispacements at
the surface is larger by about a factor of two for the case of
minimum shear plus gravitational energy as compared to the mini-
mum shear case. The same result is observed for the density
anomalies as a function of depth. The minimum gravitational
potential energy case yields much smaller density anomalies but
unrealistically large dispacements. The depth profiles for the
density perturbation show a stratification with density excesses
and deficiencies alternating with depth. The minimum total energy
is obtained when minimizing only the shear strain contribution.

The results indicate that the addition of the gravitational poten-
tial energy in the minimization process does not significantly
alter the lateral density perturbation field, as compared to the
results obtained for the minimum shear strain energy case; certainly
the inability of the mantle to withstand the resulting stresses
elastically.

Table 6D-1. Global energy magnitudes, units of 10^{30} ergs

DEGREE	Min. Shear		Min. Grav.		Min. (Shear + Grav.)	
	Grav.	Shear	Grav.	Shear	Grav.	Shear
N = 2	- 7.912	0.178	-0.086	94.639	··27.599	5.640
N = 3	- 5.966	0.167	-0.120	204.381	-13.683	1.120
N = 4	- 6.020	0.566	-0.237	586.165	-11.624	1.039
N = 5	-13.935	0.225	-0.321	1062.685	- 7.443	0.688
N = 6	- 1.412	0.070	-0.174	719.578	- 1.645	0.062
N = 7	- 0.672	0.043	-0.274	1249.120	- 3.510	2.204
N = 8	- 0.432	0.029	-0.324	1307.191	- 2.623	2.266
$\sum_N$	-36.351	1.281	-1.539	5223.762	-68.130	13.021
Total	-35.070		5222.222		-55.108	

REFERENCES AND PUBLICATIONS

Alterman, Z., H. Jarosch, and C.L. Pekeris, 1959, "Oscillations of the Earth," Proceedings of the Royal Society, A, 252.

Balmino, G., K. Lambeck, and W.M. Kaula, 1973, "A Spherical Harmonic Analysis of the Earth's Topography," Journal of Geophysical Research, 78, No. 2.

Kaula, W.M., 1963, "Elastic Models of the Mantle Corresponding to Variations in the External Gravity Field," Journal of Geophysical Research, 68, No. 17.

Lambeck, K., 1976, "Lateral Density Anomalies in the Upper Mantle," Journal of Geophysical Research, 81, No. 35.

Landisman, M., Y. Sato, and T. Nafe, 1965, "Free Vibrations of the Earth and the Properties of Its Deep Interior," Geophys. J.R. astr. soc., 9.

Lerch, F.J., C.A. Wagner, J.A. Richardson, and J.E. Brownd, 1974, "Goddard Earth Models (5 and 6)," X-921-74-145, Goddard Space Flight Center.

Rubincam, D.P., 1979, "Gravitational Potential Energy of the Earth: A Spherical Harmonic Approach," Journal of Geophysical Research, 84, No. B11.
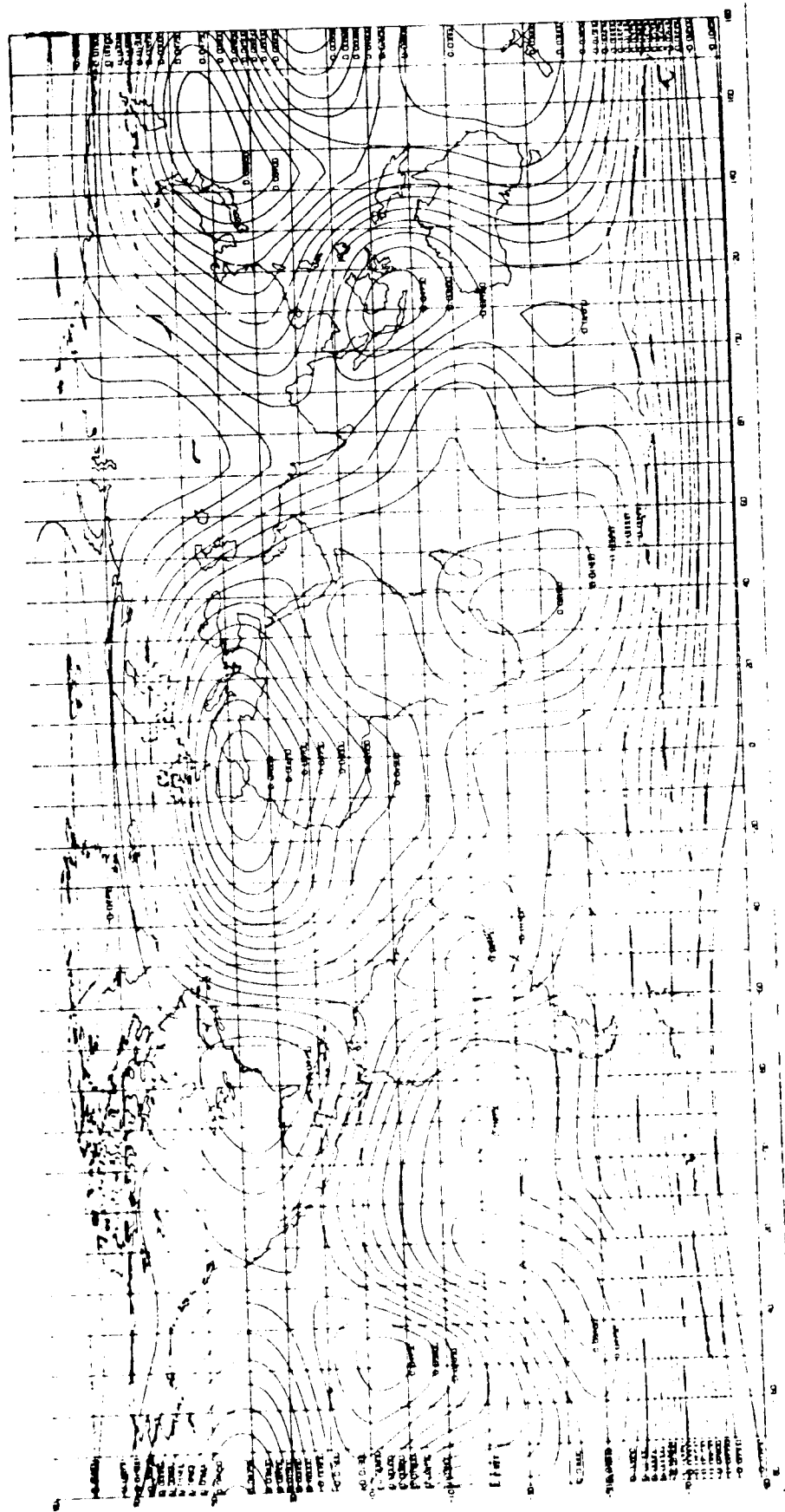
Figure 6D-1. Surfaces of equal density perturbation at the surface of the earth, units of gm/cm^3. Minimum shear strain energy case.
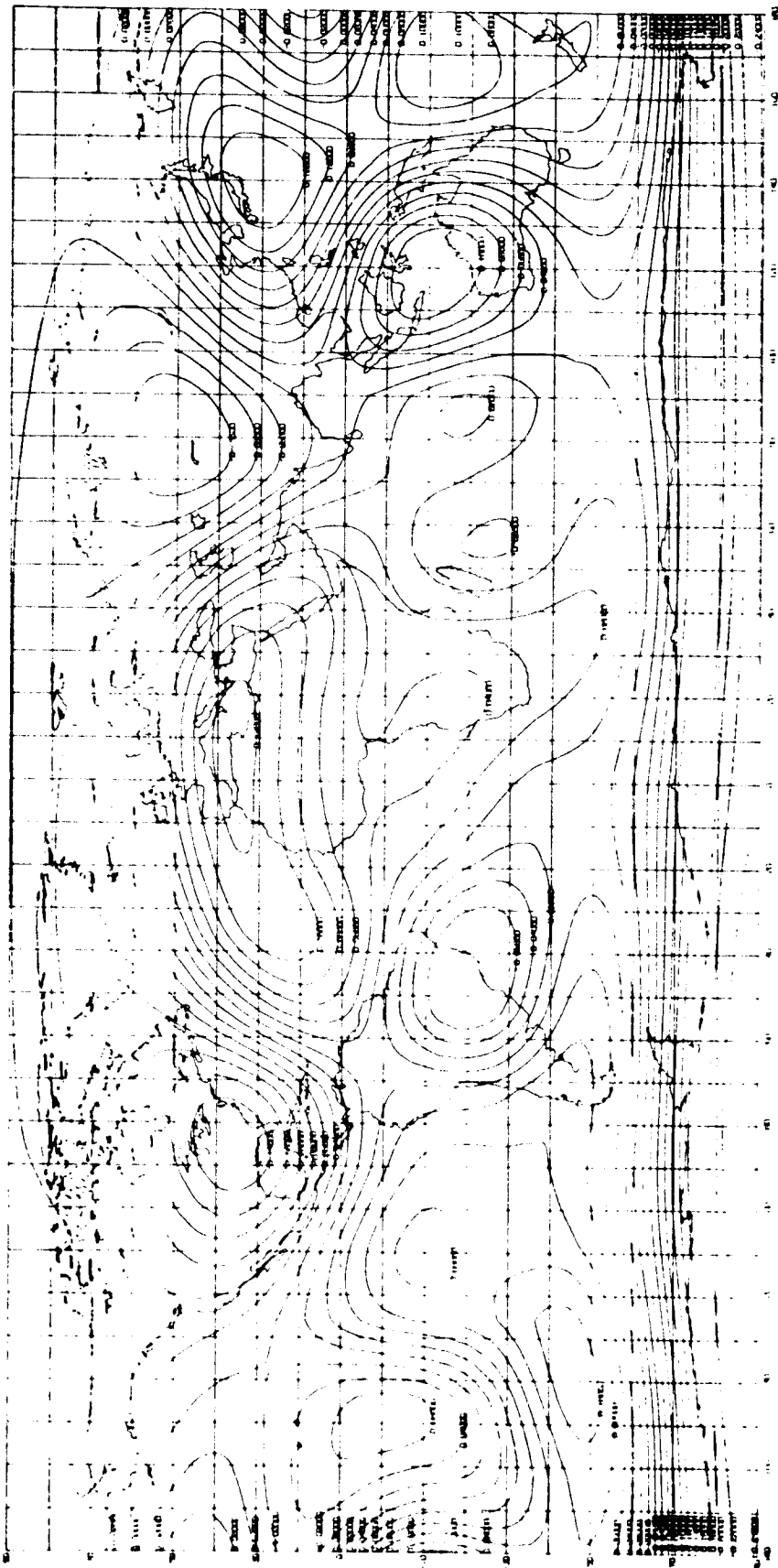
Figure 6D-2. Surfaces of equal density perturbation at the surface of the earth, units of gm/cm^3. Minimum shear plus gravitational energy case.
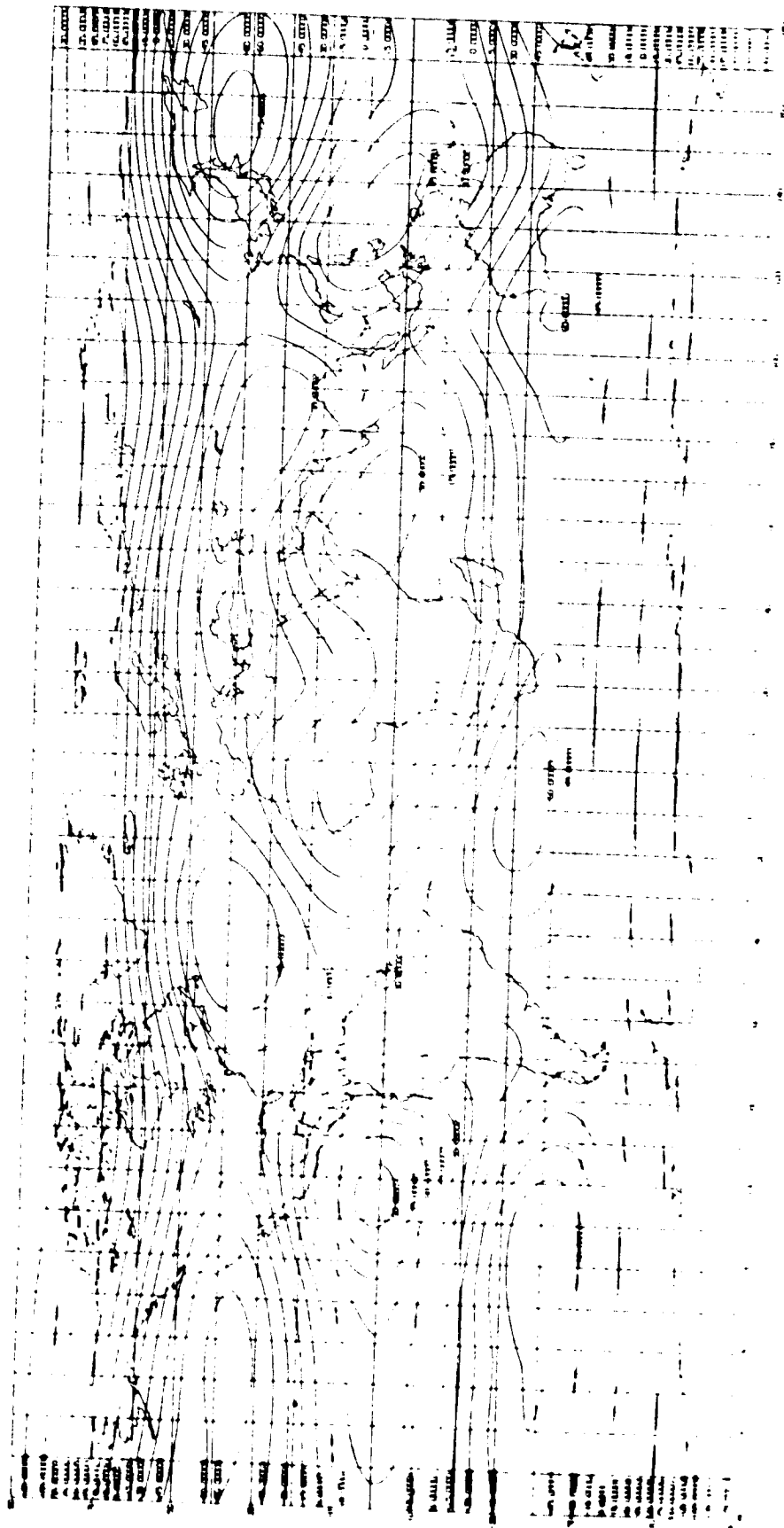
Figure 6D-3. Surfaces of equal radial displacement at the surface of the earth, units of meters. Minimum shear strain energy case.
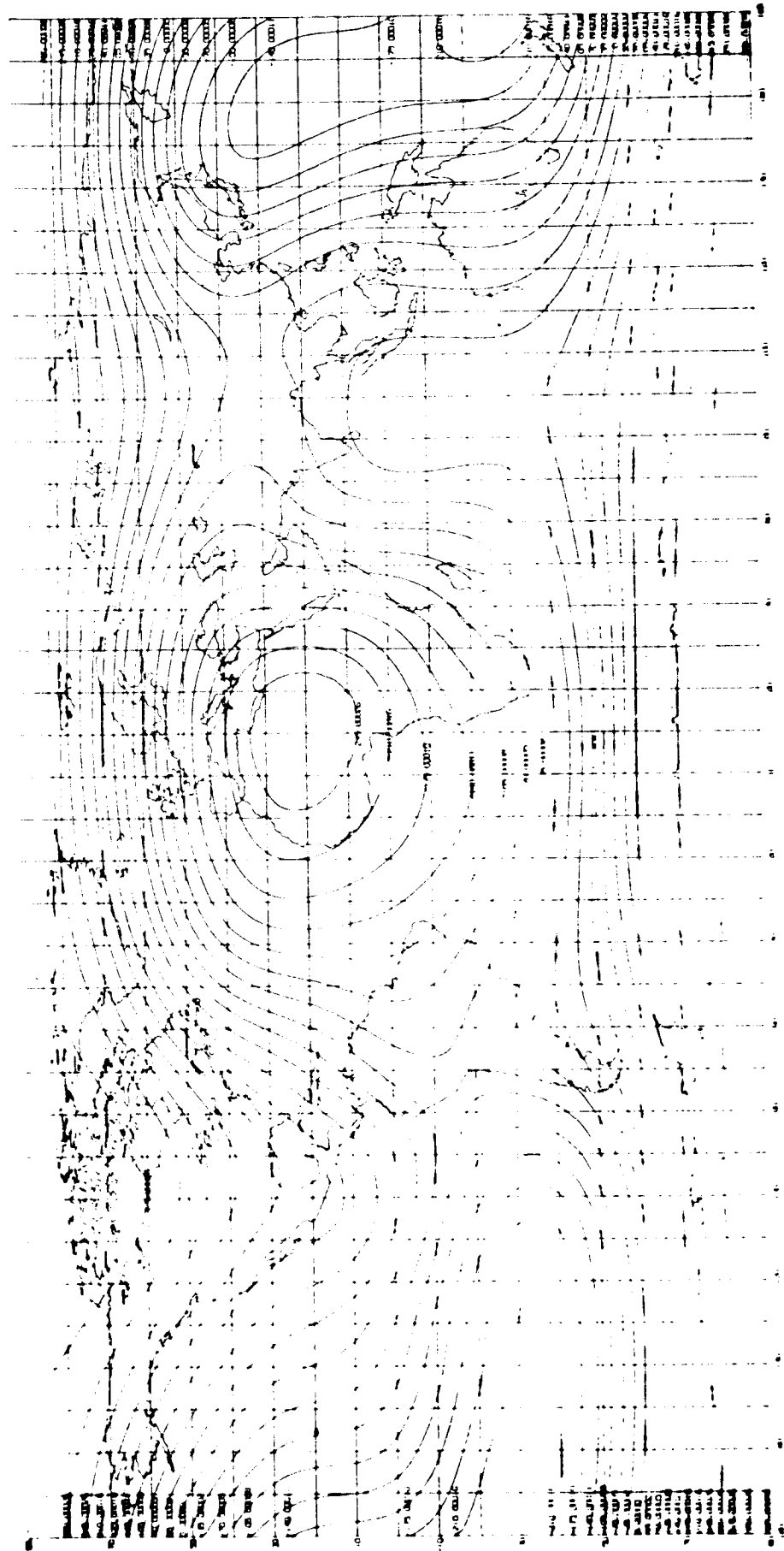
Figure 6D-4. Surfaces of equal radial displacement at the surface of the earth, units of meters. Minimum shear plus gravitational energy case.

Figure 6D-5. Surfaces of equal density perturbation on an equatorial cross-section of the earth, units of gm/cm^3. Minimum shear strain energy case.

Figure 6D-6. Surfaces of equal density perturbation on an equatorial cross-section of the earth, units of gm/cm^3. Minimum shear plus gravitational energy case.
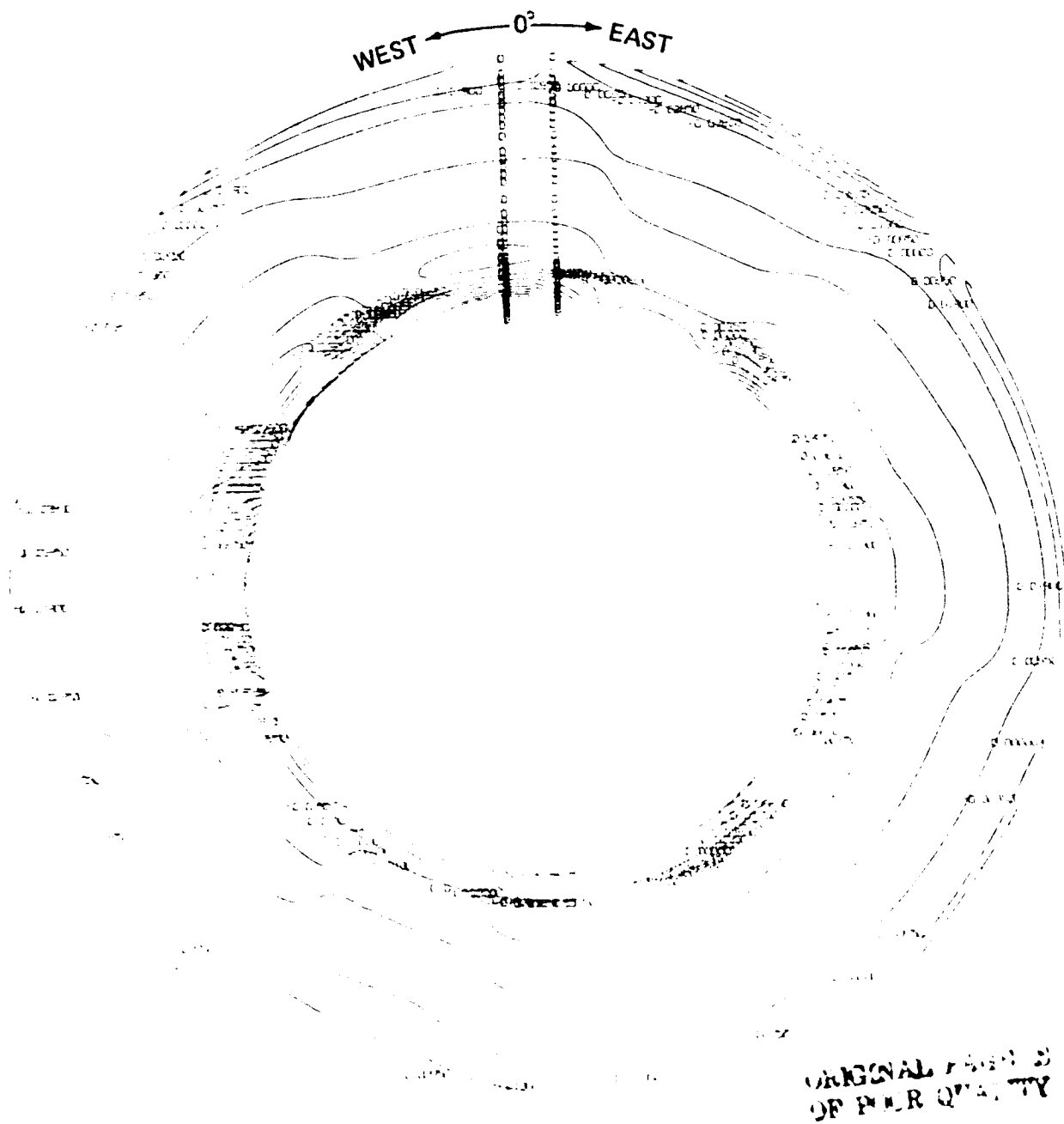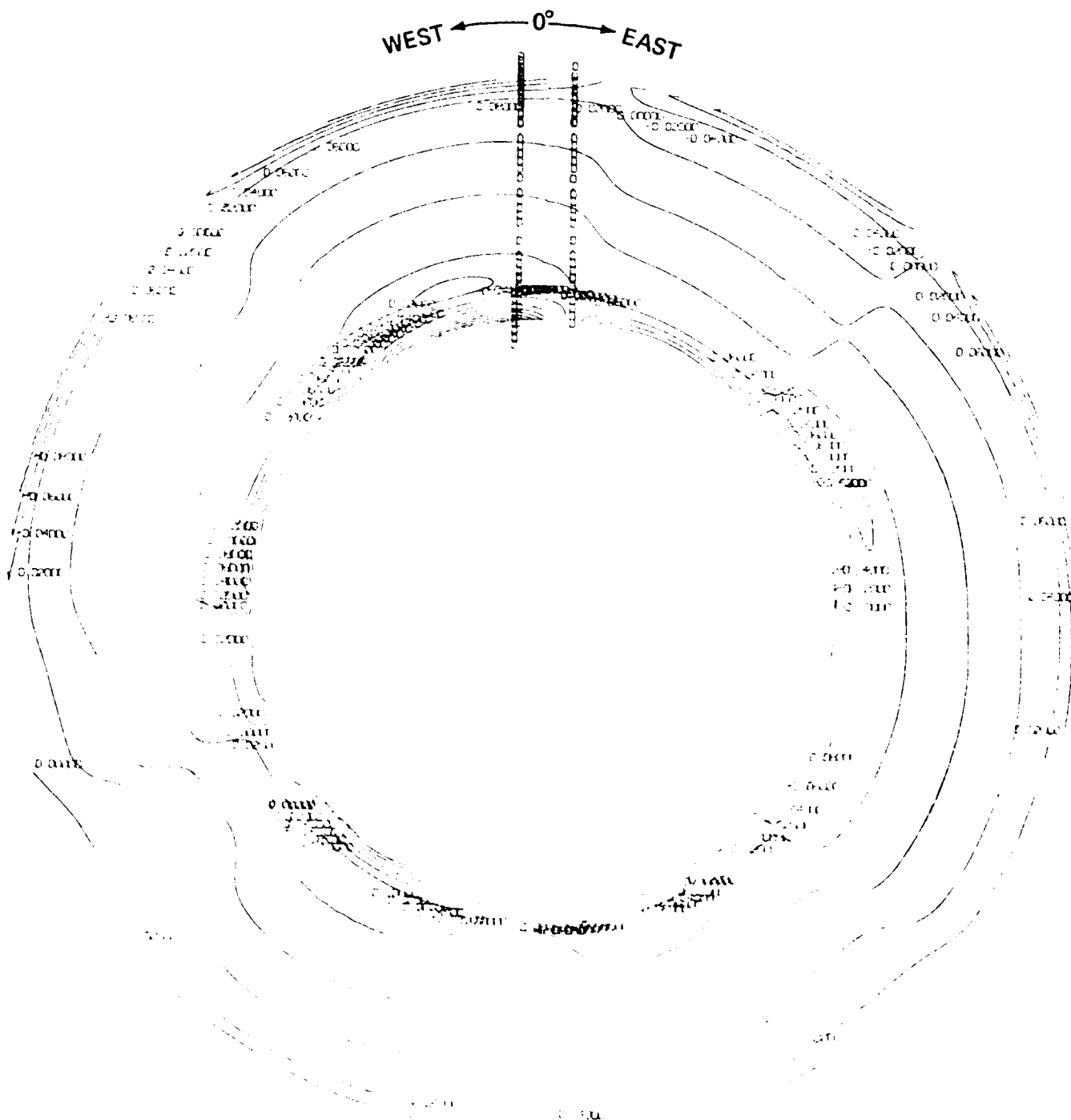
E.   STUDIES OF POLAR MOTION AND UNIVERSAL TIME WITH LAGEOS

by

D.E. Smith

OBJECTIVE

The long-range objective of this analysis is an intercomparison
of the rotation of the earth determined by satellite laser
ranging with the classical and other techniques for improved
separation of systematic errors from the geophysics. The near-
term objective is a comparison of Universal Time as determined
by laser tracking of Lageos and the Bureau de l'Heure (BIH)
based on the classical astronomical methods.

BACKGROUND

A period of 30 months of determinations of Universal Time obtained
from laser tracking of the Lageos spacecraft have been compared
with the BIH results. The Lageos values were obtained as part
of a large analysis of the data for many parameters, including
polar motion, tracking station coordinates, tidal parameters, a
solar radiation pressure parameter and an along-track acceleration
of the spacecraft. The method of analysis consisted of determining
32 monthly orbital arcs for Lageos and simultaneously solving all
32 arcs for all the parameters. The polar motion and Universal
Time (U.T.) were estimated every 5 days after the epoch of each
set of orbital elements. It was impossible to determine a value
for U.T. at the epoch of the elements in each arc because the
node of the orbit was being estimated and is inseparable from time.
The initial determinations of U.T. were therefore with reference
to the nodal value of the orbit at the epoch. In order to make
the U.T. estimate continuous over the 32-month period a correction
was applied to each value of U.T. corresponding to the difference
at the epoch between the node and the node computed from the
previous orbital arc. A set of values of U.T. were finally
obtained for the 32-month period based on the continuous nodal
precession of a single orbit. These values of U.T. were compared
with the published smoothed BIH results for the same dates.

RECENT ACCOMPLISHMENTS

In the comparison with BIH a linear trend was removed because it
represented an error in the precession of the Lageos orbit in
inertial space and two periods, 1050 days and 525 days. These
periods are caused by the K_1 and K_2 solid-earth and ocean tides
that perturb the Lageos orbit. These periods are not expected to
occur in the BIH U.T. values and therefore it is legitimate to
remove them from the comparison. Although tidal parameters were
recovered in the analysis of the data, these long period tides
would not be accounted for in the recovered tidal values. After
these two tidal periods and residual slope were removed, the
differences between Lageos and BIH U.T. had definite structure and
are shown in Figure 6E-1.

A spectral analysis of the differences shows significant power at about 182 days and a small effect near 28 days. No other spikes of significance appeared in the spectrum. An attempt to remove the peak near 182 days with a single period was un- successful and the reason is evident in Figure 6E-1. The ampli- tude of the 6-month period seems to have changed dramatically during the second half of the data thus preventing a single frequency with constant amplitude from satisfying the data. Mathematically, the near 6-month power can be absorbed by two periods near 182 days, say 180 and 185 days, which combine to give a 6-month period with decreasing amplitude. Alternatively, a more geophysically acceptable representation is a single 6-month period whose amplitude changes significantly around day 250.

SIGNIFICANCE

The cause of the 6-month period is probably the result of systematic error in the BIH data. A 6-month period is not one which might be expected in the Lageos data unless of geophysical origin, but in the BIH the observing methods have a predominantly annual and some semi-annual terms arising from seasonal effects at the observing stations.

The other period observed in the comparison is a 28-day period with an amplitude of a few hundreds of an arcsecond and is a tidal effect in the earth's rotation. It is detectable in both the Lageos data and the raw BIH data but is removed in the process itself. The fact that no other significant periods are detectable in the U.T. differences indicates that there are no amplitudes larger than about 0.001 milliseconds for periods larger than 10 days and less than about 500 days.

FIGURE 6-1. LAGEOS - BIH RESIDUALS IN U.T.
(SLOPE, AVERAGE, 1050d, 525d REMOVED)

DAYS (From 1976.0)

SECONDS
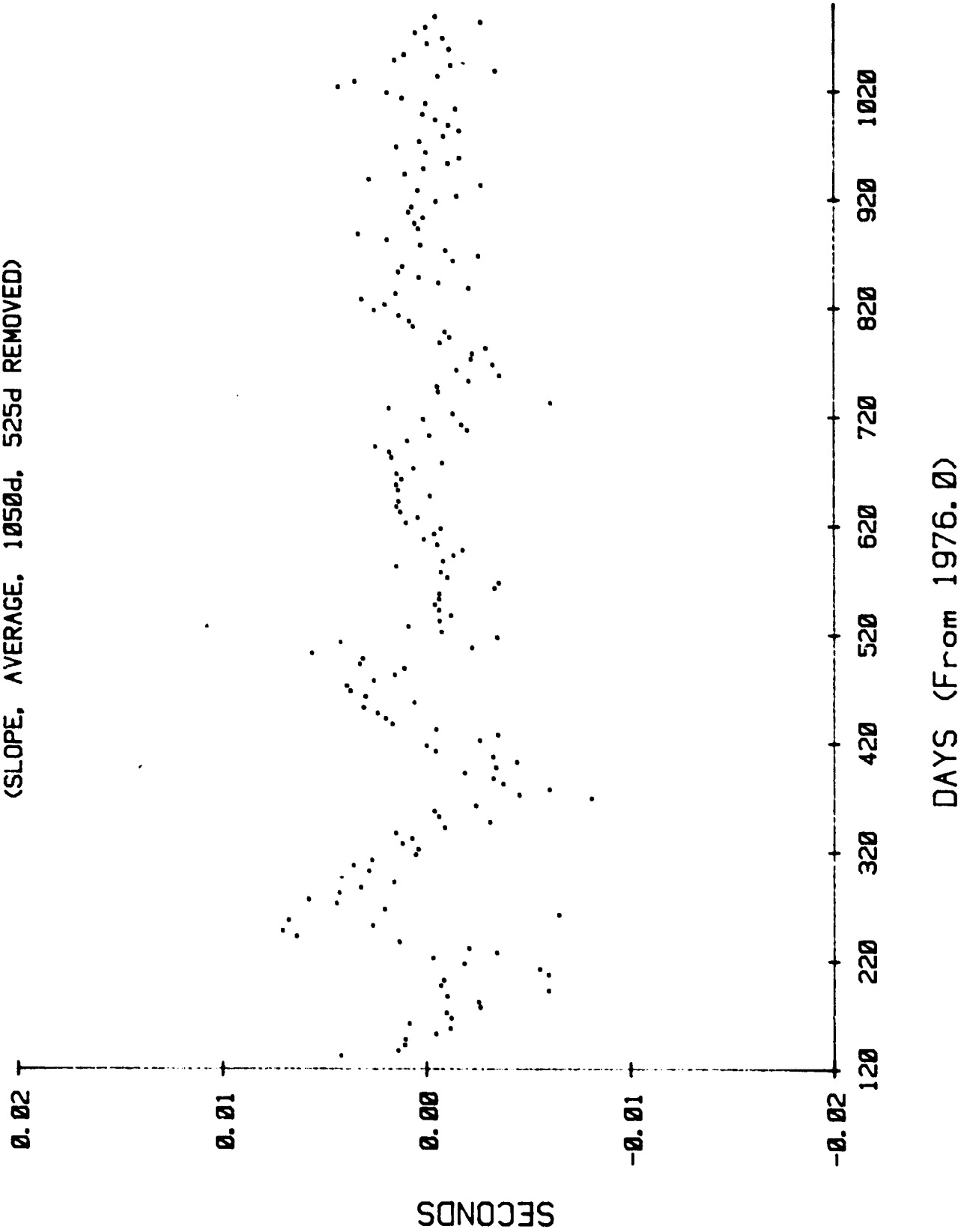
CHAPTER 7

SEA SURFACE TOPOGRAPHY

edited by

J.G. Marsh

OVERVIEW

The overall goal of this program is to apply remote sensing data to studies of dynamic ocean and Earth processes. The primary data types are satellite altimetry data, orbit perturbation data and gravity data. These data are analyzed in conjunction with surface observations, for example, ocean temperature and density measurements.

Global sets of satellite altimeter data have been collected during two satellite missions: The GEOS-3 mission (1975 to 1978) and the Seasat mission (1978).

Research programs are underway in the following areas to analyze and interpret the altimeter data:

o   The development and implementation of techniques for the calibration and performance evaluation of the altimeter systems.

o   The computation of regional as well as global mean sea surfaces which can be used as basic reference surfaces for analyzing dynamic ocean topography associated with ocean circulation.

o   Detailed analyses of the Gulf Stream and the associated eddy systems to improve our understanding of near surface as well as abyssal circulation.

o   The analyses of orbit evolution data for the computation of ocean tidal parameters which are important for studies of dynamic ocean circulation modeling and for precision orbit determination.

A description of these research programs is presented in the following sections.

Contributors to the sea surface topography work include Robert Cheney, Marie Colton, Vince Grano, Theodore Felsentreger, Ronald Kolenkiewicz and James Marsh.

A. MEAN SEA SURFACE COMPUTATION USING GEOS-3
AND SEASAT ALTIMETER DATA

by

J.G. Marsh

OBJECTIVE

The objective of this work is to compute a global mean sea surface using a combination of satellite altimeter data and precision orbital data based upon laser and Unified S-Band observations. This surface will form the basis for dynamical ocean processes analyses as well as for analyses of geophysical problems such as mantle convection.

BACKGROUND

The GEOS-3 radar altimeter experiment conducted during the period of 1975-1978 has provided a homogeneous grid of altimeter data over the oceans with a resolution in most areas of a degree or better. The precision of these data is on the order of 20 to 30 cm. The data set considered in the past year consisted of over 1.5×10^6 observations recorded during 1975 and 1976.

During the time period of July to October 1978 the Seasat radar altimeter experiment provided a global set of altimeter data with a precision of 10 cm. An 18-day global set of the Seasat data was initially preprocessed by the Jet Propulsion Lab and made available to the Seasat altiemter/orbit experiment team for evaluation. This data set consisted of about 700,000 observations and provided a grid spacing of about 1.5° at the equator.

Techniques and computer programs have been developed and implemented for: removing the effects of orbit error from the altimeter data; for editing the data; for gridding the data and forming sea surface topography maps.

RECENT ACCOMPLISHMENTS

The GEOS-3 altimeter data were recorded in the form of short arcs, most of which were a few thousand kilometers or less in length. Ground-based laser and S-Band tracking data required for precision orbit determination were available for only a portion of the altimeter data. In order to reference the altimeter data to a common center-of-mass reference system, precision orbits were computed covering 5-day arcs whenever possible. A total of 45 5-day reference orbits were ultimately computed using the GEM-10B gravity model. Since orbit error is long wavelength (i.e., once per revolution is the dominant frequency) the short altimeter passes unsupported by the ground based data could be corrected for orbit error through the adjustment of tilts and biases (Marsh, et al., 1979a). Due to the large amount of data involved, the earth was divided into 16 regions. The data in each region, except for the reference passes, were corrected using the results of the tilt and bias solutions and all the data were edited by comparing each point to the surface generated by the entire data set.

In this manner a data set covering almost the entire ocean surface was created which contained alongtrack altimeter data which had been corrected for orbital errors and edited to remove outliers. This alongtrack data set was then gridded using a 6-parameter, quadratic model of the surface at each grid point. The resulting 1° x 1° grid was contoured and is shown in Figure 7A-1. The geodetic constants of this surface were adjusted to conform to the 1979 IUGG set of constants.

The GEOS-3 data was especially dense in the GEOS-3 calibration area. Figure 7A-2 shows the groundtracks of GEOS-3 during times when altimeter measurements were being recorded.

To use this dense data coverage to reveal the local short-wavelength features of the geoid in this area, the technique used in producing the global surface was modified. In the global solution, the passes which belonged to the 5-day orbit set were not adjusted, and thus the orientation of the surface was determined by these fixed passes. For the "minimum constraint" solution, all the passes (except for 3 needed to provide a mean height and tilt to the surface) were allowed to adjust, thus removing the local effects of the orbit error as completely as possible. The data adjusted in this way were gridded, on a 0.25° x 0.25° grid, and this grid was adjusted to the IUGG spheroid, and the resulting grid contoured. This "minimum constraint" contour map is shown in Figure 7A-3.

Figure 7A-4 shows a contour map of the differences between the GEOS-3 minimum constraint altimeter surface and the GEM 8 5' detailed gravimetric geoid.

The GEOS-3 surface was adjusted to match the 5' gravimetric geoid in a relatively flat area of the Hatteras Abyssal Plain (ϕ: 23°-31°, λ: 288°-292°) by adjusting the X,Y,Z coordinate of its reference ellipsoid. Then this adjustment was applied to the entire area to produce the comparison map shown in Figure 7A-4. The differences over the Hatteras Abyssal Plain are generally less than 50 cm. The Gulf Stream is noted in the left portion of the figure. This comparison provides information on the precision of the GEOS-3 and gravimetrically-derived topography.

Figure 7A-5 shows a preliminary global sea surface which has been made using the 18-day set of Seasat altimeter data, recorded during July 28 to August 15, 1978, Marsh, et al., 1979b, 1980a. The surface computation technique employed was similar to that used for the GEOS-3 data. However, since the data was continuous and accurate orbit data (Marsh and Williamson, 1980b) could be computed for every pass of altimeter data, tilts and biases were not adjusted for a subset of the passes. Prior to surface computation analyses with the Seasat data, a timing bias analysis was necessary. The results of these analyses indicated that a timing correction of -79.4 m.s. should be applied to the data (Tapley, et al., 1979), Marsh and Williamson, 1980c.

The global GEOS-3 sea surface has been compared to the GEM-10B detailed gravimetric geoid and Seasat sea surface. All the surfaces were computed on a 1° x 1° grid. The rms differences between these surfaces are: GEOS-3 - GEM10B det. geoid, RMS = 2.69 m. GEOS-3 - Seasat, RMS = 1.30 m.

SIGNIFICANCE

Using radar altimetry and precise orbit data, techniques have been developed and utilized for the computation of mean sea surfaces on a a global as well as a regional scale. The accuracy of the global 1° x 1° GEOS-3 and Seasat surfaces is on the order of a meter or better and further improvements are expected as orbit accuracy is improved and more altimeter data are made available. Regional solutions covering a few thousand kilometers have a precision of better than 50 cm. Since the accuracy of these reference surfaces has already surpassed that which is available from gravity data, it is believed that they will provide an important reference for the measurement of temporal ocean circulation phenomena. These mean sea surfaces will also provide the basis for geophysical analyses such as mantle convection in the ocean areas.

FUTURE EMPHASIS

During the next few weeks the remainder of the GEOS-3 altimeter data, about 2/3 more than presently available, will be released by Wallops Flight Center. Also the total 70-day Seasat data set will be released by the JPL. These data will be combined for the extension of the present analyses. Regional computations will be performed as a function of time in an attempt to reveal time-dependent circulation features. Improved orbital force models, for example, new GEM gravity will be tested for improvement in computing the GEOS-3 and Seasat ephemerides.

REFERENCES AND PUBLICATIONS

Marsh, J.G., T.V. Martin, J.J. McCarthy, P.S. Chovitz, "Mean Sea Surface Computation Using GEOS-3 Altimeter Data," _Marine Geodesy_, Vol. 3, pp. 181-200, 1979a.

Marsh, J.G., R.G. Williamson, T.V. Martin, "Seasat Orbit and Altimeter Data Analyses," _EOS Transactions_, AGU, Vol. 60, No. 46, p. 806, 1979b.

Marsh, J.G., T.V. Martin, "Mean Sea Surface Computation Based Upon GEOS-3 Altimeter Data," submitted tothe _J. Geophys. Res._, 1980a.

Marsh, J.G., R.G. Williamson, "Precision Orbit Analyses in Support of the Seasat Altimeter Experiment," _Journal of the Astronautical Sciences_, Vol. XXVIII, No. 4, 1980b.

Marsh, J.G., R.G. Williamson, "Seasat Altimeter Timing Bias Estimation," submitted to the _J. of Geophys. Res._, 1980c.

Tapley, B.D., R.E. Schutz, J.G. Marsh, W.F. Townsend, G.H. Born, editors, "Accuracy Assessment of the Seasat Orbit and Altimeter Height Measurement," _Seasat Orbit Accuracy Assessmetn and Bias Calibration Workshop Report_, June 11-16, 1979, University of Texas, Austin.

FIGURE 7A-1

MEAN SEA SURFACE
TOPOGRAPHY BASED UPON
GEOS-3 ALTIMETER DATA

APRIL 1975 TO NOV. 1976
1° GRID, 2m CONTOUR
a₀·6378137m, ¹⁄f·298.257
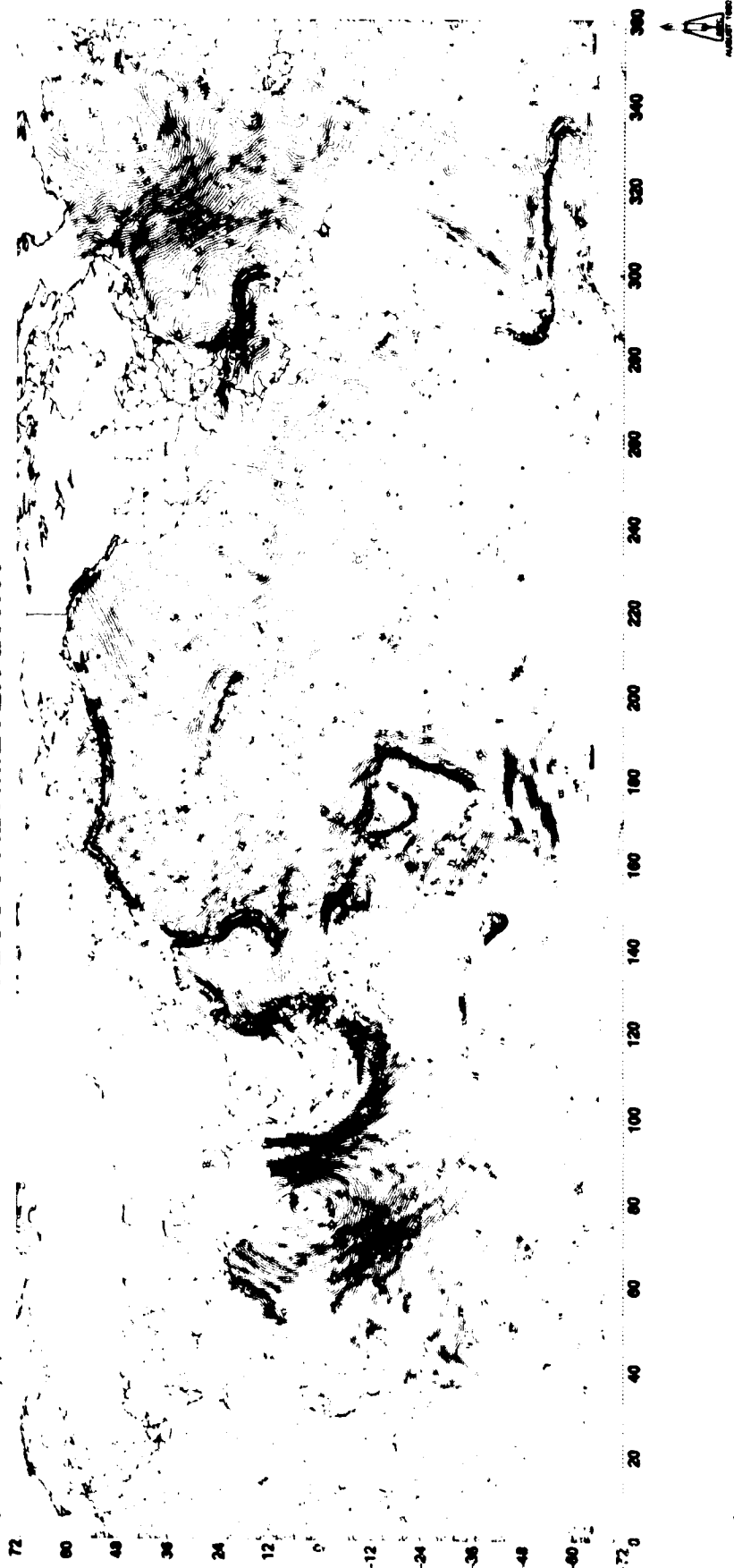
GEOS-3 ALTIMETER DATA
APRIL 1975 TO NOV. 1976
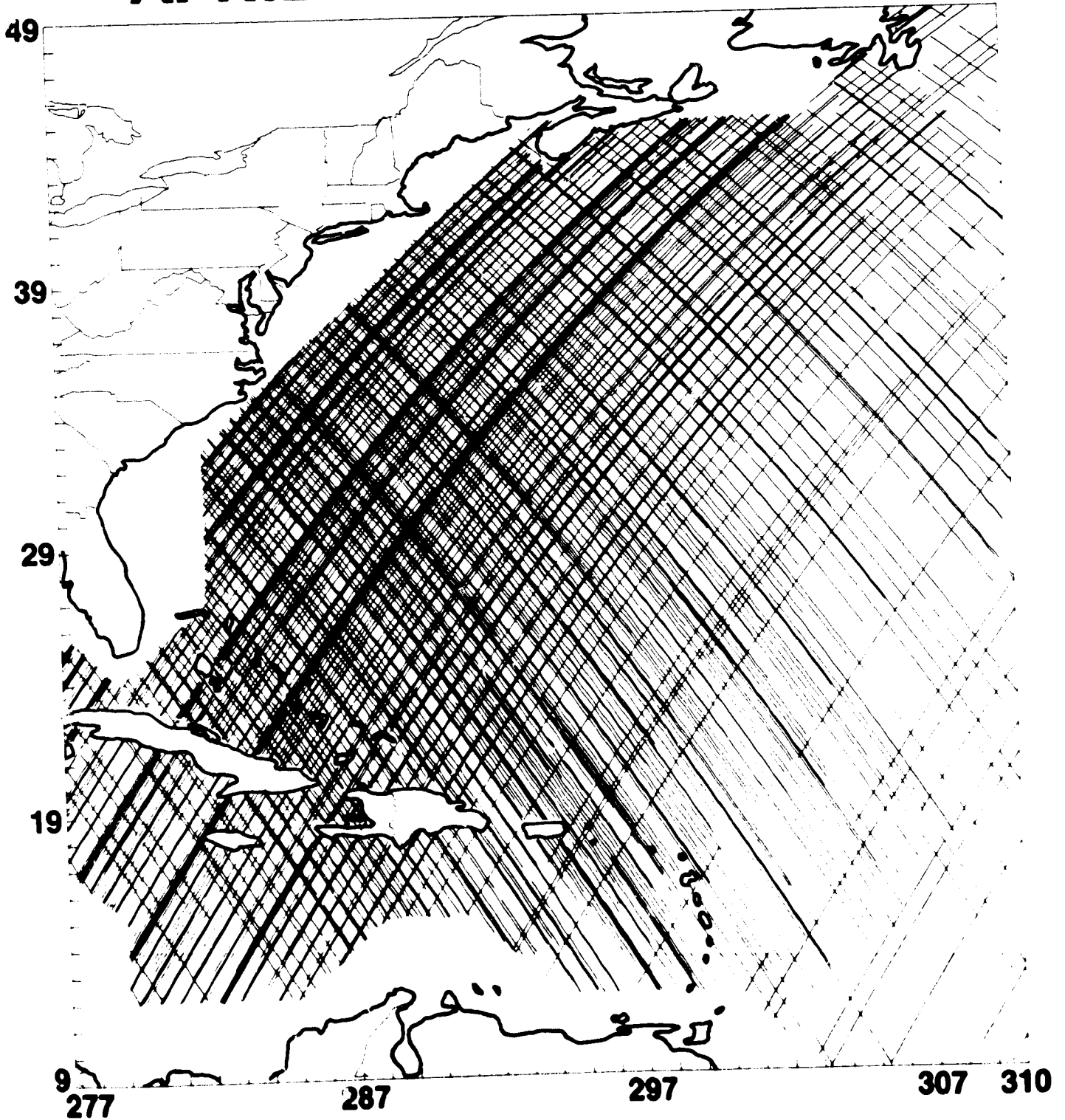
MEAN SEA SURFACE TOPOGRAPHY
BASED UPON GEOS-3
ALTIMETER DATA

APRIL 1975 TO NOV. 1976
0.25° GRID, 1m. CONTOUR
Ae = 6378 137, 1/f = 298.257

FIGURE 7A-5

MEAN SEA SURFACE
TOPOGRAPHY BASED UPON
SEASAT ALTIMETER DATA

DIFFERENCES BETWEEN THE GEOS-3
MEAN SEA SURFACE AND THE RECTIFIED
5' DETAILED GRAVIMETRIC GEOID

CONTOUR INTERVAL = 25 cm.

RECTIFICATION AREA

B. ALTIMETRIC STUDIES OF OCEAN CIRCULATION DYNAMICS
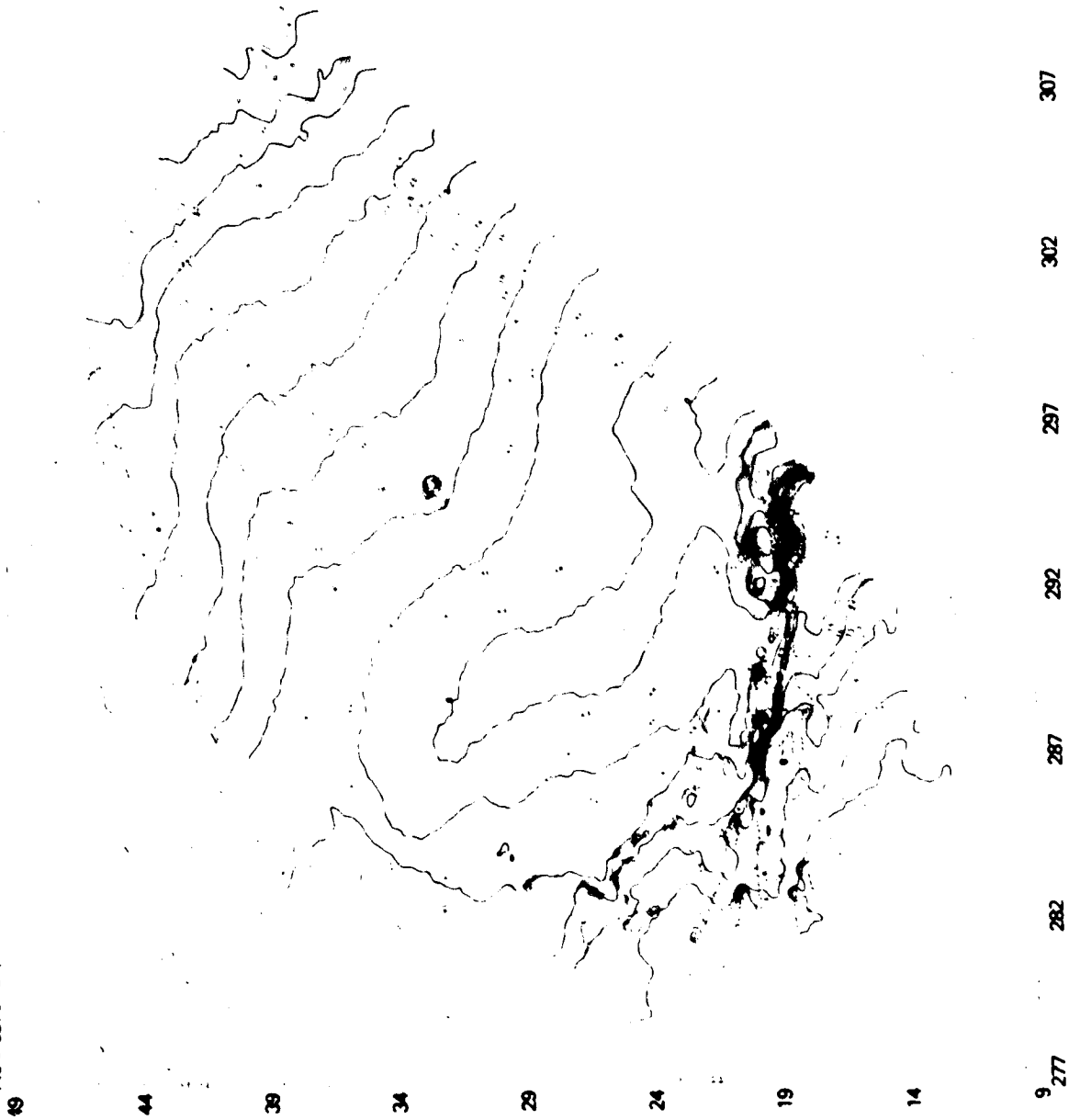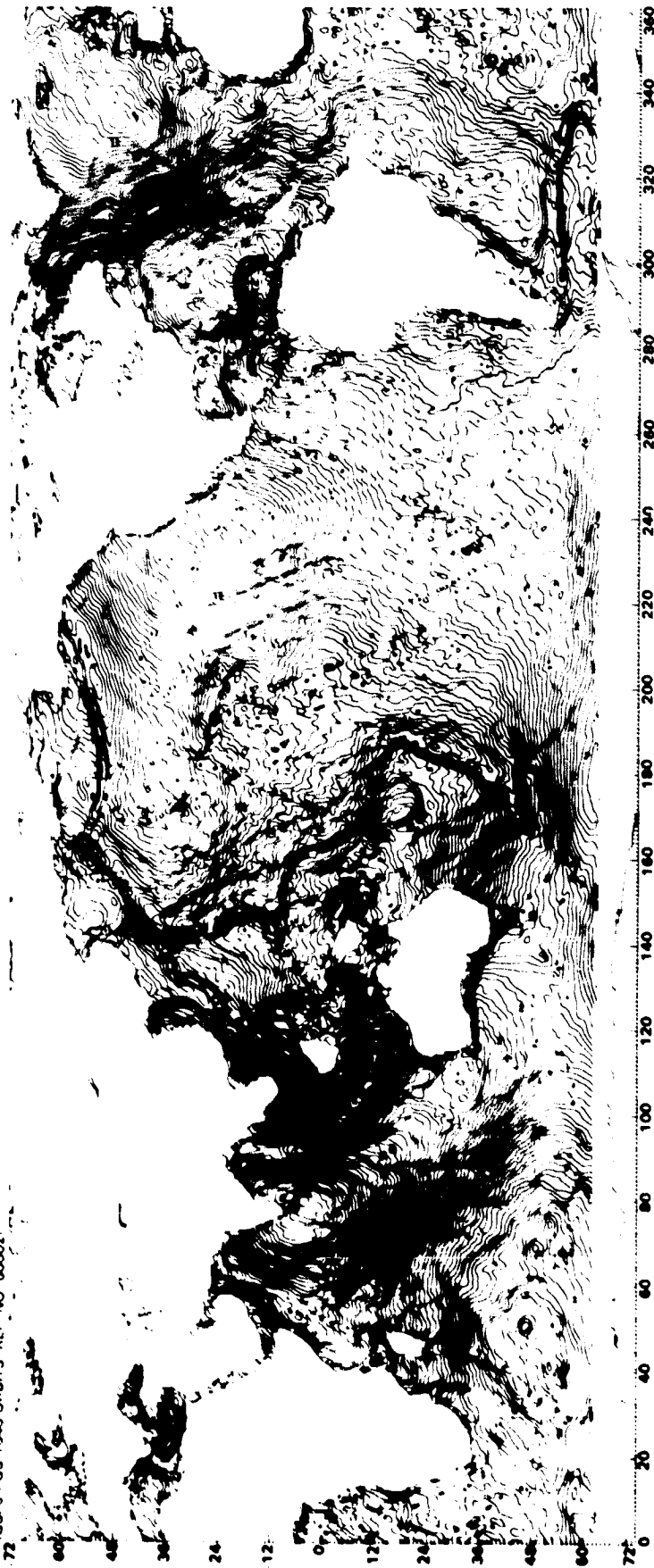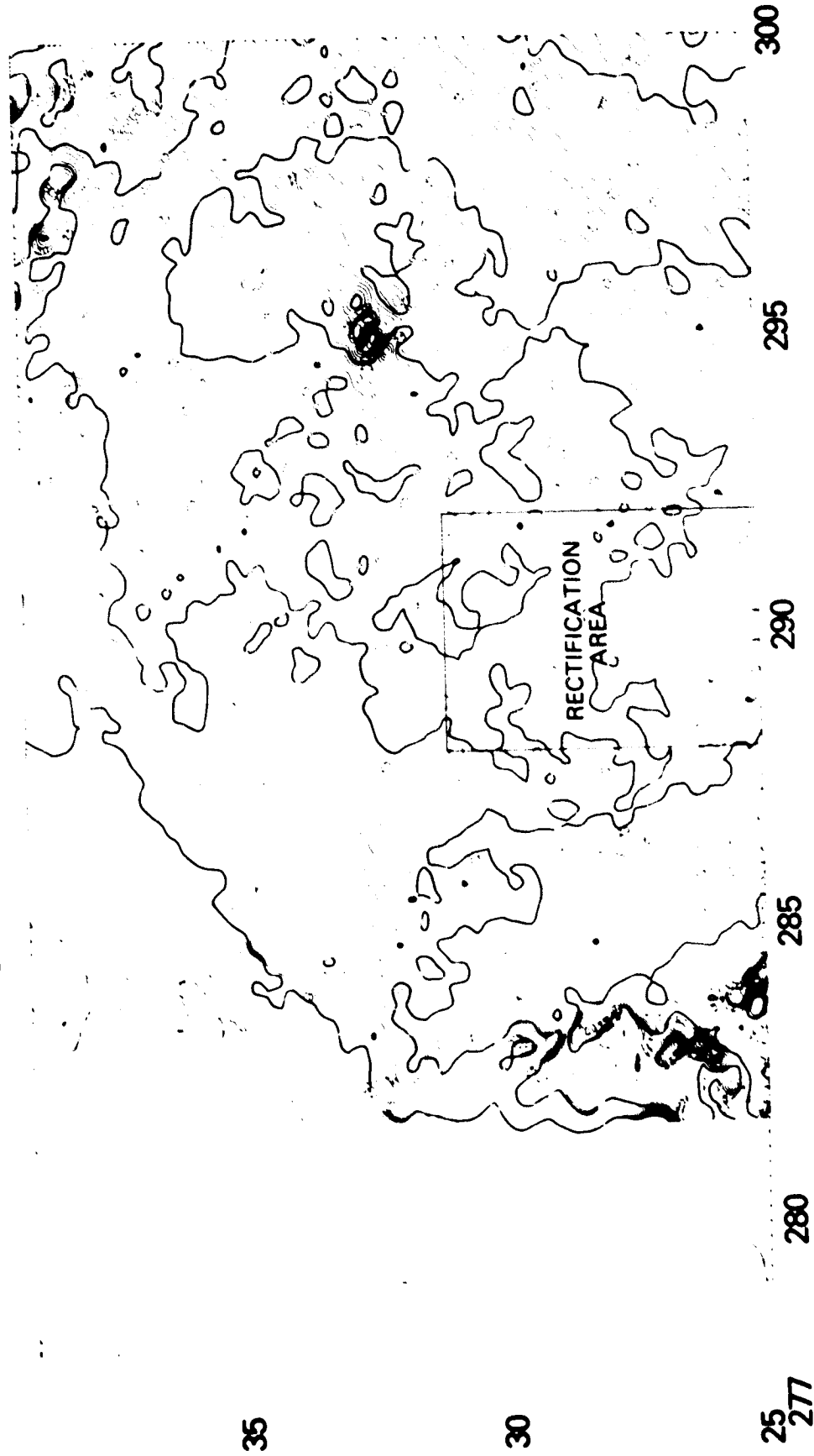
by

R.E. Cheney, J.G. Marsh, V. Grano, M. Colton

OBJECTIVES

The purpose of this work is to derive ocean circulation information from satellite altimetry. In principle, surface current speeds can be measured by combining altimeter data with geoid models to reveal dynamic sea surface slopes. While this approach has been successful in the Gulf Stream system where a detailed geoid model is available (Cheney and Marsh, 1980), such measurements are not possible elsewhere. Until improved geoids are available on a global scale, the major contribution of altimetry will be measurement of the time-variable component of flow (the eddy field). Accordingly, such analysis techniques are presently being developed in the Geodynamics Branch.

BACKGROUND

Altimeters have now been flown on two satellites; GEOS-3 gathered 25 cm data during 1975-78 and Seasat provided 10 cm altimeter data for 3 months in 1978. Orbits for these satellites were computed with an accuracy of approximately 1.5 m. The altimeter and orbit data have been combined to compute mean sea surfaces for various regions of the world oceans (Marsh, et al., 1980) and for the global ocean as a whole (Cheney and Marsh, 1980). These sea height maps provide more geodetic than oceanographic information, since heights due to ocean currents are two orders of magnitude smaller than the static topography due to gravity variations. However, the basic techniques involved in these computations can be extended to identify and measure eddy-like ocean features.

RECENT ACCOMPLISHMENTS

Two geoid-independent techniques are being investigated. Both provide quantitative as well as qualitative observations of eddy variability.

1. Crossover Differences

The point at which any ascending pass intersects any other descending pass is called a crossover. The time between the two intersecting passes can be less than a day or as long as the mission duration, 3.5 years in the case of GEOS-3. At the crossing points the geopotential contribution is the same on both tracks, so that the discrepancy in height between the two passes can provide a measure of the dynamic variability. Orbit error must first be removed by adjusting tilts and biases of the individual passes in a least squares minimization of the crossover differences.

To demonstrate this procedure, crossover difference statistics were derived in the western North Atlantic using 425 passes of GEOS-3 data taken over 1.5 years. Analysis of the 25,000 crossovers established by these passes clearly reveals the well-known energetics of the Gulf Stream system (Fig. 7B-1). The largest differences, 45-65 cm, occur in a continuous band along the mean axis of the Gulf Stream, and the level of variability gradually diminished to less than 25 cm toward the mid-ocean. These results are in agreement with similar maps derived from standard oceanographic data (Wyrtki, Magaard, and Hager, 1976; Dantzler, 1977).

2. Collinear Tracks

Altimeter profiles along identical ground tracks contain the same gravitational contributions due to sea surface topography. Time variations in sea height due to dynamic phenomena can therefore be detected in groups of collinear profiles. During the final 26 days of Seasat the ground tracks were repeated at 3-day intervals. A sample of these collinear data in the southwest Indian Ocean is shown in Fig. 7B-2. After removal of the mean from each of the eight profiles, a large transient is seen near 39°S-37°E, 800 km east of the Agulhas Plateau. The disturbance has a horizontal scale of 200 km, rms deviation about the mean of 22 cm, and the total range of sea surface height variation is 70 cm. This undulation is probably due to a migrating eddy, as observations by satellite-tracked drifters have revealed highly energetic vortices in this area.

SIGNIFICANCE

Altimeter analyses by crossover differences and collinear tracks permit investigation of global ocean variability independent of geoid knowledge. Orbit error is also not critical since both procedures involve orbit adjustment. The techniques are complementary in that the crossover approach provides good spatial resolution over long times, while collinear data allow synoptic observations but on a relatively coarse spatial grid. Together they should give a quantitative description of ocean eddy energy as well as the mean positions of major deep ocean currents.

FUTURE EMPHASIS

We plan to exploit these techniques in all ocean areas using existing altimeter data sets. Results should be especially important in remote areas such as the Southern Ocean where conventional observations are rare. Once the data are reduced to sea height variabilities, statistical analyses should provide additional information. For example, calculation of the structure function may yield dominant eddy scales. Potential real-time applications for NOSS (National Ocean Satellite System) may also emerge from these studies.

REFERENCES AND PUBLCATIONS

Campbell, W.J., R.E. Cheney, J.G. Marsh and N.M. Mognard, "Ocean Eddy Structure by Satellite Radar Altimetry Required for Iceberg Towing," Cold Reg. Sci. Tech., 1, 211-221, 1980.

Cheney, R. E., "A Search for Cold Water Rings with Seasat," Proceedings of the Symposium on Spaceborne Synthetic Aperature Radar for Radio Oceanography, The Johns Hopkins Oceanographic Studies, (in press), 1981.

Cheney, R.E., "Comparison Data for Seasat Altimetry in the Western North Atlantic," J. Geophys. Res., (submitted), 1981.

Cheney R.E. and J.G. Marsh, "Seasat Altimeter Observations of Dynamic Topography in the Western North Atlantic," J. Geophys. Res., (in press), 1980.

Cheney, R.E. and J.G. Marsh, "Determination of Mesoscale Eddy Statistics by Satellite Altimetry, EOS, (submitted) 1982.

Cheney, R.E. and J.G. Marsh, "Oceanographic Evaluation of Geoid Surfaces in the Western North Atlantic," Proceedings of the Symposium on Oceanography from Space, Venice, Italy, May 26-30, 1980, Plenum Press Marine Sciences Series, 1981.

Cheney, R.E., P.L. Richardson and B.P. Blumenthal, "Air Deployment of Satellite Tracked Drifters," J. Geophys. Res., 85, 2773-2778, 1980.

Cheney, R.E., P.L. Richardson, and K. Nagasaka, "Tracking a Kuroshio Cold Ring with a Free-Drifting Surface Buoy," Deep-Sea Res., 27, 641-654, 1980.

Dantzler, H.L., "Potential Energy Maxima in the Tropical and Subtropical North Atlantic," J. Phys. Oceanogr., 7, 512-519, 1977.

Kao, T.W. and R.E. Cheney, "The Gulf Stream Front: A Comparison Between Seasat Altimeter Observations and Theory," J. Phys. Oceanogr., (submitted), 1981.

Marsh, J.G. and R.E. Cheney, "Applications of Satellite Altimetry to Oceanography," Proceedings of the Symposium on Space Geodesy and Its Applications, Cannes, France, November 18-21, 1980.

Marsh, J.G., T.V. Martin, J.J. McCarthy and P.S. Chovitz, "Mean Sea Surface Computation Using GEOS-3 Altimeter Data," Marine Geodesy, 3, 359-378, 1980.

Wyrtki, K., L. Magaard and J. Hager, "Eddy Energy in the Oceans," J. Geophys. Res.,81, 2641-2646, 1976.
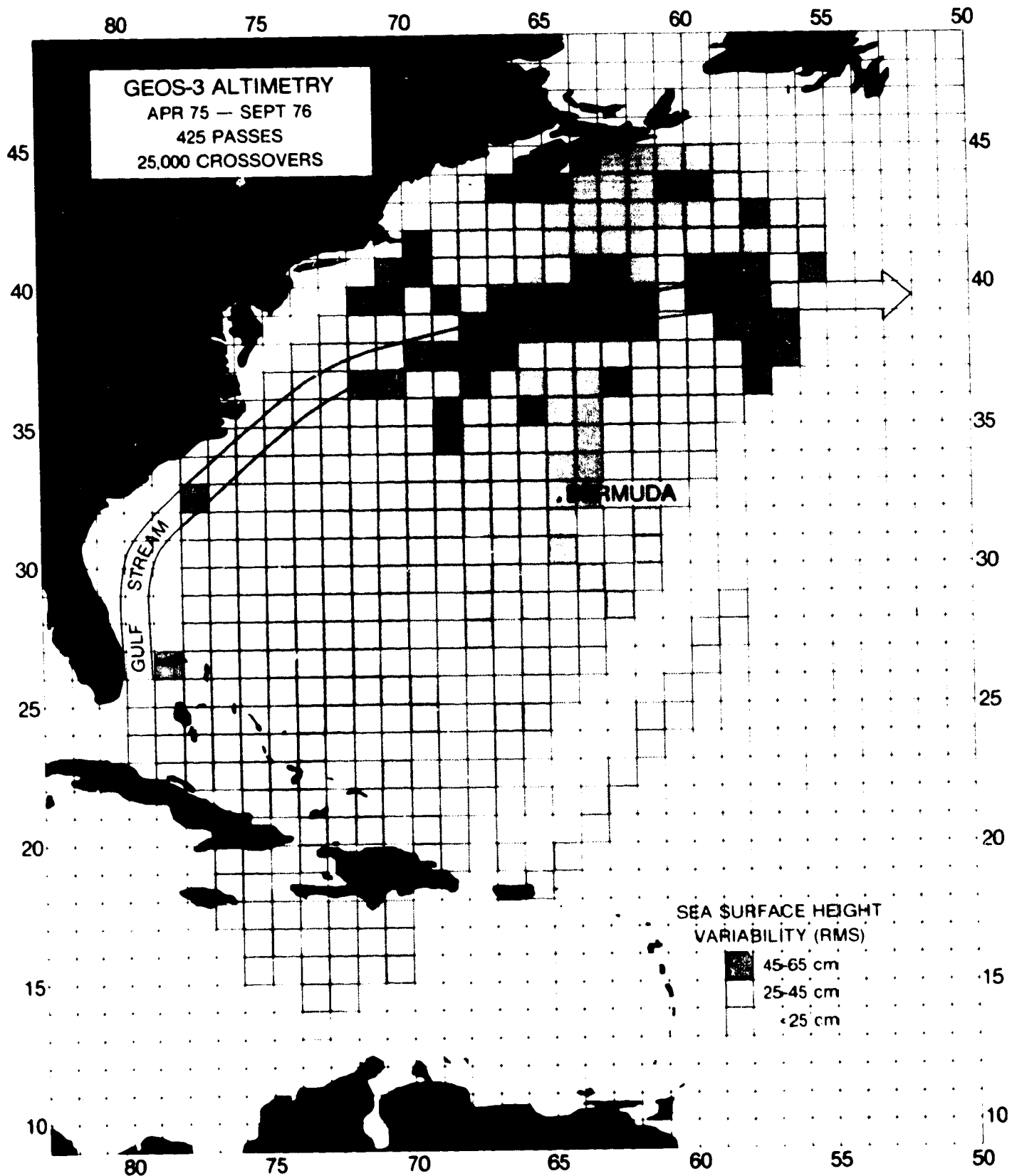
Fig. 7B-1. GEOS-3 altimeter data applied to detection of ocean current variability by analysis of crossover differences.
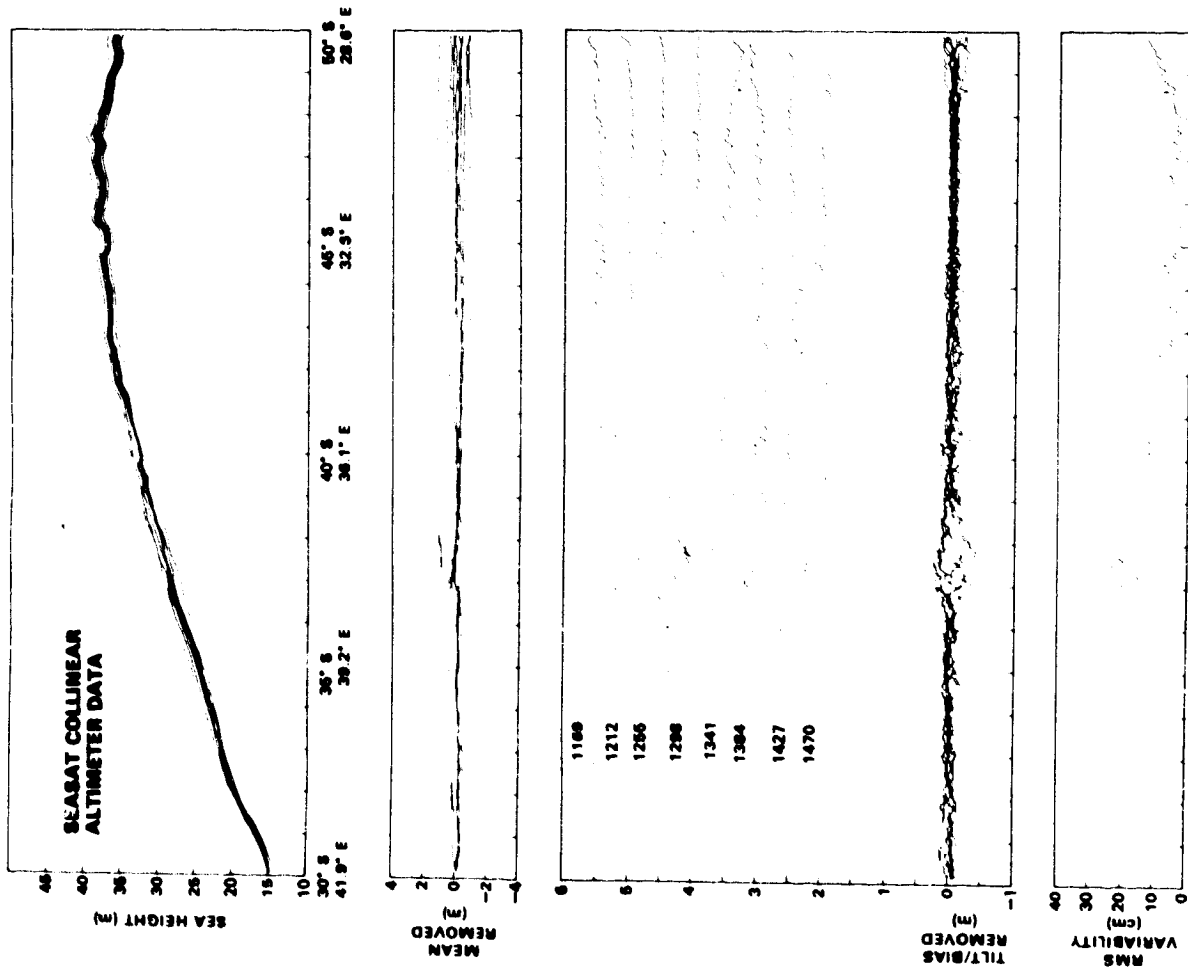
7-13

Fig. 7B-2. Analysis of 8 collinear altimeter profiles collected by Seasat in the southwestern Indian Ocean, September 16 to October 7, 1978. The feature at 39°S is thought to be a migrating eddy.

C.   <u>THE SEASAT ALTIMETER HEIGHT CALIBRATION</u>

by

R. Kolenkiewicz

OBJECTIVE

The objective of the Seasat-Altimeter height calibration effort
is to obtain an accurate value of the precision of the altimeter
measurement, the bias in the altimeter measurement after it has
been subjected to the process of correcting for the instrument
and geophysical effects during the computation of the altimeter
data tape and the bias in the time tag assigned to the measurement.
Applications of this information include, e.g., determination of
the semimajor axis of the ellipsoid best approximating the geoid.

BACKGROUND

The Seasat A spacecraft was launched from Vandenburg Air Force
Base on June 26, 1978. Until spacecraft failure on October 10, 1978,
the Seasat altimeter has taken data on several thousand passes.
In order to obtain full usage of these data a calibration (or
height bias determination) of the altimeter is necessary.

The validation of the altimeter measurement from the spacecraft
to the mean sea surface requires situations in which this distance
can be accurately inferred, independent of the altimeter data
itself. Effectively, this can be done using satellite passes which
are nearly overhead at island laser tracking sites. This technique
has the advantage that an accurate <u>a priori</u> knowledge of geoid
heights is not required.

In support of altimeter height bias calibration, the Seasat orbit
was adjusted on September 10, 1978, to obtain a repeating (every
43 revolutions, approximately 3 days) groundtrack which passes as
close as possible to the Bermuda laser site. Between September 10
and the spacecraft power failure on October 10, 1978, there were
10 North to South Bermuda overflights with the groundtracks shown
in Figure 7C-1. All passes were supported by the NASA Spacecraft
Tracking and Data Network (STDN), with four passes supported by the
Bermuda laser. These laser supported passes provide the primary
information for absolute bias calibration and stability analysis
of the Seasat Altimeter. The remaining six passes are useful,
however, for analyzing errors in smoothed and extrapolated altimeter
data across Bermuda. With extensive analysis, these passes could
also be used to help develop a geoid model in the vicinity of the
Bermuda laser and thus simplify future altimeter calibration efforts.

The Seasat altimeter calibration technique is based on GEOS-3
experience (Martin and Kolenkiewicz, 1980). It consists basically
of the use of altimeter passes over Bermuda with laser tracking
support (for accurate orbit height determination) and altimeter
tracking, on both sides of Bermuda, which can be extrapolated to
obtain equivalent sea surface height measurements on the island
itself. The objective is to create an equivalent altimeter

measurement over the laser tracking site which can be related to sea surface heights several kilometers away from the island with an accuracy compatible with a total calibration error budget of 7 cm. A bias of this accuracy can then be used to produce corrected altimeter data which will have the proverbial 10 cm accuracy (Martin, 1977). Available geoid models cannot provide the desired accuracy, so it is necessary to use the altimeter data itself to provide the water-land extrapolation. No geoid model was used ·in the calibration analyses discussed below.

To demonstrate the elements of the overhead calibration technique, consider the basic calibration geometry as shown in Figure 7C-2. Assuming a pass directly over a laser tracking station with continuous laser and altimeter tracking, the measurements directly over the tracking station can be used for bias estimation by equating the altimeter measurement, corrected to the ellipsoid, with the laser measurement also corrected to the ellipsoid. Equating the two measurements shown in Figure 7C-2,

$$h_a - b + h_t = \delta h + h_{ga} = h_{gs} + h_m + R \tag{1}$$

where

h_a = measured altimeter height above the sea surface corrected for instrumental and atmospheric propagation effects and spacecraft center of mass offset.

b = bias in the altimeter measurement,

$h_t + \delta h$ = tide measurement as determined by the tide guage at the time of the altimeter pass. This measurement includes non-tidal temporal sea surface variations,

h_{ga} = geoid height at the altimeter subsatellite point,

R = measured distance from the laser tracking station to the laser corner cube reflectors corrected for instrumental and atmospheric propagation effects and spacecraft center of mass offset,

h_m = height of the tracking station above mean sea level (the geoid) at the tracking station,

h_{gs} = geoid height at the tracking station.

The altimeter measurement bias can thus be determined using Equation (1), from the expression:

$$b = h_a + h_t + \delta h + h_{ga} - [R + h_{gs} + h_m] \tag{2}$$

The terms in brackets on the right-hand side of Equation (2) constitute the ellipsoidal height normally calculated in orbit determination programs, while the terms outside the brackets give the ellipsoidal height based on the altimeter measurements, a measured tide, and a geoid model. The right-hand side is thus the "observed" minus "computed" measurement, normally referred to as the measurement residual. The residual can be calculated whether the satellite is directly over the laser site or not, although only at the direct overhead point will the two geoid heights be identical and thus cancel.

In practice, the altimeter cannot accurately track directly over the laser site because of land in the altimeter footprint, and the laser does not track directly overhead because its Az-El mount cannot follow the high azimuth rates in the vicinity of the point of closest approach (PCA). However, the latter is not a problem because an accurate overhead orbit can be estimated with a gap in the data around the PCA.

After deleting measurement points which have been significantly influenced by the presence of land in the footprint, the altimeter data can be smoothed across Bermuda to obtain extrapolated alti- meter residuals at the groundtrack point of closest approach to the laser site. These extrapolated residuals can then be used along with the laser orbit and various corrections to obtain the altimeter height bias.

RECENT ACCOMPLISHMENTS

As the altimeter cannot produce sea surface measurements across the island, the "residuals" were computed, using Equation (2), for the period when the altimeter was not significantly influenced by land and extrapolated across the island. Waveforms for data points in the vicinity of Bermuda were analyzed for all four calibration passes, Table 7C-1, to determine any evidence of land effects. AGC records for this data were also analyzed as an aid in detecting the influence of land in the altimeter footprint, although AGC effects on height are only second order. All points with any evidence of land in the waveforms were deleted. Any additional points which showed evidence of anomalous height behavior near Bermuda were also deleted. The resulting data set, shown in Figure 7C-3, with edited points indicated by O's and accepted measurements indicated by X's can be used to estimate geoid heights along the ground truth across Bermuda for each of the four calibration passes.

There are some simplifications that were made in Equation (2), primarily in the h_a term. In practice, this quantity must be obtained from the measured altitude data, corrected for propaga- tion effects, instrumentation errors, and sea state effects. Most of these corrections are at the centimeter or decimeter level. In addition, there are a few other corrections to be made due to idiosyncrasies of some of the data and/or reductions.

The raw smoothed altimeter residuals for a typical Bermuda over-flight are shown in Figure 7C-4. The smoothed residuals were obtained by using the ALTKAL smoother (Fang and Amann, 1977). The points of closest approach to the laser site are indicated, and the residuals at these times are listed in Table 7C-2 as the starting point for the bias estimations. If these passes were all over the laser site, we would have four different calibration values. However, none of them cross directly over the laser. Figure 7C-5 shows the different corrected residuals, plotted as a function of distance from the laser site (measured in the northwest direction). Assuming the geoid to be linear along this direction, as has been confirmed by GEOS-3 altimeter data (Martin and Butler, 1978), a straight line fit has been made to the four points in order to estimate the corrected residual at the laser site. The best estimate of the intercept with the zero distance is 39.90 ± 0.07 m.

One final correction which has not yet been applied to the alti-meter residuals is the effects of acceleration lag. The acceleration lag error is $Accel/K_A$., where $K_A = 6.5/sec^2$. For all four passes at the closest approach to laser point, the lag correction is approximately 7 cm. Adding this correction and the geoid height at the laser to the residual obtained from Figure 7C-5 have:

	Residual at laser site		39.90 m
+	Acceleration lag correction		.07 m
+	Geoid height at laser site		-39.97 m
	Bias	=	0.00 m

It is thus concluded that if the Seasat altimeter data is accurately corrected for propagation effects, and is corrected for sea state bias with a procedure equivalent to the one used in the analysis, the appropriate bias for the altimeter 0.0 ± 0.07 m. Assuming a data noise level of 7 cm, which was in fact observed at even the 10/sec data rate for all the cali-bration passes, the Seasat altimeter is indeed a 10 cm altimeter.

SIGNIFICANCE

The absolute bias calibration for the Seasat-A altimeter has been measured. This correction can be applied to these data to enable investigators to determine important geophysical parameters.

FUTURE EMPHASIS

This work has been completed. Results will appear in a special Seasat issue of the Journal of Geophysical Research.

REFERENCES AND PUBLICATIONS

Born, G.H., H.H. Hagard, M.E. Parke, J.M. Diamante, B.C. Douglas, C.C. Goard, R. Kolenkiewicz, and J.G. Marsh, "Altimeter Height Timing Bias Report," presented at Oceans '79, The Institute of Electrical Engineers, Inc. and the Marine Technology Society, San Diego, CA, 1979.

Fang, B.R. and D.W. Amann, "ALTKAL--An Optimum Linear Filter for GEOS-3 Altimeter Data," NASA CR-141429, August 1977.

Kolenkiewicz, R., and C.F. Martin, "Preliminary Determination of the Seasat Altimeter Height Bias," presented at the 1979 Spring Meeting of the American Geophysical Union, Washington, DC; EOS Transactions, American Geophysical Union, Vol. 60, No. 18, May 1979.

Kolenkiewicz, R. and C.F. Martin, "The Seasat Altimeter Height Bias Using Four Bermuda Overflights," presented at the Seasat Colloquium, Scripps Institution of Oceanography, LaJolla, CA, October 29-31, 1979.

Kolenkiewicz, R., and C.F. Martin, "Refinement of the Seasat Altimeter Height Bias Using 12 Bermuda Overflights," presented at the 1979 Fall Meeting of the American Geophysical Union, San Francisco, CA, EOS Transactions of the American Geophysical Union, Vol. 60, No. 46, November 1979.

Kolenkiewicz, R. and C.F. Martin, "Seasat Altimeter Height Calibration," NASA TM 82040, October 1980.

Martin, C.F. and M.L. Butler, "Calibration Results for the GEOS-3 Altimeter," NASA CR-14143, September 1977.

Martin, C.F., and R. Kolenkiewicz, "Calibration Validation for the GEOS-3 Altimeter," NASA TM 80710, June 1980.

Tapley, B.D., G.H. Born, H.H. Hagar, J. Lorell, M.E. Parke, J.M. Diamante, B.C. Douglas, C.C. Goad, R. Kolenkiewicz, J.G. Marsh, C.F. Martin, S.L. Smith, III, W.F. Townsend, J.A. Whitehead, H.M. Burne, L.S. Fedor. D.C. Hammond, N.M. Mognard, "Seasat Altimeter Calibration, Initial Results," Science, Vol. 204, pp 1410-1412.
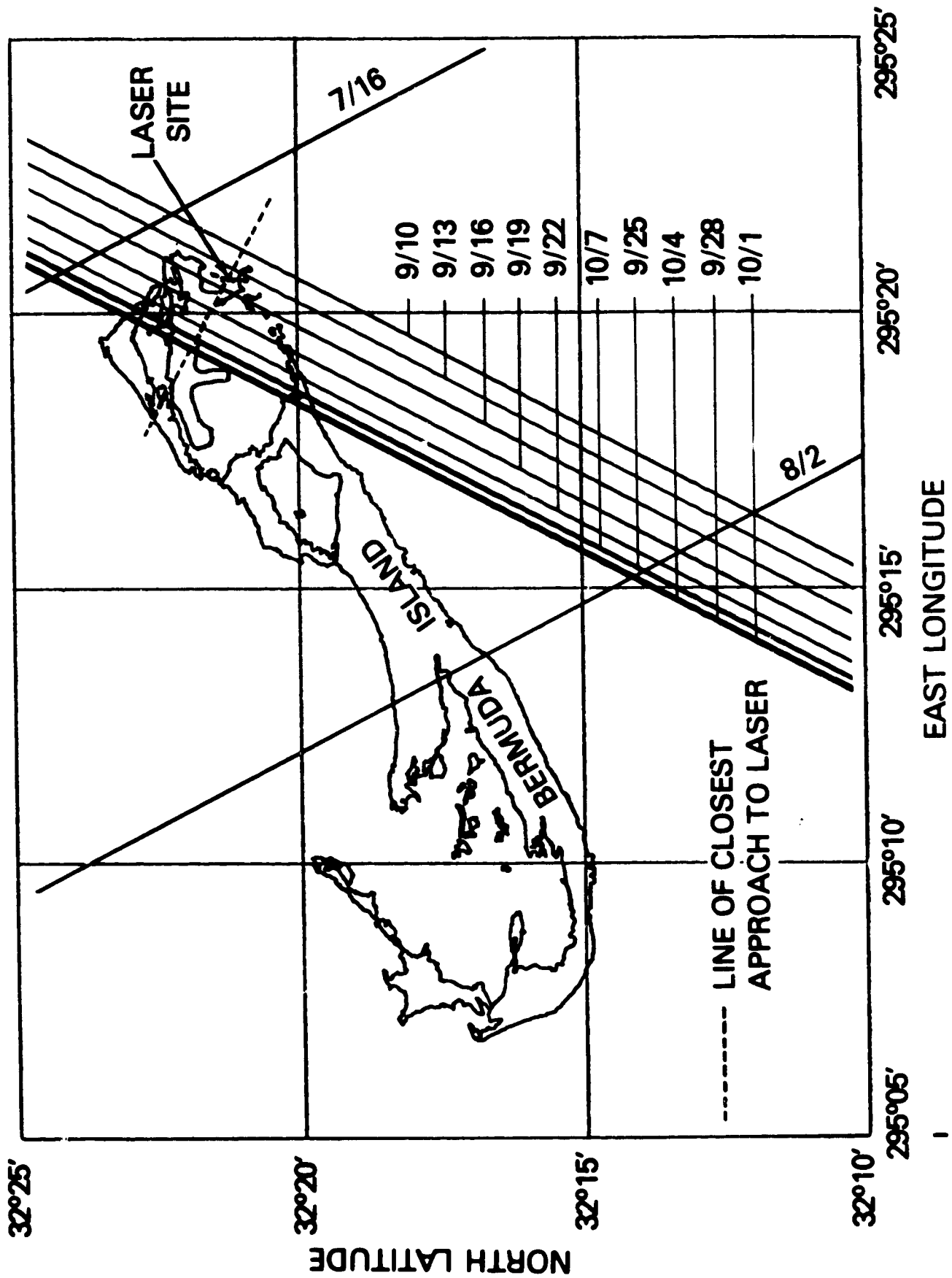
Fig. 7C-1. Groundtracks for Bermuda calibration overflights.
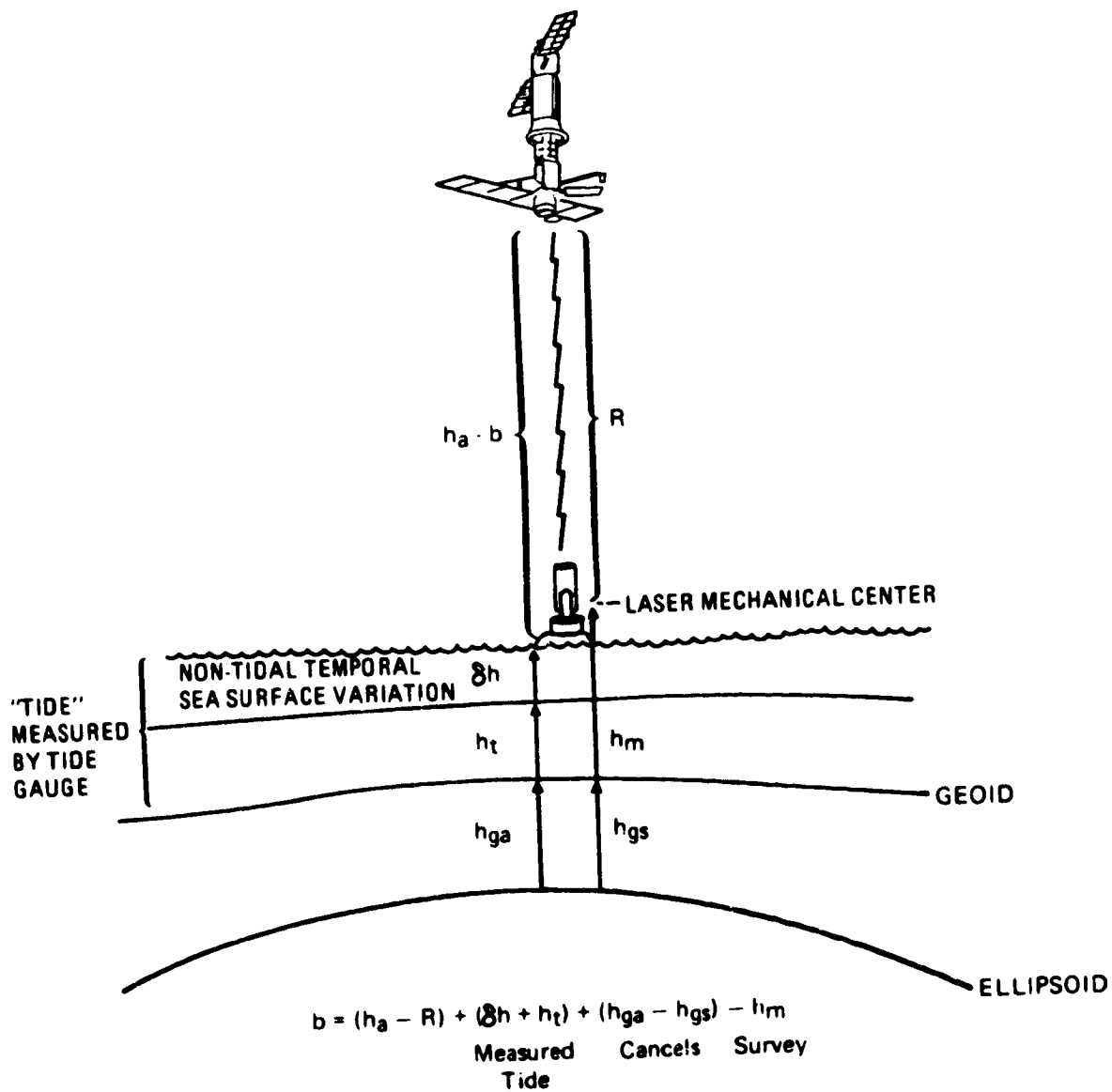
Fig. 7C-2. Calibration geometry using overhead pass.

$$b = (h_a - R) + (\delta h + h_t) + (h_{ga} - h_{gs}) - h_m$$

Measured   Cancels   Survey
Tide
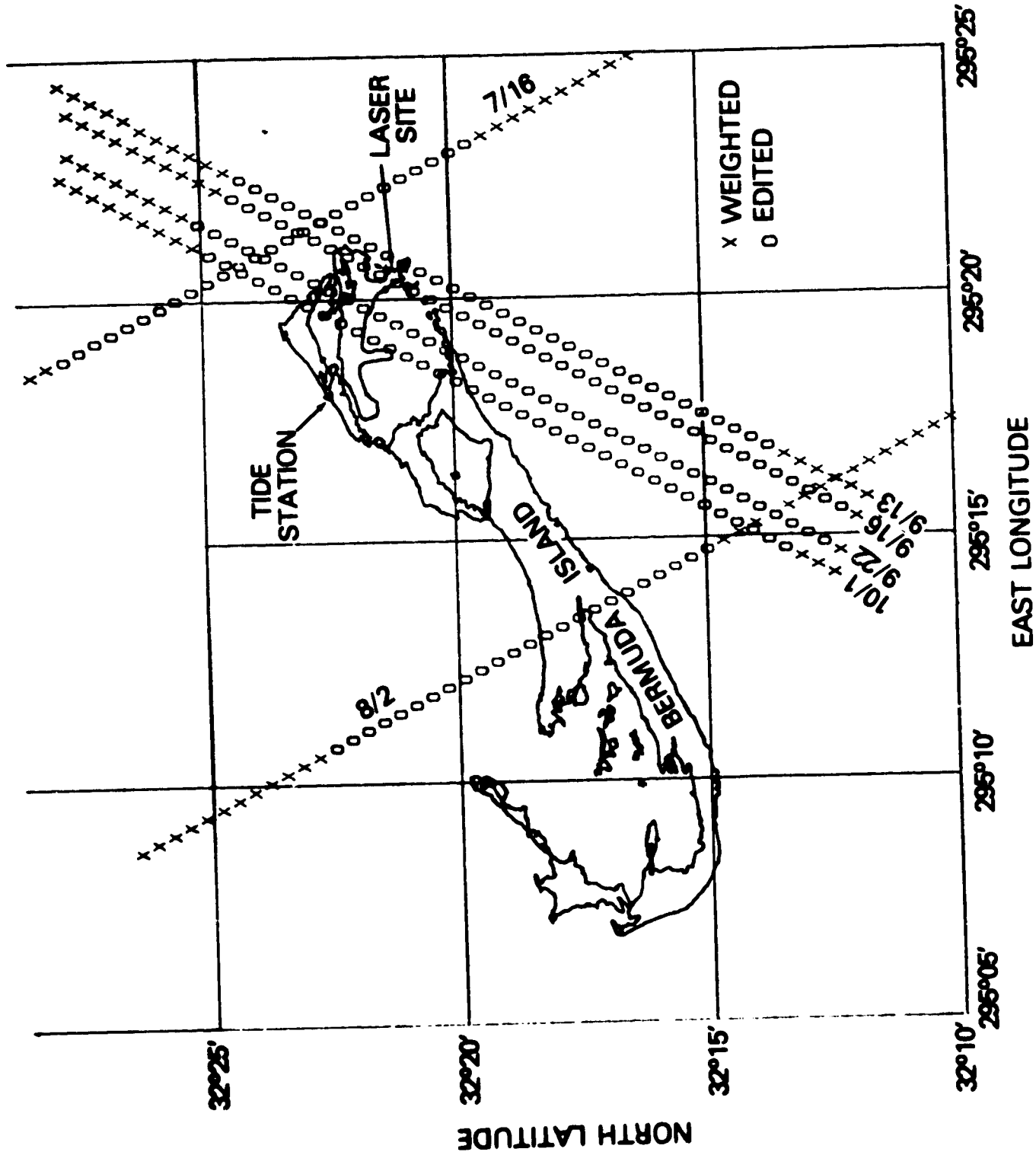
Fig. 7C-3. Groundtracks for four laser-supported north to south Bermuda overflights showing edited data segments.
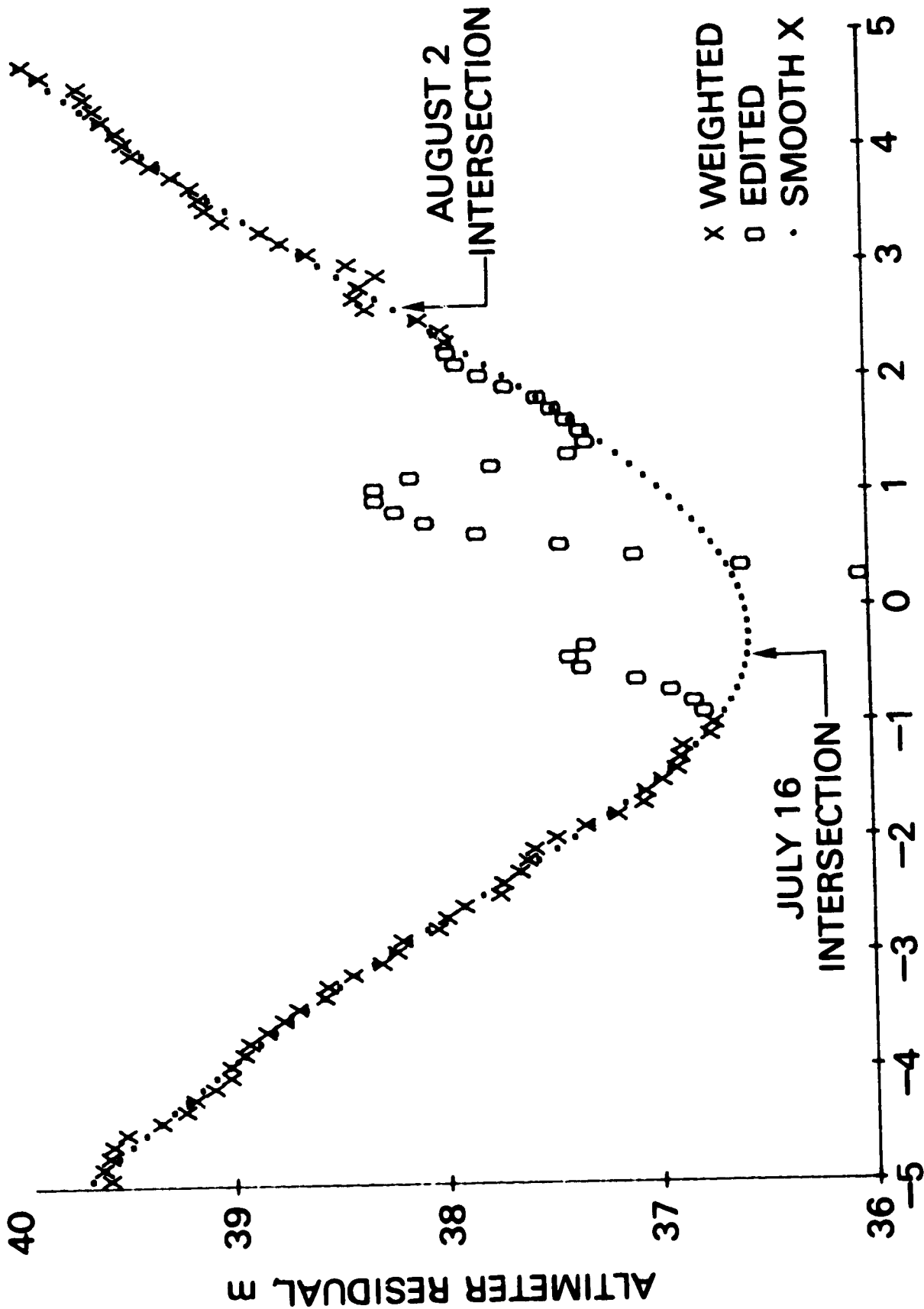
Fig. 7C-4. Altimeter residuals for Seasat pass on September 13.
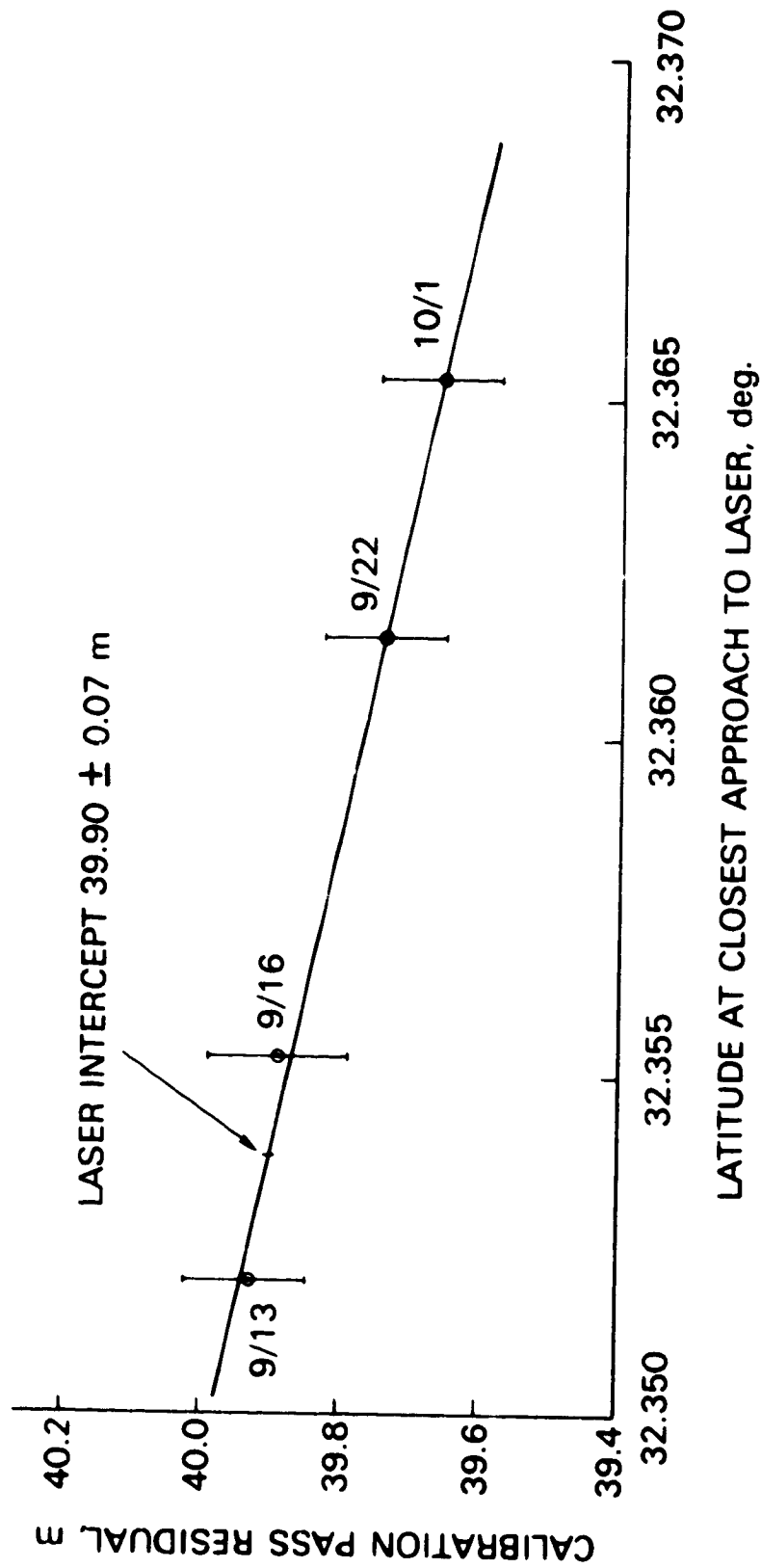
Fig. 7C-5. Smoothed altimeter residuals at closest approach to laser.

TABLE 7C-1. TRACKING SUPPORT USED FOR CALIBRATION ORBIT ESTIMATION

Date of Pass	9/13/76	9/16/76	9/22/76	10/1/76
Data Start Time	$2^h58^m43^s$	$1^h50^m40^s$	$3^h38^m1^s$	$3^h0^m50^s$
Data End Time	$4^h43^m47^s$	$4^h59^m40^s$	$5^h21^m57^s$	$6^h5^m30^s$
Laser Support on Overflight Pass	Bermuda, Grand Turk	Bermuda, Grand Turk	Bermuda, Goddard	Bermuda, Grand Turk
Laser Support on Pass Following Overflight	Patrick	None	Patrick, Goddard	None
S-Band Stations Used	None	Santiago, Merritt Island, Bermuda	None	Santiago, Merritt Island, Bermuda

TABLE 7C-2. TIMES, LATITUDES, AND RESIDUALS FOR CLOSEST APPROACH TO LASER

DATE OF PASS in 1978 (M/D)	TIME (H:M:S)	LATITUDE (DEG.)	CORRECTED RESIDUAL (m)
9/13	03:02:06.9541	32.3520	39.93
9/16	03:14:52.6862	32.3553	39.88
9/22	03:40:23.7821	32.3615	39.73
10/1	04:18:37.8574	32.3653	39.66

CHAPTER 8

LAND RESOURCES

edited by

C. Lisette Dottavio

OVERVIEW

Over the years, man is becoming more aware of the utility and importance of land resources such as timber, soils, and wetlands. The management and conservation of these resources has become a priority to insure their availability in the future. Successful management is, in part, dependent upon the acquisition of accurate and timely land cover and land use information. Satellite remote sensor systems such as the Landsat Multispectral Scanner, are uniquely capable of providing this information because of the satellite's repetitive and synoptic view of the Earth's surface. Personnel within the Land Resources Group of Goddard's Earth Resources Branch are dedicated to evaluating and improving remote sensing systems and analysis techniques to provide the information required for intelligent resource management decisions.

The Land Resources Group consists of seven quantitative resource discipline scientists with remote sensing backgrounds. Their research activities include forest disturbance assessment, urban land and forest land change detection, applied software development, and improved land cover classification studies. The projects represent a diversity of land resources applications, yet their results can often be integrated to provide a greater understanding of how best to monitor and assess resource conditions using remotely sensed data.

A major research effort underway is coordinated with the AgRISTARS Renewable Resource Inventory (RRI) Activities. The Land Resources Group is developing, and testing image analysis techniques that will facilitate the use of remotely sensed data to accurately detect, classify, and assess the areal extent and severity of forest disturbances. In addition to improving analysis techniques, personnel are examining the spectral and spatial properties of numerous forest disturbances, and the use of satellite data to detect major changes in forest canopy conditions. This AgRISTARS/RRI research is a product of previous research on the use of Landsat to monitor gypsy moth defoliation of hardwood forests. Another outgrowth of that work is a three year Applications Pilot Test with the Pennsylvania Department of Environmental Resources to demonstrate the technical feasibility of conducting automated, annual assessments of insect defoliation of hardwood forests using Landsat digital data.

Considerable effort is also being devoted toward examining the utility of future satellite systems such as the Landsat-D Thematic Mapper (TM) for resource evaluations. Studies will emphasize the use of TM data to monitor rural areas disturbed by strip mining, to inventory wetland habitats and forests, and to examine urban land cover.

Two other investigations are currently underway which address urban land cover and applied software development. The former study will finalize the development, evaluation, and documentation of urban area change detection techniques which were initiated under a previous NASA/Census Bureau Applications Pilot Test. The latter study is designed to develop a method to classify high resolution remotely sensed data into land use classes, such as industrial, commercial, or residential based on the relative distribution of image components such as roofs, pavement, trees, and lawn.

The variety of research topics listed herein illustrates the diverse interests and expertise available within the Land Resources Group. To facilitate the research activities, Goddard has access to a number of image processing and computer systems. Studies continue to expand so that a more complete understanding of how to utilize remotely sensed data in natural resource management can be obtained.

A. DETECTION, CLASSIFICATION AND MEASUREMENT OF FOREST DISTURBANCES

by

C.L. Dottavio and D.L. Williams

OBJECTIVES

A major effort underway at Goddard's Earth Resources Branch involves the remote monitoring of natural and man-induced forest disturbances. This research effort is designed to develop and test new or existing techniques that will facilitate the use of remotely sensed data to accurately detect, classify, and assess the areal extent and severity of forest disturbances and stress conditions.

BACKGROUND

For the past several years, research has been conducted by Goddard personnel to determine the feasibility of using Landsat multispectral scanner (MSS) data to identify hardwood forest stands that have been defoliated by the gypsy moth caterpillar during the insect's summer feeding cycle. As a result of the defoliation research, Goddard has been requested to participate in the AgRISTARS/Renewable Resources Inventory (RRI) research activities.

The AgRISTARS/RRI research program initiated in FY80 is a six year program which emphasizes the development and evaluation of new remote sensing technology to be applied in the inventory, monitoring, and managing of forest land and rangeland renewable resources. Goddard is assuming total responsibility for a number of key research tasks under AgRISTARS/RRI Problem Area 4 - Detection, Classification, and Measurement of Forest Disturbances. Among these tasks are included a sensor parameter study, a forest disturbance assessment study, forest change detection technique development, and an advanced change monitoring system. During the past year, activities were initiated on the first two tasks listed. Subsequent research will involve all the areas mentioned.

RECENT ACCOMPLISHMENTS

Previous results in the gypsy moth defoliation study had shown that aspect may modify the spectral response of various hardwood canopy conditons such that healthy vegetation and stressed vegetation are often confused when classifying Landsat MSS data. A preliminary field investigation was recently completed to examine the radiometric properties of a hardwood forest as a function of canopy conditions, aspect, time, and date. The study was also designed to develop a standardized, quantitative ground based technique to calibrate Landsat classification results.

Diffuse radiance measurements were taken using a Mark II Three Band Radiometer. The instrument is designed to measure energy in three

wavelength regions that correspond to Landsat D's Thematic Mapper bands TM3 (red, 0.63-0.69 µm), TM4 (reflective infrared, 0.76-0.90 µm) and TM5 (middle infrared 1.55-1.75 µm). Radiance was measured by holding the radiometer 45 cm above a levelled barium sulfate plate located on the forest floor (see Figure 8A-1). The measurements were taken under different hardwood forest canopy conditions throughout the 1980 summer season and were used in subsequent statistical analyses.

Preliminary statistical analyses indicate that although percent canopy closure accounts for most of the variability in diffuse radiance measurements, the remaining variance can be explained by the interaction of other environmental variables, such as aspect, time and date of measurement, and canopy uniformity. The interaction of aspect with date and time are particularly significant for the red and reflective infrared radiance measurements. These interactive effects are most likely indicative of effective solar angle, that is, incident radiation as a function of topography and zenith angle. A singular effect attributed to aspect, as might be expected from previous gypsy moth studies, is not evident.

Another important observation made during the analyses centers on diffuse radiance values for middle ranges of percent canopy closure. As the percent of canopy closure decreased, the variability of radiance measurements increased. Although a direct correlation between the field radiance values and Landsat reflectance values cannot be made, the field data gives several indications which are useful to future Landsat based studies. For example, moderate defoliation (30-60% canopy removed) may have such high spectral variability that the class cannot be identified on Landsat data unless other environmental parameters such as topography and zenith angle are considered.

The general conclusions reached through the results of this project are in need of further research and evaluation. Anticipated research efforts will involve a second field radiometer study as well as a spectral reflectance investigation to begin in the spring of 1981.

A second study, initiated during the past year, involves the use of ancillary data such as digital topographic terrain data, for improved forest canopy condition assessment. Previous investigations into the use of Landsat MSS data to identify insect defoliation indicated that areas on northwest slopes which were identified on ground reference data as light defoliation were classified as moderate defoliation using Landsat data. To alleviate this problem, Digital Elevation Model (DEM) topographic data produced by the U.S. Geological Survey has been processed to produce a slope orientation classification for a study area in central Pennsylvania. The DEM slope classification is being superimposed onto corresponding Landsat MSS data which contains insect defoliation and onto a Landsat based forest/non-forest mask. Using a layered classification approach to separate out forests on particular slope classes, the analyst will then classify defoliation classes. Results of this activity will be documented in subsequent reports.
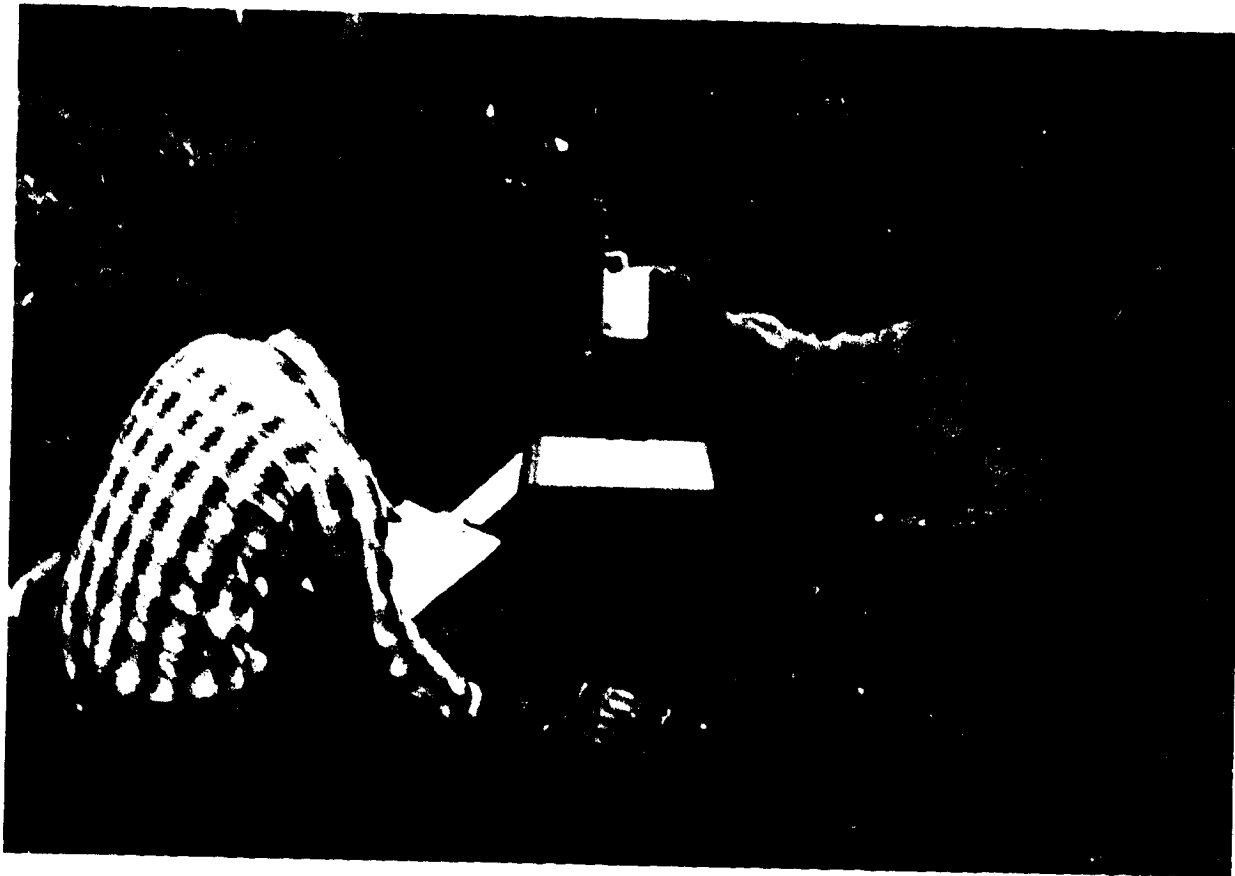
Figure 8A-1.   Diffuse radiance measurements were made in three
               wavelength regions using a Mark II-Three Band Radiometer.

SIGNIFICANCE

Ancillary data sets, such as topographic data, may help to eliminate Landsat classification errors due to aspect. However, the field radiometer study indicates that many parameters other than aspect effect the radiometric response associated with forest canopy conditions. As more research is carried out to identify these environmental parameters and compounding interactions, the ability to identify and assess forest disturbances and stress conditions from satellite altitudes will be greatly improved.

FUTURE EMPHASIS

The field radiometer study will be completed and a standardized, quantitative, ground-based technique for assessing the density of the forest canopy in order to calibrate remotely sensed estimates of canopy stress will be developed. In addition, an evaluation of (1) Thematic Mapper Simulator data and (2) ancillary information, such as digital topographic terrain data, for improved forest canopy condition assessment will continue.

Numerous other research activities will commence under the AgRISTARS effort during the next year. Under the sensor parameter study, three separate activities are currently underway or in the planning stages. These include:

    1. Selection of optimum Thematic Mapper bands suited to identify forest disturbances such as defoliation, fire, and clearcutting (to begin 11/80)

    2. Determination of the size distribution of various forest types and forest disturbances and their relation to instantaneous field of view (current activity)

    3. Documentation of classification accuracies as a function of resolution element size, for forestry and land resources targets having varying levels of spatial complexity (current activity).

Another major effort, to be initiated, will examine forest change phenomenon five acres or larger in size. An advanced forest change monitoring system utilizing Landsat digital data and computer-aided analysis techniques will be developed. In addition, on-going research activities relative to the development, refinement and evaluation of image analysis techniques to detect, monitor, and assess insect defoliation of hardwood forests will continue.

PUBLICATIONS

Dottavio, C.L., D.L. Williams, B.L. Markham, and M. Labovitz. 1980. Sensor Parameter Study: Literature Review and Experimental Plan. A final report prepared for AgRISTARS/Renewable Resources Inventory, Task 4.1. NASA Technical Memorandum TM-82034. 24 pages.

Dottavio, C.L. 1980. Preliminary Results: Effect of Forest Canopy Closure on Incoming Solar Radiance. NASA Technical Memorandum, under review.

B. MONITORING INSECT DEFOLIATION OF HARDWOOD FORESTS USING LANDSAT

by

R.F. Nelson, C.L. Dottavio and D.L. Williams

OBJECTIVE

The defoliation of hardwood forests by insects is a serious problem
in the northeastern United States. The gypsy moth caterpillar, which
was introduced to this country during the nineteenth centry, has
defoliated millions of acres of hardwood forests during the last
decade. Over the past 10 years, the state of Pennsylvania has attributed
the loss of $32 million worth of timber resources to this insect.
Resource managers must continually monitor insect movement and damage
to plan and implement appropriate pest management activities. This
research effort is designed to develop, test, and evaluate an automated
system to annually estimate the extent and severity of insect
defoliation of hardwood forest using computer analysis of Landsat
digital data.

BACKGROUND

An ongoing research effort at NASA's Goddard Space Flight Center
(GSFC) involves the use of Landsat multispectral scanner (MSS) data
to detect and monitor insect defoliation of hardwood forests. Results
have shown that defoliation of hardwood forests by the gypsy moth
caterpillar is more readily identifiable using multitemporal data
sets which represent forest canopy conditions before and after
defoliation. The procedure for utilizing multitemporal data sets
to monitor insect infestation involves obtaining a Landsat image
of a given area prior to infestation. This image is classified
using computer-aided analysis techniques to identify the extent
of forest cover versus non-forest cover. A second image over the
same area is obtained after insect damage has occurred and is then
digitally overlain onto the forest/non-forest classification map
derived from the previous image. By following this procedure,
forested areas can be isolated on the image exhibiting insect
defoliation and subsequent analysis can be excluded to those areas
only.

Throughout these activities, the Pennsylvania Division of Forest
Pest Management, Bureau of Forestry, has been informally cooperating
with Goddard by providing ground truth information and field
expertise. Their interest in the gypsy moth project has lead
to the initiation of a three year Applications Pilot Test (APT)
project. The objective of the APT is to develop and transfer remote
sensing technology to the Pennsylvania agency so they can conduct
annual surveys of defoliation damage using Landsat MSS data. The
project is divided into three phases: an initial test phase in which
the survey techniques will be identified and developed; a quasi-
operational phase in which a Landsat data base will be created for the
state of Pennsylvania; and finally a technology transfer phase. This
report will describe the results of the initial test phase.

RECENT ACCOMPLISHMENTS

Intrinsic to monitoring forest cover conditions is the determination of the best time to observe changes in the forest canopy. A study was undertaken to determine the temporal window within which the extent and severity of gypsy moth defoliation could be monitored using Landsat data. Subsections of six relatively cloud-free Landsat scenes were obtained during the summer of 1977 over Williamsport, Pennsylvania. The subscenes, which spanned 73 days between May 22 and August 2, were examined to determine the nature and magnitude of the spectral reflectance changes in healthy and defoliated forest over time. Study areas were located in healthy, moderately defoliated, and heavily defoliated hardwood forest and their mean reflectances and variances computed. This information was used to determine the separability of the defoliated and non-defoliated areas throughout the summer. Results indicated that (1) defoliated areas are most readily distinguished in late June; and (2) a two month window (from early June to late July) exists within which Landsat data is suitable for assessment of gypsy moth related damage. Consequently, the effects of insect damage can be assessed at times other than peak defoliation, allowing greater flexibility in the acquisition of cloud-free Landsat imagery for damage assessment. It should be noted that the date of peak defoliation, as well as the length of the available window for damage assessment, may vary from year to year due to environmental influences on biological development.

Another goal of the APT is to find a reliable, method for classifying defoliated forest. Previous work had shown that certain non-forested land cover types were often confused with defoliated forest. In order to avoid these errors, a forest non-forest mask was generated using a non-defoliated Landsat data set. The mask is created using a single class, two channel, Bayesian procedure to classify the Landsat data, which is then density sliced to produce the final forest classification. After the forest mask was created, the defoliated Landsat data set was overlain onto the classification and insect damage assessment began in the isolated forested areas. Landsat data covering defoliated forest were used to investigate four methods of classifying forest defoliation to determine which provided the most satisfactory results.

A 52,900 hectare area north of Harrisburg, Pennsylvania, was classified using a supervised classification approach (Bayes), a band 7/band 5 ratio approach (RVI), a second ratio approach using the Transformed Vegetative Index (TVI), and a band 4, 5, and 6 polynomial transformation approach devised by the Calspan Corporation (Calspan). The Ratio and Transformed Vegetation Indices relate the Landsat spectral measurements to various vegetation density indicators such as green leaf biomass.

A software package called ASSESS2 was used to investigate which of the four classification approaches most effectively delineated the gypsy moth defoliation. The results of the four classifications

were compared to a "ground truth" image manufactured by combining the forest/non-forest mask and digitized aerial photointerpretation information.

Results indicated that the Bayes approach produced the most consistent and intuitively reasonable results. The RVI and TVI approaches tended to classify defoliated areas accurately, but did poorly in healthy forest. The Calspan approach had the highest per-pixel classification accuracy, but did poorly in classifying moderately defoliated areas. The very low classification accuracies common to all four approaches suggest problems with the photointerpretation information used as ground reference data. The ground reference data is being evaluated to determine if revisions are necessary.

SIGNIFICANCE

A timely, accurate survey technique is being developed for forest insect damage assessment. Current pest survey techniques, which include aerial surveillance, ground surveillance, and aerial photography, do not meet the criteria needed for a standardized, timely, and cost effective monitoring procedure. The repetitive and synoptic coverage provided by Landsat, plus the simple analysis techniques being developed under this APT, make the satellite sensor system an attractive survey medium for monitoring widespread insect damage over large areas.

The tendency of Vegetation Index classifiers to accurately identify defoliated areas indicate that these simple procedures may be useful for monitoring forestry related problems if modifications can be made to identify healthy forests with equal accuracy. The forest/non-forest mask technique increases defoliation classification accuracy. Finally, identification of the temporal window for insect damage assessment will provide greater flexibility in acquisition of cloud free imagery for defoliation assessment.

FUTURE EMPHASIS

Evaluation of the Vegetation Index classification methods will be continued and the best approach will be further refined for forestry applications. In addition, APT Phase II activities will commence. Goddard will acquire imagery and computer compatible tapes for the most recent, nondefoliated, and relatively cloud free Landsat coverage of the entire state of Pennsylvania. These data will be used to create a forest/non-forest data base for the entire state. Personnel will oversee the generation of a digitally mosaiced Landsat data base and data management system for the entire state. Pennsylvania foresters will then be able to utilize this data base for annual statewide defoliation assessments.

PUBLICATIONS

Nelson, R.F. 1980. Defining the Temporal Window for Monitoring Defoliation using Landsat. Presented at 1981 Annual International Symposium on Remote Sensing, American Society of Photogrammetry. Washington, DC.

TABLE 8B-1. VEGETATIVE INDEX RATIOS

Ratio Vegetative Index (RVI)   MSS7/MSS5

Difference Vegetation Index (DVI)   2.4 X MSS7 - MSS5

Transformed Vegetative Index (TVI) $\dfrac{MSS7 - MSS5}{MSS7 + MSS5} + 0.5$

Green Vegetation Index (GVI)   -0.29 X MSS4 - 0.56 X MSS5 +
                                       0.60 X MSS6 + 0.49 X MSS7

Perpendicular Vegetative Index
  (PVI) $(SOIL5 - MSS5)^2 + (SOIL7 - MSS7)^2$

                                       Where

                                       SOIL5 = 0.85 X MSS5 + 0.35 X MSS7
                                       SOIL7 = 0.35 X MSS5 + 0.15 X MSS7

Linear Vegetative Index (LVI)   -2.59 X MSS4 - 7.28 X MSS5 + 0.88
                                       X MSS6 + 3.59 X MSS7

C. SURFACE MINE MONITORING

by

J. R. Irons

OBJECTIVE

A study was conducted to quantitatively compare the utility of several remote sensing systems for the inventory and monitoring of coal surface mines in the Eastern United States. The study addressed the impact of spectral and spatial resolution improvements planned for future spaceborne sensors.

BACKGROUND

The study was conducted in cooperation with the Environmental Monitoring and Support Laboratory/Las Vegas of the Environmental Protection Agency (EPA). The EPA was interested in efficient and accurate procedures for surface mine inventory and monitoring.

Remotely sensed data were acquired over three Pennsylvania study areas during the Fall of 1978 and the Spring of 1979. The data were obtained from the following sensors: the Landsat-2 Multispectral Scanner Subsystem (MSS); an airborne Thematic Mapper Simulator (TMS) multispectral scanner; and a high altitude aerial photographic system (Wild-Heerbrugg RC-10 cameras carried aboard NASA's U-2 aircraft). The study areas were located within the Main Bituminous Coal Field of the Appalachian Plateau. The areas consisted mainly of forest and agricultural land which had been extensively disturbed by surface mining. Twenty 150-hectare mine sites located within the three areas were selected for intensive study. The sites provided a comprehensive cross-section of active, reclaimed, and abandoned mines. A hierarchical classification scheme was developed for the thematic mapping of the study areas. The scheme emphasized land cover categories which were useful for the assessment of mine reclamation and which were amenable to recognition through the analysis of multispectral scanner data.

Prior to classification, the digital data from each of the multispectral scanners were preprocessed to reduce geometric distortions. The TMS data were also resampled to simulate data acquired at the 30 meter resolution planned for the Thematic Mapper. Thematic maps were then generated via the digital analyses of each preprocessed data set. The areal extent of each land cover category within the 150-hectare mine sites was estimated by the automated counting of the number of pixels classified into each category.

The high-altitude color and color infrared aerial photographs were enlarged to a scale of 1:12,000 and manually photointerpreted. For each 150-hectare site, the area of each category was determined by planimetering.

The accuracy of the area measurements were assessed by a quantitative comparison to ground reference data. The ground reference data consisted of low-altitude, photointerpreted, color and color infrared aerial

photography acquired in the Fall of 1978. For each mine site, area measurements were obtained by planimetering, and the photointerpretation was field checked.

RECENT ACCOMPLISHMENTS

The objectives, methods, and results of this study were presented in a poster board session at the Fourteenth International Sympoisum on Remote Sensing of Environment, and a paper will appear in the proceedings. The reported results are summarized in Table 8C-1 which compares the accuracy of area estimates derived from the different data sets.

SIGNIFICANCE

Although Landsat MSS data proved useful for accurately identifying surface mines, the detailed categories listed in Table 8C-1 could not be consistently recognized via the digital analysis of MSS data. These categories represent the diversity of land cover found within mines, and this detailed information is required for the effective monitoring of mine operation and reclamation. As shown in Table 8C-1, the areal extent of these categories were accurately mensurated using simulated Thematic Mapper data. Thus, the launch of the Thematic Mapper should significantly enhance the utility of space-acquired remotely sensed data for surface mine monitoring.

FUTURE EMPHASIS

Additional digital data have been acquired over the study areas by the Seasat Synthetic Aperature Radar (SAR) and 11-channel, airborne, Modular Multispectral Scanner (M^2S). The M^2S data were acquired in the Spring of 1980. The collection of data for the Pennsylvania study areas presents an excellent opportunity for further research into the potential utility of Thematic Mapper data, the utility of SAR data, optimum spectral band selection, and change detection. Future research into these topics will depend on the funding situation.

A more rigorous evaluation of the potential utility of Thematic Mapper data will be the first priority. Additional radiometric preprocessing of the TMS data will be considered to more closely simulate the data expected from the Thematic Mapper. Alternate approaches to the derivation of thematic maps from the TMS data will be investigated. Ground reference data will be digitized and registered to the TMS data. The digitization and registration will allow the expression of thematic map accuracy in terms of the portion of pixels correctly classified.

REFERENCES AND PUBLICATIONS

Anderson, A.T., et al. 1977. Landsat Imagery for Surface-Mine Inventory. Photogrammetric Engineering and Remote Sensing, Vol. 43, No. 8: 1027-1036.

Irons, J.R., H. Lachowski, and C. Peterson. 1980. Remote Sensing of Surface Mines: A Comparative Study of Sensor Systems. Proceedings, Fourteenth International Symposium on Remote Sensing of Environment, San Jose, Costa Rica, April 23-30.

Table 8C-1.   Accuracy* of Surface Mine Category Area Measurements

Category Level II	Level III	Thematic Mapper Simulator	Daedalus Scanner Fall 1978	Daedalus Scanner Spring 1979	Color Infrared High Altitude Aerial Photography	Ground Reference (hectares)
Barren		0.95	0.88	0.60	0.86	776.8
	Graded	0.89	0.96	0.88	0.69	413.9
	Upgraded	0.88	0.63	0.21	0.85	357.9
	Coal	**	0.91	**	**	4.9
Revegetated		0.93	0.70	0.49	0.93	758.7
	Grass	0.93	0.70	0.26	0.71	380.0
	Trees	0.71	**	0.72	0.95	377.9

*Accuracy = 1-(Area Estimate - Ground Reference/Ground Reference)

**(Area Estimate - Ground Reference/Ground Referece)>1

D. **LAND COVER CLASSIFICATION ACCURACY AS A FUNCTION OF**

SENSOR SPATIAL RESOLUTION

by

B.L. Markham, J.R.G. Townshend* and M.L. Labovitz

OBJECTIVES

The objective of this study is to provide an understanding of how the spatial resolution of a satellite sensor system affects the accuracy of land cover classifications derived from the sensor data. This information will be used to provide spatial resolution design recommendations for future land observing satellite systems.

BACKGROUND

A review of previous studies indicated that there are two counteracting factors affecting per-pixel image classification accuracies as a function of spatial resolution (Townshend 1980). The first factor involves the high frequency spatial variations in the spectral response of some land cover classes, called scene noise. These variations tend to increase the variances of training statistics at high spatial resolutions, causing more overlap between land cover classes. This results in potentially lower classification accuracies than would be achieved with coarser resolutions. The second factor is related to the higher percentage of boundary (mixed) pixels associated with coarser resolutions. The fewer mixed pixels at finer resolutions produce better classification accuracies.

Prior research on the combined effects of scene noise and boundaries on classification accuracy has been limited, with conflicting results. These disparate results are a consequence of the differences in the internal characteristics and sizes of the land cover types evaluated. In this study, a number of terrain situations are being evaluated, with varying land cover target sizes and internal characteristics, in order to provide a more complete, explainable picture of the relationship of classification accuracy to spatial resolution.

RECENT ACCOMPLISHMENTS

Two separate approaches are being used to evaluate the spatial resolution classification accuracy interaction. The first is a more empirical approach involving the use of aircraft mulispectral scanner data which is degraded to simulate coarser resolutions. The second approach is more theoretical, using a gridding algorithm to simulate the scanning process and a digitized land cover map to represent the ground scene.

For the empirical study, two sets of aircraft multispectral scanner

data were collected at a nominal 5 meters resolution. Modular Multispectral Scanner (M^2S) Data in eleven channels were collected on April 11, 1980 and Thematic Mapper Simulator Data were collected on August 27, 1980.

Target areas were the same for both flights, consisting of three flightlines of marsh, agricultural, forest and urbanized land in eastern Maryland. Digital data for the April flight was received on June 30, 1980. Data from the August flights has not yet been received.

A spatial resolution degradation filter developed by Sadowski and Sarno (1976) was used to create data sets with 10, 20, 40 and 80 meter resolutions for the April data. Statistics were generated at each resolution level for the same training areas of various land cover types. A maximum likelihood decision rule was used to classify the degraded images.

Land cover data has been interpreted for one test area consisting of predominantly salt marsh and water from aerial photographs imaged simultaneously with the scanner. The land-water boundary was digitized, registered to the scanner data and gridded @ 2.5 meters resolution. Two images of the photointerpreted data were generated: (1) a bit image with "1's" in pixels containing a boundary and (2) an image where each grid cell (pixel) contained a number corresponding to the dominant land use type (i.e., land or water) in that cell. The first image was used to determine the number of boundary pixels at each resolution level. The second image was compared pixel by pixel with the classified images to determine overall classification accuracies. This image was also combined with the boundary image to determine pure (non-boundary) pixel classification accuracies.

For the one test site completed, scene noise was relatively low. For the water training class, no change in variance was apparent with changing resolution (Fig. 8D-1). The salt marsh training class showed a moderate decrease in variance with resolution degradation. As expected, in this case with low scene noise and relatively distinct spectral signatures of the two classes, classification accuracies of pure pixels were high at all spatial resolutions, increasing only slightly at 30 meters (Figure 8D-3). Boundary pixels were important in this area (Figure 8D-2). As a result, boundary effects dominated, resulting in improved overall classification accuracies with improved spatial resolution (Figure 8D-3).

In the theoretical study, the major accomplishments have been the development of a sophisticated gridding algorithm and the digitizing of two wetland cover type data sets. This gridding algorithm takes a digitized cover map and calculates the area of intersection of each grid cell with the land cover polygons, essentially simulating a scanner's operation. It generates frequency histograms of percentage area of intersection of grid cells and target types. This can be done

8-15

for different sizes and shapes of cells and thus enables evaluation of the boundary pixel problem, e.g., one can examine the number of pure pixels, 90% pure pixles, etc. at many resolution levels. Two data sets, covering wetland areas (one inland, one coastal) have been digitized and edited and are ready to be run through the gridding algorithm.

SIGNIFICANCE

This study is currently in the data analysis stage with only preliminary results available. The empirical results for the one test site completed indicate that continued improvement in digital classification accuracy is possible with increasing resolution (to 5m). Although intuitively plausible, similar results have rarely been shown to occur with actual data. A significant achievement of this effort is that two procedures have been developed and tested for evaluating classification accuracy with varying spatial resolution, laying the foundation for continued research.

FUTURE EMPHASIS

Work is continuing on both aspects of this study. A minimum of two data sets which are more complex than the initial wetland site will be evaluated under the empirical approach. Under the theoretical study, the already digitized wetland data will be analyzed with the existing algorithm. For both studies, the targets evaluated will be shifted more towards the forestry discipline. In particular, gypsy moth and spruce budworm damage will be examined with the theoretical approach, pending the availability of suitable data. In addition, refinements of the gridding algorithm may be instituted to allow evaluation of the scene noise problem.

REFERENCES

Sadowski, F. and J. Sarno. 1976. "Forest Classification Accuracy as Influenced by Multispectral Scanner Spatial Resolution". Environmental Research Institute of Michigan, Report 109600-71-F, 130 p.

PUBLICATIONS

Townshend, J.R.G. 1980. "The Spatial Resolution Power of Earth Resources Satellites: A Review". NASA/GSFC TM-82020 (A preprint of an article to appear in Physical Geography).
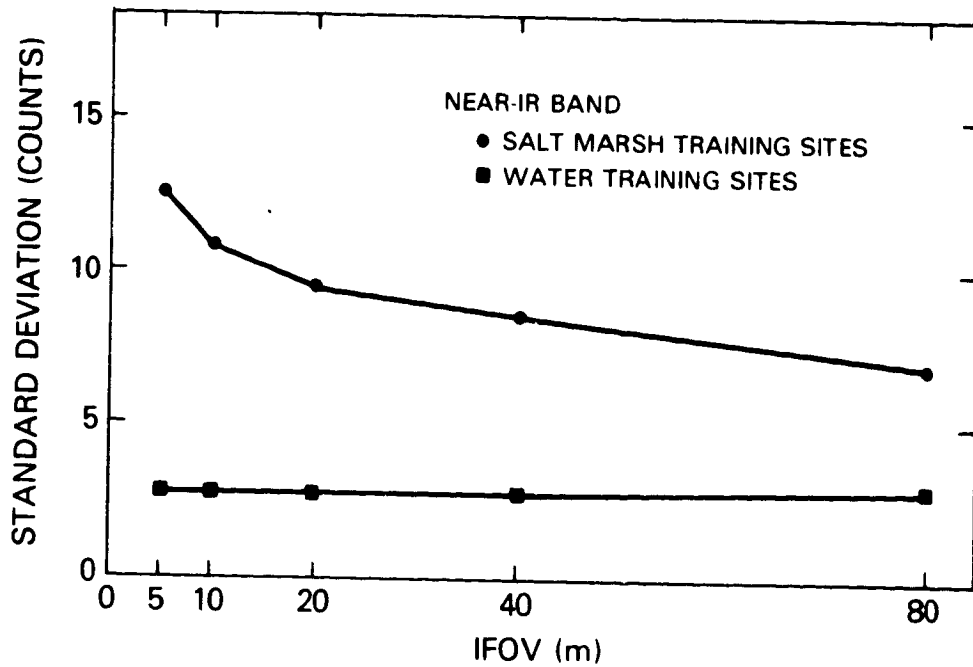
Figure 8D-1.   Noise in training sites as a function of spatial
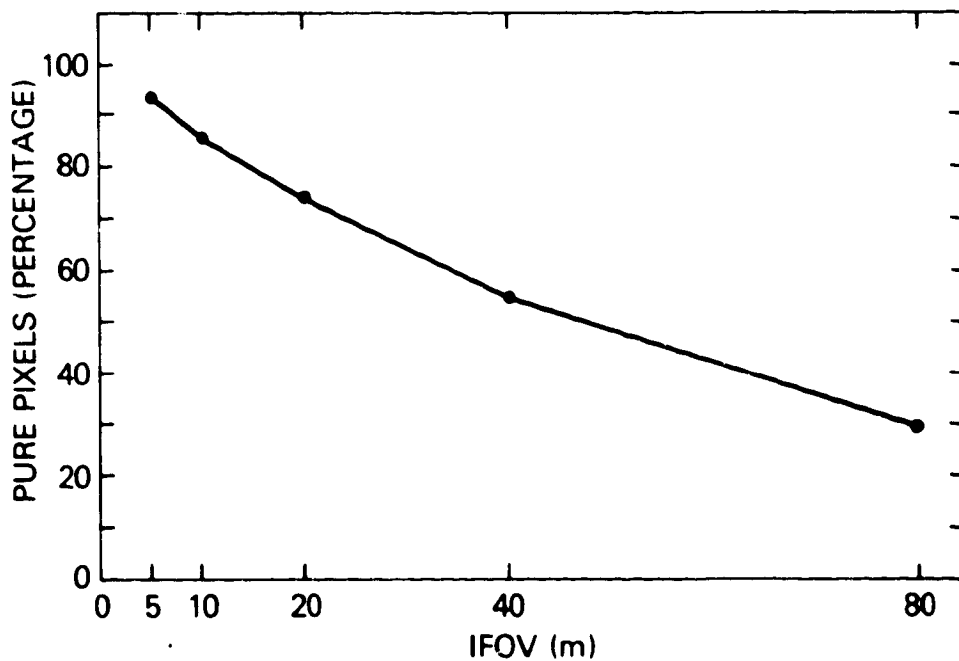resolution for the near-IR (0.76-0.86 μm) band

Figure 8D-2.   Percentage of pure pixels as a function of spatial
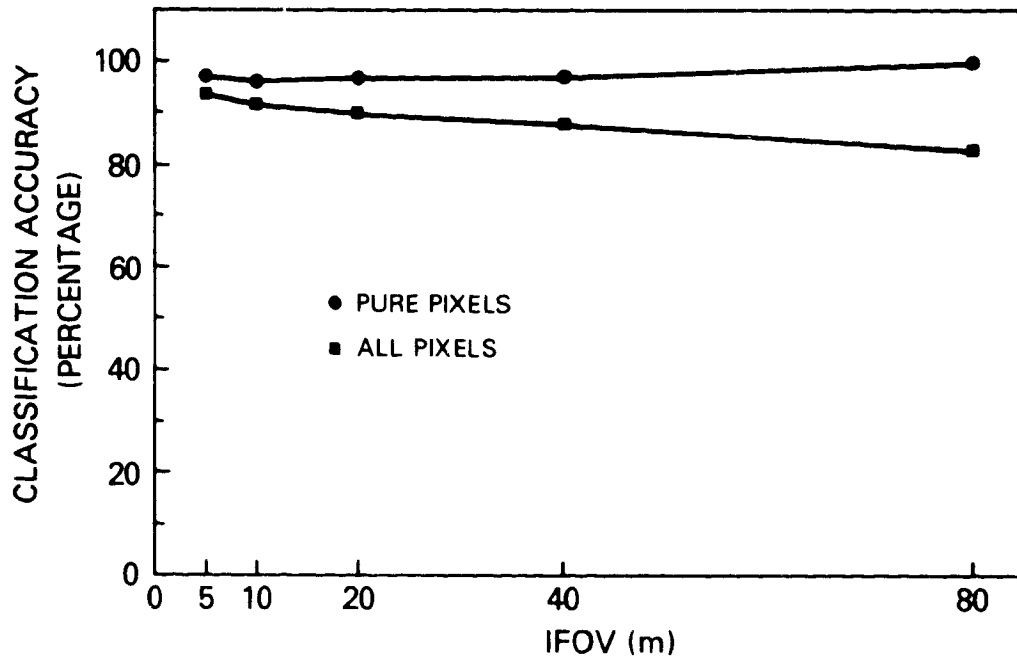resolution for the salt marsh test area.

8-17

Figure 8D-3. Classification accuracy as a function of spatial
resolution for the salt marsh test area

E. THE CENSUS BUREAU/NASA URBANIZED AREA APPLICATION PILOT TEST

by

D. L. Toll

OBJECTIVES

The overall objective of this Applications Pilot Test (APT) is to
develop and evaluate remote sensing techniques to delineate and
periodically update urbanized area boundaries in the United States.
The primary objective is to develop procedures using Landsat MSS data
for accurately detecting changes from non-urban to urban land cover.
Other objectives include: (1) assessment of the cost-effectiveness,
accuracy, timeliness and increased capability of using Landsat
technology operationally, (2) training of Census Bureau personnel,
and (3) evaluation of sensor payloads in addition to Landsat MSS,
including the proposed Space Shuttle Payload, Landsat Thematic Mapper
simulator data and Seasat Synthetic Aperture Radar data.

BACKGROUND

The Census Bureau/NASA Urbanized Area Application Pilot Test
is concluding its fourth and last year of a program to develop
procedures utilizing satellite data for the Urbanized Area Boundary
Program at the Census Bureau. The specific approach utilized in the
APT has been to evaluate the use of satellite data to replace or enhance
the use of aerial photography and ground site visits for the preliminary
delineation of urbanized areas occurring within the approximately
300 Standard Metropolitan Statistical Areas. Initial work in the APT
successfully demonstrated the utility of digitally processed Landsat
enhancements and classifications in the delineation of urbanized areas.
In another approach, multitemporal Landsat imagery were used to detect
changes in urban expansion. As a result of an evaluation by Census
Bureau geographers, they recommended that change detection procedures
be the primary area for further development. Hence, the emphasis for
the last year has been to develop cost-effective and accurate procedures
to detect non-urban to urban land cover change. Due to budget cutbacks,
however, these procedures will not be evaluated for Census Bureau
applications in Fiscal Year 1981.

RECENT ACCOMPLISHMENTS

Of the various change detection procedures evaluated using Landsat MSS
data, an "image differencing" approach provided the highest accuracies
for detecting urban expansion (see Table 9E-1). This approach utilizes
two Landsat scenes, where radiance values from one date are subtracted
from the corresponding location of the second date. Typically, Landsat
MSS band 5 (.60-.70 µm), the vegetative cover discrimination band,
provided the overall highest accuracies. An evaluation of various
preprocessing methods to improve accuracies for an image differencing

change detection analysis indicated that overall accuracies were generally reduced. These methods included a principal component transformation, low and high pass filter, and data normalization procedures. An analysis of the optimum time of year to conduct change detection has indicated that the entire vegetative season is adequate for change detection analysis. Wide temporal differences between Landsat scenes used in change detection (i.e., non-anniversary dates), however, also resulted in changes occurring from differences in solar elevations and phenology as well as to land cover changes.

Because Landsat MSS data was the only digital remote sensing data routinely available for urbanzied area evaluation, nearly all of the analysis procedures were completed using Landsat MSS data. However, because of the potential of other remote sensing systems to meet Census Bureau geographer goals, other system payload were examined. This included: (1) the Landsat-D payload, (2) the Space Shuttle payload, and (3) the Seasat Synthetic Aperature Radar. Preliminary analyses have indicated that all of these sensor systems provide capabilities for use in urban area delineation.

SIGNIFICANCE

By effectively developing and evaluating procedures to delineate urbanized areas, it is possible to upgrade procedures in the urbanized area boundary program at the Census Bureau. This work is also advancing the state of the art in change detection methodology.

FUTURE EMPHASIS

Because of budget cut-backs there will not be a cost-benefit analysis or a transfer of technology during FY81. Emphasis will be placed on the analysis and documentation of change detection work completed during FY80.

REFERENCES

Computer Sciences Corporation. 1980. "Change Detection Methodology for Urbanized Areas", Technical Memorandum in Preparation, Silver Spring, MD.

Friedman, S.Z. and R.K. Fretz. 1980. "Evaluating the Utility of Remote Sensing Techniques through the Analysis of Regional Variation of Geographic Phenomena", IEEE Workshop on Picture Data Description and Management, Pacific Grove, CA.

General Electric Company. 1980. A Review of the Capabilities of the Proposed Shuttle Payload for Monitoring Urban Expansion, NAS5-25707, Beltsville, MD.

General Electric Company. 1980. "Change Detection Method Development, Census Urban Area Application Pilot Test", NAS5-25707, Mod. No. 2, Beltsville, MD.

Riordon, C.J. 1980. "Non-Urban to Urban Land Cover Change Detection Using Landsat Data, Summary Report", NAS5-26127, NASA/Goddard Space Flight Center, Greenbelt, MD.

PRESENTATIONS AND PUBLICATIONS

Toll, D.L., J.A. Royal and J.B. Davis. 1980. "Urban Area Update Procedures Using Landsat Data", ASP Fall Technical Meeting at Niagra Falls, American Society of Photogrammetry, Falls Church, VA.

Toll, D.L. 1980. "Urban Area Delineation by Remote Sensing", Technical Memorandum in preparation, NASA/Goddard Space Flight Center, Greenbelt, MD.

Toll, D.L., J.A. Royal, S.Z. Friedman and J.B. Davis. 1980. "Urban Area Update Procedures Using Remote Sensing Data", in preparation, to be submitted to the American Cartographer, American Association of Geographers, Washington, DC.

Description	Overall Change Detection Accuracy (%)	Non-Urban to Urban Change Detection Accuracy (1-Omission Error) (%)	Commission Error (%)
Richmond			
MSS band 4 differencing	91	54	6
MSS band 5 differencing	89	76	9
MSS band 6 differencing	85	61	13
MSS band 7 differencing	81	33	14
MSS band 5 low passed differencing	88	69	9
MSS band 5 high passed differencing	86	68	12
principal component transformation prior to differencing (first component)	87	50	9
principal component transformation prior to differencing (second component)	87	55	9
post-classification comparison	87	69	10
Denver			
MSS band 4 differencing	79	63	14
MSS band 5 differencing	85	61	6
MSS band 6 differencing	83	61	10
MSS band 7 differencing	71	70	28
principal component transformation prior to differencing (first component)	78	56	16
principal component transformation prior to differencing (second component)	79	48	11
post-classification comparison	69	61	23

Table 8E-1. Summary of change detection accuracies/errors

F. CLASSIFICATION OF HIGH RESOLUTION REMOTELY SENSED DATA

VIA COMPONENT FREQUENCY ANALYSIS

by

S. W. Wharton

OBJECTIVES

The objective of this study was to: (1) demonstrate the need for
classification procedures designed to process high spatial resolution
remotely sensed data; and (2) develop an alternative classification
method to classify informational classes such as industrial, commercial,
or residential, based on the relative distribution of image components
such as roofs, pavement, trees, lawn, etc. surrounding each picture
element (pixel).

BACKGROUND

The spatial resolution of remotely sensed data determines the number
and type of informational classes which can be identified using
computer assisted classification methods. For example, Landsat data
gathered over an urban residential area at 80 m resolution could
allow broad information classes (i.e., land) such as industrial,
commercial, residential, etc. to be extracted by direct analysis.
However, imagery gathered by an aircraft sensor at a 7 m resolution
would contain data representing separate individual cover types,
including roofs, paved surfaces, lawns, trees, etc. These
constituent subclasses make up the 80 m informational classes.
Classification procedures which have been primarily designed to
process Landsat or similar resolution data, tacitly assume that
all of the informational target classes can be mapped by a simple,
direct analysis. These procedures may not be effective in classifying
land use with high resolution data.

An alternative classification method was developed for high spatial
resolution data using color infrared aerial photography and Linear
Array Pushbroom Radiometer (LAPR) (7.2 m resolution) data collected
over Laurel, Maryland in June 1979. The study area is characteristic
of communities undergoing residential expansion and industrial
development in the Baltimore-Washington metropolitan area and contains
a number of land cover types amenable to this type of analysis.

RECENT ACCOMPLISHMENTS

Using visual analysis of the aerial photography, the study area
was segmented into four broad groups representing various aggregates
of category subtypes, namely, low density single unit dwelling
residential (Type I); high density single unit dwelling residential
(Type II); multiunit dwelling apartment complex (Type III); and
industrial/commercial (Type IV). The major distinguishable cover
subtypes were roofs (R), paved areas (P), trees (T), and lawn or

field (L). Other less heterogeneous categories such as forests, brushland and open fields could not be divided into cover subtypes. An estimate (Table 8F-1) was made of the areal proportion of the category subtypes within each broad category by repetitively counting the number of dots within each subtype on a grid covering the aerial photography.

Based upon these results, it was concluded that conventional classifiers could not classify land use with high resolution imagery. Three classification methods including a parallelepiped classifier on the GE Image-100, an ESOCLS cluster analysis program on the HP3000 IDIMS image analysis system, and a supervised training approach using the IDIMS maximum likelihood classifier were applied to the LAPR imagery. These classifiers were unable to distinguish the four broad categories; rather they categorized the image into subcover types.

An alternative approach to classify land use was developed which consisted of two stages, namely: (1) derivation of sub-category signatures by grouping data with similar spectral responses (cluster analysis) and production of a classification map; and (2) identification of informational categories by analysis of the relative distribution of sub-categories within the classified image. Existing cluster analysis procedures were used for the first stage. Research emphasis was placed upon the development of methods to analyze spatial distributions.

A series of six programs was developed, using the Pennsylvania State University computer system. The category distribution (CDIST) program computes the relative distribution of categories within selected neighborhoods (windows) around each pixel. The remaining programs are used to cluster the data output from CDIST and to produce a classification map of the clustered data.

The programs were tested using randomly generated synthetic data which were developed to simulate the four broad categories found in the Laurel imagery. The data were then processed using various window sizes, noting the accuracy in discriminating between the four blocks in each case (Table 8F-1). A window is the area centered about each pixel from which the frequency distribution is computed. It is obvious that the smaller sized windows (5 by 5 or less) do not contain enough pixels to reliably sample the sub-category distributions. As expected, the accuracy increases with increased window size since the frequency distributions are estimated from a larger number of samples. These results demonstrate that the component frequency analysis is a useful methodology for classifying high resolution data.

SIGNIFICANCE

Existing classification procedures are not effective in extracting informational categories from high resolution data such as 7.2 m resolution Linear Array Pushbroom Radiometer data. An alternative approach is needed to fully utilize high resolution data from the

30 m resolution Thematic Mapper and from multilinear array sensors which are currently under development. This research will facilitate the acceptance and utilization of high resolution data in the user community by demonstrating that conventional informational classes (such as land use) can be extracted from the data.

FUTURE EMPHASIS

Further work is needed to test the new procedure's accuracy in processing real data, and to determine optimal program parameters for its use. Land use maps derived from low (80 m) and high (7 m) resolution will be compared for accuracy and mapping detail. The 7 m data will be degraded to simulate various lower resolutions to determine the resolution at which land use classes are divided into image components.

Table 8F-1. Percentage of category subtypes listed by category.

(P = pavement, R = residential, L = lawns, T = trees)

Land Use Category	P	R	L	T
Multi-unit dwelling	36	27	19	18
Single unit dwelling (low density)	19	18	33	30
Single unit dwelling (high density)	22	28	17	33
Industrial/Commercial	53	41	6	0

Table 8F-2. Classification accuracies from test data for various sized windows.

Window Size (pixel)	3x3	5x5	7x7	9x9	11x11	15x15	25x25	35x35	49x49
Accuracy (%)	47	77	85	90	93	94	94	94	87

Chapter 9

REMOTE SENSING OF VEGETATION AND SOILS

edited by

C. J. Tucker

OVERVIEW

Remote sensing studies of vegetation and soils in the optical and
thermal regions of the spectrum are directed in the Earth Resources
Branch toward the objective of using these methods to monitor
natural resources and terrestrial vegetation in particular. The
importance of these research activities lies in the ability to use
remote sensing techniques to assess vegetation condition, vegetation
type, crop yield, total dry matter accumulation, episodes of plant
stress, and related inferences. With the growing pressures on the
terrestrial biosphere which have resulted from population and
development pressures, various orbital remote sensing techniques
offer a unique synotpic perspective for the inventory and assessment
of the terrestrial plant biomass or phytomass. However, in order
to utilize remotely sensed data from earth resources satellites,
controlled ground-based studies are necessary to understand the
many variables which influence and/or control the interaction of
electromagnetic energy with terrestrial vegetation. This understanding
maximizes our remotely sensed information and leads to the optimization
of future satellite sensor systems.

The various studies presented in this section cover research which
is grouped into four major sections: studies on agronomic variables
and spectral response; bidirectional reflectance/radiance studies;
topographic effect studies; and the development of new instrumentation
necessary for ground-based remote sensing studies. Studies such
as those described herein contribute to a greater understanding of
spectral data collected by earth resources satellites from vegetated
targets. The importance of this understanding for inventory and
assessment of the environment needs no emphasis when one considers
the unique and fragile nature of the terrestrial phytomass and the
dependence of this planet's human population upon it for food,
fiber, and a climate which can support life as we know it.

A. TEMPORAL RELATIONSHIPS BETWEEN SPECTRAL RESPONSE

AND AGRONOMIC VARIABLES OF A CORN CANOPY

by

D.S. Kimes, B.L. Markham, C.J. Tucker and J.E. McMurtrey III

OBJECTIVES

The objective of this study was to document relationships between
agronomic variables of a corn canopy and the spectral response
of the canopy in thematic mapper bands TM3 (0.63-0.69 um), TM4
(0.76-0.90 um), and TM5 (1.55-1.75 um).

BACKGROUND

A field (approx. 0.9 ha) of well-drained Elkton silt loam soil located
on the USDA Beltsville Agricultural Research Center was selected for
this study. Corn (Zea mays L.) was planted on May 12, 1979. A total
of 43 randomly selected plots were measured during the growing season
from June 15 through October 3, 1979 at approximately six day
intervals. Table 1 presents the dates and the number of samples for
each date along with the corresponding plotting symbols used in the
figure of this paper.

The spectral radiances from these plots 1.9m in diameter were
measured using a three band radiometer elevated 3.7m above the
ground. The three spectral bands used corresponded to NASA's
Landsat-D thematic mapper bands TM3 (0.63-0.69 um), TM4 (0.76-0.90 um),
and TM5 (1.55-1.75 um). Each plot was destructively sampled and
the following agronomic variables were measured: wet and dry total
biomass, plant height, fraction of ground cover by plants, wet and
dry green leaf biomass, green leaf area index, fraction of leaf
chlorosis, and total plant water content. Ratio combinations of
the spectral data were correlated with the agronomic data.

RECENT ACCOMPLISHMENTS

Significant relationships were found between ratio combinations of the
radiance data and the wet and dry total biomass, plant height,
fraction of ground covered by plants, wet and dry green leaf biomass,
green leaf area index, fraction of leaf chlorosis, and total plant
water content. Figure 9A-1 and Table 9A-1 show excellent relationships
between the normalized difference of TM bands 3 and 4 [ND34 = (TM4-
TM3)/(TM4+TM3)] and the green leaf area index. Some of these
relationships were found to be redundant since several of the agronomic
variables were highly correlated to one another by physiological
and anatomical principles. For example, the linear correlation
coefficient between the green leaf area index and green leaf biomass
was 0.99. In addition, the TM5 band did not provide any marked

improvement in the relationships to the agronomic variables.

The conclusions of the study were as follows.

1. Under conditions of no plant water stress, band TM3 and TM5 (1.55-1.75 µm) were highly correlated with a correlation coefficient (r) of 0.97, thus making these 2 bands redundant, for these conditions.

2. The green leaf area or green leaf biomass were found to be the most highly correlated agronomic variables with the spectral data. Estimated canopy cover was found to be substantially less correlated with the spectral data than were the green LAI or green leaf biomass.

3. Green leaf biomass determinations were highly correlated to the green leaf area index. Green leaf biomass measurements are suggested for future studies of corn canopies to reduce the laboratory measurement time while providing quantitative data highly correlated with corn canopy spectral response. Similar relationships were found between total leaf biomass and total LAI as well as chlorotic leaf biomass and chlorotic LAI.

4. Significant relationships were found between the spectral data and associated ratio combinations and many of the agronomic variables sampled. In addition, many of the agronomic variables were highly interrelated because of their relationship(s) to crop growth and development.

SIGNIFICANCE

Nondestructive remote sensing techniques can be applied to corn canopies to estimate agronomic variables highly related to corn canopy physiological status. These same inferences may be extended to large areas by Landsat-D's thematic mapper when this earth resources mission is launched in early 1982.

FUTURE EMPHASIS

This project has been completed and manuscript has been submitted for publication.

PUBLICATIONS

Kimes, D.S., B.L. Markham, C.J. Tucker, J.E. McMurtrey III. 1980. "Temporal Relationships Between Spectral Response and Agronomic Variables of a Corn Canopy". Remote Sensing of Environment (submitted).

Table 9A-1. Number of plots measured on each date with corresponding symbol used in Figure 1. A total of 43 plots were measured.

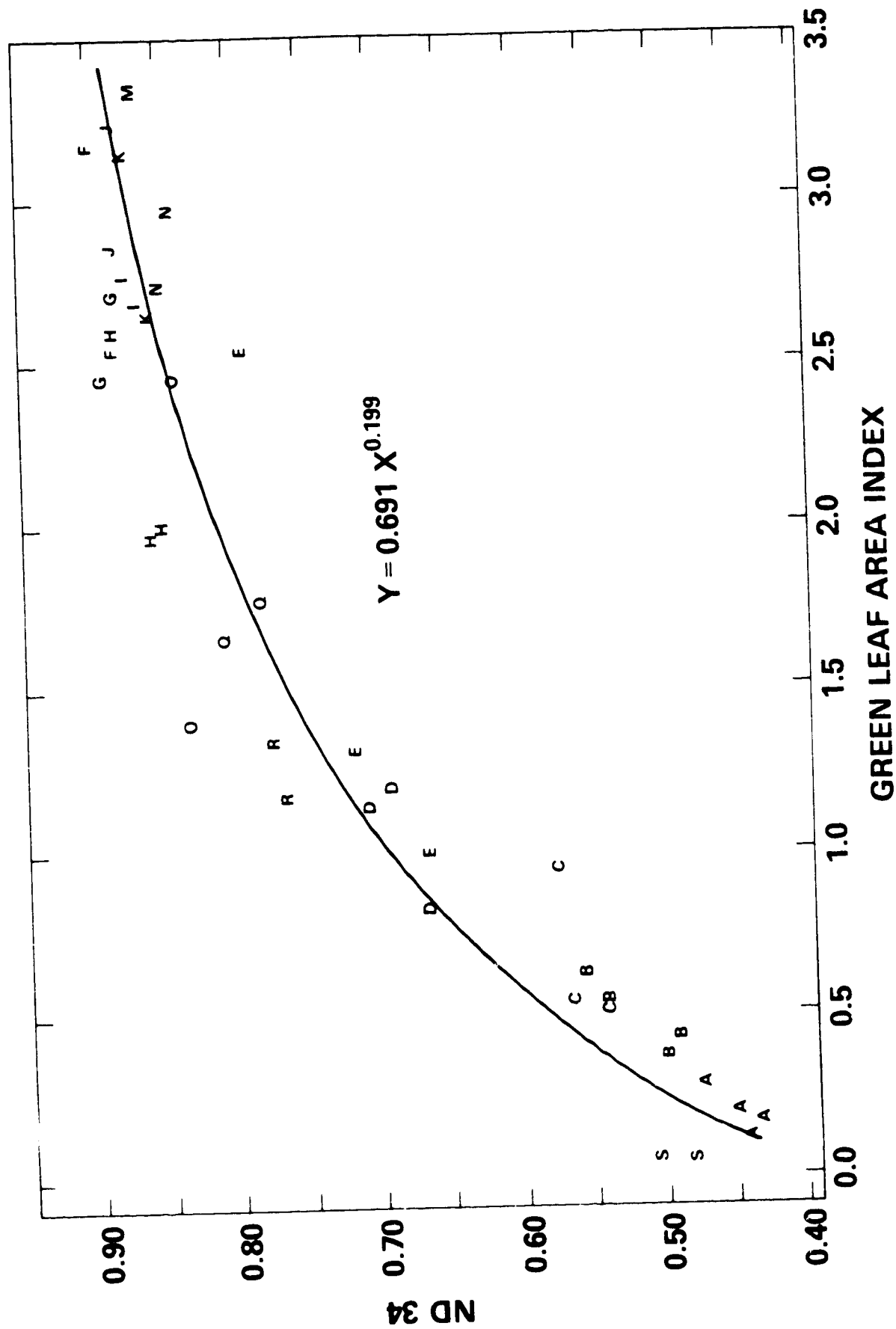| Date	Number of Plots Measured	Plotting Symbol	Date	Number of Plots Measured	Plotting Symbol
06/15/79	4	A	07/31/79	2	J
06/22/79	4	B	08/06/79	2	K
06/27/79	3	C	08/13/79	2	L
07/03/79	3	D	08/20/79	1	M
07/06/79	3	E	08/30/79	2	N
07/18/79	2	F	09/04/79	2	O
07/19/79	2	G	09/11/79	2	Q
07/23/79	3	H	09/18/79	2	R
07/27/79	2	I	10/03/79	2	S

Figure 9A-1. Non-linear relationship of ND34 versus green leaf area index. Data point symbols refer to sampling dates as shown in Table 9A-1.

B. SPECTRAL STUDY OF WHEAT COMPONENTS

by

J.B. Schutt

OBJECTIVES

This ongoing investigation was undertaken to identify differences in
the spectral responses of the structural elements of wheat, which
could have a bearing on yield estimation.

BACKGROUND

The observation that the absorption regions of chlorophyll a
(437,676 nm) and b (468,651 nm) broaden and increasingly overlap
as leaves mature is well known. Gates et al. (1965) seem to have been
the first group to document this effect using a laboratory reflectance
spectrometer. Their results were reported for oak (dicot) leaves.
Collins (1978) has reported the effect as a "red shift" (745-785 nm) in
wheat (monocot) leaves using an aircraft mounted spectrometer. We have
observed the effect in cotton (dicot) leaves taken from the same
plant; the effect could not be identified from between plant
comparisons due to interplant variability. In the case of wheat,
the development of chlorophyll absorption can only be an indirect
indicator of yield because leaf maturation is completed prior to
heading. After the head emerges, the leaves on the plant commence
to senesce. It is the relationship between the spectra of these
components during emergence and ripening which we are investigating
on a continuing basis.

RECENT ACCOMPLISHMENTS

Spectral measurements were taken in the laboratory from 0.36 to 2.5 μm
on heads and flag leaves of field grown wheat plants. The results
are summarized in Figure 9B-1. Spectral areas are given for a mature
and senesced flag leaf and for a nearly empty and fully ripened seed
containing head. The spectral differences from 0.8 to 1.2 μm
between both the leaf and the head for each state are striking. As
the flag leaf senesced, its spectral structure disappeared while
its reflectance increased. During the same time periods, the head
gained in reflectance as it matured, but contrary to leaf behavior,
a spectral structure developed as the carbohydrate level increased.
Both the senescing leaf and the ripening head produce a reverse
"red shift" or a shift in the long wavelength chlorophyll absorption
toward the blue.

SIGNIFICANCE

These results demonstrate that leaf and head spectra from 0.8 to 1.2 μm
are distinct, and provide a basis for their partial separation using
off nadir viewing.

FUTURE EMPHASIS

Recently a greenhouse planting of wheat has been undertaken to
provide an additional check on these results, to identify for the
"red shift", and to shed some light on the effect of fertility on the

spectra of heads during ripening. Pending verification of these
results, the study will be pursued in the field during the upcoming
growing season.

REFERENCES

Gates, D.M., Keegan, J.H., Schleter, J.C., and Weidener, V.R.,
  "Spectral Properties of Plant", Appl. Optics, 11-20 (1965).

Collins, W., "Identification of Crop Type and Maturity" Photogram.
  Engr. and Remote Sens. 44(1): 43-55 (1978).

SPECTRAL SHIFTS IN WHEAT
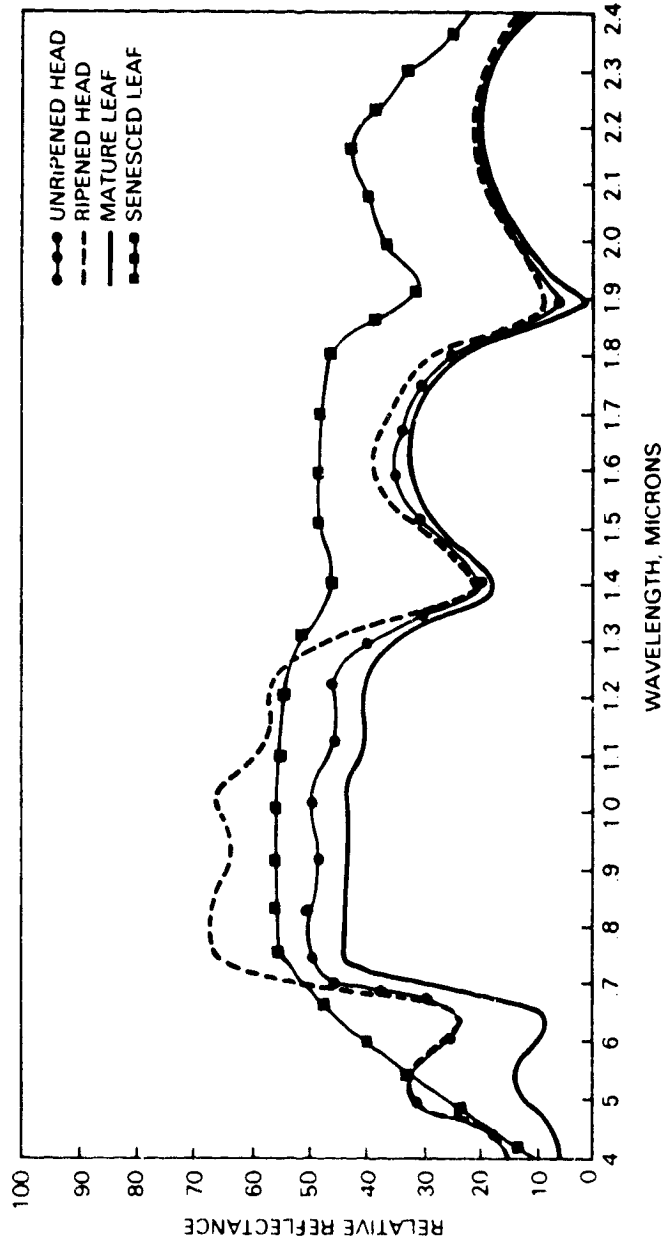
Figure 9B-1. Relative spectral responses of a head of wheat and a flag leaf. Each component is shown in two spectral states important in remote sensing.

C. **REMOTE SENSING OF TOTAL DRY MATTER ACCUMULATION IN WINTER WHEAT**

by

C.J. Tucker, B.N. Holben, J.H. Elgin, and J.E. McMurtrey

OBJECTIVES

To investigate the prediction of total dry matter accumulation by
integrating frequently collected spectral data from winter wheat.
Discuss possible extrapolations to the carbon dioxide question data
requirements.

BACKGROUND

The global carbon dioxide (CO_2) cycle has been the subject of much
recent interest and continues to be the subject of serious international
concern. Remote sensing, with its unique synoptic perspective,
has been mentioned as a possible means of monitoring the terrestrial
vegetation biomass or phytomass. The role of the phytomass in
the global CO_2 cycle is extremely important and involves the amount of
carbon stored in various plant communities of the world, with special
emphasis on forested areas and, in particular, tropical forests.
Remote sensing techniques might be employed in attempts to satisfy
three interrelated requirements for information about the terrestrial
phytomass: the distribution of the various plant communities; changes
in the distribution of the plan communities with time and, particularly,
deforestation; and the net primary productivity of the various plant
communities, including regrowth following deforestation. Remote sensing
unfortunately cannot be used for direct measurement of the carbon
stored as above-ground phytomass.

We report herein on a technique that can be used to assess net primary
productivity or total dry-matter accumulation from frequently collected
red and photographic-infrared spectral data for winter wheat canopies.
The same technique is thought to be extendable to terrestrial vegetation
in general.

Our experiment was conducted in a 1.2-ha soft red winter wheat
(Triticum aestivum L.) field at the Beltsville Agricultural Research
Center, Beltsville, Maryland.

Twenty 2- x 3-m plots in the wheat field were selected during the
winter dormant period. Four pairs of red and photographic-infrared
spectral measurements were taken per plot with a hand-held digital
radiometer. Data were collected on 21 dates between March 21, 1978
(Julian date 80), and June 23, 1978 (Julian date 174), at intervals
ranging from 1 to 9 days.

The red (0.65 - 0.70 μm) and photographic-infrared (0.775-0.825 μm)
spectral-radiance data were used to form the IR/red ratio and the
normalized difference (ND), where:

$$ND = (IR-red)/IR+red) \tag{1}$$

The four pairs of spectral measurements per plot were averaged to
account for the spatial variability present in each plot. All spectral

data were collected under sunny skies within plus or minus 90 minutes of local solar noon, and measured normal to the ground surface.

Throughout the growing season average plant height, estimated percentage of cover, and phenological development were recorded for the field area . The crop reached harvest maturity in late June 1978. On June 28, 1978 (Julian date 179), a 0.9- x 3.0-m swath was cut from the center of each plot with a small sickle-bar mower. Total biomass and grian yield were recorded. The entire above-ground biomass was oven dried at $60^{\circ}C$ for 72 hours and weighed; the resulting total dry-matter accumulation was expressed in g/m^2.

RECENT ACCOMPLISHMENTS

Red and photographic-infrared spectral data collected on 21 dates over the growing season with a hand-held radiometer were quantitatively correlated with total dry-matter accumulation in winter wheat. The spectral data were found to be highly related to vigor and condition of the plant canopy. Two periods of drought stress and subsequent recovery from it were readily apparent in the spectral data. Simple ratios of the spectral radiance data compensated for variations in solar intensities and, when integrated over the growing season, explained 79% of the variation in total above ground accumulation of dry matter. A satellite system is proposed to provide large-area assessment of total dry accumulation or net primary production from terrestrial vegetation.

SIGNIFICANCE

1. Red and photographic infrared spectral data were found to be highly related to canopy vigor of winter wheat and its response to rainfall after mild drought.

2. The IR/red radiance ratio and the normalized difference integrated over spectral sampling dates were found to be strongly related to above-ground total accumulation of dry matter in winter wheat.

3. A coarse spatial resolution satellite system is proposed to allow large-area assessment of net primary production or total dry matter accumulation. This information would have immediate use in addressing some of the questions associated with the role of the terrestrial phytomass in the carbon dioxide cycle. In addition, this information would provide large-area primary production data for monitoring desertification, drought, deforestation, acid rain, and many other occurrences which adversely affect plant growth and development.

FUTURE EMPHASIS

The technique described herein is being applied to different plant communities. This will determine the extent to which this technique is applicable.

REFERENCES

Tucker, C.J., B.N. Holben, J.H. Elgin and J.E. McMurtrey. 1981 "Remote Sensing of Total Dry Matter Accumulation in Winter Wheat". Remote Sensing of Environment (in press).

D. REMOTE SENSING OF TEMPERATURE PROFILES IN VEGETATION

CANOPIES USING MULTIPLE VIEW ANGLES AND INVERSION

TECHNIQUES

by

D. S. Kimes

OBJECTIVES

The objective of this study was to demonstrate and evaluate a mathematical inversion technique based on physical principles which utilizes a series of sensor view angles and a priori information of vegetative geometric structure to predict temperature profiles of vegetation canopies.

BACKGROUND

There has been great interest in utilizing remote sensing in the thermal infrared region (3-20 μm) to gain additional information concerning the status of land resources. In the vast majority of remote sensing applications, vegetation canopies are encountered. Often the vegetation itself is the target of interest as is the case in agriculture, forestry, and range applications; however, in many applications such as agronomy, geology, and hydrology the substrate underlying the vegetation (e.g., soil, rock, snow, etc.) is of interest. A mixture of vegetation and substrate components within the field of view of a sensor often complicates accurate scene interpretation. Wide variability in mixture of natural scenes occurs, causing wide variability in spectral response (both reflective and emitted regions) and difficulty in making accurate inferences. Furthermore, strong vertical temperature profiles occur within vegetation that affect sensor response and prevent accurate inferences of plant water status, disease conditions, etc. A remote sensing technique is needed which uniquely separates composite sensor response(s) into a unique temperature profile (vertical profile of vegetation temperatures and substrate temperature).

In this study a technique was proposed that utilized a physically based deterministic model to relate the vertical temperature profile and the geometric structure of the vegetation to the directional, thermal infrared sensor response. Using a series of off-nadir sensor view angles and a priori information of vegetation geometry as input variables, the model was mathematically inverted to solve uniquely for the vertical temperature profile. The technique was evaluated on data from several wheat canopies at different stages of development.

RECENT ACCOMPLISHMENTS

Kimes (1980a) presented a deterministic equation based on physical principles which expressed the directional sensor response as a function of vegetation geometry and the temperature profile of horizontal layers of vegetation. In this study the equation was expressed as a system of linear equations as follows:

$$A\bar{t} = \bar{s} + \bar{\epsilon} \qquad (1)$$

$$A = \begin{pmatrix} a_{11} & a_{12} \cdots \cdots a_{1m} \\ & \ddots \\ a_{21} & \\ \vdots & \\ a_{n1} \cdots \cdots \cdots a_{nm} \end{pmatrix} ; \quad \bar{t} = \begin{pmatrix} t(x_1)^4 \\ t(x_2)^4 \\ \vdots \\ t(x_n)^4 \end{pmatrix} ; \quad \bar{s} = \begin{pmatrix} s(\theta_1,\emptyset_1)^4 \\ s(\theta_2,\emptyset_2)^4 \\ \vdots \\ s(\theta_n,\emptyset_n)^4 \end{pmatrix} ; \quad \bar{\epsilon} = \begin{pmatrix} \epsilon_1 \\ \epsilon_2 \\ \vdots \\ \epsilon_n \end{pmatrix}$$

Where $s(\theta_i,\phi_i)$ is the effective radiant temperature (ERT; also referred to as apparent temperature) in degrees Kelvin of an m-layered canopy system (layer 1 to m proceeds from the top of the canopy to the substrate) as measured by a sensor viewing the canopy at zenith and azimuth angles θ_i and ϕ_i respectively, $t(x_j)$ is the mean ERT in degrees Kelvin of the components in the canopy layer with vertical position x_j, and is the error vector. The components of the A matrix (a_{ij}) characterize the vegetation geometry and are the relative proportions of surface elements in layer x_j that present themselves to direct view to a sensor with view angle θ_i,ϕ_i. Calculations of this matrix were reported by Kimes et al. (1980).

Field studies were conducted at Phoenix, Arizona, on irrigated wheat field. Measurements of the $S(\theta,\phi)$, $T(x)$ and a_{ij} values for eight canopies of various geometric structure for thirty-three measurement periods were made (Kimes, 1980b). This data set served as validation data for testing various inversion techniques. Several cases were solved including cases of an exact 2 x 2 system (n sensor view angles and m canopy layers), an exact 4 x 4 system, and also overdetermined systems of these exact systems. Sensitivity analyses of these systems were performed.

The results showed that the four layered systems were extremely sensitive; a $1^{\circ}C$ change in nadir sensor ERT can drastically change the predicted canopy layer ERT ($20^{\circ}C$ or more). These ill conditioned systems are not appropriate for the accuracies of measurements experienced in most remote sensing applications. However, by employing a two layered system (vegetation and soil) and two or more sensor view angles, the mean vegetation and soil temperatures can be inferred, relatively accurately. For example, the root-mean-square prediction accuracy of vegetation temperatures of the data set was $1.8^{\circ}C$ for a system using $0^{\circ}/40^{\circ}$ zenith view angles. Using this system the prediction of vegetation temperature is a 2.4 and 2.2 times more accurate than the measurement of a single sensor measurement at 0° and 40° zenith view angles, respectively. From sensitivity analyses it was found that one can expect relatively accurate inferences of vegetation temperatures for canopies having intermediate and dense vegetation densities, and relatively poor inference of vegetation temperatures for sparse canopies. The converse is true for inferring substrate temperatures.

SIGNIFICANCE

These findings have significant implications for remote sensing research and applications in agriculture, hydrology, geology, forestry,

and other earth resources disciplines where the scene of interest
is the vegetation canopy or the underlying substrate rather than the
composite scene. For specific vegetation geometries this technique may
provide a means for uniquely separating mean vegetation and
substrate temperatures when a priori knowledge of vegetation geometry
and two or more sensor view angle measurements can be obtained.

FUTURE EMPHASIS

This study has been accepted for publication. Future work will
involve preprocessing of the data, including smoothing and physical
constraints based on known thermal properties of canopies, to
improve the prediction accuracies.

PUBLICATIONS AND REFERENCES

D.S. Kimes, 1980a. "Effects of Vegetation Canopy Structure on
Remotely Sensed Canopy Temperatures," Remote Sensing of Environment
(in press).

D.S. Kimes, 1980. "Remote Sensing of Temperature Profiles in
Vegetation Canopies using Multiple View Angles and Inversion
Techniques". IEEE Transactions on Geoscience and Remote Sensing
(in press).

D.S. Kimes, S.D. Idso, P.J. Pinter, Jr., R.D. Jackson, and R.J. Reginato,
1980. "Complexities of Nadir-Looking Radiometric Temperature
Measurements of Plant Canopies". Applied Optics 19(13): 2162-2168.

E. ANGULAR CONSIDERATIONS IN OFF-NADIR VIEWING OF

SOIL AND VEGETATION

by

C.J. Tucker and B.N. Holben

OBJECTIVES

The objective of this study was to measure the bidirectional reflectance/radiance distribution function of soil and vegetation. This was accomplished by a series of rapid field measurements where 56 hemispherical radiance measurements were made from the same area in two spectral bands. Data in support of this objective were collected at eight azimuthal positions and for seven sensor view angles per azimuthal position.

BACKGROUND

The reflectance of a surface is a very complex assemblage of specular and diffuse radiant fluxes eminating from a surface relative to the direct and diffuse radiant flux impinging upon that surface. For many remote sensing investigators, the reflectance has been assumed constant for a given cover type primarily because geometric conditions of observation have been relatively constant (i.e., a nadir viewing sensor, standard time of observation, and a horizontal target). More portable and flexible field equipment and future off-nadir looking satellites (proposed NASA satellites and French SPOT satellites) present the opportunity to investigate spectral reflectances from variable light source-target-sensor geometries.

Remote sensing involves the acquisition of electromagnetic radiation eminating from a target surface and impinging upon a sensor surface. In order to relate the sensor information to specific propeoties of the surface, a detailed accounting of the radiation transfer must be taken. For the visible and reflective infrared portions of teh electromagnetic spectrum, this is accomplished by describing the reflected radiant flux from a surface relative to the incident radiant flux.

Several 6-m x 6-m experimental plots were selected for detailed experimental study at the Beltsville Agricultural Research Center, Beltsville, Maryland. One plot of bare soil and one plot of uniformly distributed nut sedge (sedgei nute) were selected. Nut sedge is a commonly occurring grass-like weed. The bare soil plot was kept clear of all vegetation by applications of herbicide.

Red (0.65 - 0.70 μm) and photographic infrared (0.775 - 0.825 μm) spectral data were collected at zenithview angles of $0°$, $10°$, $20°$, $30°$, $40°$, $50°$ and $60°$ from eight compass positions (N, NE, E. SE, S, SW, W, and NW) using a two-channel hand-held radiometer. The hand-held portion of the radiometer was mounted on a camera tripod to which a protractor was attached for angular determinations. Plot areas of homogenous composition were carefully selected as the field of view gradually increased with increasing sensor view angle. A

complete set of 7 sensor view angles measured at 8 compass positions
was measured in 15 to 30 minutes total elapsed time, reducing
variations caused by the apparent movement of the sun. Barium
sulfate reference measurements were made before and after each
series of spectral measurements. These data were collected on
5/39/78 for the bare soil plot and 6/29/78 for the 20% ground
cover nut sedge plot. Solar elevations and solar azimuths (measured
clockwise from north) for the plots were 50° and 257° respectively
for the bare soil and 74° and 187° for the nut sedge.

The zenith view angles measured for each compass position form a
plan perpendicular to the ground (see Figure 9E-1). The azimuth of
each plane, called a view azimuth, was calculated clockwise
with respect to the solar azimuth, hence a view azimuth of 90° 270°
are perpendicular to the principal plane of the sun and a view azimuth
of 180° is parallel to the principal planewith the sensor looking
toward the solar azimuth.

The spectral data presented in this report will be the measured spectral
radiances, the ir/red radiance ratio, and the normalized difference (ND)
of (ir-red)/(ir+red). The radiances were uncalibrated instrument
readings which were directly convertable into spectral reflectances
by simply dividing them by the measured $BaSO_4$ value.

RECENT ACCOMPLISHMENTS

Ground collected red and photographic infrared spectral radiances
were measured from the eight principal compass positions at zenith
view angles of 0° to 60° in 10° increments. Data were collected
from a plot of bare soil and a vegetated plot. Significant
relationships to phase angle, zenith view angle, and view azimuth of
the sensor were found for both red and photographic infrared spectral
radiances for bare soil and for the red radiance, ir/red radiance
ratio, and normalized difference for the vegetated plot. The sensor
response to the bare soil plot was found to be essentially equal
when viewed within the plane perpendicular to both the principal
plane of the sun and the ground. This suggested a possible "atmospheric
correction" target for off-nadir viewing satellites. In addition,
phase angle may be an important model input for relating off-nadir
spectral data to nadir spectral data calibrated to green leaf area
index.

SIGNIFICANCE

1. Spectral data collected form bare soil with the sensor's
view situtated perpendicular to both the principal plane of the sun
and the ground were found to be constant with zenith view angle. This
equal spectral response could have utility for atmospheric corrections
using off-nadir looking satellites. The relationship of phase angle
to the red and photographic infrared spectral response from bare
soil explained the zenith view angle and view azimuth effects.

2. Backscattering was enhanced by large zenith view angles in
both bands for the bare soil. Red spectral response decreased with
increasing zenith view angle for the vegetated plot as a result of
projected leaf area index of the erectrophile sedge canopy geometry
and showed little variation with zenith view angle in the photographic
infrared band.

3. Phase angle was inversely related to spectral response for bare soil suggesting that spectral response could be modeled in part by a phase angle relationship.

4. Red responses to bare soil and vegetation were identical to the photographic infrared respones to bare soil. However, a heiarchial linear relationship of photographic infrared radiances to the nut sedge canopy was found. The heiarchial relationship may be successfully modeled in part by phase angle to normalize uncalibrated off-nadir spectral data to a nadir calibrated standard.

5. The IR/red radiance ratio and normalized difference both exhibited view azimuth, zenith view angle, and phase angle relationships which corresponded to changes in projected leaf area index of the nut sedge canopy.

FUTURE EMPHASIS

Additional field data collection efforts are anticipated as well as mathematical modeling of these types of soil and/or vegetation scenes.

REFERENCES

Tucker, C.J. and B.N. Holben. 1981. "Angular Consideration in Off-Nadir Viewing of Soil and Vegetation". International Journal of Remote Sensing. 2: (in press).
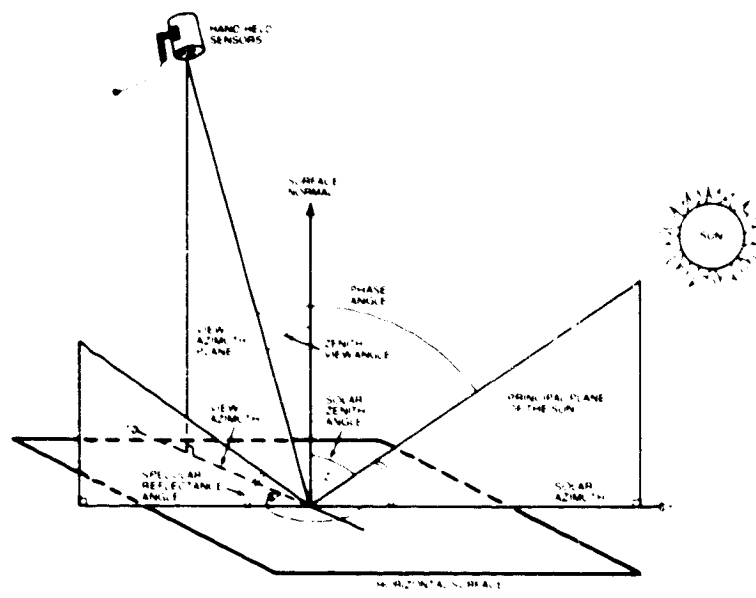
Figure 9E-1. Diagram illustrating the specular reflectance angle,
              phase angle, solar zenith angle, zenith view angle,
              view azimuth plane and principal plane of the sun.
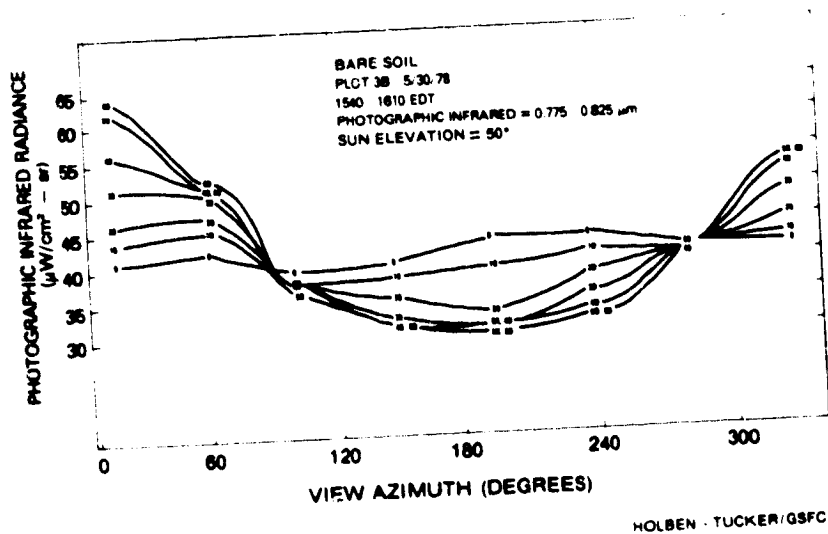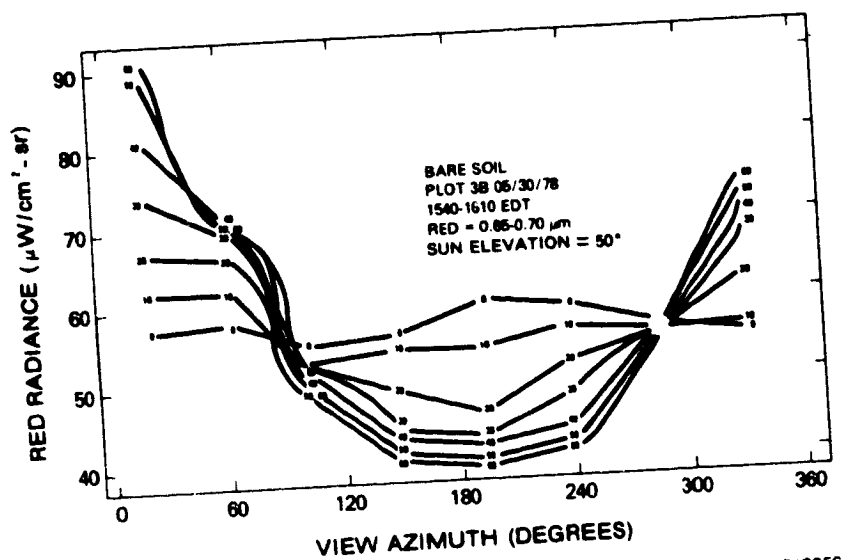
Figure 9E-2. View azimuth vs (a) red radiance and (b) photographic infrared radiance for bare soil on 5/30/78. Note the nodal points approximately perpendicular to the principal plane of the sun.
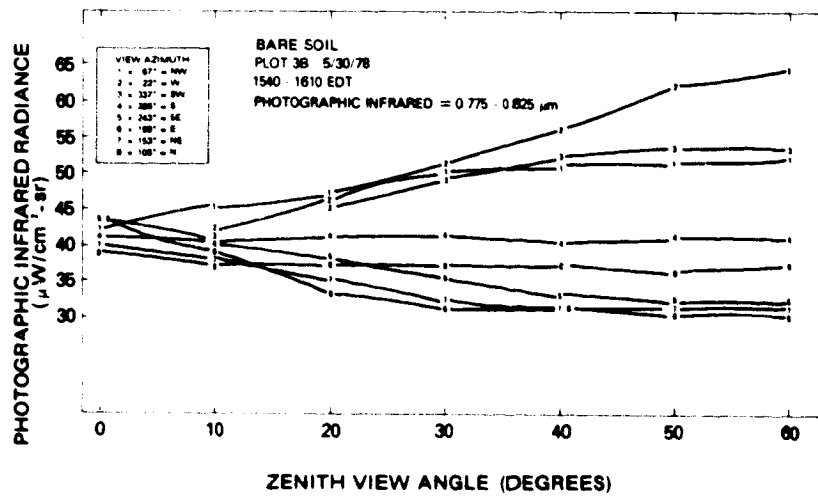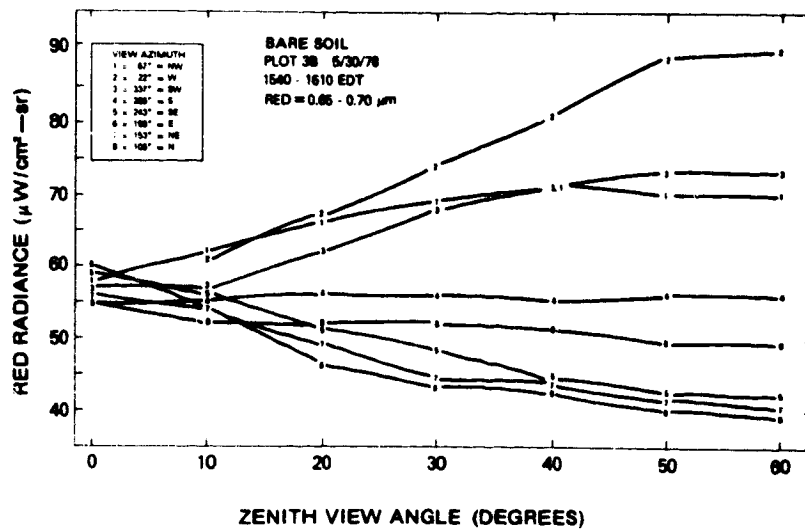
Figure 9B-3. Zenith view angle plotted vs (a) red radiance and
(b) photographic infrared radiance for bare soil on
5/30/78. Separation of the view azimuth curves increased
with increasing zenith view angle.
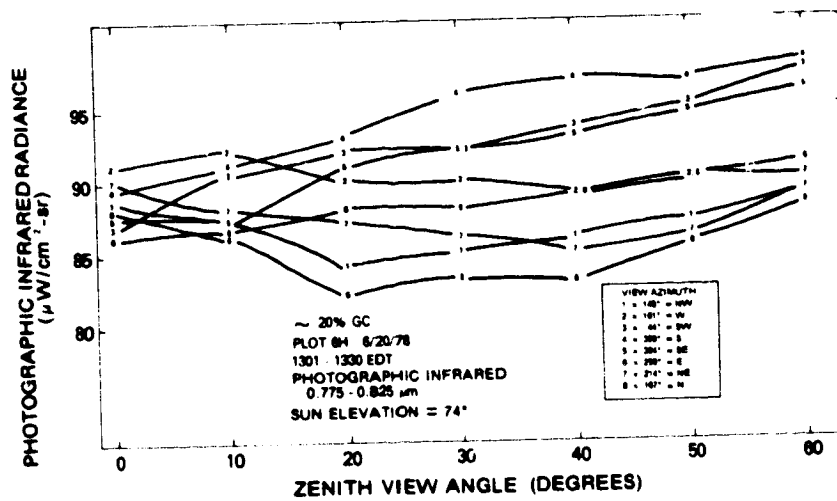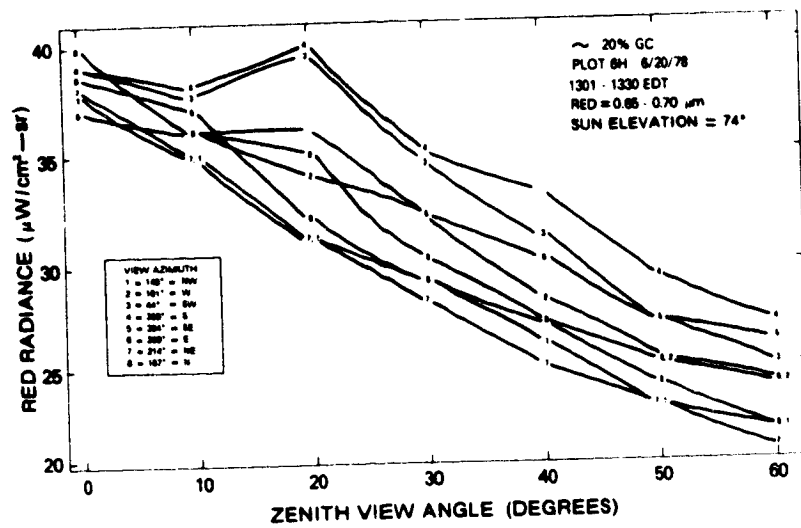
Figure 9E-4. Zenith view angle plotted vs (a) red radiance and (b) photographic infrared radiance for ¯20% green cover on 6/20/78. Note a decrease in red radiance with increasing zenith view angle for the red radiance only.
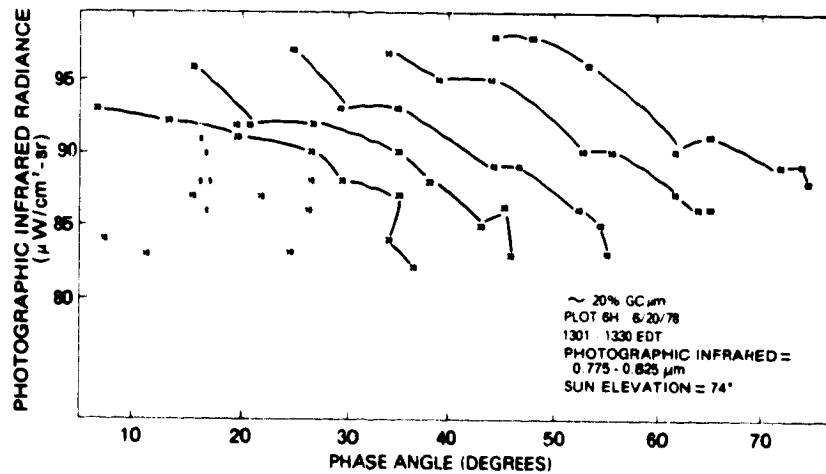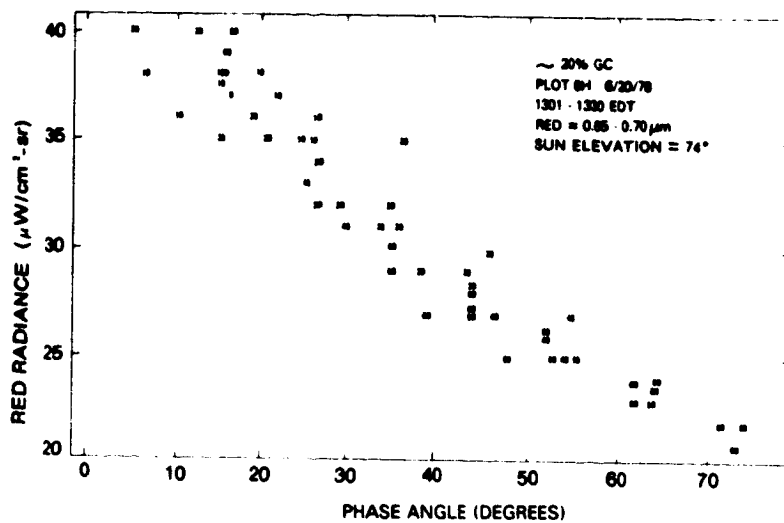
Figure 9E-5.   Phase angle vs (a) red radiance and (b) photographic
                infrared radiance were plotted for ~20% green cover on
                6/20/78. Note the response differences between red and
                photographic infrared. The data points are numbers
                corresponding to zenith view angles.

F. SIMULATED DIRECTIONAL RADIANCES OF VEGETATION

FROM SATELLITE PLATFORMS

by

J.A. Kirchner, C.C. Schnetzler and J.A. Smith

OBJECTIVES

The purpose of the study was to examine, via simulation techniques, the effects of off-nadir viewing, vegetation canopy geometry and density, solar zenith angle, and atmospheric condition on the spectral radiance and normalized difference index (ND) as viewed from a satellite.

BACKGROUND

The potential development of pointable earth observation satellite sensors provides not only the opportunity to improve the temporal resolution of a scene by looking across adjacent swaths, but also raises the necessity of understanding the radiometric and geometric effects of viewing a given target off-nadir. The scope of this problem is quite broad since sun/sensor geometries, atmospheric conditions, spectral bands, and the bidirectional reflecance properties of the surface must all be considered. Each of these factors influences the radiance observed from a given target at a given time. Under natural conditions, it is difficult to isolate and observe the effects of each singly; hence, the use of mathematical simulation models. Such models, effectively used, can aid in understanding the complexities of off-nadir viewing, eventually leading to new remote sensing applications or improvement of existing capabilities.

RECENT ACCOMPLISHMENTS

Simulation data used in this study were taken from the data base established by Smith et al. (1980) for ORI, Inc. Kriebel (1976) showed that the directional radiance of a target was determined by the distribution of radiation impinging upon the target. In the study conducted by Smith, et al. (1980) the atmospheric radiative transfer model developed by Turner (1974) was used to supply the necessary incoming radiance values as well as to predict the radiance perceived by a sensor at a given altitude, zenith angle, and azimuth look angle with respect to the sun. Atmospheric path radiance was taken into account. The model was modified by replacing the Lambertian surface normally found in the model with bidirectional reflectance factors typical of various vegetated surfaces. These factors were derived using the Solar Radiation Vegetation Canopy model of Smith and Oliver (1972). For a satellite altitude, spectral responses at two wavelengths, 0.68 μm in the chlorophyll absorption band of vegetation, and 0.80 μm in the near infrared, were simulated at nine sensor zenith angles, five sensor azimuths and nine solar zenith angles for seven vegetation canopies under three atmospheric conditions. Only the data for a grass canopy, modeled with two different geometries at low, medium, and high biomass levels, were used in the present study.

The simulated radiance data were used to calculate the value of the normalized difference index (IR-RED/IR+RED), a green biomass indicator. Data analysis included construction of polar plots of radiances and normalized differences according to the scheme presented in Figure 9F-1. The data were then contoured according to their <u>percent change from the nadir value</u>. Plots to help visualize the effects of various sun angles, view angles, canopy geometries and densitites, and atmospheric conditions were grouped accordingly. Figures 9F-2 and 3 illustrate the off-nadir variability of the spectral radiance and normalized difference of a grass canopy under clear atmospheric conditions for spherical and planophile canopy geometries, respectively.

SIGNIFICANCE

1. Off-nadir viewing effects were found to be more pronounced in the red spectral band than in the infrared.

2. The magnitude of off-nadir viewing effects is a function of canopy geometrical structure.

3. The normalized difference index tends to remove some of the variability due to off-nadir look angles that is exhibited by individual spectral bands.

4. A "hot spot" in plots of red radiance is located such that contours about it tend to align with a relative azimuth of 120°. Thus, viewing near this azimuth should give rise to the least variation of data values over a range of sensor zenith angles since the fewest contours are crossed.

5. Off-nadir variability of scene radiance and normalized differences decreases with increasing biomass at given sun and view angles.

6. Increasing solar zenith angles greatly increase the magnitude of variations observed by looking off-nadir, but actually tend to lessen the variations seen within a sensor zenith angle range of 0 to 35° due to the movement of the hot spot out of this range.

7. Atmospheric haze wipes out useful surface information by magnifying scattering effects.

FUTURE EMPHASIS

The project described was completed and submitted to a journal.

REFERENCES AND PUBLICATIONS

Kirchner, J.A., C.C. Schnetzler, and J.A. Smith, "Simulated Directional Radiances of Vegetation from Satellite Platforms". Submitted to International Journal of Remote Sensing.

Kriebel, K.T. 1976. "On the Variability of the Reflected Radiation Field Due to Differing Distributions of the Irradiation". Remote Sensing of Environment. 4: 257-264.

Smith, J.A. and R.E. Oliver. 1972. "Plant Canopy Models for Simulating
Composite Scene Spectroradiance in t'e 0.4 to 1.04 Micrometer
Region". Proceedings of the Eighth International Symposium on Remote
Sensing of Environment, University of Michigan, Ann Arbor, pp. 261-
274.

Smith, J.A., K.J. Ranson, and J.A. Kirchner. 1980. "A Simulation
Analysis of Bidirectional Reflectance Properties and their Effects
on Scene Radiance". ORI, Inc., Silver Spring, MD. 125 p.

Turner, R.E. 1974. "Radiative Transfer in Real Atmospheres", Report No.
190100-24-T. ERIM, Ann Arbor, MI. 108 p.
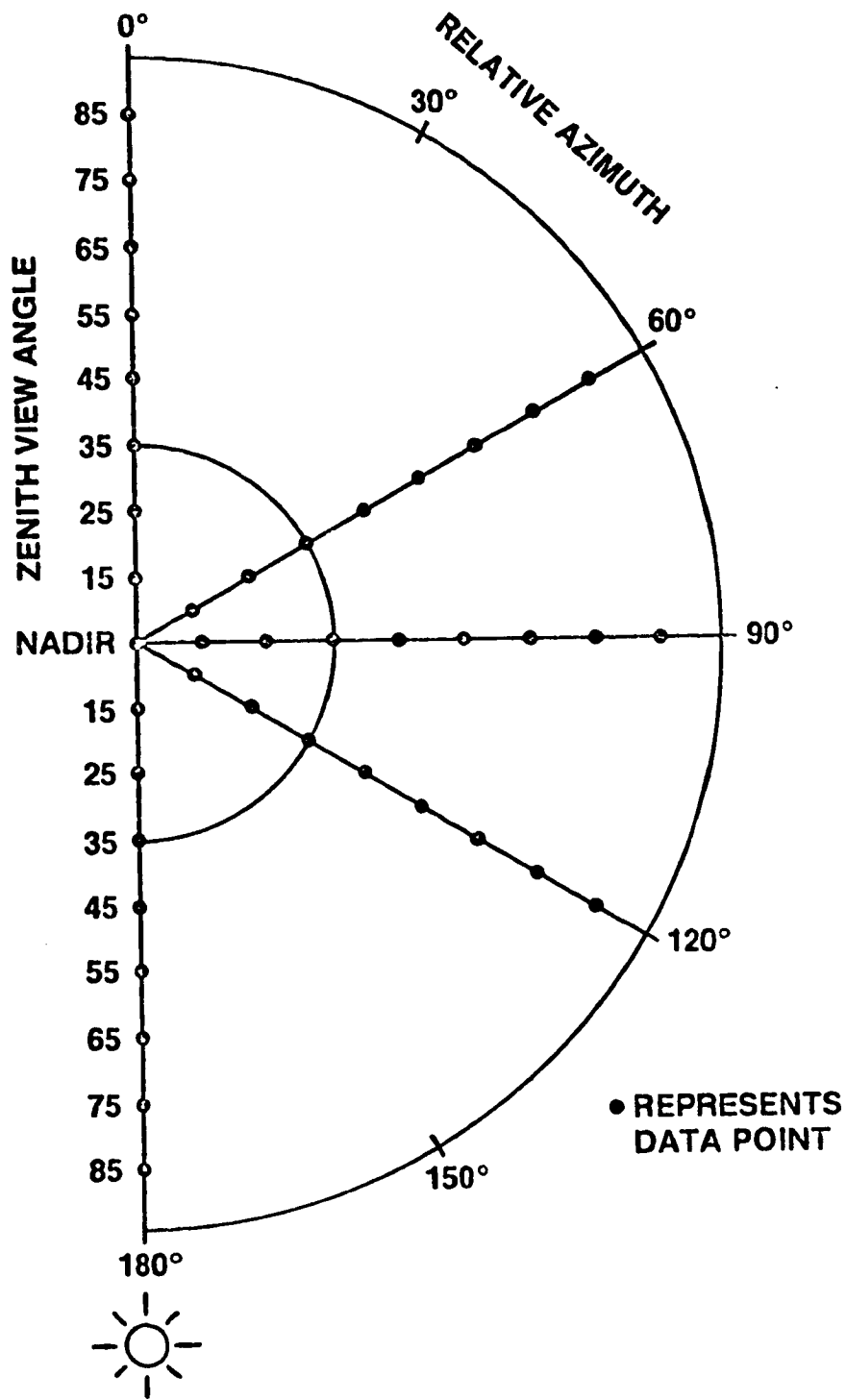
Figure 9F-1 . Scheme for plotting and contouring radiances
and normalized differences according to their
percent change from the nadir value. Data were
plotted for nine sensor zenith and five sensor
azimuth angles. The nadir value is the average
of the 5° sensor zenith angle values for the 5
azimuth angles. Solar azimuth is always 180
degrees. The semi-circle at 35° zenith represents
a suggested maximum sensor pointing angle.

SPHERICAL GRASS CANOPY (MID-BIOMASS)

**LAI = 1.2
SOLAR ZENITH ANGLE 35°
VISIBILITY 23 km**

$$ND = \frac{IR\text{-}RED}{IR\text{+}RED}$$

RED RADIANCE (0.68 μm)
NADIR=3.25 mW cm^{-2}sr^{-1}

IR RADIANCE (0.80 μm)
NADIR=8.99 mW cm^{-2}sr^{-1}

NADIR=0.469
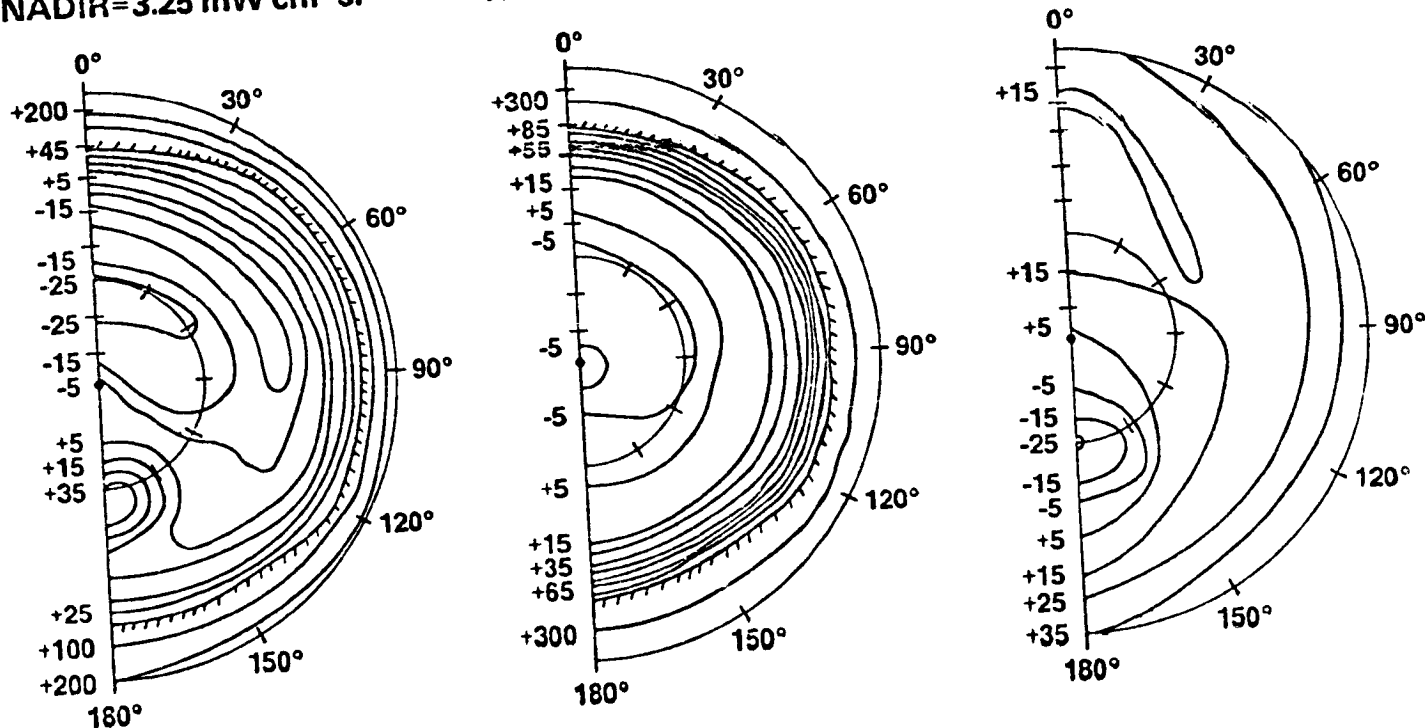
Figure 9F-2 . Polar plots showing off-nadir variability of a) red radiance, b) IR radiance, and c) normalized difference, for a medium biomass, spherical grass canopy at a solar zenith angle of 35° under clear atmospheric conditions. Contour lines represent percent change from the nadir value. Contour interval is 10%. Hatched lines indicate some contour lines have been omitted.

PLANOPHILE GRASS CANOPY (MID-BIOMASS)

LAI = 1.2
SOLAR ZENITH ANGLE 35°
VISIBILITY 23 km

$$ND = \frac{IR-RED}{IR+RED}$$

RED RADIANCE (0.68 μm)
NADIR=3.63 mW cm⁻²sr⁻¹

IR RADIANCE (0.80 μm)
NADIR=12.7 mW cm⁻²sr⁻¹

NADIR=0.555

Figure 9F-3. Polar plots showing off-nadir variability of a) red radiance, b) IR radiance, and c) normalized difference, for a medium biomass, planophile grass canopy at a solar zenith angle of 35° under clear atmospheric conditions. Contour lines represent increments of 10% change from the nadir value. Hatched lines indicate some contour lines have been omitted.

G. MODELING THE EFFECTS OF VARIOUS RADIANT TRANSFERS IN

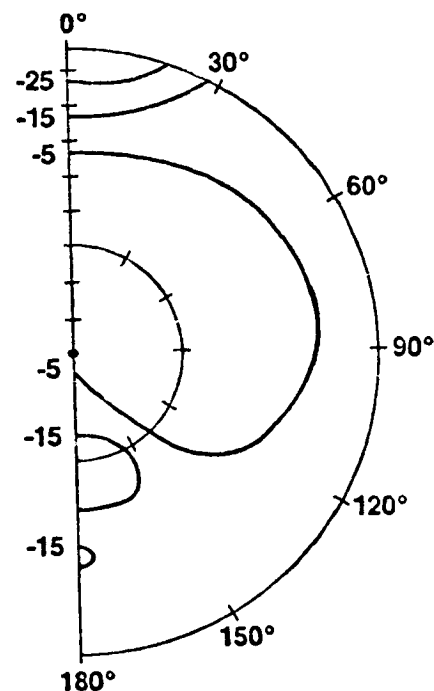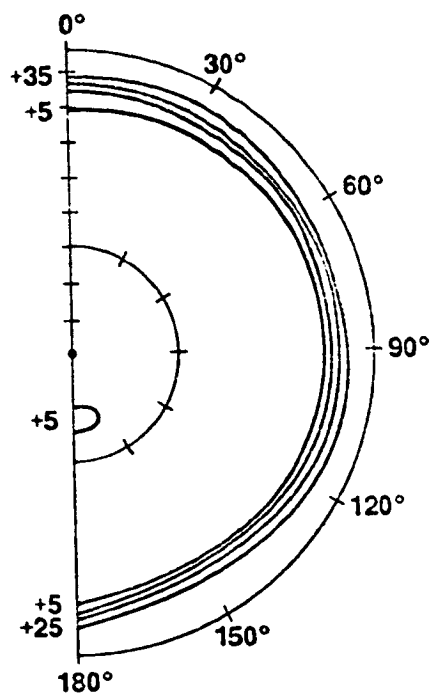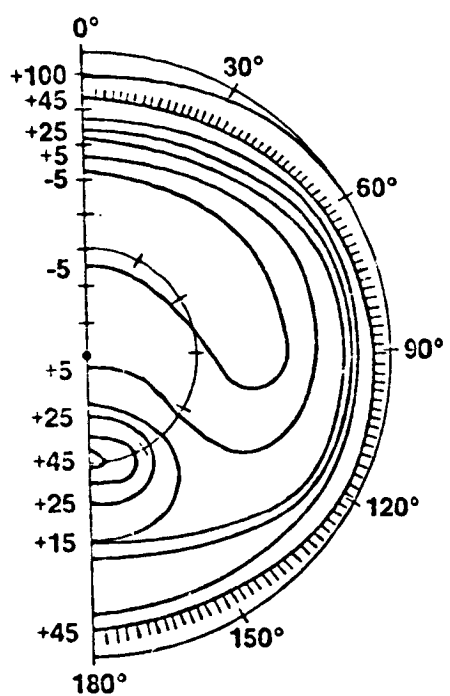## MOUNTAINOUS TERRAIN ON SENSOR RESPONSE

by

J.A. Kirchner and D.S. Kimes

OBJECTIVES

The purpose of this study was to develop a model capable of simulating the effects of anisotropic sources of irradiance and bidirectional reflectance properties of the target surface on sensor response for various slope orientations, and to use this model to examine the errors associated with two practical techniques for accounting for the topographic effect on sensor response.

BACKGROUND

The analysis of remotely sensed spectral data has potential for providing effective management of natural resources in areas of mountainous terrain. Recent studies have shown problems in the interpretation of multispectral data in mountainous areas due to topographic effects on sensor response. These effects are caused by variations in slope orientation with respect to sources of incident radiation (as opposed to variations in surface cover conditions) and need to be considered before accurate classification of multispectral data from mountainous terrain can be achieved. The radiant transfers in such terrain are of such complexity that an accurate understanding of the causes of sensor response variability is difficult to achieve without the aid of a comprehensive, physically based model.

RECENT ACCOMPLISHMENTS

A model was developed which simulates the effects of variations of direct solar radiance, anisotropic sky radiance, anisotropic radiance of surrounding topography and bi-directional reflectance of the target slope on the directional sensor response for various sun and target slope orientations. The simulated topographic scene consisting of the target slope and adjacent slopes was modeled as a set of two or more contiguous planes. Spherical coordinate systems were used exclusively to describe all radiant energy transfers.

Two coordinate systems were defined, as shown in Figure 9G-1, to account for the radiant transfers. The target plane represents the slope of interest, and the target point represents the location of the sensor field of view on the slope. The target point can occur at any location on the target plane. The inclination and aspect angles of the target plane were described by $\vee$, and γ, respectively, in the standard XYZ

coordinate system. Inclination of the adjacent slope was described by τ (Figure 9G-2). Both the XYZ and X'Y'Z' systems were discretized into a finite number of sectors as defined by azimuth ($\Delta\phi$) and inclination ($\Delta\theta$) intervals (Figure 9G-3). The discretization of the hemisphere into sectors was a convenient numerical technique for accounting for the anisotropic distributions of radiation, both from the sky and from adjacent terrain reflections.

The spectral radiance from the target point, L_r, in any direction (θ'_r, ϕ'_r), is exactly determined by

$$L_r (\theta'_r, \phi'_r) = \int_0^{2\pi}\int_0^{\pi/2} \rho^B(\theta'_i, \phi'_i; \theta'_r, \phi'_r) L_i (\theta'_i, \phi'_i)$$
$$\sin \theta'_i \cos \theta'_i \, d\theta'_i d\phi'_i.$$

where (ρ^B) is defined as the relation of that part of the total spectral radiance d $L_r (\theta'_r, \phi'_r)$ reflected in the direction θ'_r, ϕ'_r which originates from the direction of incidence θ'_i, ϕ'_i to the total spectral irradiance $L_i (\theta'_i, \phi'_i) \sin (\theta'_i) \cos (\theta'_i) \, d\theta'_i d\phi'_i$ impinging on a surface from the direction (θ'_i, ϕ'_i). In the context of the model framework, however, the outgoing radiance in the direction of each X'Y'Z' source sector was calculated as a numerical approximation of this equation where the integral over the hemisphere was a summation of the individual source sectors. The directions of these radiance values were rotated to the XYZ system for reporting of the directional sensor response.

Simulations of the model were compared with results of two different techniques which attempt to account for topograhic effects for a variety of slope-aspect orientations. The first technique was a simple cosine correction which ignored diffuse radiation from both the sky and adjacent slopes, while the second technique included diffuse skylight, but still ignored flux from adjacent terrain. For each simulation, the differences between the target radiances calculated by the comprehensive model and the respective techniques were used to evaluate the accuracy of each technique.

SIGNIFICANCE

In this study the model was utilized to explore the errors associated with two practical techniques for accounting for the topographic effect on sensor response. The results showed that the topographic effect needs to be considered in mountainous terrain before accurate inferences from sensor data can be made. For the specific anisotropic irradiance conditions and Lambertain scenes of this study, it was clear that relatively significant errors can occur at all wavelengths when accounting for the topographic effect in terrain with slopes greater than 20° if only a direct solar source is considered (simple cosine correction). This error was diminished by greater than 50% when both direct solar and diffuse sky sources were considered. The latter technique had a maximum 4% error in reflectance for all simulated

scenes except for highly reflected wavelengths and extreme slopes (30° slopes). With the recent development of methods for integrating digital terrain data with remote sensing data it has become possible to apply such techniques.

FUTURE EMPHASIS

In future model applications the variability in sensor response for non-Lambertian surfaces will be explored.

PUBLICATIONS

Kimes, D.S. and J.A. Kirchner, "Modeling the Effects of Various Radiant Transfers in Mountainous Terrain on Sensor Response". Accepted for publication by IEEE Transactions on Geoscience and Remote Sensing.
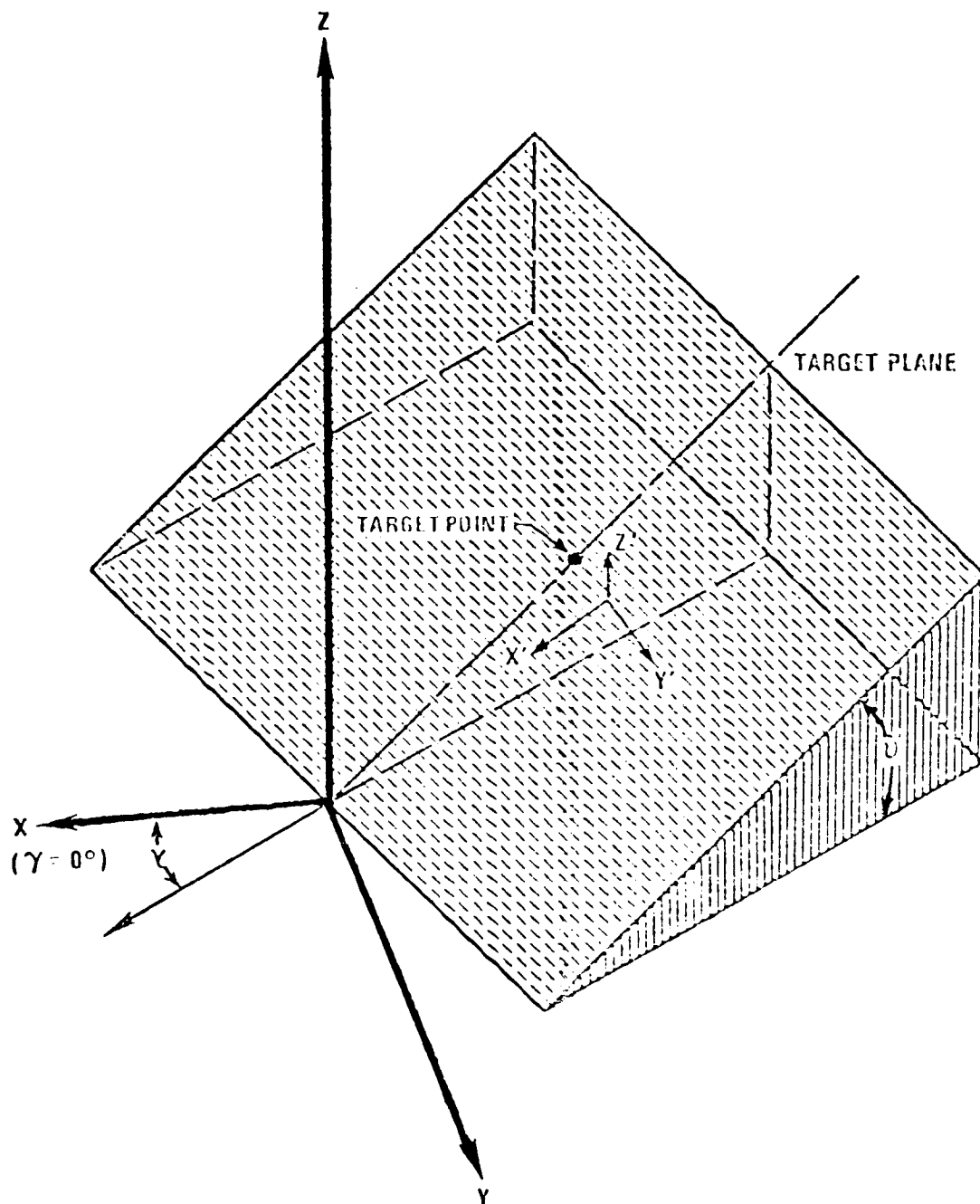
Figure 9G-1. Two coordinate systems used to account for radiant tranfers between the target point and the surrounding topography and sky. XYZ is the standard three-dimensional Cartesian coordinate system where the zenith and North directions are represented by the Z and X axes respectively. The base of the target plane lies within the XY plane and passes through the origin. X'Y'Z' is the three dimensional Cartesian coordinate system relative to the target plane where Z is normal to the target plane, X' and Y' lie within the target plane, X' is oriented toward the XY plane so that the Euclidian distance is minimal, and the origin is arbitrary relative to XYZ. Both coordinate systems are discretized into sectors. The target plane inclination ( ) and aspect ( ) are shown in the XYZ coordinate system.
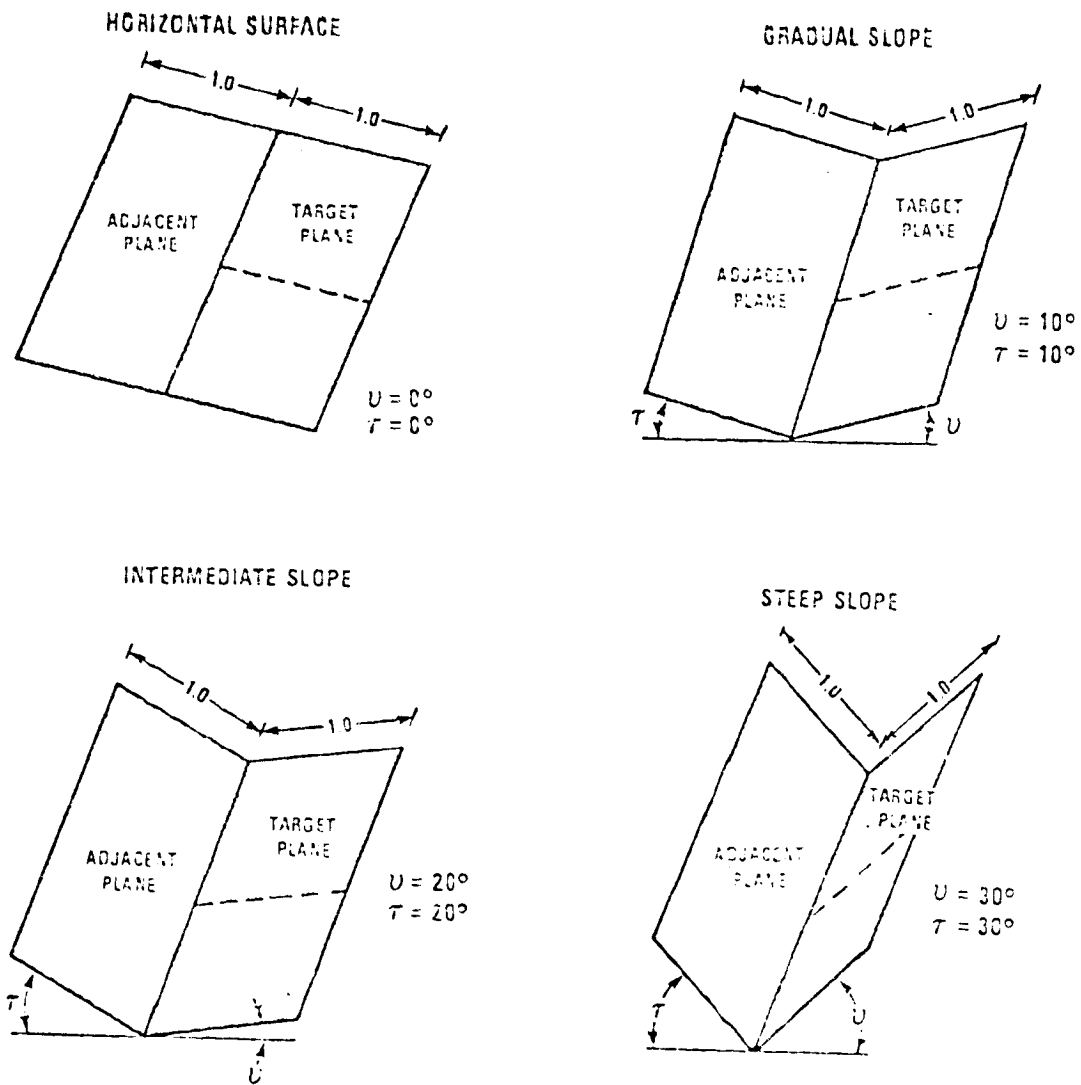
Figure 9G-2. Four theoretical valleys with their respective slope
inclinations (the target and adjacent slope inclinations
are ., and ;, respectively) and relative lengths (1.0).
In all cases the valley slope was zero degrees. The
target point of the sensor can be placed anywhere along
the dashed lines.
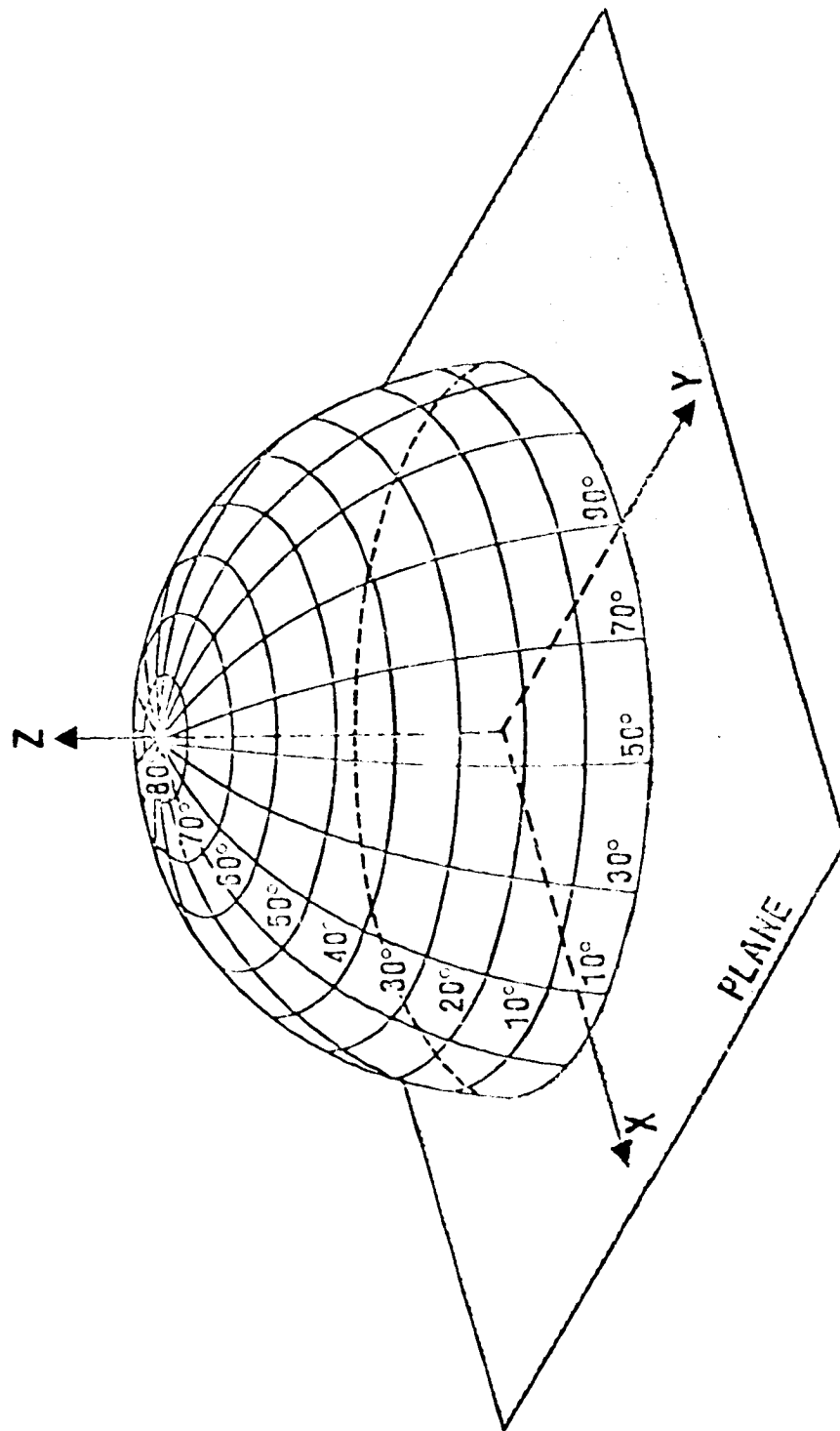
Figure 9(-3. Three dimensional view of the contiguous sectors of coordinate system XYZ defined by $\Delta\theta = 20°$ and $\Delta\phi = 10°$ increments as indicated. Normal vectors X and Y lie within the plane and vector Z is normal to the plane.

H. AN EXAMINATION OF SPECTRAL BAND RATIOING TO REDUCE THE TOPOGRAPHIC EFFECT ON REMOTELY SENSED DATA

by

B.N. Holben and C.O. Justice

OBJECTIVES

The effectiveness of ratioing red and photographic infrared spectral radiance for removing the topographic effect in remotely sensed scenes was evaluated in a ground control experiment.

BACKGROUND

The "topographic effect" is manifested on Landsat multispectral images by the visual appearance of terrain ruggedness and is caused by the differential spectral radiance due to surface slope angle and aspect variations. The topographic effect is most pronounced in areas of rugged terrain and results in a wide range of radiance values for each cover type. Some studies have stated that the topographic effect can be reduced by ratioing spectral bands and visual examination of ratioed Landsat images have confirmed this statement.

Quantitative analysis of the topographic effect on Landsat data is a complex task due to difficulties in ground location, variation in surface cover, and limited slope and aspect distributions. The authors, therefore, attempted to reduce some of the complexity by analyzing the topographic effect using radiance data collected with a nadir pointing hand-held radiometer from a uniform sand surface inclined at various combinations of slope and aspect.

Ratioing of multispectral channels in its simplest form consists of dividing the radiance value in one channel by the corresponding radiance value in a second channel to reduce environmental effects and enhance the data. The rationale behind the use of ratios is rarely discussed in the literature though the factors causing radiance variation are defined as:

$$L_\lambda = E_\lambda(\theta, t) \cdot \rho_\lambda(\theta, t) \cdot T_\lambda(\theta, t) + \beta_\lambda(\theta, t).$$

multiplicative term + additive term

where: L_λ = Spectral radiance received at the sensor

$E_\lambda(\theta, t)$ = Direct spectral irradiance impinging the target at time t

$\rho_\lambda(\theta, t)$ = Target reflectance at time t

$T_\lambda(\theta, t)$ = Atmospheric transmittance at time t

$\beta_\lambda(\theta, t)$ = Scattered radiation by the atmosphere to the sensor's field of view at time t

θ = Angular parameters

We assumed that radiance angular interdependencies had equal
multiplicative effects for all wavelengths, hence band ratioing
of multispectral data was seen as a potentially powerful tool
for reducing these multiplicative effects on the radiance received
at the sensor. The topographic effect, as a function of surface
incidence and exitance angles of direct sunlight is embodied within
the multiplicative terms and therefore may be reduced by ratioing.
Ratioing multispectral channels was demonstrated by the following
example in which the ratio of two adjacent narrow band channels is
invariant for a given target. This example assumes all additive
factors are negligible or have been subtracted out.

Consider a simple case in which the same target is sensed under
two different sun-target-sensor geometries (A and B) with all
other factors constant. The radiances (L) and, therefore, signals
for channels i and j under conditions A and B are ratioed:

$$\frac{L_i^A}{L_j^A} \quad \text{and} \quad \frac{L_i^B}{L_j^B}$$

Assuming an identical change in surface geometry occurs for each
channel, then

$$L_i^A = kL_i^B$$

$$L_j^A = kL_i^B$$

for all multiplicative factors k. Then the two ratios are identical:

$$\frac{L_i^A}{L_j^A} = \frac{kL_i^B}{kL_j^B} = \frac{L_i^B}{L_j^B}$$

A similar argument can be made for any other combination of
multiplicative factors.

RECENT ACCOMPLISHMENTS

Our approach for examining the effect of ratioing on the topographic
effect was to minimize the environmental variables which contribute
to the additive terms and control those variables which contribute
to the multiplicative terms. This was accomplished by employing a
hand-held radiometer similar to that described by Pearson et al.,
(1976), to sense a uniform sand surface. The radiometer was filtered
for the red (0.63 - 0.69 μm) and photographic infrared (0.775 - 0.825 μm)
channels. The uniforms sand surface was oriented to all combinations
of slopes, ranging from 0 to 60° in 10° increments, and aspects ranging
from 0 to 360° in 22.5° increments, for 11°, 35°, 40°, and 62° solar

elevations. All observations were taken under cloudless conditions with a nadir pointing sensor. Less than one-half hour was required to complete collection of a data set, thereby reducing errors due to the apparent movement of the sun. All surrounding surfaces were painted black to eliminate any major scattering from adjacent sources. The surface aspect was measured in degrees, clockwise from the sun's azimuth. This angle is termed the "azpect" of the surface (Holben and Justice, 1979). Red and photographic infrared radiance data pairs were collected in data subsets called azpect strings, that is slopes of $0-60^\circ$ for each azpect. An additional data set was collected to examine the effect of the scattered light additive factor on the ratioed data. The scattered light measurements were obtained by obscuring the solar disc, which is a standard method for collecting skylight data. The global radiance (i.e., the total radiance impinging on the surface) was measured consecutively with the skylight data.

The radiance data were coded and ratio values were calculated for each observation pair. Means and standard deviations were calculated for all data sets and the results presented in the following section. For the additional data set the radiance measurements for the scattered light illuminated surface were subtracted from the global radiance measurements prior to analysis.

The topographic effect can be quantified by calculating the percent change in radiance for each slope from a reference radiance measurement. For this study the reference radiance was taken to be the radiance for a horizontal surface. To show the variation in the ratio values (i.e., the remaining topographic effect), the percentage change in the ratio value from the ratio for the horizontal surface was calculated for all azpects for a moderate solar elevation data set. The mean percentage change for each slope is plotted in Figure 9H-1.The largest mean percentage change in ratio values (5%) was calculated for the 60° slope angle. Ratio values deviated less from the horizontal surface ratio for slope perpendicular to the solar azimuth and more for slopes into and away from the solar azimuth (i.e., in the principal plane). These results show that the ratio values for different surface geometries were not constant and therefore it can be concluded that the topographic effect was not totally eliminated by ratioing but has been considerably reduced (from 40% to 5%).

Examination of the ratio values associated with the four solar elevations shows that the ratio values vary between data sets. These variations in ratios are summarized in Table 9H-1, where the mean standard deviation, and range of the ratios for each data set are presented.

The smallest range in ratios (0.88-0.90) corresponded to the high solar elevation, i.e., the data set with the least topographic effect. The greatest range in ratios (0.67-0.79) corresponded to the low sun elevation data set, i.e., the greatest topographic effect. The range in ratioed values shows that the topographic effect was not totally normalized for any of the data sets.

Table 9H-1

Summary of all Ratioed Observations for Each Data Set

Solar Elevation Date	62° 8/24/78	40^{0} 9/25/78	35° 9/4/78	11° 9/26/78
Number of Aspect Strings	9	17	17	18
Mean Ratio Value	.889	.696	.880	.720
Standard Deviation of the Ratio Values	.0060	.0080	.0118	.0361
Range of Ratio Values	.88-.90	.68-.71	.86-.90	.67-.79

SIGNIFICANCE

a.   Ratioing did not completely eliminate the topographic effect within the field measured radiance data.

b.   Ratioing reduced the topographic effect in the radiance data for the range of slopes ($0-60^{\circ}$) and solar elevations ($11-62^{\circ}$) examinined by an average of 83%.

c.   The remaining topographic effect within the ratioed data was due to uncorrected additive radiance terms.

d.   Subtracting the scattered light component of the global irradiance prior to ratioing was shown to further reduce the topographic effect.

e.   The proposed explanation for the small remaining variation in the ratioed data with the diffuse light subtracted was the wavelength dependency of the scattering properties of the surface

f.   Ratioing will not be effective for reducing the topographic effect on shaded surfaces which are illuminated solely by scattered light.

From this study, certain implications can be made concerning the application of the ratioing technique to multispectral satellite data. First, ratioing of multispectral channels is perhaps the simplest technique for reducing a large proportion of the topographic effect within multispectral satellite data. Second, direct inference from these results to those that can be expected from ratioing statellite data should be made with great care. Certain of the additive terms minimized in this study will play an important part in confounding the reduction in topographic effect on satellite data. Third, complete removal of the scattered skylight component cannot be achieved when using multispectral satellite data, although subtraction of a mean diffuse value obtainable from known shaded surfaces may

lead to some improvement in reducing the ratio variations. The degree of improvement achievable by this method makes the utility of reduction of the diffuse component somewhat questionable.

Results for this study show that ratioing will be most effective for areas of extreme ruggedness exhibiting a marked topographic effect, although it will be obvious that many parts of the world have few slopes of greater than 30° and the topographic effects exhibited by the radiance data used in this study will rarely be so extreme.

FUTURE EMPHASIS

Application and evaluation of spectral band ratioing to Landsat data are being undertaken for a variety of covertypes.

REFERENCES

Holben, B.N., and C.O. Justice, 1979. "The Topographic Effect on the Spectral Response of Nadir Pointing Sensors". Photogramm. Eng. and Remote Sens. 46(9): 1191-1200.

Justice, C.O., and B.N. Holben, 1979. "Examination of Lambertian and non-Lambertian Models for Simulating the Topographic Effect on Remotely Sensed Data". NASA TM 80557, Goddard Space Flight Center, Greenbelt, Maryland 20771.

Justice, C.O., and B.N. Holben, 1980. "The Contribution of the Diffuse Light Component to the Topographic Effect on Remotely Sensed Data". NASA TM 80727. Goddard Space Flight Center, Greenbelt, MD 20771.
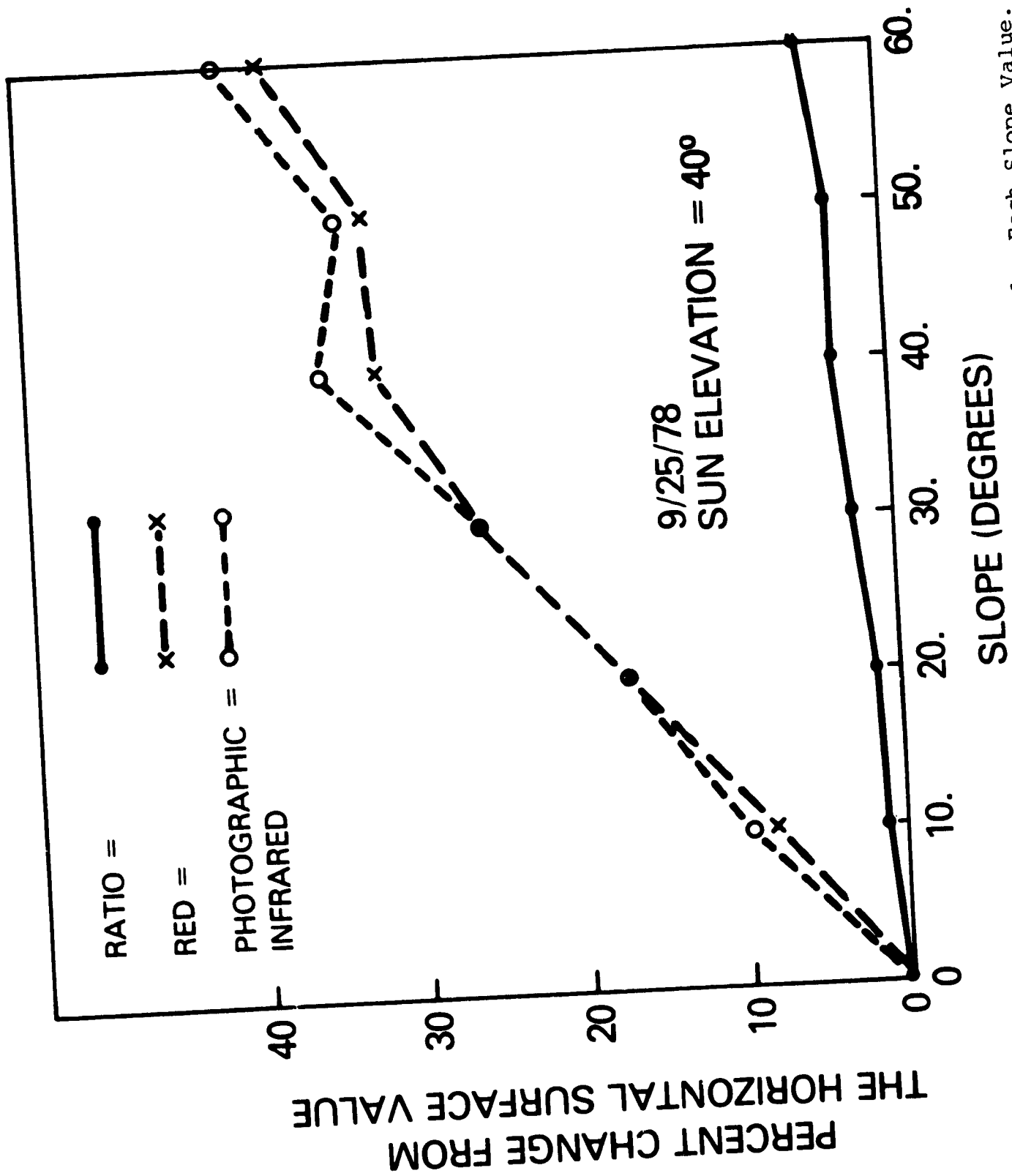
Figure 9H-1. The Mean Percent Change in Ratios Plotted for Each Slope Value.

I. THE CONTRIBUTION OF THE DIFFUSE LIGHT COMPONENT TO THE TOPOGRAPHIC EFFECT ON REMOTELY SENSED DATA

by

B.N. Holben and C.O. Justice

OBJECTIVE

The topographic effect is measured by the difference between the global radiance from inclined surfaces as a function of their orientation relative to the sensor position and light sources. The shortwave radiant energy incident on a surface is composed of direct sunlight, scattered skylight and light reflected from surrounding terrain. The latter two components are commonly known as the diffuse component. The objective of this study was to examine the contribution of the diffuse light component to the topographic effect and to assess the significance of this diffuse component with respect to two direct radiance models, to spectral band ratioing and to simulated Landsat data.

BACKGROUND

Modeling the radiation incident on surfaces has been undertaken for a number of applications. Recent developments in modeling the radiation from surfaces have been made for remote sensing applications, whereas previous insolation modeling had predominantly meterological and solar energy applications. Several of the early models assumed an isotropic distribution for diffuse light under clear sky conditions. However, several studies have shown the adverse effects of applying the isotropic diffuse sky assumption, and others show that the isotropic assumption is accurate for slopes facing perpendicualr to the principal plane and for slopes of less than 45°.

For remote sensing studies and in particular examination of the topographic effect we are concerned with radiance emanating from the surface and not solely the insolation or irradiance impinging the surface and thus we need to consider the reflection of both the direct and diffuse components. The radiance measured from a surface is a function of the reflectance properties of the surface, the atmosphere between the ground and the sensor, the sensor geometry, and the incident radiation. Examination of the diffuse radiance component in the context of remote sensing will help us to model the topographic effect more accurately and to assess its significance in models applied to satellite remotely sensed data. For non-Lambertian surfaces, the radiances will be determined by the directional scattering properties of the surface, the intensity and direction of radiation sources, and the exitance angle and therefore radiance modeling will undoubtedly be more complex than for Lambertian surfaces.

RECENT ACCOMPLISHMENTS

The approach adopted for quantifying the diffuse light component to the topographic effect was to measure diffuse and global radiances from surfaces tilted at a range of slopes and aspects. Radiances were measured consecutively from a non-Lambertain coarse sand surface and a $BaSO_4$ reference surface. The $BaSO_4$ surface approximates a Lambertian surface and has a reflectance of approximately 98%, for the wavelengths and view angles examined in this study. At steeper view angles a $BaSO_4$ surface approximates a Lambertian surface far less.

Radiance measurements were obtained for both surfaces, inclined at all combinations of slope angles, ranging from 0-60 degrees in 10° increments and aspects for the 16 compass points, in 22.5° increments. The surface aspect was measured in degrees clockwise from the sun's azimuth. The angle is termed the "azpect" of the surface (Holben and Justice, 1979). Red and photographic infrared radiance data pairs were collected in data subsets called "azpect strings," that is slopes between 0-60° in 10° increments for each azpect. The measurements, in π radiances, were taken using a two-channel nadir pointing handheld radiometer filtered for the red (0.63-0.69 µm) and photographic infrared (0.76-0.90 µm) bands. These channels are equivalent to the proposed Thematic Mapper bands 3 and 4 of Landsat-D.

The surfaces surrounding the target were painted flat black to minimize terrain scattering. Global and diffuse radiances were measured for both surfaces at each slope/azpect combination. The diffuse observations were obtained by shielding the solar disc with a small opaque panel. Three data sets were taken under clear sky conditions for solar elevations of 23°, 29°, and 39°, which correspond to the Landsat sensing time for midlatitude solar elevations occuring during late fall, winter and early spring, or for high latitude solar elevations occuring during late spring, summer and early fall respectively. Each data set was collected in less than 45 minutes and each azpect string in less than 3 minutes. The measurement apparatus was reoriented to the sun's azimuth after collection of radiance measurements for each azpect string subset, to reduce errors due to the apparent movement of the sun.

The diffuse light was found to produce a topographic effect which varied from the topographic effect for direct light. The topographic effect caused by diffuse light was found to increase slightly with solar elevation and wavelength for the channels examined. The correlations between data derived from two simple direct radiance simulation modles and the field data were not significantly affected when the diffuse component was removed from the radiances. Diffuse radiances contributed largely to the variation in ratioed data. Subtraction of the diffuse radiance prior to ratioing resulted in a 50 percent average decrease in the standard deviation of the ratioed data.

In an extreme case of radiances from a 60 percent reflective surface, assuming no atmospheric path radiance, the diffuse light topographic effect contributed a maximum range of 3 pixel values in simulated Landsat data from all aspects with slopes up to 30 degrees. Such a variation is sufficiently small compared with other variations

which are likely to occur in the data, to indicate that the diffuse component does not warrant modeling prior to cover classification analysis.

SIGNIFICANCE

The contribution of the diffuse light topographic effect to the overall topographic effect within global radiances, varies with azpect; the diffuse radiances generally increase with slope for azpects facing into sun and decrease with slope for azpects perpendicular and away from sun. These results indicate than an isotropic sky assumption cannot be used to adequately describe the diffuse component.

Assessment of the significance of the diffuse component was undertaken first by examining the effect in two direct radiance models. Only slight improvements were found in the correlation between the radiance and the theoretical data derived using the Lambertian Model, whereas an average improvement of 26 percent in the correlation coefficient was calculated for data derived using the non-Lambertian model when the diffuse component was subtracted.

The significance of the diffuse component to band ratioing was also assessed. Subtraction of the diffuse component led to a 50 percent average decrease in the standard deviation of the ratios associated with the uniform surface, over the range of slopes and azpects examined. The greatest reduction in the standard deviations was found for slopes perpendicualr to solar azimuth.

The Landsat simulation study showed that for clear sky conditions over a range of solar elevations associated with typical mid-latitude Landsat passes, that the diffuse light radiances in cases of extreme reflectance and slope variation would constitute only a maximum 3 pixel variation in the Landsat measured global radiances. In this event, it is unlikely that such a maximum variation could be taken into consideration to improve cover classification accuracies, by reducing the diffuse light topographic effect. It should be understood that areas of shadow will have 100 percent diffuse radiance and the higher Landsat quantization values associated with these shadowed areas are essentially due to atmospheric path radiance. The effect of varying atmospheric path radiance between the target and sensor were not examined in this study.

Diffuse light causes a topographic effect on remotely sensed data which will vary in significance with the application in question. The ground based study showed that the diffuse component caused a detectable variation in the ratioed spectral data which potentially could be modeled and hence the effect eliminated from the data. For Landsat studies a maximum possible variation of 3 pixel values for the conditions specified does not at present warrant further detailed modeling and in most cases the variation due to the diffuse component will be substantially less.

FUTURE EMPHASIS

Because anisotropic sky diffuse radiance had a rather small effect on simulated Landsat pixel values, no further efforts are planned for evaluating this effect. Further research on the effects of terrain scattering on measured radiance is being conducted.

REFERENCES

Holben, B.N. 1975. "The Development and Sensitivity Analysis of a Model for Estimating Insolation Climate in Mountainous Topography." Masters Thesis, Colorado State University, Fort Collins, 159 pp.

Holben, B.N. and C.O. Justice 1979. "The Topographic Effect on The Spectral Response from Nadir Pointing Sensors." Photogramm. Eng. and Remote Sens. 46(9): 1191-1200.

Holben, B.N. and C.O. Justice, 1980. "An Examination of Spectral Band Ratioing to Reduce the Topographic Effect on Remotely Sensed Data." NASA/GSFC Tech. Mem. 80604, p. 28. (In Press International J. Remote Sens.)

Justice, C.O. and B.N. Holben, 1979. "Examination of Lambertian and non-Lambertian Models for Simulating the Topographic Effect on Remotely Sensed Data." NASA/GSFC Tech. Mem. 80557

J. ## APPLICATION OF DIGITAL TERRAIN DATA TO QUANTIFY AND REDUCE

THE TOPOGRAPHIC EFFECT ON LANDSAT DATA

by

C.O. Justice, B.N. Holben and S.W. Wharton

OBJECTIVES

The objective of this study was to quantify and reduce the topographic effect found in Landsat data for an area in central Pennsylvania.

BACKGROUND

The topographic effect is defined as the variation in radiances from inclines surfaces compared to radiance from a horizontal surface as a function of the orientation of the surfaces relative to the light source and sensor position. On Landsat images of rugged terrain, this effect is manifested by the visual impression of relief. The authors measured the topographic effect on remotely sensed data and showed the effect to be most extreme at low solar elevations and greatest for slopes in the principal plane of the sun. They also showed by a Landsat simulation study that the topographic effect can produce a considerable variation in radiances associated with a given cover type and may lead to poor cover-classification results. It has been demonstrated that reflectances vary as a function of slope and aspect and that such terrain variations complicate the task of discriminating woodland categories with remotely sensed data.

Two types of data were integrated to provide the data base used in this study; namely, Landsat multispectral scanner (MSS) data and digital terrain data. The Landsat data chosen for this study were for July 19, 1976, with a solar elevation of 55°. The digital terrain data used in this study were the 30-m Digital Elevation Model (DEM) data obtained from the U.S. Geological Survey (USGS) Digital Applications Team, Reston, Virginia. Four techniques for reducing the topographic effect were examined in this study, namely, spectral-band ratioing and application of a Lambertian model, a modified Lambertian model, and a non-Lambertian model.

RECENT ACCOMPLISHMENTS

This project was subdivided into four major areas. The first area describes the measurement of the topographic effect for the Landsat data taken at a 55° solar elevation by examination of randomly selected test sites. Second, a detailed analysis of the topographic effect for six sample transects was made across the mountain ridge. Third, the variability of the Landsat radiance data for the six transects was examined after the application of spectral-band ratioing and the Lambertian and non-Lambertian normalization models to reduce the topographic effect. The final emphasis includes application of the optimum normalization procedure to the Landsat data and comparison of the corrected and the uncorrected radiance data.

Field checking of the randomly selected test sites before the analysis had shown no observable differences in the woodland cover for the three locations. The differences in the mean pixel values were therefore associated primarily with the topographic variation. The

highest mean pixel values associated with the oak woodland cover
were in MSS 6 for the southeast aspect. However, the highest
individual radiances were for MSS 7, which was quantized to 64
levels, half the quantization level of the other three channels.
The northwest-aspect moderate-slope radiances for MSS 6 and MSS 7
were higher than the steep-slope radiances for the same aspect.
Three distinct ranges of mean pixel values were obtained for the
three slope-aspect classes for MSS 6 and 7. For MSS 6 a difference
of 17 pixel values separated the mean values for the sites associated
with the southeast and northwest aspects. Such a large range indicates
that selection of training sites for cover classification from one
slope-aspect location may not adequately describe the radiances
from the same cover from other locations. The degree to which this
may affect the classification results depends largely on the location
and distribution of other cover-class radiances within the classification-
feature space.

Six sample transects of Landsat data across the mountain ridge were
taken to examine the topographic effect in detail and to assess the
statistical relationship between the Landsat radiances and the
data derived with the proposed models. The statistical relationship
between the radiances and the data derived from the models was
assessed for each transect with Pearon's product-mounted correlation
coefficient. The correlation coefficient gives an indication of the
strength of the linear relationship between two variables. Correlation
coefficients (r) were insignificant at the 0.05 level for MSS 4 and 5
for all three models. Strong positive relationships ($r > 0.84$) were
found for data derived with the Lambertian and non-Lambertian models,
and a strong negative relationship was found for data derived with the
modified Lambertian model for all transects. There was no substantial
difference in the size of the r values among the three models.

Coefficients of variation (CV) indicated a greater variation in the MSS
7/5 ratio that in the MSS 6/5 ratio, because of the higher
variation in MSS 7. The CVs for MSS 6/5 and 7/5 ratioes decreased
slightly from the CVs for the raw MSS data for three out of six transects.
The poor reduction in the topographic effect by the MSS 6/5 and 7/5
ratios is due to the negligible variation in MSS 5. The relatively
constant radiance in MSS 4 and MSS 5 is associated with the high
absorption of the green leaves of the deciduous woodland and means
that ratioing is effectively dividing MSS 7 and MSS 6 by a constant
value.

Application of the Lambertian model to the data to reduce the topograhic
effect (i.e., division of each pixel by cos i) led to a large increase
in the CV for each transect over the variation for the raw data. This
increase in the CVs is presumably due to the inapplicability of the
Lambertian assumption for the woodland cover type in question. A
modified Lambertian model was a considerable improvement over the
Lambertian model in reducing the topographic effect, but for all
transects, it increased the topography-induced variation above that
found in the raw Landsat data. The CVs for the non-Lambertian model
were markedly smaller than the CVs for raw MSS 6 and 7 data. The
maximum reduction in the CVs was from 10.5 to 3.9 for MSS 6 and from
15.0 to 4.0 for MSS 7. The non-Lambertian model was shown to be the
best correction procedure for reducing the topographic effect. This
model reduced the difference between the mean values of the test sites

(slopes) by approximately 86% for MSS 6 and 7.

SIGNIFICANCE

1. Spectral-band ratioing (MSS 7/5, MSS 6/5) slightly decreased the variation of the Landsat data for 50 per cent of the transects. Because of the small variation in MSS 5, ratioing could not eliminate the direct-light topographic effect, as the denominator of the ratio was virtually constant. This reasoning also may explain the poor results obtained by with band-ratioing techniques.

2. When applied to the Landsat data, the Lambertian model increased the topographic effect. This degradation of the radiance is due to the inapplicability fo the Lambertian assumption to model the bidirectional reflectance characteristics of the woodland surface.

3. The modified Lambertian model developed, decreased the variation produced by applying the Lambertian model but gave even higher variances than those found in the raw Landsat data.

4. The non-Lambertian model developed, markedly decreased (~86 per cent) the variation of the Landsat data, and, therefore, reduced the topographic effect.

5. Although the non-Lambertian model did not completely eliminate the topographic effect, it considerably reduced the variation. The difference between the mean pixel values associated with the two extreme slope-aspect sites was reduced from about 86 per cent in MSS 6 and MSS 7.

In conclusions, this study has demonstrated that high-quality digital terrain data such as the USGS DEM data can be used via modelling to enhance the utility of multispectral satellite data. Digital terrain data can be used to develop and test improved radiative transfer models, which, in turn, may lead to improved cover classification of Landsat data.

FUTURE EMPHASIS

Further development of the existing model is required for application of the technique to more complex surface-cover conditions.

REFERENCES

Cicone, R.C., W.A. Malila, and E.P. Crist, 1977. "Investigation of Techniques for Inventorying Forested Regions". Final Report: Vol. II Forestry information system requirements and joint use of remotely sensed and ancillary data. NASA-CR-ERIM 122700-35-F2.

Holben, B.N. and C.O. Justice, 1979. "The Topographic Effect on the Spectral Response for Nadir Pointing Sensors". Photogramm. Eng. and Remote Sens. 46(9): 1191-1200.

Holben, B.N. and C.O. Justice, 1980. "An Examination of Spectral Band Ratioing to Reduce the Topographic Effect on Remotely Sensed Data". NASA TM 80640, Goddard Space Flight Center, Greenbelt, MD.

Justice, C.O. 1978. Proc. Am. Soc. Photogramm. Fall Mtg., Albuquerque, New Mexico, pp. 303-328.

Justice, C.O. and B.N. Holben, 1979. "Examination of Lambertian and non-Lambertian Models for Simulating the Topographic Effect on Remotely Sensed Data". NASA TM 80557, Goddard Space Flight Center, Greenbelt, MD.

Justice, C.O. and B.N. Holben, 1980. "The Contribution of the Diffuse Light Component to the Topographic Effect on Remotely Sensed Data". NASa TM 85290, Goddard Space Flight Center, Greenbelt, MD.

Smith J.A., T.L. Lin and K.J. Ranson, 1980. "The Lambertian Assumption and Landsat Data". Photogramm. Engng. Remote Sensing (in the press).

K. **A COMPARISON OF THE REFLECTIVITY OF TFE - A WASHABLE**

SURFACE - WITH THAT OF BaSO4

by

J.E. Schutt and B.N. Holben

OBJECTIVES

To check the utility of the hydrophobic and soiling resistance
properties of TFE in the preservation of its optical properties,
a series of optical measurements in conjunction with a soiling-
cleansing cycle were carried out.

BACKGROUND

Numerous white diffusely reflecting materials and coating compositions
have been developed and applied in novel ways for use in radiometric
calibration procedures and in bidirectional reflectance measurements
as, for example, are carried out in conjunction with remote sensing
studies. Some of the more studied substances are magnesium oxide,
both smoked and pressed forms, pressed magnesium carbonate, barium
sulphate either pressed or bound together with polyvinyl alcohol
(PVA) or potassium sulphate, sodium chloride, sulfur (highly reflective
in the IR) and alpha aluminum oxide either singly or admixed with
magnesium oxide and bound with an alkali-metal silicate. Of these
compositions, barium sulphate weakly tethered with a water soluble
form of polyvinyl alcohol has received widest acceptance. For other
than laboratory applications, however, a standard reflective diffuser
is required whose infrared reflectance is not sensitive to changes in
humidity, and whose initial reflectance can be recovered once is has
been soiled by rinsing with a spray of demineralized water. We have
attempted to formulate Halon into a coating composition for application
by spraying rather than by tamping into a lubricant matrix. Specifically,
we chose to diperse the TFE in a methyl acetate concentrate of vinyl
acetate-alcohol copolymer, which was diluted for heavy loading with
TFE using ethyl alcohol, a low residue vehicle. After application,
the ratio of binder solids to TFE was about 1 to 111.

RECENT ACCOMPLISHMENTS

The TFE coating, for which the formulation is disclosed above, was
evaluated optically under field and laboratory conditions in three
states: as applied, after being rolled to reduce porosity, and after
being covered with earth, shaken sufficiently to force particles in
to a portion of the existing pores, and sprayed vigorously with
demineralized water to flush debris from the pores. After trail
applications of the coating a thickness of 0.48 to 0.50 mm was
decided upon in order to optimize physical properties. The coating was
applied over aluminum surfaces primed with aluminum oxide in potassium

silicate, Dow-Corning Z-6075 primer and an unprimed surface. These surface preparations were for the purpose of comparing reflectances, since the TFE is transparent and recommended for use at 6 mm and promoting adhesion. For comparison purposes laboratory measurements were carried out for $BaSO_4$. PVA, while under field conditions measurements on $BaSO_4$. PVA were bracketed by measurements on TFE.

Absolute reflectance measurements were made in the laboratory from 0.36 to 2.5 μm using a Beckman DK-2A spectrophotometer outfitted with a Gier-Dunkle integrating sphere. Figure 9K-1 compares the reflectances of sprayed TFE with itself after being covered with earth and washed, and with $BaSO_4$. PVA. Table 9K-1 lists reflectance values for all treatments and surface preparations at the central wavelengths of each of the six Landsat-D thematic mapper bands: 0.45-0.50 μm (TM1), 0.52-0.60 μm (TM2), 0.63-0.69 μm (TM3), 0.76-0.90 μm (TM4), 1.55-1.75 μm (TM5), and 2.08-2.35 μm (TM6). $BaSO_4$. PVA data are included for comparison purposes. Note that the aluminum oxide primer gives the maximum reflectance indicating that the coating is not totally opaque; rolling has little effect; rolling and washing reduces reflectance by about 0.5 percent.

Comparing the soiled and washed surfaces of the rolled and unrolled samples, it appears that the unrolled surface is more resistant to soiling and is cleansed more readily; $BaSO_4$. PVA has a higher reflectance than our TFE preparation by about 2 percent except at 2.21 μm.

Field data collection was carried out using a three channel radiometer filtered to display irradiances from thematic bands 3, 4 and 5 (listed above). The radiometer, adapted for mounting either an HN22 or an HR Polaroid polarizer, was mounted in a nadir looking position on a small gantry such that it viewed a tiltable support from about 1 m on which was mounted one of the reference panels. The radiometer support apparatus was rotated with the sun such that the radiometer viewed the sloping reference surfaces only in the principal plane of the sun, i.e., the plane of maximum observable radiance range for a nadir pointing sensor.

The reference panel was tilted from horizontal at a 50° slope in 10° increments. At each increment, a polarizing filter was rotated clockwise through the sequence of angles 0°, 45°, 90°, 135°. The transmission axis was set at 0°. Spectral data were taken at each slope/polarization angle combination. Approximately three minutes were required to complete a data set. To account for the slight apparent movement of the sun in comparing spectral radiance of TFE to $BaSO_4$, a TFE-$BaSO_4$-TFE sequence was followed requiring approximately 9-10 minutes to complete. All data were taken under cloudless and relatively haze-free conditions on July 30, 1980 near Beltsville, Maryland.

The reflective characteristics of the surfaces were evaluated
by comparing the standard deviations (s) and coefficients of
variation (CV) of the means of the first Stokes parameter normalized
for incidence angle. The average value of the two TFE data sets
were calculated for comparison with $BaSO_4$ for each treatment
(Table 9K-2). The differences in the coefficient of variation of
the TFE relative to the $BaSO_4$ (ΔCV) was calculated (Table 9K-2).
Examining any of the three channels showed that the ΔCV was no
greater than 1.69 percent regardless of treatment. Inspection
of individual channels between treatments indicated no trends in
the ΔCV. The evidence strongly suggests that a TFE reference panel
may be periodically washed without significantly altering is radiance
values when compared to the $BaSO_4$. PVA monitor data.

The reflective properties were statistically evaluated by examining
the means and standard deviations of the polarizations at the
95 percent confidence limit (Table 9K-3). As the mean of the polarization
component approaches zero, the reference surface becomes more
diffuse. Inspection of the data by treatment reveals that the
polarized component is less than 1.6 percent in the case of TFE
and less than 1.7 percent for $BaSO_4$. Applying confidence limits
showed that 95 percent of all TFE radiometric observations would
have a polarization component of less than 2.7 percent for all
treatments, less than the 3.6 percent predicted for $BaSO_4$ paint
(Table 9K-3). These same data showed there to be less than a 1 percent
difference in the polarization component for 95 percent of the
observations between TFE treatments. There was no evidence indicating
that the polarization component of TFE was any different from
$BaSO_4$ or that any TFE treatment had polarization characteristics
different from the others under field conditions.

SIGNIFICANCE

In general it was apparent from these data that the reflective properties
of TFE were comparable to $BaSO_4$ and that no distinction could be made
between the optical properties of TFE sprayed, TFE lightly rolled
or TFE washed under field conditions. Laboratory analysis indicated
that $BaSO_4$. PVA was approximately 2% more reflective and that there
was no advantage to lightly rolling TFE.

This study indicates that TFE has recoverable reflective properties
after soiling through washing with demineralized water. Unlike
$BaSO_4$. PVA, TFE may be used as a reference standard in remote
sensing applications after repeated soiling - washing cycles.

FUTURE EMPHASIS

Evaluation of the stability of $BaSO_4$. PVA vs TFE are being
conducted under various irradiational levels over time. Additionally
the Lambertian characteristics of each must be compared.

Table 9K-1. Reflectance values at thematic mapper wavelengths for TFE, treated samples, of TFE and $BaSO_4$. PVA.

Sample-Treatment*	0.485μm	0.560μm	0.660μm	0.830μm	1.55μm	2.21μm
TFE-1	95.6	95.7	95.6	94.0	91.9	88.9
TFE-2	93.9	94.2	93.9	92.2	90.6	88.4
TFE-3	94.1	94.3	94.2	92.5	91.3	89.2
TFE-1R	95.8	95.3	95.5	93.8	91.1	87.9
TFE-2R	94.6	94.1	94.1	92.5	90.7	88.7
TFE-3R	95.0	94.6	94.5	93.1	91.4	89.2
TFE-1RW	94.6	94.8	94.9	93.8	91.0	87.9
TFE-2RW	94.1	93.9	94.2	92.9	91.3	89.1
TFE-3RW	94.7	94.0	94.2	92.4	90.6	88.7
TFE-1	95.9	95.7	95.8	94.1	91.7	88.6
TFE-2	94.5	93.5	94.1	92.5	90.6	88.4
TFE-3	94.5	94.0	94.2	92.7	91.1	89.1
TFE-1W	95.6	95.4	95.4	94.0	91.2	87.8
TFE-2W	94.8	94.1	94.0	92.6	90.7	88.8
TFE-3W	95.2	94.9	94.7	93.0	91.4	89.4
$BaSO_4$-1	97.5	97.3	97.5	96.2	93.6	87.8
$BaSO_4$-A	97.0	96.9	97.1	95.7	92.9	87.7

*Al_2O_3 and potasium silicate = 1, Z-6075 primer = 2, untreated = 3, R = rolled, W = soiled and washed, A = acrylic primer

C - 4

Table 9K-2. Means ($\bar{X}$), standard deviations (s), coefficient of variation (CV) and differences between the $BaSO_4$ and TFE coefficient of variation (ΔCV) calculated from the first Stokes parameter for each TFE treatment.

	TFE-1*				$BaSO_4$-1		
	$\bar{X}$	s	CV	ΔCV	$\bar{X}$	s	CV
TM3	35.9	2.14	5.96	-1.69	37.6	2.50	6.65
TM4	93.2	8.07	8.66	+1.54	98.7	7.03	7.12
TM5	10.8	1.16	10.74	+0.03	11.2	1.20	10.71

	TFE-1R				$BaSO_4$-1		
	$\bar{X}$	s	CV	ΔCV	$\bar{X}$	s	CV
TM3	36.9	4.52	12.24	-1.23	38.3	5.16	13.47
TM4	96.6	4.80	4.96	-0.67	101.9	5.74	5.63
TM5	9.58	0.52	5.42	-0.18	10.0	0.56	5.60

	TFE-1RW				$BaSO_4$-1		
	$\bar{X}$	s	CV	ΔCV	$\bar{X}$	s	CV
TM3	38.2	3.08	8.06	+1.38	40.1	2.68	6.68
TM4	95.5	8.59	8.99	+1.61	102.1	7.54	7.38
TM5	11.0	1.22	11.09	-0.15	11.3	1.27	11.24

* 1 = Al_2O_3 and potassium silicate primer

R = Rolled

W = Soiled and Washed

Table 9K-3 Means ($\bar{X}$), standard deviation (s) and 95 percent confidence limits calculated from polarization data for $BaSO_4$ and treated TFE surfaces.

	TFE-1*			$BaSO_4$-1		
	$\bar{X}$	s	95%	$\bar{X}$	s	95%
TM3	0.0145	0.0061	2.67	0.0174	0.0094	3.62
TM4	0.0108	0.0052	2.12	0.0121	0.0055	2.31
TM5	0.0134	0.0049	2.32	0.0122	0.0049	2.20

	TFE-1R			$BaSO_4$-1		
	$\bar{X}$	s	95%	$\bar{X}$	s	95%
TM3	0.0125	0.0053	2.31	0.0114	0.0042	1.98
TM4	0.0064	0.0044	1.52	0.0041	0.0031	1.03
TM5	0.0112	0.0040	1.92	0.0060	0.0041	1.42

	TFE-1W			$BaSO_4$-1		
	$\bar{X}$	s	95%	$\bar{X}$	s	95%
TM3	0.0159	0.0053	2.62	0.0151	0.0048	2.47
TM4	0.0066	0.0028	1.22	0.0068	0.0019	1.06
TM5	0.0137	0.0030	1.97	0.0168	0.0036	2.40

*1 = Al_2O_3 and Potassium silicate primer

R = Rolled

W = Soiled and Washed
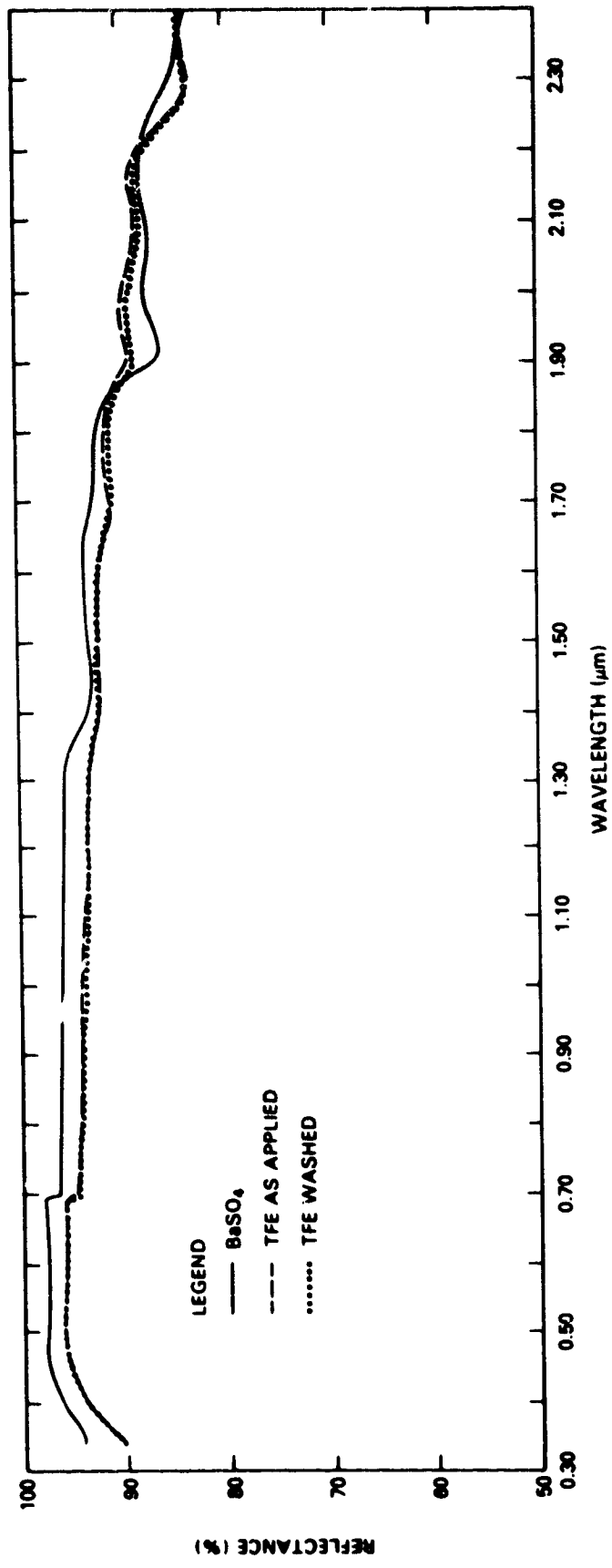
Figure 9K-1. Reflectance vs Wavelength for three reference surfaces.

LEGEND
——— BaSO₄
— — — TFE AS APPLIED
······ TFE WASHED

WAVELENGTH (μm)

REFLECTANCE (%)

L. THE GSFC MARK-II THREE BAND HAND-HELD RADIOMETER PROJECT

by

C.J. Tucker and W.H. Jones

OBJECTIVES

To develop and produce a simple, self-contained, portable, hand-held radiometer designed for field use.

BACKGROUND

The applications of remotely sensed data for environmental monitoring have increased substantially since the launch of Landsat-1 (formerly (ERTS-1) in 1972. The uses of this new technology have extended into many disciplines where the unique features of satellite remote sensing can be employed to address various resource questions. The majority of remote sensing research to date has utilized Landsat data. Several workers have come to realize that ground-based in situ remote sensing studies were needed to better understand the basic relationships between natural materials and reflectance or radiance as a function of wavelength. This realization resulted from the apparent fact that Landsat MSS imagery is not an optimum method of conducting more basic remote sensing research of natural materials. The difficulties of concurrently sampling ground experimental areas of ~0.4 ha, quantifying atmospheric variability, compensating for sun angle effects, accounting for instrument responses, etc., and the interaction(s) between these sources of experimental variation are considerable.

Ground-based spectrometers have been utilized by several research groups in an attempt to collect in situ spectral reflectance data. These efforts have largely been successful and, at the same time, have demonstrated the limitations of spectrometers. The limitations include the cumbersomeness of spectrometers, the cost of maintaining and operating of these devices, and the lack of mobility, among other factors. It should be clearly understood that spectrometers do provide basic information about natural materials and their resulting reflectances as a function of wavelength. This is not only important per se but has provided the experimental basis for the development of hand-held radiometers.

Hand-held radiometers, as used in this report, refers to a discrete waveband device which can be hand carried and operated. These instruments are spectraly configured by placing a filter in the pathlength of the detector(s) in question. For example, the three-band device described in this report has 2 silicon detectors (sensitivity range ~0.4 - 1.0 µm) and one lead sulfide detector (sensitivity range ~1.0 - 3.0 µm). By placing interference filters of 0.63 - 0.69 µm and 0.76 - 0.90 µm in the pathlength of the silicon channels and a 1.55 - 1.75 µm filter in the pathlength of the lead sulfide channel, the resulting device is configured spectrally to thematic mapper band TM3, TM4 and TM5. The three band device described in this report was intended primarily to support Landsat-D's thematic mapper by in situ data collection.

RECENT ACCOMPLISHMENTS

A self-contained, portable, hand-held radiometer designed for field useage has been constructed and preliminarily tested. The device, consisting of a hand-held probe containing three sensors and a strap supported electronics module, weighs 4½ kilograms, is powered by flashlight and transistor radio batteries, utilizes two silicon and one lead sulfide detectors, has three liquid crystal displays, sample and hold radiometric sampling, and the spectral configuration of the device corresponds to Landsat-D's thematic mapper bands TM3 (0.63 - 0.69 µm), TM4 (0.76 - 0.90 µm) and TM5 (1.55 - 1.75 µm). The device was designed to support thematic mapper ground-truth data collection efforts and to facilitate in situ ground-based remote sensing studies of natural materials. Prototype instruments have been extensively tested under laboratory and field conditions with excellent resutls obtained.

Forty-five instruments have been manufactured as of June, 1980 and are in field operation throughout the United States and elsewhere in Senegal, Thailand, France, and South Korea. Users in the U.S. include the USDA, various universities, and a sugar growers cooperative in Hawaii.

In addition, four instruments have been modified slightly and are in use in various museums to study light-caused deterioration of valuable museum objects. Museums involved include the North Carolina Museum of Art; the Smithsonian Institution, Washington, DC; Winterthur Museum, Wilminton, Delaware; and Carneggie-Mellon Institute, Pittsburg, Pennsylvania.

SIGNIFICANCE

A relatively inexpensive instrument designed for extended field use by agronomists, ecologists, and other ground-based remote sensing researchers has been built, tested, and placed in the hands of researcher workers. Modifications to the instrument have resulted in a companion museum testing program as well. The significance of this project is the availability of a $5,000 instrument which has the capabilities of instruments costing several times this amount.

FUTURE EMPHASIS

A report describing the instrument has been accepted for publication by Science. The production (and sales) of the instrument has been transferred to a small business concern in Beltsville, Maryland.

REFERENCES AND PUBLICATIONS

Tucker, C.J., W.H. Jones, W.A. Kley, and F.J. Sundstrom. 1981. "The GSFC Mark-II Three-Band Hand-Held Radiometer". GSFC TM-80641, 29 pp.

Tucker, C.J., W.H. Jones, W.A. Kley, and G.J. Sundstrom. 1980. "A 3-Band Hand-Held Radiometer for Field Use". Science (in press).

M. AN OFF-NADIR VIEWING FIELD INSTRUMENT

by

D.W. Deering

OBJECTIVES

The purpose of the instrument development activity reported herein
is to build a highly mobile field instrument that will enable very rapid
radiance measurements in selected spectral channels for numerous
viewing angles.

BACKGROUND

Sensor viewing geometry can have a significant affect on the resultant
measurements of spectral radiance of a given scene. The complexity
of the effect is compounded by the addition of different solar
positions and scene element orientations. These complexities,
coupled with atmospheric effects, make the prediction of off-nadir
viewing effects extremely difficult. Intensive data collection and
scene modeling research are needed to understand and predict these
effects.

Sensor view angle effects on current earth resources satellites
are largely ignored due to the relatively small scan angles. For
example, on the Landsats the scan angle is only $\pm 5.5^{\circ}$. On the
Landsat-D Thematic Mapper the scan angle will be increased to $\pm 7.5^{\circ}$.
However, even the $\pm 5.5^{\circ}$ scan angle of Landsats 1, 2 and 3 gives rise
to a 10% across image variation in MSS4 on March 22 and a 25% change in
total radiance on June 22 at $30^{\circ}-40^{\circ}$ N latitude. For Landsat-D
the June 22 radiance variation across the image will be increased
to 35% (Barker, et al., 1976). Atmospheric path radiance changes
in off-nadir viewing are sufficient to cause substantial degradation
of recognition results unless corrections are applied (Turner et al.,
1974).

The differential bidirectional reflectance response due to viewing
geometry effects for plant canopies has been well documented and
summarized by Smith and Ranson (1979). Most of the bidirectional
reflectance data, however, are too limited or suffer from insufficinet
controls or lack of supporting data to make them useful for predictive
modeling and scene synthesis. The capability for obtaining adequate
spectral measurements of scenes for obtaining the bidirectional
reflectance distribution function (BRDF), which is necessary for
modeling and scene simulations, is severely limited by instrumentation.
Consequently, in order to enable the acquisition of scene radiance
data suitable for determining the BRDF for a large number of vegetation
types under a wide variety of conditions, the AIRMASS (Anisotropic
Irradiance and Radiance Measurement Apparatus for Spectral Sampling)
instrument is being developed.

RECENT ACCOMPLISHMENTS

In order to obtain adequate bidirectional reflectance field data for scene modeling it is necessary to obtain radiance measurements at numerous, accurately positioned nadir and off-nadir angles and rapidly enough to prevent any changes in the sky or target during the sampling period. It is desirable also to sample the incident radiation at various angles and to sample at several important wavelength bands simultaneously.

Portability of the instrumentation is an important consideration because it must be capable of being taken into large fields (or plant communities) and easily manageable within a field in order to obtain a statistically adequate number of samples to sort out the true bidirectinal effects. It is also desirable that it be portable enough to travel to different regions for sampling different types of vegetation and even for mounting on airborne platforms for more synoptic scene sampling. Thus, a compact and completely self-contained instrument is desirable. These were among the considerations of GSFC Code 923 Scientists and Code 944 Engineers for designing the AIRMASS instrument.

The AIRMASS instrument is basically a 3-channel, rotating head radiometer consisting of three primary units, the sensor head, data recording unit, and power pack (Figure 9M-1).

The sensor head is composed of a motor-driven two-axis gimbel on which three detector units are mounted. The three detectors include two silicon and one germanium solid state detectors, which are initially configured to correspond with Thematic Mapper spectral bands 3, 4 and 5 (.63-.69 um, .76-.90 um, and 1.55-1.75 um), respectively. The detector cones confine their individual fields of view to 15°. The two-axis, two-motor rotation of the head enables a near-complete sampling of the entire sky/ground sphere. There is a 15° exclusion area toward the mounting device due to mechanical limitations.

The data recording unit is a small suitcase-sized box (1 ft. x 1 ft. x .75 ft.) containing the tape recorder, control panel and electronic circuits.

The scan system is designed such that sampling can be done in a continuous helical pattern or in circular, stepped increments. The data is recorded serially in digital form. There is also a nadir "calibrate" hold position. In the helical sampling mode a complete data set can be taken in only 22 seconds followed by a one minute data dump to the tape recorder from the buffer. A minimum of twenty data sets can be stored on one tape.

The power supply unit is carried separately and is a 12 volt sealed lead-acid battery with a 25 ampere-hour capacity. The battery is approximately "six-pack" sized, and could be mounted to the data recording unit for ease of transport. A smaller battery pack is being

evaluated which could be built into the data box.

The sensor head can be mounted at the end of a tripod mounted boom (Figure 9M-1) or can be supported at the end of a truck boom, such as a "cherry picker". Because of its portability and self contained power supply it would be amenable to mounting on various other platforms including helicopter, airplane, etc.

The sensor head weighs 7 lbs. The data recording unit weighs approximately 10-13 lbs. The tripod with extension pole and mount weighs about 30 lbs. The large detached battery pack weighs 23 lbs.

The AIRMASS instrument designing has been completed and component parts are currently being fabricated. It is anticipated that the instrument will be assembled in January and February 1981 and ready for operational field use by late March 1981.

SIGNIFICANCE

The AIRMASS instrument will enable rapid off-nadir sky and scene field data acquisition. This will result in significant improvement in the quantity and quality of bidirectional reflectance data, which will increase scene understanding and allow more reliable scene modeling for predicting off-nadir viewing effects.

REFERENCES

Barker, J.L. et al., 1976. "Analysis of the Effects of Equatorial Crossing Times on Earth Resources Applications for Landsat Follow-On", NASA Report, April 21, 1976 (unnumbered and unpublished).

Smith, J.A. and K.J. Ranson. 1979. "MRS Literature Study of Bidirectional Reflectance and Atmospheric Corrections, II: Bidirectional Reflectance Studies Literature Review". Prepared for NASA/GSFC, 250 p.

Turner, R.E., W.A. Malila, R.J. Nalepka, and F.J. Thompson. 1974. "Influence of the Atmosphere on Remotely Sensed Data". SPIE Proceeding 51: 101-114.
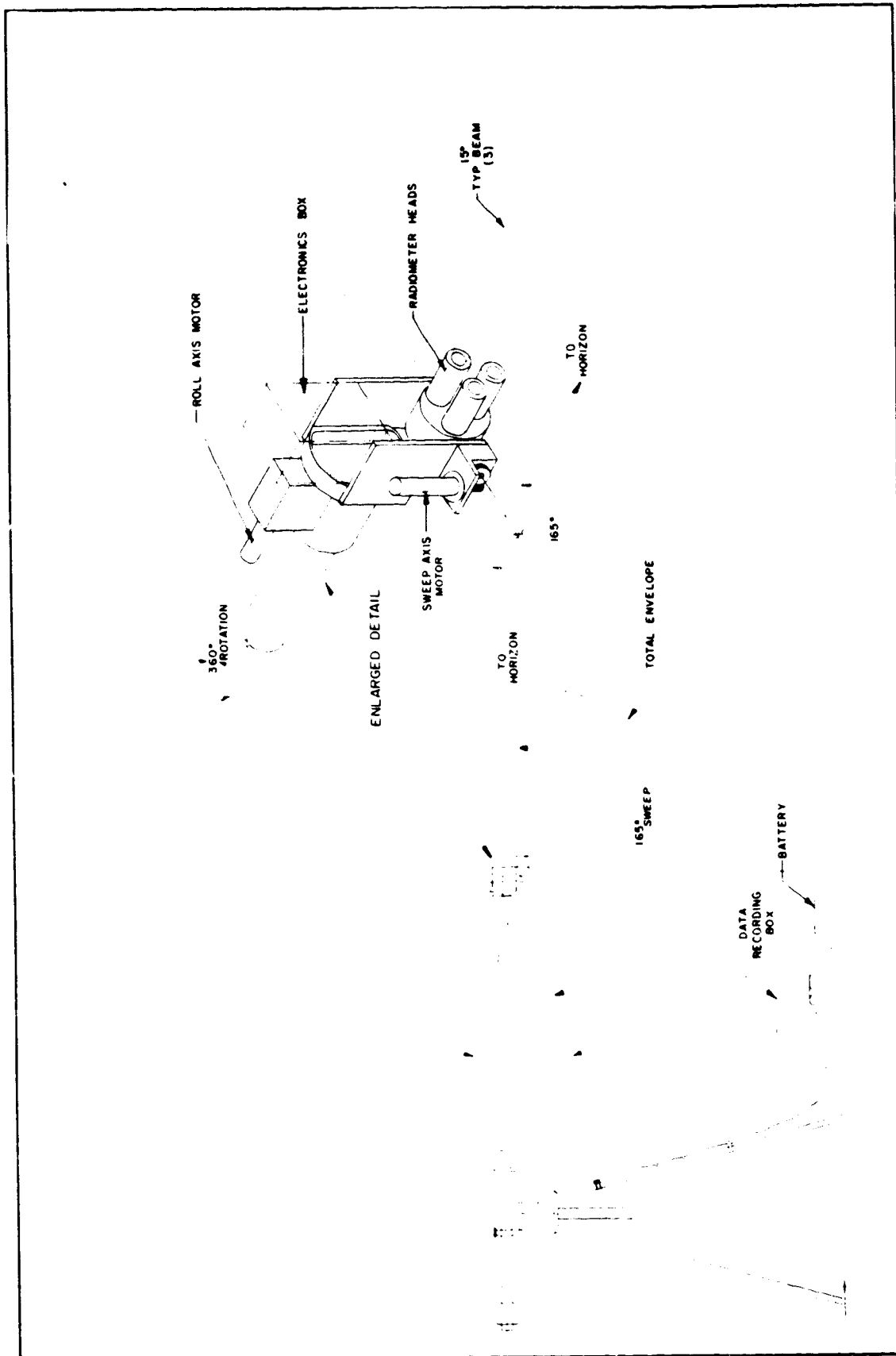
Figure 9M-1. AIRMASS instrument for bidirectional reflectance studies shown in tripod boom mount configuration.

CHAPTER 10

HYDROLOGICAL SCIENCES

edited by

Beverly K. Hartline

OVERVIEW

Recent research in the Hydrological Sciences has concentrated on developing
or applying remote sensing capabilities in three areas: monitoring soil
moisture, monitoring snowpacks, and predicting river flow and flood hazard.
In addition, we are demonstrating the value of satellite-borne sensors for
studying the hydrological regime in parts of the world that are fairly
inaccessible, for example, the Arctic.

SOIL MOISTURE

Our soil moisture research program focuses on developing the techniques and
sensors that will allow the spatial and temporal variations of soil moisture
to be determined remotely. Accurate information on soil moisture is
important for managing water resources, monitoring crop vigor, forecasting
crop yield, and assessing erosion potential. Moreover, soil moisture
influences the weather and climate because it is a boundary condition for
atmospheric processes. Since the amount of moisture in the soil is one
factor controlling the emission and reflection of radiation from the ground,
there exists a potential for monitoring soil moisture from space.

Our contribution to the soil moisture research effort* is to develop theoretical
models of the electromagnetic (especially microwave) signature of soil moisture
and to perform field and aircraft experiments to acquire the data needed to
validate those models. By this method we hope to zero in on a sensor combination
that allows the amount of moisture in the soil to be inferred accurately.

In analyzing the data and in refining the models, the real challenge has been
and remains to extract information about soil moisture from the radiation
emitted and/or reflected from the soil surface. The problem is that other
features, such as vegetation and surface roughness, affect the signal from
the soil moisture. Furthermore, the inherent variability of soil moisture
limits the accuracy of ground truth measurements.

We have reached the point where we are fairly confident of our modelling
and interpretation of the microwave response for a wide range of soil condi-
tions. Consequently, we have begun to focus our field and theoretical
studies on the more difficult and more practical problem of using the remotely
sensed measurements of surface moisture to estimate the moisture content of
the entire root zone.

---

*Soil Moisture studies are part of a multiagency, cooperative project
(AgRISTARS--Agriculture and Resources Inventory Through Aerospace Remote
Sensing). The approach and direction of NASA's soil moisture research is
guided by a research plan (PRISMS--Plan of Research for Integrated Soil
Moisture Studies).

SNOW

The thrust of our research on snow is to develop the techniques and sensors that will allow properties of the snowpack—its depth, water equivalent, wetness—to be determined remotely. Snow provides as much as 70 percent of the water supply for the western states of the U.S. In order to anticipate floods and allocate water for irrigation and hydroelectric power generation, users need accurate and timely information on the amount of snow and its readiness to melt. Conventionally, such data are collected at snow survey points that may or may not be representative of the entire watershed.

Satellites, due to their large, synoptic view of the ground, are in a good position to survey the snow cover, and obtain the needed snow data economically. Already, data from Landsat and NOAA satellites can be used to measure the area covered by snow. Use of that information improves runoff forecasts.

Since it is not the area covered by snow but the amount of water comprising the snow that provides the runoff, remote measurements of this parameter—the water equivalent—could boost the accuracy of forecasts even further. Our research is directed toward devising ways to make this measurement, and currently microwave sensors appear promising. Microwaves sample the interior of the pack, because they penetrate snow to a depth on the order of 10 to 100 times their wavelength. Furthermore, the microwave signature of snow depends, among other things, on its water equivalent. Two other advantages of microwaves are that they see through most clouds, and that the signature of wet snow is distinct from that of dry snow.

We have developed a theoretical model of the microwave emission of snow and we are collecting data using satellite- and aircraft-borne and truck-mounted sensors to validate the model. As in soil moisture research, the challenge is to disentangle the effects on the microwave signal of all the variables, such as crystal size, snow density and layering, the texture and state of the underlying ground and the presence of liquid water, in order to extract the information on water equivalent. We hope to separate these effects using a multifrequency approach.

HYDROLOGICAL MODELLING

Timely remotely sensed data can improve hydrological modelling for forecasting river runoff and evaluating flood hazard. Our research over the past few years has culminated in two recently completed Applications Systems Verification and Transfer Projects dealing with snow mapping and water management and control that demonstrate the value for hydrological applications of data obtained by satellites. In the tested applications, however, the remotely sensed data were used in conventional, empirically based models.

We are working with researchers from the University of Maryland and from the USDA Hydrological Laboratory in Beltsville, Maryland to develop and validate new models that are designed expressly to take satellite data as input. These models should optimize the usefulness of remotely sensed hydrological data.

ARCTIC HYDROLOGY

Permafrost dominates the hydrological regime of the Arctic. Since the Arctic is inhospitable and relatively unpopulated, satellite imagery provides, in many cases, the first data and certainly the least costly data, from which hydrological phenomena unique to an area of permafrost can be explored and monitored.

We recently completed a study of the nature and source of aufeis (ice that overflows in discrete patches in river channels), that convincingly calls into question previous hypotheses advanced to explain its occurrence. In addition, we are collaborating with scientists from the U.S. Army Cold Regions Research and Engineering Laboratory to monitor the recovery of a patch of tundra that was burned in 1977. We determined that damage to the tundra and the regrowth of vegetation can be assessed reliably using Landsat digital data. This study provides a data base for evaluating damage--inflicted by man's activities or by nature-- to the tundra and the near-surface permafrost, and for estimating the rate of recovery from the damage.

A. AIRCRAFT REMOTE SENSING OF SOIL MOISTURE AND HYDROLOGIC PARAMETERS

by

P. E. O'Neill, T. Schmugge and J. Wang

OBJECTIVE

The objective of this cooperative investigation with the U.S. Department of Agriculture (USDA) Beltsville Agricultural Research Center (BARC) is to examine the ability of airborne microwave sensors to detect variations in soil moisture content. An eventual goal is to evaluate the capability of remote sensing to supply soil moisture data needed by water resource agencies to predict runoff and to evaluate irrigation requirements.

BACKGROUND

Since microwave emission or backscatter from a terrain surface is largely dependent on its dielectric properties, the possibility of measuring soil moisture rests upon the large disparity in the dielectric constant of water and soil. Aircraft platforms provide an opportunity for making large-scale simultaneous observations of soil moisture over a wide range of surface conditions which may be encountered in water resource applications.

During the past few years a series of aircraft data flights were arranged over several agricultural test sites in semi-arid regions of Oklahoma and South Dakota and in humid regions of Georgia and Florida. Ground measurements of near-surface soil moisture, soil temperature and surface vegetation cover were coordinated with overflights by a NASA C-130 research aircraft equipped with visible, infrared, and passive and active microwave sensors.

RECENT RESULTS

Analysis of the aircraft data demonstrates that L-band (1.4 GHz, 21 cm wavelength) microwave radiometers reliably respond to soil moisture content in the top 5 cm of the soil. Correlations of approximately −0.88 (r^2 = .78) have been obtained between microwave brightness temperature and soil moisture for the South Dakota test site independent of vegetation cover. For the Oklahoma and Georgia/Florida sites the correlation was ~ -0.7 (Figure 10A-1). When these data are separated by land use or crop types, correlations in most categories increase. Results using data from the aircraft's active microwave scatterometers indicate that the best relationship between microwave backscatter and near-surface soil moisture is obtained a. C-band frequency (4.75 GHz, 6.3 cm wavelength) at an incidence angle of 15° off nadir (Fig. 10A-2). These results confirm the active microwave soil moisture research conducted by the University of Kansas.

FUTURE EMPHASIS

Data collected during three NASA aircraft flights this summer over very dry test watersheds in Oklahoma complement measurements obtained from these same watersheds under moist conditions in 1978. Now that a complete range of soil wetness conditions and different environments have been sampled, the field observations are being used to refine and validate microwave emission models. Future effort will focus on the effects of vegetation cover/crop type and non-homogeneous terrain on the response of microwave sensors to varying levels of soil moisture.

PUBLICATIONS

"Soil Moisture Sensing with Microwave Radiometers," by T. Schmugge, long paper presented at the 6th Purdue Symposium on Machine Processing of Remotely Sensed Data, Lafayette, Indiana, pp 346-354, 1980.

"Aircraft Remote Sensing of Soil Moisture and Hydrologic Parameters," by T. J. Jackson, T. J. Schmugge, G. C. Coleman, C. Richardson, A. Chang, J. Wang and E. T. Engman, USDA/SEA Agricultural Research Results ARR-NE-8, 1980.

"Active Microwave Measurements for Estimating Soil Moisture in Oklahoma," by T. J. Jackson, A. Chang, T. J. Schmugge, paper presented at the Fall Technical Meeting of the American Society of Photogrammetry, 1980.

"Spatial Relationships of Surface Soil Moisture," by T. J. Jackson and T. J. Schmugge, submitted for publication to Journal of Hydrology, 1980.

"Analysis of Surface Moisture Variations Within Large Field Sites," by K. R. Bell, B. J. Blanchard, T. J. Schmugge, and M. W. Witczak, Water Resources Research, 16, 796-810, 1980.

"Estimation of Soil Moisture with API Algorithms and Microwave Emission," by B. J. Blanchard, M. J. McFarland, T. J. Schmugge and E. Rhoades, submitted for publication to Water Resources Bulletin, 1980.

Figure 10A-1. Comparison of 21 cm emissivities measured from an aircraft platform. These data were obtained from 9 flights during 1976-1978 over Hand County, South Dakota. The dashed line is the regression result for data obtained over a Phoenix, Arizona site.
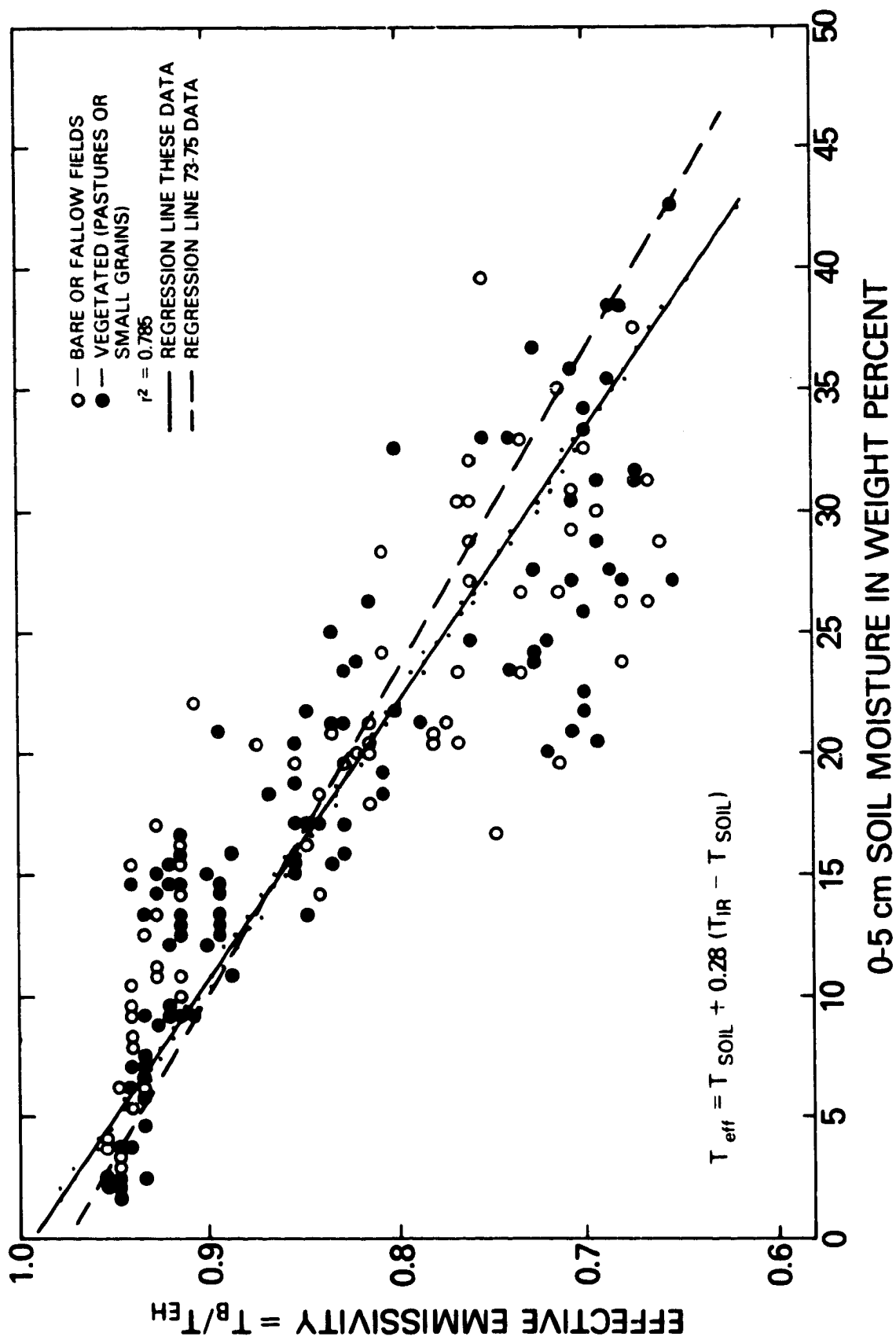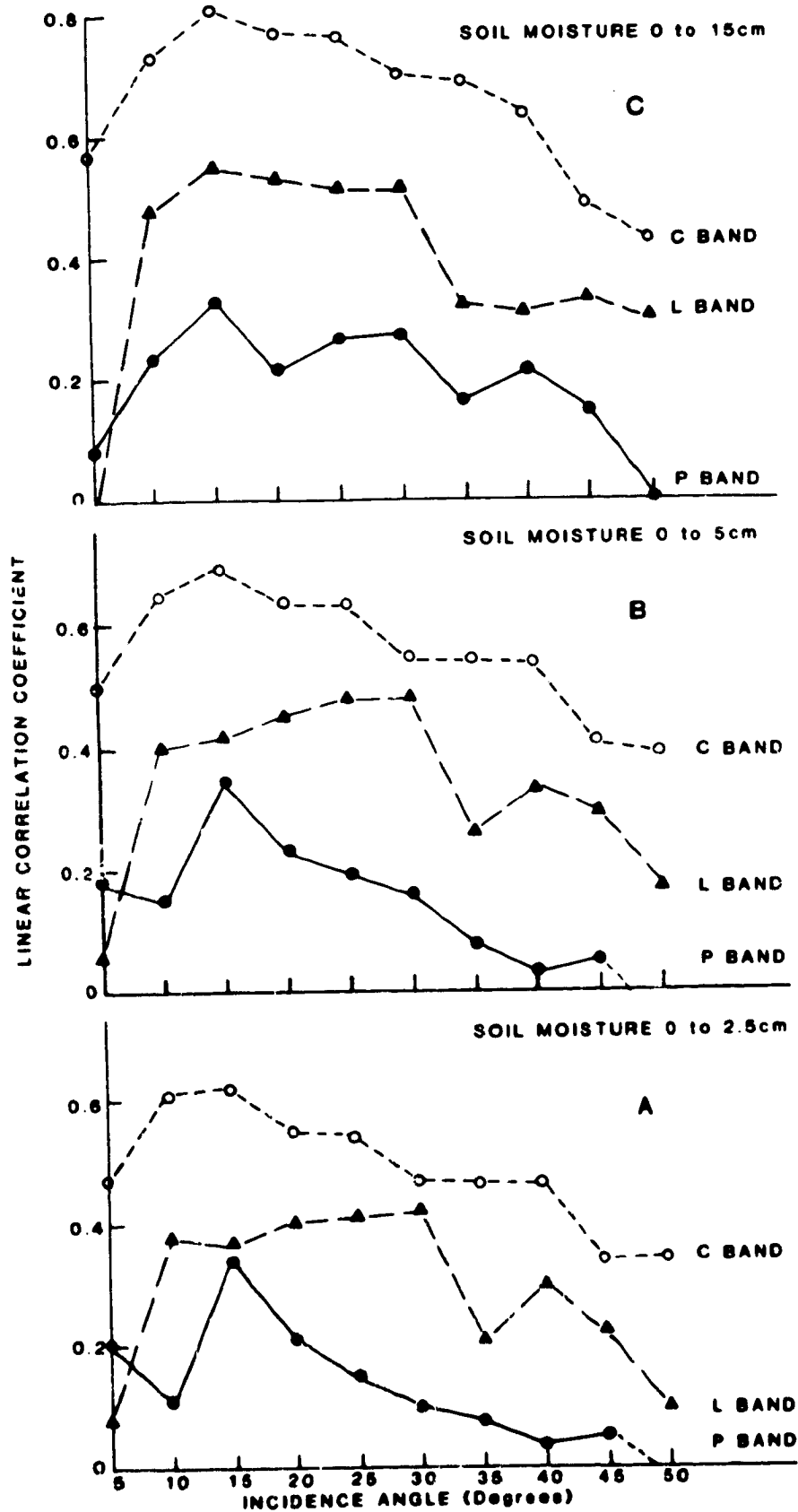
Figure 10A-2. Variation of the linear correlation between volumetric soil moisture and the radar backscattering coefficient as a function of incidence angle and band for different soil moisture depths.

B. GROUND-BASED MEASUREMENTS OF SOIL MOISTURE THROUGH A VEGETATION CANOPY

by

P. E. O'Neill, T. Schmugge and J. Wang

OBJECTIVE

The goal of this Goddard Space Flight Center (GSFC) experiment (codes 924 and 946), in cooperation with U.S. Department of Agriculture/Beltsville Agriculture Research Center (USDA/BARC), is to understand quantitatively the effects of sensor parameters such as frequency, polarization and angle of incidence, and target parameters such as moisture content, surface roughness and vegetation cover on the ability of microwave radiometers to determine soil moisture content.

BACKGROUND

Microwave emission data were acquired under controlled conditions by GSFC's truck-mounted microwave radiometers at 1.4 GHz and 5 GHz over both bare and vegetated fields at the USDA/BARC test site. Soil at the test site is a sandy loam, and vegetation covers include grass, soybean and corn. Due to unavoidable constraints, field data collection consisting of measurements of microwave emission, soil moisture content, soil temperature and vegetation biomass was limited to October 1979.

RECENT RESULTS

The bare field measurement results at 1.4 GHz agree fairly well with radiative transfer model calculations with appropriate values for surface roughness factor and mixing ratio (Fig. 10B-1). In addition, because the soil at the USDA/BARC site is similar to the soil in a soil moisture test area studied by Jet Propulsion Laboratory researchers in 1979, for the first time the performance of different 1.4 GHz microwave radiometer systems can be directly compared. Although acquired under a different range of soil moisture conditions, the two data sets are consistent with each other in that they demonstrate the same relationship between microwave brightness temperature and soil moisture content (Fig. 10B-2 and Fig. 10B-3).

The presence of a vegetation canopy was found to produce higher microwave brightness temperatures than those expected from a bare field, thus reducing radiometer sensitivity to the underlying soil moisture content. At 1.4 GHz this sensitivity reduction ranged from about 20 percent for 10 cm tall grass to greater than 50-60 percent for a dense soybean field; at 5 GHz the corresponding reduction in sensitivity ranged from approximately 70 percent to 90 percent of the bare field case. Based on this study, the obscuring effect of a vegetation cover on the microwave response to soil moisture increases with radiometer frequency and with the biomass of the vegetation as would be expected (Fig. 10B-4).

FUTURE EMPHASIS

Work is continuing on quantification of the biomass relationship, using new radiometric and ground truth data sets acquired at the BARC test site during July through September 1980. This year's dry field observations will complement those obtained in 1979, when wet soil conditions predominated during the period of radiometric measurement.

PUBLICATIONS

"An Empirical Model for the Complex Dielectric Permittivity of Soils as a Function of Water Content," J. R. Wang and T. J. Schmugge, IEEE Trans. Geosci. Remote Sensing, GE-18, 4, 288, 1980.

"Passive Microwave Remote Sensing of Soil Moisture: The Effect of Tilled Row Structure," J. R. Wang, R. W. Newton and J. W. Rouse, IEEE Trans. Geosci. Remote Sensing, GE-18, 4, 296, 1980.

"The Dielectric Properties of Soil-Water Mixtures at Microwave Frequencies," J. R. Wang, Radio Science, 15, 5, 977, 1980.

"Microwave Remote Sensing of Soil Moisture Content Over Bare and Vegetated Fields," J. R. Wang, J. C. Shiue and J. E. McMurtrey, III, Geophys. Res. Letters, 7, 10, 801, 1980.

"Remote Sensing of Soil Moisture Content Over Bare Fields at 1.4 GHz Frequency," J. R. Wang and B. J. Choudhury, accepted for publication by J. Geophys. Res., 1981.

"Thermal Microwave Emission from Vegetated Fields: A Comparison Between Theory and Experiment," J. R. Wang, J. C. Shiue, S. L. Chang and M. Dombrowski, submitted for publication to IEEE Trans. Geosci. Remote Sensing, 1980.

"Remote Measurements of Soil Moisture by Microwave Radiometers at BARC Test Site," J. Wang, J. Shiue, E. Engman, J. McMurtrey, III, P. Lawless, T. Schmugge, T. Jackson, W. Gould, J. Fuchs, C. Calhoon, T. Carnahan, AgRISTARS Technical Report SM-G0-00471, Oct., 1980.

"System Calibration of the 1.4 GHz and 5 GHz Radiometers for Soil Moisture Remote Sensing," J. Wang, J. Shiue, W. Gould, J. Fuchs, E. Hirschmann and W. Glazar, NASA TM 82043, GSFC, Nov. 1980.

"Comparison of Radiative Transfer Models for Predicting the Microwave Emission from Soils," T. J. Schmugge and B. J. Choudhury, NASA TM-80688, submitted for publication to Radio Science, 1980.

"Effect of Soil Texture on the Microwave Emission from Soils," by Thomas Schmugge, NASA Tech Memo 80632, IEEE Trans. on Geoscience and Remote Sensing, GE-18, 353-361, 1980.
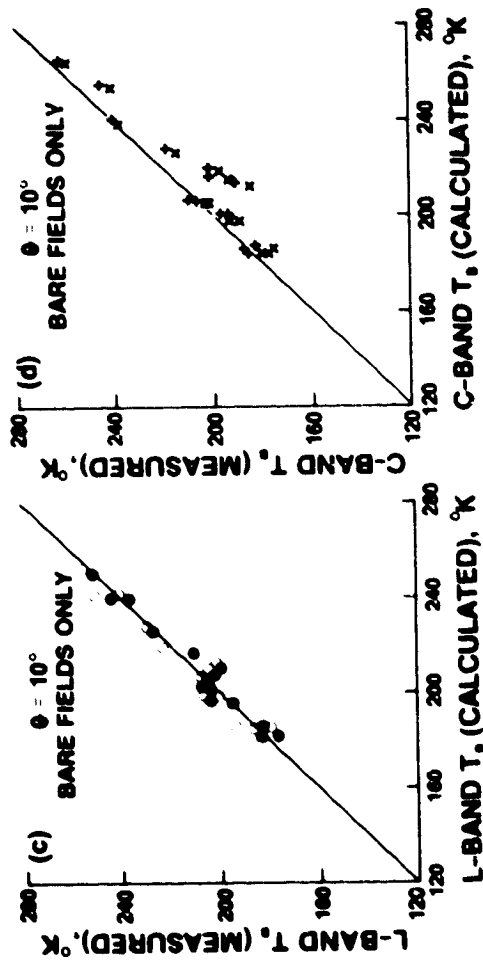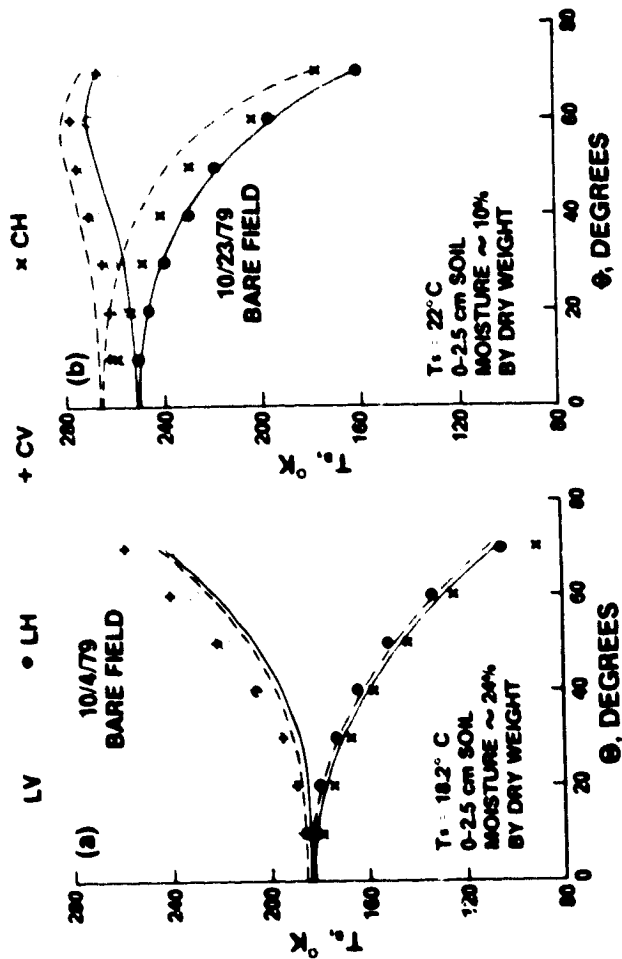
Figure 10B-1. The antenna temperatures vs. incident angles for a bare field when soil was wet. (b) The antenna temperatures vs. incident angles for a bare field when soil was dry. (c) A comparison of L-band measured and calculated antenna temperatures for bare fields at θ = 10°. (d) A comparison of C-band measured and calculated antenna temperatures for bare fields at θ = 10°

1.42 GHz NORMALIZED BRIGHTNESS TEMPERATURE (T_B) VS. SOIL MOISTURE

INCIDENCE ANGLE = 25°

- = 1979 SAN JOAQUIN VALLEY DATA
  0-2.0 cm SOIL MOISTURE
  n = 34
  r = −.93

x = 1979 BELTSVILLE DATA
0-2.5 cm SOIL MOISTURE
n = 14
r = −.92

COMBINED r = −.96

BARE FIELDS
SANDY LOAM SOIL

NORMALIZED T_B : L-BAND HORIZONTAL POLARIZATION
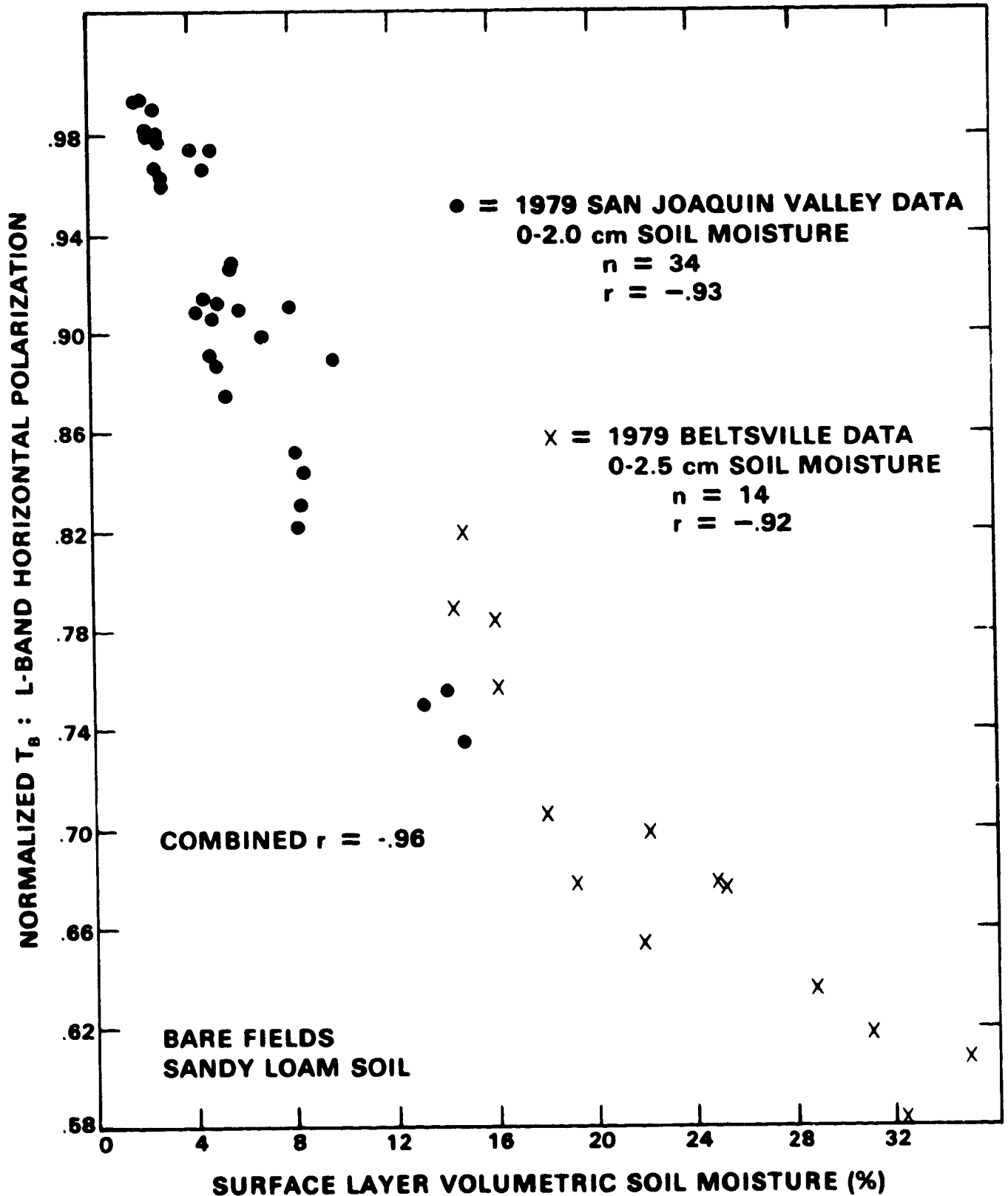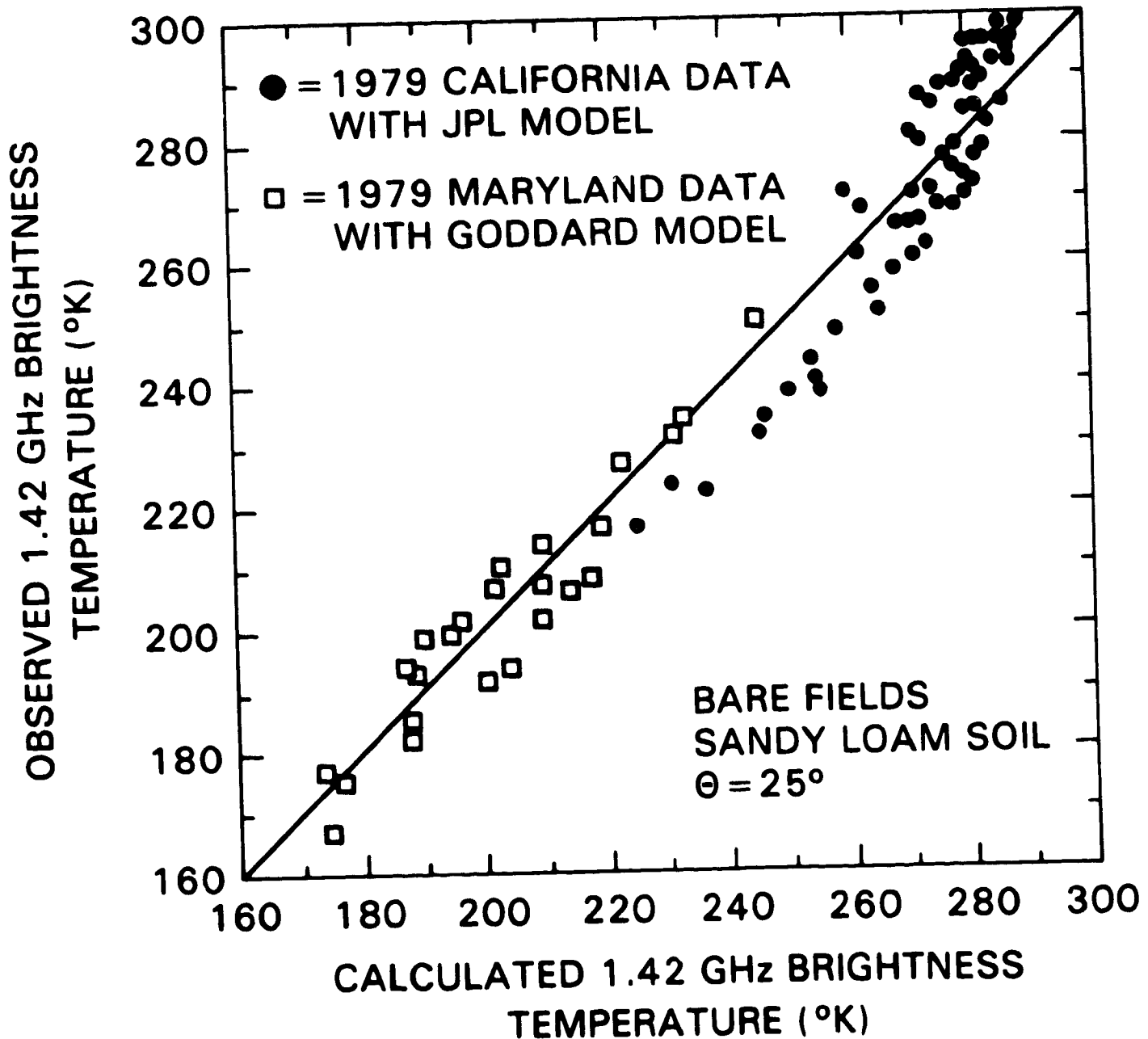
SURFACE LAYER VOLUMETRIC SOIL MOISTURE (%)

COMPARISON BETWEEN OBSERVED AND CALCULATED 1.42 GHz MICROWAVE BRIGHTNESS TEMPERATURE
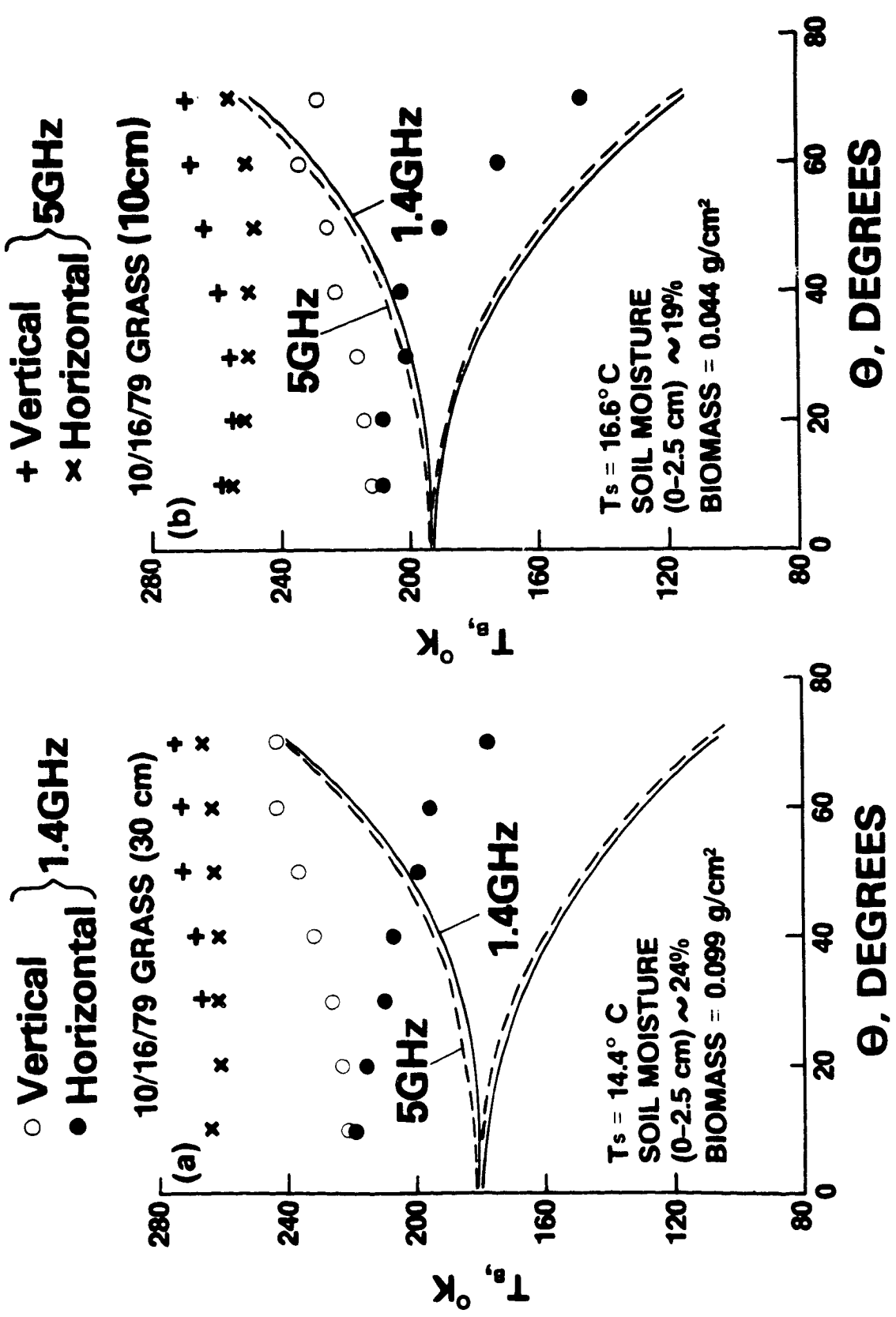
(INCLUDES BOTH HORIZONTAL AND VERTICAL POLARIZATION)

Figure 10B-4. The Measured Brightness Temperatures Plotted Against the Incident Angles for Grasslands; (a) 30cm Tall Grass; (b) 10cm Tall Grass. The Smooth Curves (solid ones for 1.4GHz and dashed ones for 5GHz) are the Calculated Results Assuming the Fields were Bare. Ts is Soil Temperature at Top 2.5 cm Layer.

C. DETERMINATION OF SNOWPACK PROPERTIES BY MICROWAVE RADIOMETRY: THEORETICAL MODEL AND EXPERIMENTAL VALIDATION

by

A. T. C. Chang, J. L. Foster, D. K. Hall, A. Rango and B. K. Hartline

OBJECTIVE

The objective of this study is to develop a way to infer properties of a snowpack from observations made by satellite-borne sensors. Our recent efforts have focussed on microwave radiometry, because that technique shows promise for providing information on the water equivalent of snow.

BACKGROUND

Water stored in the snowpacks provides as much as 70 percent of the water supply for the western states of the U.S. In order to accurately monitor the snow water content, measurements of snow-covered area, depth, density, and free water content are essential. Conventionally, these data are collected by skiers, by use of snowmobiles, and from a few isolated stations instrumented with pressure pillows or other sensors. These data collection methods are time consuming and only limited data are collected at points in selected snow survey courses. Recently, visible and near infrared sensors on-board the operational satellites have provided information on snow-covered area (Rango, 1975). Because these sensors see only the surface of the snowpack, they cannot measure the water equivalent of the snow. Since microwave sensors respond to emissions from within the snowpack, they have considerable potential for monitoring snowpack properties, such as water equivalent (Rango, et al., 1979). Moreover, the dielectric properties of water are sufficiently different from those of dry snow crystals that information on the wetness of the snow--a measure of its readiness to melt--is also contained in the microwave emissions.

RECENT ACCOMPLISHMENTS

In order to determine snowpack properties quantitatively by microwave radiometry, it is necessary to understand the microwave interactions within the snowpack. A microscopic scattering model (Chang, et al., 1976) has been developed to calculate the microwave emissions from a snowpack. At present, our major effort is concentrated on relating the measurements taken by truck-mounted systems and airborne sensor systems to the snow water equivalent, and comparing these measurements with predictions from the model.

Snow water equivalent predicted using the model and the measured brightness temperatures at 37 GHz are compared with the measured snow water equivalent in Tables 10C-1 and 10C-2. For shallow snowpacks, the agreement between measured and predicted values is quite good. But when the snowpack is deep, predicted and measured values are disparate. In part, the poor correlation is due to the fact that 37 GHz radiation penetrates only approximately 1 meter of snow. However, we suspect that uncertainties in choosing the mean crystal size assumed in the model are the major cause of the disagreement in the deep-snowpack cases. This finding underlines the importance of grain

size, and suggests that it is one of the snow properties that ought to be measured in field studies of microwave emission from snow.

FUTURE EMPHASIS

This study will be extended to sample many different snow conditions. The theoretical model will be refined by utilizing data obtained by airborne and spaceborne microwave systems.

REFERENCES AND PUBLICATIONS

Chang, A. T. C., P. Gloersen, T. Schmugge, T. T. Wilheit and H. J. Zwally, "Microwave Emission from Snow and Glacier Ice," Journal of Glaciology, 16, p 23-29, 1976.

Chang, A. T. C., and J. Shiue, "A Comparative Study of Microwave Radiometer Observations over Snowfields with Radiative Transfer Model Calculations," NASA TM-80267, (in press), Remote Sensing of Environment, 1980.

Chang, A. T. C., J. Shiue and A. Rango, "Remote Sensing of Snow Properties by Passive Microwave Radiometry: GSFC Truck Experiment," NASA Microwave Snow Property Workshop, NASA CP-2153, 1980.

Chang, A. T. C., J. L. Foster, D. K. Hall and A. Rango, "Monitoring Snowpack Properties by Passive Microwave Sensors on Board Aircraft and Satellite," NASA Microwave Snow Property Workshop, NASA CP-2153, 1980.

Foster, J. L., A. Rango, D. K. Hall, A. T. C. Chang, L. Allison and L. Diesen, "Snowpack Monitoring in North America and Eurasia Using Passive Microwave Satellite Data," NASA TM-80706, (in press), Remote Sensing of Environment, 1980.

Foster, J. L., D. K. Hall, A. T. C. Chang, A. Rango, L. Allison and L. Diesen, "The Influence of Snow Depth and Surface Air Temperature on Satellite-Derived Microwave Brightness Temperature," NASA TM-80695, 1980.

Rango, A., A. T. C. Chang and J. L. Foster, "The Utilization of Spaceborne Microwave Radiometers for Monitoring Snowpack Properties," Nordic Hydrology, 10, p 25-40, 1979.

Rango, A. (Editor), "Operational Applications of Satellite Snow Cover Observations," National Aeronautics and Space Administration, Washington, D.C., NASA SP-391, 430 p., 1975.

Table 10C-1. Test of Theory Using Data from Truck-Mounted Microwave Systems

Test Site	Brightness Temperature T_B (37 GHz)	Incidence Angle	Polarization*	Snow Water Equivalent	
				Measured Ground Truth	Predicted from T_B
Truckee, CA (Edgerton, et al.)	233K	45°	V	10 cm	9 cm
	210K	45°	V	20 cm	16 cm
Steamboat Spring, CO (Stiles and Ulaby)	205K	57°	H	10 cm	9 cm
	188K	57°	H	20 cm	15 cm
Fraser, CO (Chang, et al.)	210K	50°	V	21 cm	16 cm
Davos, Switzerland (Hofer and Mitzler)	210K	55°	V	50 cm	16 cm

*V = vertical; H = horizontal

Table 10C-2. Test of Theory Using Data from Aircraft Microwave System

| Test Site | Brightness Temperature | | Polarization | Snow Water Equivalent | | Ground Cover |
	T_B(37 GHz)	T_B(10.7 GHz)*		Measured Ground Truth	Predicted from T_B	
Steamboat Spring, CO March 1976	165°K	245 V 199 H	0.10	16.1± 7 cm	17 cm	Wet
Walden, CO March 1976	235	268 V 258 H	0.02	2.8± 1.5 cm	3 cm	Frozen
Steamboat Spring, CO March 1977	200	---	---	10.4± 3.7 cm	11 cm	Frozen
Walden, CO March 1977	254	---	---	0.12 cm	0 cm	Frozen
Rabbit Ears Pass, CO February 1, 1980	234	263 V 245 H	0.04	49.3± 13 cm	4 cm	Frozen
Steamboat Spring, CO February 1, 1980	197	---	---	19.8± 2 cm	12 cm	Frozen
Steamboat Spring, CO March 1980	162	255 V 210 H	0.10	30.9± 5.6 cm	29 cm	Wet
Walden, CO March 1980	194	---	---	9.9± 4.8 cm	12 cm	Wet

*V = vertical; H = horizontal

D. SNOWPACK MONITORING USING PASSIVE MICROWAVE DATA FROM NIMBUS SATELLITES

by

A. Rango, A. T. C. Chang, J. Foster and D. K. Hall

OBJECTIVES

This study was part of an effort to increase the amount of information about snow cover that is available from remote sensing. Its purpose was to test the feasibility of using passive microwave sensors on satellites to measure snow depth or the water equivalent of the snowpack. An Electrically Scanning Microwave Radiometer (ESMR) is on board Nimbus 5 (wavelength 1.55 cm) and Nimbus 6 (wavelength 0.8 cm). Nimbus 7 carries a Scanning Multichannel Microwave Radiometer (SMMR; wavelengths 0.8, 1.4, 1.7, 2.8, and 4.6 cm).

BACKGROUND

Currently the area covered by snow is the only snow parameter that is monitored using data from satellites, and that information, derived from visible and near-infrared imagery, can be obtained only when the weather is clear. Yet from the standpoint of predicting streamflow and allocating water use, it would be extremely useful to have an estimation of the amount of water stored as snow. Moreover, it would be nice to be able to keep an eye on the snow, even when the sky is cloudy.

In principle, microwave radiation from snow could provide the information to answer both of these needs. Microwaves penetrate clouds and the microwave emission from snow is sensitive to conditions within the snowpack to a depth of 10 to 100 times the wavelength. Such factors as snow temperature, thickness, grain size, water equivalent, and the presence of liquid water contribute to the microwave emissivity of snow, thereby influencing the intensity of microwave emission, known as brightness temperature (T_B).

We selected three study areas: the high plains of Canada (southern Alberta and Saskatchewan), the high plains of the U.S. (eastern Montana and western North Dakota), and the central steppes of Russia. Brightness temperatures from ESMR or SMMR overpasses of these areas were compared with snow depths reported by meteorological observers on the ground.

RECENT RESULTS

Microwave brightness temperature appears to be a promising measure of snow depth under the dry snow conditions typical in these study areas. (Fig. 10D-1)

- Microwave brightness temperature decreases with snow depth and water equivalent. Snow accumulation and depletion at specific locations cause variations in passive microwave brightness temperatures observed from Nimbus satellites. Qualitative monitoring of snowpack build-up and disappearance during the winter appears feasible in a given area.

- Since the snow was relatively shallow (less than 40 cm deep), the short wavelength ESMR (Nimbus 6) measurements and the short wavelength SMMR data produced the strongest correlations with snow depth.

- Because different geographic areas have different snowpack conditions, ground cover, underlying soil conditions and surface temperatures, it is difficult to extrapolate relationships between microwave brightness temperature and snow depth from one area to another.

- Passive microwave signatures of snow cover are not obscured by cloud cover and observations can be made at night.

FUTURE EMPHASIS

The challenge in the analysis of microwave emissions from snow lies in the fact that snowpack conditions are complex, continually changing, and that microwave radiation from snow is not completely understood. We plan to continue to explore empirical correlations between snowpack properties and brightness temperatures measured by the Nimbus satellites. In particular, we will exploit the multichannel feature of the SMMR to see whether important snowpack properties can be inferred from the multispectral signature of microwave emissions from snow.

PUBLICATIONS

Foster, J. L., A. Rango, D. K. Hall, A. T. C. Chang, L. J. Allison, and B. C. Diesen: Snowpack Monitoring in North America and Eurasia Using Passive Microwave Satellite Data. Remote Sensing of the Environment (in press) 1980.

Foster, J. L., D. K. Hall, A. Rango, A. T. C. Chang, L. J. Allison, and B. C. Diesen: The Influence of Snow Depth and Surface Air Temperature on Satellite-Derived Microwave Brightness Temperature. NASA Technical Memorandum TM-80695, 1980

Hall, D. K., A. Rango, J. L. Foster, and A. T. C. Chang: Progress and Requirements of Passive Microwave Remote Sensing of Snowpack Properties. Proceedings of the Workshop on Polar Surface Microwave Properties for Climate Research, Greenbelt, Maryland, 1980.

Chang, A. T. C., J. L. Foster, D. K. Hall, and A. Rango: Monitoring Snowpack Properties by Passive Microwave Sensors on Board of Aircraft and Satellites. Microwave Snow Properties Workshop, Ft. Collins, Colorado, 1980. NASA Conference Publication 2153, 235-248.
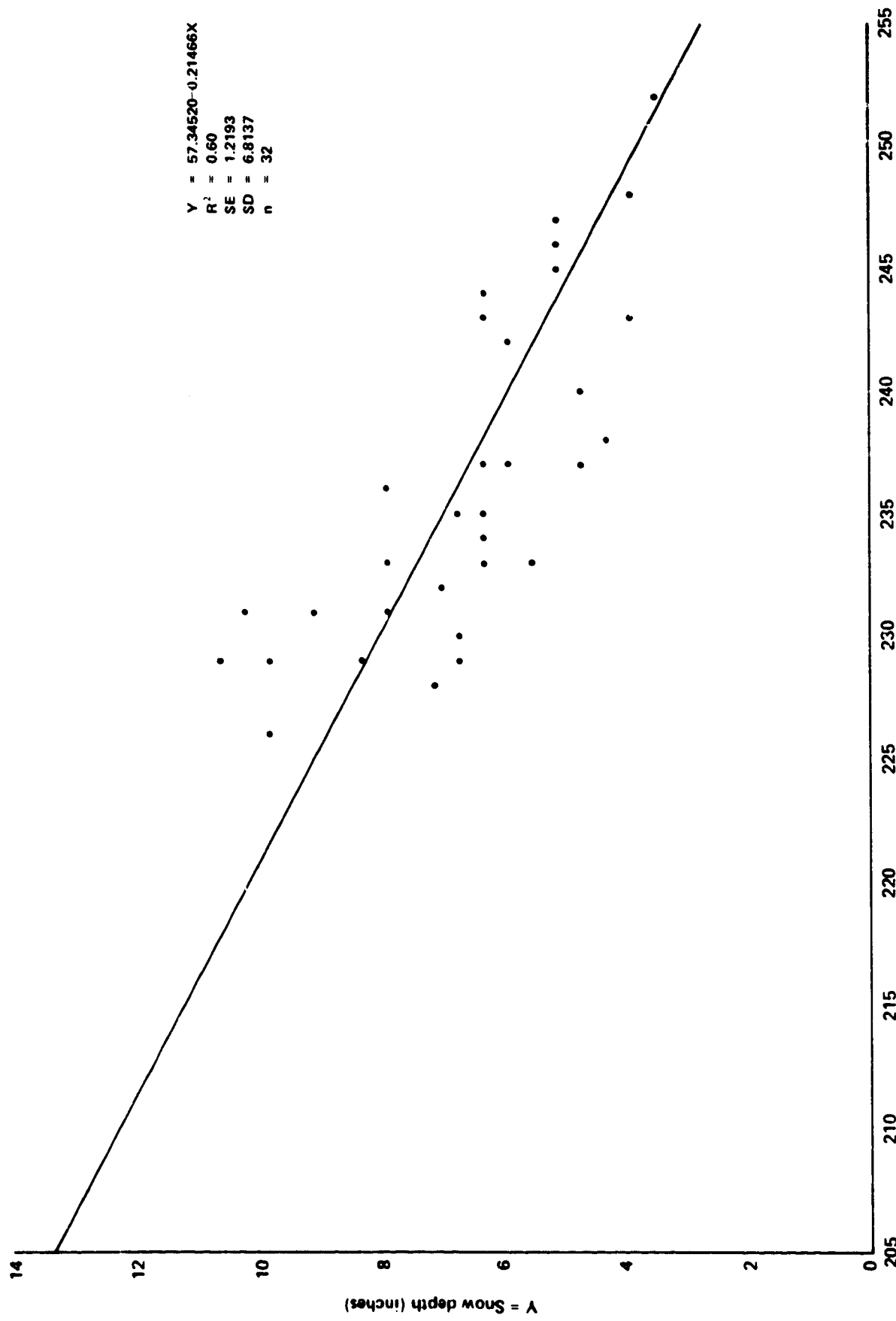
Figure 10D-1. Snow depth in Central Russia plotted as a function of brightness temperature measured by Nimbus 6.

E. SNOW MAPPING APPLICATIONS SYSTEMS VERIFICATION AND TRANSFER PROJECT

by

A. Rango

OBJECTIVE

The purpose of this study was to test the operational usefulness of measurements of snow covered area from images taken by Landsat and NOAA satellites.

BACKGROUND

In the western United States, snowmelt provides most of the water that is consumed by agriculture, industry, and residences, or used to generate hydroelectric power. In the spring, melting snow can cause rivers to flood. Thus, many agencies are concerned with predicting snowmelt runoff, both to allocate water optimally and to minimize damage due to flooding. To make their predictions, these agencies need to know how much snow is in each river basin.

Since 1972, when Landsat-1 and NOAA-2 satellites were launched, it has been hypothesized that satellite data could be used to measure snow-covered area and thereby assist in snowmelt runoff prediction. The Snow Mapping Applications Systems Verification and Transfer (ASVT) project was begun in 1975 to determine whether satellite observations of snow-covered area can be used operationally by agencies to increase the accuracy of their runoff predictions. In order to sample a broad range of snow, vegetation and climatic conditions, study basins in California, Arizona, Colorado, and the Pacific Northwest were selected for the ASVT. Data collection was completed in 1979.

RECENT RESULTS

This ASVT has proven that satellite-sensed snow-covered area can be used to reduce the error in snowmelt runoff predictions in a cost-effective manner. For example, in California test basins, use of the remotely sensed data reduced runoff forecast errors from 15 percent (conventional) to 10 percent (Landsat). Modelling studies on the Boise River in Idaho indicated that the error in short term (5-day) forecasts could drop as much as 9.6 percent when satellite measurements of snow-covered area are used.

The use of the satellite data is not fully operational, however, because there is too long a time lag between Landsat data acquisition and receipt by the user. In addition, the frequency of coverage from Landsat is not optimum. NOAA satellite data are available with the required frequency and quick turnaround, but the resolution is much poorer than Landsat, and as a result they are more difficult to manipulate for snow mapping, especially in small to moderate-sized basins. Truly operational application of satellite data will only be possible in the eleven western states when the data turnaround time is reduced to 72 hours, and the water management agencies can be assured of a continuing supply of data from space.

SIGNIFICANCE

In the areas studied, the remote sensing data were estimated to be capable of reducing snowmelt runoff forecast error by 1-5 percent. Extrapolated over the eleven western states, a 1 percent absolute improvement in forecast accuracy was found to be worth approximately $38 million per year ($28 million from irrigation benefits and $10 million from hydropower benefits).

FUTURE EMPHASIS

In this ASVT remotely sensed data were input into river forecast models that were designed to use conventional data. We are working now on developing models that are tailored to take snow-covered area as input data. We are testing these forecast models operationally on basins that are large enough that their snow cover can be mapped with sufficient accuracy from the coarse-resolution NOAA images.

PUBLICATIONS

Rango, A. and R. Peterson, 1980: Operational Applications of Satellite Snow-cover Observations, NASA Conference Publication CP-2116, National Aeronautics and Space Administration, Washington, D.C., 302 pp.

Rango, A., 1980: Operational applications of satellite snow cover observations, Water Resources Bulletin, Vol. 16, No. 6, 8 pp.

F. SNOWMELT RUNOFF MODELING USING REMOTE SENSING DATA

by

A. Rango

OBJECTIVE

The overall objective of this study is to test whether snowmelt runoff in operational-size (> 100 km^2) basins can be forecast successfully using models based on satellite remote sensing data.

BACKGROUND

In order to practice effective water resources management various agencies have come to depend on the use of hydrologic models to assist them in this function. Many agencies in the western United States are in the process of switching over to modeling of the snowmelt runoff process as opposed to statistically based approaches. Few models currently have the capability to accept remote sensing data, however, there are a few excellent models, such as the SSARR (Streamflow Synthesis and Reservoir Regulation) and Martinec models, that require basin-wide snow cover estimates that can only be obtained from some form of remote monitoring. The Martinec model was developed in Europe on small experimental basins (< 50 km^2) and applied using aircraft data. To be useful, such a model must be applied to larger, operational-type basins (> 100 km^2) with a potential need for runoff forecasts. When Landsat data became available, it was decided to test this model on operational basins in the western United States and assess its ability to simulate runoff using satellite and limited conventional data. Basins in the Wind River Mountains of Wyoming and the Rocky Mountains of Colorado were selected for testing.

RECENT RESULTS

Four basins have been tested thus far (Dinwoody Creek, WY - 228 km^2; Bull Lake Creek, WY - 484 km^2; South Fork, CO - 558 km^2; and Conejos River, CO - 730 km^2) with successful application of the model in each case. Because normal temperature and precipitation measurements from conventional stations have been employed, it appears that satellite snow cover is a critical input variable which allows application of the model to these operational size basins. In the Wind River Mountains comparisons of simulated and measured streamflow indicate that simulated seasonal (6-month) volumes are within 5 percent of actual, and that about 82-86 percent of the variation in actual daily runoff values is explained by the modeling approach. In the Colorado Rockies, the predicted seasonal flow volume averaged to within 2 percent of the observed volume, and about 88 percent of the variation in daily flows is explained.

SIGNIFICANCE

The model has the potential for the operational prediction of snowmelt runoff for varying time periods, and it also can be applied to ungauged basins. Such a modeling capability provides a means for applying the satellite remote

sensing data operationally by a water resources agency. Regulation of reservoirs for flood control, irrigation, and hydropower can thus be improved.

FUTURE EMPHASIS

The snowmelt runoff model will be applied to the entire Rio Grande River Basin above Del Norte, Colorado ($3419 \ km^2$) for eventual operational use by the U.S. Department of Agriculture and the Colorado Division of Water Resources. In addition, the model will be converted for use in the forecasting mode and tested on the Colorado basins.

In order to make more effective use of remote sensing data, a task force will focus on the development of a family of remote-sensing-compatible hydrological models. These models will be designed for use with spatially obtained remote sensing information and not with conventional point measurements. Both non-snowmelt and snowmelt situations will be covered.

PUBLICATIONS

Rango, A. and J. Martinec, 1979: Application of a snowmelt-runoff model using Landsat data, Nordic Hydrology, 10, 225-238.

Rango, A., 1980: Remote sensing of snow covered area for runoff modelling, Hydrological Forecasting (Proceedings of the Oxford Symposium), IAHS-AISH Publication No. 129, International Association of Scientific Hydrology, Oxford, U.K., pp. 291-297.

Hawley, M. E., R. H. McCuen, and A. Rango, 1980: Comparison of models for forecasting snowmelt runoff volumes, Water Resources Bulletin, 16, 5, 914-920.

G. WATER MANAGEMENT AND CONTROL APPLICATIONS SYSTEMS VERIFICATION AND TRANSFER PROJECT

by

A. Rango

OBJECTIVE

The purpose of this study was to test the utility of Landsat hydrologic land use data as input for hydrologic engineering models that are used to generate discharge frequency curves.

BACKGROUND

For flood control planning and construction purposes, up-to-date hydrologic land use information is required for model simulations of flood flows under existing land cover conditions. Agencies charged with the management of flood flows need the most current information possible for use in these studies. The Corps of Engineers, as an example, conducts approximately 75 watershed studies each year. Initial research had indicated that Landsat classifications of land use could be used in place of conventional data in these studies at potentially significant cost savings. To test this idea, the water management and control Applications Systems Verification and Transfer (ASVT) project was begun in cooperation with the Corps of Engineers. In order to sample a broad range of watersheds currently undergoing land use change, the Corps of Engineers selected six study basins distributed across the U.S. Landsat data were used to classify the present land use and were tested against conventional data in the simulation of the flood flows from the six basins.

RECENT RESULTS

The Water Management and Control ASVT has proven that Landsat land use data can be used to generate discharge frequency curves virtually identical to the conventional curves on all basins tested (Figure 10G-1). The selection of the Landsat-based curve would result in the design of a flood control system that would be no different from the conventional approach. On a watershed basis, Landsat land use classifications differed from conventional ones by only 2-8 percent. In addition, it was found that the Landsat data could be directly incorporated in the Corps of Engineers grid cell data bank, thereby providing an automated environment for applying Landsat classifications in routine hydrologic investigations.

SIGNIFICANCE

The potential for significant cost savings by employing Landsat hydrologic land use data has been demonstrated on the study watersheds. The Landsat costs are approximately one quarter to one half the costs of the conventional methods on basins greater than 10 mi^2 (25 km^2). Associated analysis of the ASVT data indicates that differences in relative effectiveness of the

conventional and Landsat methods for obtaining land use for hydrological modeling purposes for each of the test basins are insignificant.

FUTURE EMPHASIS

The degree of improvement in hydrologic land use classifications using improved resolution Landsat-D data will be tested. The Corps of Engineers will participate in this phase of the study in specific locations such as the Upper Mississippi River basin. Applications for hydrologic modeling and floodplain information surveys will be examined.

LANDSAT AND CONVENTIONAL DISCHARGE FREQUENCY CURVES GENERATED USING THE STORM MODEL FOR THE PENNYPACK CREEK BASIN (55.74 MI^2)
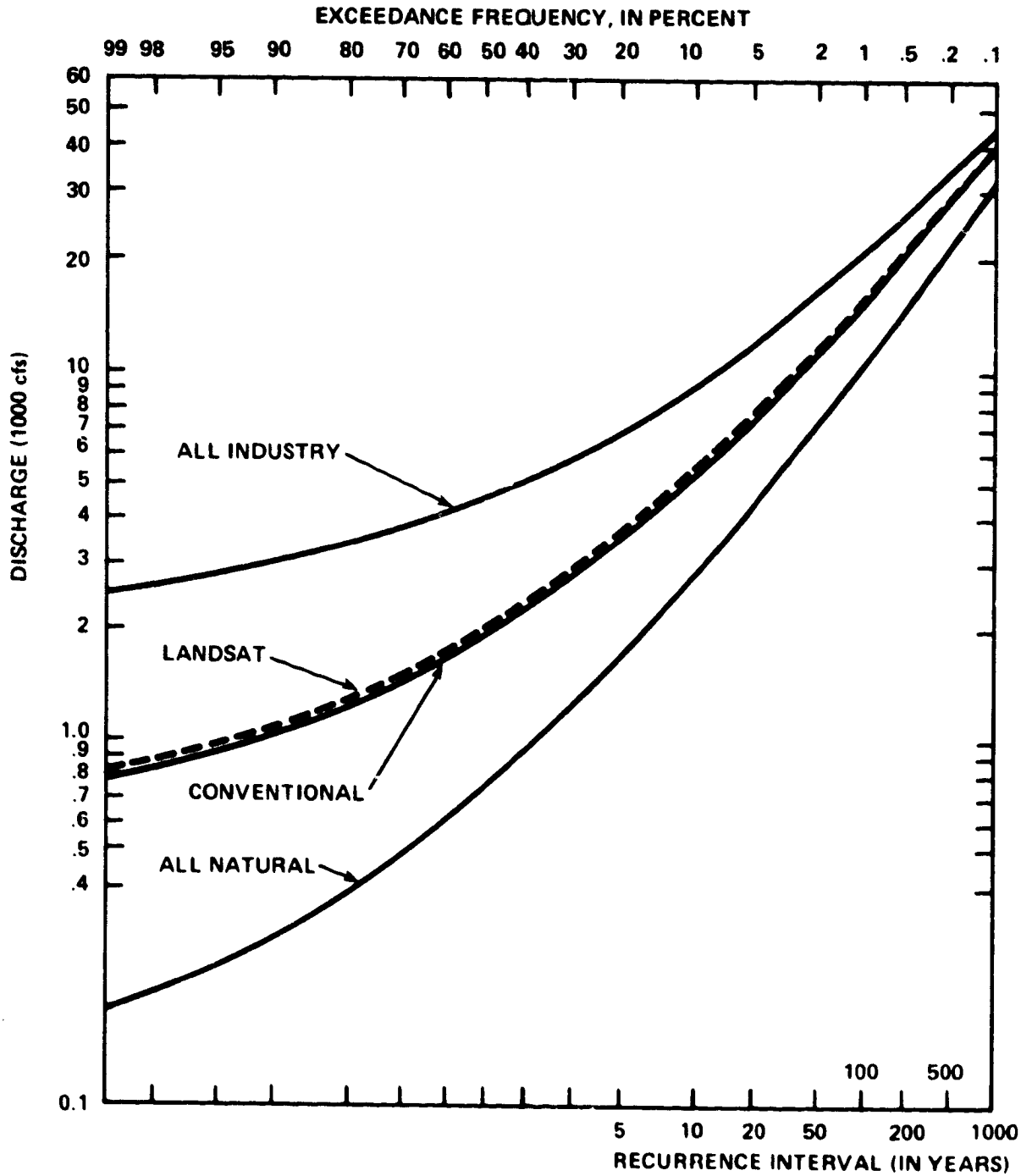
H. ANALYSIS OF AUFEIS SOURCE WATER ON THE ARCTIC SLOPE OF ALASKA

by

D. K. Hall

OBJECTIVE

The objective of this work was to determine the origin of the water which forms large aufeis fields (river icings) in the continuous permafrost region of the Arctic Slope of Alaska.

BACKGROUND

In July of 1978 and 1979, field parties took measurements of aufeis extent and thickness, and collected samples of aufeis water for subsequent laboratory analysis. A NASA Convair-990 overflight accompanied the field work in July of 1978. Aerial photographs were obtained and used to determine the precise location of the aufeis within the stream channel, and the shape and extent of the aufeis for comparison with aufeis as seen on Landsat imagery. June Landsat data were used to measure the maximum extent of aufeis fields on the eastern Arctic Slope of Alaska. These measurements were used to determine the interannual variability of the maximum extent of aufeis on the Arctic Slope of Alaska.

RECENT ACCOMPLISHMENTS

Through measurement of the interannual variability of aufeis extent using June Landsat MSS and RBV imagery (1973 - 1979), it was determined that the areal extent of larg aufeis fields does not follow meteorological trends, contrary to theory. Thus, the aufeis feed-water could not be local (i.e.from streamflow). Field and laboratory measurements corroborated this when the melted aufeis water was found to contain large amounts of calcium carbonate which is abundant only in the Brooks Range and foothills approximately 100 km to the south, but not in adjacent upstream stream water. The average amount of calcium (as $CaCO_3$) in the aufeis samples was 321.6 mg/l; the adjacent river water contained only 44.7 mg/l of calcium.

The aufeis feed-water travels northward through a network of unfrozen zones within the continuous permafrost which is probably comprised of an interconnecting system of tectonic faults. Tectonic faults are prevalent on the eastern Arctic Slope where the aufeis is located, and rare on the western Arctic Slope where no large stream aufeis exists.

SIGNIFICANCE

Aufeis can cause much damage during construction in permafrost regions and can be inadvertently created by man if the natural flow of groundwater is interrupted and the dynamics of aufeis formation is not understood. Its existance can be beneficial because it is fresh (spring) water, and potable

water is scarce in the Arctic especially during the winter. In addition, the results of this research indicate that there are probably more tectonic faults in the eastern Arctic Slope than have been mapped, because the feed-water needs passageways through which to flow within the impermeable permafrost.

FUTURE EMPHASIS

The June aufeis extent will continue to be measured in subsequent years using Landsat MSS and RBV data. This will enable quantitative determination of the relationship between meteorological factors (precipitation and severity of freezing (as expressed in freezing degree days)) and aufeis extent.

PUBLICATIONS

Hall, D. K., 1980: Mineral Precipitation in North Slope River Icings. Arctic, V. 33, pp. 343-348.

Hall, D. K., 1980: Analysis of the Origin of Water Which Forms Large Aufeis Fields on the Arctic Slope of Alaska Using Ground and Landsat Data. Unpublished Ph.D. thesis, Univ. of MD, 120 pp.

Hall, D. K., 1980: Use of Landsat Data for River and Lake Ice Engineering Studies. To appear in River and Lake Ice Engineering, a book to be published jointly by the U.S. Army CRREL and the IAHR Committee on Ice Problems, 12 pp. (Also NASA TM 80686.)

Hall, D. K. and C. Roswell, 1980: Analysis of the Origin of Aufeis Feed-Water on the Arctic Slope of Alaska. NASA TM 81992, 41 pp.

I. LANDSAT DIGITAL ANALYSIS OF THE RECOVERY OF BURNED TUNDRA IN ALASKA

by

D. K. Hall and J. P. Ormsby

OBJECTIVE

The main objectives of this study were: A) to evaluate the regeneration of tundra following a wildfire; B) to categorize burn severity (within the burned area); C) to compare ground and satellite observations for use in estimating vegetation regrowth following a tundra fire.

BACKGROUND

Between July 26 and August 12, 1977, a wildfire burned a 48 km^2 area in north-western Alaska near the Kokolik River. In August 1977 and 1978, field measurements were made by Cold Regions Research and Engineering Laboratory (CRREL) scientists on the site of the tundra fire, and in July 1978 imagery was obtained during a NASA Convair-990 aircraft overflight of the site. Landsat digital tapes of the area were obtained for four time periods: before the fire occurred (July 1977), during the fire (early August 1977), less than 1 month after the fire stopped (August 1977) and approximately 1 year after the fire stopped (August 1978). Portions of these tapes were analyzed using the Atmospheric and Oceanographic Image Processing System (AOIPS).

RECENT ACCOMPLISHMENTS

Three categories of burn severity were delineated based on spectral reflectance of Landsat Band 7 data. The spectral reflectances within the categories: lightly-, moderately- and severely-burned tundra were measured for the August 21, 1977, and the August 14, 1978 subscene. Table 10I-1 shows that the spectral limits increased in 1978 in all three categories of burn severity. This corresponded to an increase in regrowth of vegetation which was observed in the field. Portions of the lightly-burned category were inferred to be fully recovered based on the Landsat data because the spectral response of these portions was the same as that of nearby unburned tundra. This was confirmed in the field for selected areas.

SIGNIFICANCE

The amount of time required for recovery of tundra following a fire is unknown. Damage is dependent upon various factors including: type of vegetation, proximity of ground ice to the surface, elevation, drainage, and meteorological conditions (rain and wind) prior to and during the fire.

Landsat recorded the events during and after the Kokolik River tundra fire. Landsat data proved to be a convenient and inexpensive way to monitor vegetation regrowth (and thus infer recovery) following a wildfire, and to evaluate the effects of fire in this remote area. The response of tundra to surface disturbances is important especially in light of the increasing use of the Arctic for oil exploration.

TABLE 10I-1. Spectral Limits of the August 21, 1977 and August 14, 1978
Subscenes of the Burned Area from Band-7 Density Slices

		Spectral Limits	
Theme	Name	August 21, 1977	August 14, 1978
1	Water	0 – 3	0 – 8
2	Severely burned and smaller lake	4 – 12	9 – 31
3	Moderately burned	13 – 24	32 – 51
4	Lightly burned	25 – 44	52 – 64

FUTURE EMPHASIS

CRREL scientists are continuing to measure tundra regeneration at the site
of the fire. After more Landsat tapes are acquired at GSFC (e.g. August 1979,
1980 and 1981), the spectral reflectances will again be compared with the
in-situ measurements and with the August 1977 and 1978 results in order to
determine longer term recovery characteristics of burned tundra.

PUBLICATIONS

Hall, D. K., J. Brown and L. Johnson, 1978: The 1977 Tundra Fire in the
Kokolik River Area of Alaska. Arctic, V. 31, pp. 54-58.

Hall, D. K., J. Brown and L. Johnson, 1978: The 1977 Tundra Fire at Kokolik
River, Alaska. CRREL SR 78-10, 11 pp.

Hall, D. K., J. P. Ormsby, L. Johnson and J. Brown, 1980: Landsat Digital
Analysis of the Initial Recovery of Burned Tundra at Kokolik River,
Alaska. Rem. Sens. of Environ., V. 11.

Chapter 11

ADVANCED STUDIES

edited by

John Barker

OVERVIEW

The goal of the Earth Resources Advanced Studies Group is to
provide performance simulation capability to assist in the
feasibility, definition, design, and fabrication trade-off
studies of future sensor systems for applications in renewable
and non-renewable resources. The approach is both passive and
active; that is, to maintain a familiarity with research and
development efforts of others, as well as maintaining and developing
a capability to model key phases in the end-to-end system in our
own facilities, from spectral and spatial characteristics of
typical targets, through sensor and supporting spacecraft systems,
through processing and finally through value assessment. Part
of this goal is to identify critical areas where new research
should be done in order to evaluate the potential impact on
future satellite missions.

Previous efforts of the advanced studies group have included:
(1) Simulating of the expected performances of Landsat-D for
Crop Production Forecasting ("Sigma Squared"), (2) designing
and implementing a field research program in collaboration with
USDA in Beltsville, Maryland for collecting spectra of crops under
measured conditions for simulating the performance of future
sensors, and (3) evaluating the potential and designing a research
plan for the use of remotely sensed data for improving decisions
in the management of crops ("AM1", Agricultural Management
Information).

Two 1979 efforts (Williams et al., 1979, and Irons and Wharton, 1979)
were not active during 1980 but are expected to become active again
in 1981. One was the Landsat-D Assessment System activity which
has the objective of providing a facility and capability to perform
analyses that will quantify the engineering and technological
advantages afforded by the Thematic Mapper Scanner, relative to
MSS capability. Funds have not been available for Landsat-D
assessment studies in 1980. The other effort was analysis of data
from aircraft flights of a linear array pushbroom radiometer (LAPR)
to demonstrate and evaluate the utility of data acquired by a
linear array instrument for remote sensing applications. A publi-
cation was produced on this 1979 work (Wharton, Irons and Huegel,
1980). Consideration is being given to further MLA aircraft flights
and analysis in 1981.

In 1980, the major effort was to support the engineers in a value assessment part of a multispectral linear array (MLA) sensor feasibility study for an operational land observing system (OLOS). It involved inputs from more than fifty perople, approximately half of them were remote sensing specialists at Goddard. Results are documented in the Final Report of the feasibility study, primarily in the appendices. Titles and authors for three of the activities in advanced studies reported on for 1980, are given below, by section:

A. Value Assessment of an Operational Land Observing System
    John Barker

B. Simulating Information Content of Digital Imagery
    Mike Forman

C. Simulating Landsat Sensor Performance from Field Spectra
    Brian Markham, John Barker and Charles Schnetzler

Work in 1981 will center around both the Landsat-D assessment activity and the MLA/OLOS research activities. In addition, some effort needs to be given to the "ultimate" sensors and missions, primarily in the area of thermal and geostationary missions for land resources.

PUBLICATIONS

Irons, J. and S. Wharton, "C. Linear Array Pushbroom Radiometer Data Analysis", in Chapter 9: Advanced Studies of "Earth Survey Applications Division Research Report - 1979", NASA TM-80642 (1980), pp. 9-9 to 9-12.

Wharton, S.W., J.R. Irons and F. Huegel, "LAPR: An Experimental Aircraft Pushbroom Scanner", NASA TM-80729, July 1980, pp. 24.

Williams, D., D. Deering, K. Meehan and J. Tucker, "Landsat-D Assessment System", in Chapter 9: Advanced Studies of "Earth Survey Applications Division Research Report - 1979", NASA TM80642 (1980), pp. 9-2 to 9-5.

A. <u>VALUE ASSESSMENT OF AN OPERATIONAL LAND OBSERVING SYSTEM</u>

by

J. Barker

OBJECTIVE

The objective of this "value assessment" activity was to provide
the basis for the selection of the "most probable" sensor for the
U.S. Operational Land Observing System (OLOS) for the decade of
the 1990's.

BACKGROUND

In November, 1979, the President provided the framework within
which a civil operational land remote sensing satellite system
should be implemented under the management of the National Oceanic
and Atmospheric Administration (NOAA) in the Department of Commerce.
OLOS would provide images of the Earth for applications in many
areas of renewable and non-renewable resources, including: early
warning of changes in crop conditions, crop production forecasting
around the world, oil and gas exploration, mapping of land, charting
shallow waters, rangeland and forest management, water resource
management, urban and regional land-use planning, and monitoring
various types of episodic events. Since 1972, the National Aeronautics
and Space Administration (NASA) has been managing the experimental
precursors to OLOS, namely the three Landsat satellites. In the
1980's, NASA will probably build two or three more Landsat satellites
with a "Thematic Mapper (TM)" sensor in place of the current "Multispectral
Scanner Subsystem (MSS)". OLOS would replace these mechanical scanners
in the late 1980's with large multispectral linear arrays (MLA) of
solid state detectors. These arrays are oriented perpendicular to
the direction of the spacecraft flight and can be used to sense both
reflected and emitted radiation from the Earth. In effect, the satellite
sweeps the optics for the thousands of detectors over the ground track,
thereby providing an alternative to the rapidly oscillating mirrors
in the current cross-track mechanical scanning systems. This pushbroom
MLA technology has been identified as the sensor design for OLOS.

There are three primary advantages of using MLA technology for
satellite remote sensing. First, it has inherently better sensitivity
by a factor of up to 1000:1 due to the longer dwell time of each
detector. This can be translated into spectral bands as narrow as
10 nanometers while at the same time achieving a spatial resolution
of at least 10 meters for a ground-instantaneous-field-of-view (GIFOV).
Secondly, there are no moving optical parts during imaging which along
with the fixed position of the detectors can be used for more accurate
geometric location of points for map production. Thirdly, it has
the ability to adaptively select sampling rates which permits an

instrument to be flown at a variety of orbital altitudes and achieve a range of spatial resolutions. There are two major disadvantages of using MLA technology, both of which will presumably disappear with time. In the first place, large infrared MLA detectors need developing. In order to maintain a launch date in the 1980's, this means parallel mission definition and short wave infrared focal plane development (SWIR, 1.0-2.4 μm, micrometers). It also means an even longer time for thermal infrared array development (TIR, 2.5-15 μm), for possible addition of a separate thermal sensor to later missions. Secondly, calibration of thousands of detectors over a 15° field-of-view is required. This will require an unprecedented development of calibration methods and sources in order to achieve both spectral and radiometric equivalence to better than 0.5%. The clear inherent advantages of MLA technology are assumed to outweigh its current developmental di,advantages.

In late spring of 1980, a team of engineers and scientists at Goddard Space Flight Center began the effort of examining the existing information on the feasibility of using MLA sensors for OLOS. Scientists were asked to develop an approach to the value assessment of the various sensor options that were found to be useful and feasible by scientists and engineers. Study work was completed in July and documented in the fall.

Three approaches to value assessment were pursued in parallel: (1) survey and evaluate the scientific state-of-the-art capabilities, (2) compile, quantify and evaluate surveys of users collected by NOAA in 1980, and (3) identify and quantify a couple of illustrations of the economic value of OLOS data.

ACCOMPLISHMENTS

Scientific evaluation was obtained in two forms, reviews by specialists on key issues and interviews of key scientists both before and after the conducting of the feasibility study. The results were written up in the Value Assessment Chapter of the Final Report of the "Multispectral Linear Array Sensor Feasibility Study". An overview of OLOS scientific questions and twelve individual papers were included in Appendix C of that report (see Table of Contents of Appendix in Table 11A-1).

It was concluded that if one is restricted to six spectral channels in the 400 to 2500 nm (nanometers) range, the most probable bands would be at the approximate locations of those proposed for the Thematic Mapper. However, the design should remain flexible enough to change the exact location and width of the spectral bands as close to the launch date as possible, since several alternative bands have been identified which require further scientific study.

Existing thermal evidence strongly favored a TM thermal sensor for both discrimination and absolute temperature measurements if the overpass was at points of maximum thermal contrast close to solar noon and early in the morning. However, there was insufficent experimental evidence to demonstrate the utility of a 930 AM overpass which will occur at intervals greater than every day or so.

11-4

Spatially, there was evidence that new applications would be enabled as one went to better resolution, although there might be a necessity to average spatial elements together for some specific objectives where the error is classification of thematic categories might be increased because more detail was visible than desired. A sharpening band at two or three times the resolution of the other bands in the system was strongly favored for two reasons: (1) boundary definition can be significantly increased for visual interpretation and training site selection, and (2) errors in supervised classification procedures can be significantly reduced by the labeling of picture elements, pixels, which contain more than one type of category.

This evaluation, extensively documented in the papers listed in Table 11A-1, summarized the scientific information from which requirements for specific applications can be derived. It was then possible to provide scientific input to guide in the selection of the eleven spectral and spatial sensor options that were used in the systematic compilation of user surveys (Table 11A-2). Both user requirements and economic value assessments were then used in making an objective quantitative decision on what was the "most probable" sensor for an operational land observing system.

In 1980, NOAA assembled a comprehensive data base of user surveys for the purpose of determining OLOS sensor requirements. A major portion of our value assessment activity involved the systematic and quantitative extraction of requirements from this NOAA data base. User objectives were compiled for federal, state, local and private communities. Three quantitative procedures were developed for obtaining a single relative estimate of the value of each of eleven options identified by scientists and engineers. One measure was the annual required volume of 185 by 185 km images and the second was a measure of the fraction of programmatic requirements that were met by particular options. The third measure was a independent check on the first two. It used surveys of four discipline panels, each consisting of about five remote sensing specialists. These specialists were cognizant of research that many of the users had not seen. In addition, the panels were asked some questions that were necessary for a definition of an OLOS mission which had been omitted from the user surveys, such as required frequency of cloud-free coverage.

Results from user "Volume Requirements", "User Scores", and "Panel Scores" agreed in most major features between the eleven options identified in Table 11A-2. Naturally, the options with the higher capabilities received higher value scores. In order to identify a "most probable" OLOS sensor, these value estimates were divided by the relative cost of each option. Resulting value-to-cost ratios are given in Table 11A-3. The conclusion is that options 6, 7 and 8 are all about equally desirable according to this criterion. However, from an engineering standpoint option 8 would signficantly jeopardize an early launch of OLOS because large arrays of thermal sensors will require several years to develop. Future addition of a separate

thermal sensor requires an immediate parallel thermal sensor development program, along with a scientific effort to define the thermal requirements. Option 7 is a clear choice over option 6 because of the large incremental value expected from the sharpening band, especially for production of maps. Option 7 is therefore the current best estimate of the "most probable" sensor, based on the perceived needs by both the user and scientific communities.

Economic value assessment proceeded in parallel with the scientific and user survey activities. Two applications were researched efficiently to provide additional numerical estimates of the relative economic value of each sensor option. They were crop production forecasting and map production. These two applications are illustrative of agricultural and land use requirments. A non-quantitative survey was also undertaken of the potential benefits from reduced expenditures for the exploration of gas and oil, perhaps the largest economic benefit to be derived from remote sensing in the next twenty years. Finally, a literature research was conducted and documented for past economic analyses. Further work is needed to identify the exact mechanisms by which an economic benefit can be expected from remotely sensed data.

The one accepted economic model was for benefits realized because of more efficient storage of grain from improved monthly forecasts of expected wheat production. This wheat benefit model was parametized for error in area estimation as a function of spatial resolution. There were no useful experimental or theoretical results to permit simulations of the effect of adding SWIR or TIR bands to the four bands in the visible and near infrared region (760 to 1000 nm). Value-to-cost ratios for wheat benefits in Table 11A-3 show that a 30-meter system, options 4-8, captures most of the value for wheat, which is grown in large fields.

A second measure of economic value was made for map-making, which is currently done largely by aerial reconnaissance and represented a 900 million dollar market in 1979. Projections were made of map requirements in 1995. Analysis showed that more than 60% of the maps will be at the new 1:20,000 metric scale primarily from topographic, census and road maps. Without ground control points, registration of images will produce absolute ground locations from OLOS to an accuracy of about 100m, and none of the eleven options could be used to produce acceptable position locations for 1:20,000 scale maps. With ground control points, pixels can be located relative to their neighbors to an accuracy of better than half a pixel, thereby enabling map production of a 1:20,000 scale from a 10-meter OLOS system, namely options 9-11, at an altitude of 705 km. If these relatively infrequent mapping requirements are met while a satellite is still at its pre-boost altitude of 283 km from the space shuttle, then the 30-meter OLOS options with a sharpening band, namely options 5, 7 and 8, are satisfactory. Value-to-cost results for the 705 km orbit are also summarized in Table 11A-3 for the illustrative mapping examples.

In summary, all value assessment procedures showed a significant maximum in value-to-cost for 30-meter systems. Map production showed an apparent need for a 10-meter system which might be met with a 30-

meter system flown at its lower initial insertion orbit from the space
shuttle; this possibility requires serious further examination since a
separate MAPSAT mission is not likely in addition to an OLOS mission.
Scientific panel members saw a 50% incremented value from the addition
of SWIR bands to the current bands in the visible/near infrared regions.
Neither user nor panelists saw more than a 20% increase in value from
further addition of a thermal band; which is probably due to lack
of familiarity with experimental data rather than to the absence
of value in a TIR band. The "most probable" sensor is therefore expected
to be option 7 initially, with possible addition of a separate thermal
sensor at a later time.

SIGNIFICANCE

Objective reproducible value assessment procedures were developed and
implemented in the MLA Sensor Feasibily Study. Goddard engineers
produced requests in December, 1980 for follow-on sensor definition
studies from contractors, with procurement requests sufficiently
focused on option 7, or better, to permit a concrete evaluation of
the proposals. Finally, these evaluations have also helped identify
the potential scientific and applied research studies which are a
necessary compliment to the SWIR and TIR sensor development activities
and to the OLOS mission feasibility studies.

FUTURE EMPHASIS

Sensor science support will continue as part of the SWIR development
activity. Some level of scientific study is also needed in conjunction
with the TIR array development activity. Supporting science activities
are also planned under the OLOS mission feasibility study.

It is anticipated that all of the above MLA/OLOS Supporting Requirements
and Assessment Activities will be coordinated by the OLOS Study
Scientist and be grouped into three categories: (1) OLOS Requirements
and Integration Tasks, (2) OLOS Information and Assessment Tasks,
and (3) OLOS Economic Assessment Tasks. The overall objective of
this effort is to provide information and value assessment support
during the feasibility studies, definition, fabrication, trade-off
and assessment activities of MLA sensor and OLOS projects. In order to
accomplish this objective it will be necessary to develop quantitative
analytical capabilities of information and value assessment, including
illustrative results.

PUBLICATIONS

"Multispectral Linear Array Sensor Feasibility Study", Goddard
    Draft Final Report dated November, 1980, 224 pp.

Barker, J.L., V.V. Salomonson, P.J. Cressy and C.C. Schnetzler,
    "Landsat Observing Systems in the 80's and Value to Users," talk
    presented at American Institute of Aeronautics and Astronautics
    Conference on Sensor Systems for the 80's in Colorado Springs,
    Colorado, 2-4 December, 1980.

Table 11A-1

Final Report of MLA Sensor Feasibility Study
Appendix: Table of Contents
by
Goddard Space Flight Center
December, 1980

Table 11A-2

SPECTRAL AND SPATIAL CHARACTERISTICS OF MLA SENSOR OPTIONS
(185 KM SWATH AT 705 KM ALTITUDE)

SPECTRAL REGION	NOMINAL BAND LOCATION (MICRO METERS)	TM*	INSTANTANEOUS-FIELD-OF-VIEW (IFOV) BY OPTION (METERS)										
			1	2	3	4	5	6	7	8	9	10	11
			80m SYSTEMS			30m SYSTEMS					10m SYSTEMS		
VISIBLE (VIS)	TM1 0.45-0.52	30	80	80	80	30	30	30	30	30	10	10	10
	TM2 0.52-0.60	30	80	80	80	30	30	30	30	30	10	10	10
	TM3 0.63-0.69	30	80	40	40	30	15	30	15	15	10	10	10
NEAR INFRARED (NIR)	TM4 0.76-0.90	30	80	80	80	30	30	30	30	30	10	10	10
SHORTWAVE INFRARED (SWIR)	TM5 1.55-1.75	30	–	–	80	–	–	30	30	30	–	20	20
	TM6 2.08-2.35	30	–	–	80	–	–	30	30	30	–	20	20
THERMAL INFRARED (TIR)	TM7 10.4-12.5	120	–	–	–	–	–	–	–	120	–	–	60
ASSUMED OPTION IFOV		30	80	60	60	30	22	30	22	22	10	10	10

KEY TO SENSOR OPTIONS			1	2	3	4	5	6	7	8	9	10	11
	VIS/NIR		80	80/40	80/40	30	30/15	30	30/15	30/15	10	10	10
	SWIR		–	–	80	–	–	30	30	30	–	20	20
	TIR		–	–	–	–	–	–	–	120	–	–	60

SOLID STATE MSS   ADVANCED SOLID STATE TM*

*THEMATIC MAPPER SCANNER SCHEDULED FOR LAUNCH ON LANDSAT IN 1982

Table 11A-3

RELATIVE VALUE-TO-COST COMPARISONS FOR OLOS/MLA SENSOR OPTIONS

PERCENT OF MAXIMUM VALUE BY SENSOR OPTION

	1	2	3	4	5	6	7	8	9	10	11
RELATIVE COST											
COST TO GOVERNMENT	34	36	37	41	45	46	48	53	84	93	100
VALUE-TO-COST RATIOS											
VOLUME REQUIREMENTS	75	72	84	86	79	100	95	95	51	58	71
USER SCORES	69	70	79	83	79	92	90	100	44	50	54
PANEL SCORES	41	50	77	68	67	93	94	100	38	59	60
WHEAT DISTRIBUTION BENEFITS	34	79	77	100	92	90	86	79	50	45	42
MAP RECTIFICATION VALUE (WITH CONTROL POINTS)	31	41	50	40	38	44	45	50	100	94	93
MAP REGISTRATION VALUE (WITHOUT CONTROL POINTS)	58	73	95	88	81	99	94	100	49	54	64

KEY TO SENSOR OPTIONS	1	2	3	4	5	6	7	8	9	10	11
VIS/NIR	80	80/40	80/40	30	30/15	30	30/15	30/15	10	10	10
SWIR	-	-	80	-	-	30	30	30	-	20	20
TIR	-	-	-	-	-	-	-	120	-	-	60

SOLID STATE MSS (column 1)

ADVANCED SOLID STATE TM* (column 8)

*THEMATIC MAPPER SCANNER SCHEDULED FOR LAUNCH ON LANDSAT IN 1982

11-11

B.   SIMULATING INFORMATION CONTENT OF DIGITAL IMAGERY

by

M. Forman

OBJECTIVE

The goal of this effort is to obtain, maintain and evaluate digital imagery of terrestrial scenes for the purpose of quantifying the characteristics and capabilities of future satellite sensor systems. Sources of imagery include aircraft and satellite scanners, digitized photography and computer generated scenes.

This project has the following specific objectives:

    a.   Collect and analyze existing data sets which are suitable for general simulation studies.

    b.   Analyze aircraft sensor data which may be applicable to simulation studies.

    c.   Disseminate data to interested parties.

    d.   Generate requirements for new sets of data utilizing existing instrumentation.

    e.   Develop software for the purposes of simulation from synthetic and real data.

BACKGROUND

When new instruments are considered for remote sensing applications, it is often advantageous to have access to data sets which can be used to simulate predicted spacecraft responses. Effects of abnormal instrument or spacecraft performance on the output data can also be analyzed.

A few years ago, there was an interest in assessing classifier accuracy as a function of data compression method. There was no absolute truth to compare against. Therefore, a computer program was developed to generate a random ground truth map for a given number of classes. Spectral signatures drawn from a "bank" could then be associated with each class, spatial resolutions could be assigned, and the data set could then be degraded to simulate satellite data.

ACCOMPLISHMENTS

This past year, a study was undertaken to simulate underlap in the TM Scanner. Another problem, relating to the detection of similar signals in the presence of noise, led to the acquisition of some LACIE super site data, along with associated ground "truth" observations digitized and registered to the imagery.

During the past year various data sets have been acquired, but not analyzed in depth. These are listed in Table 11B-1.

11-12

Table 11B-1

SCENE	TYPE	RESOLUTION	BANDS	SIZE PIXELS
1	Cultural	3m	1	4096 x 4096
2	Geologic	3m	1	4096 x 4096
3	LACIE Site A	80m	4	196 x 118
4	LACIE Site B	80m	4	196 x 118

Scenes 1 and 2 are digitized aircraft photographs and have use in applications relating to spatial analysis. Scenes 3 and 4 are both multispectral and temporal and have associated ground truth maps and photos.

The 3-meter resolution scenes have been used to simulate expected Landsat-D performance, including studies of underlap data acquisition by the Thematic Mapper (TM) caused by satellite height variations, and studies relating to jitter caused by vibrational interactions of the TM, Multispectral Scanner (MSS) and the antenna. The Multispectral data scenes are being used as input for a planned demonstration of the Massively Parallel Processor (MPP) classification capability.

The calibration data which is routinely acquired by the Thematic Mapper Simulator (TMS) was found to have a radiometric value much below the specified 8 bit level in the visible and near infrared regions. Additionally, the single lamp, single point calibration methods used are unreliable and inaccurate. Thus data acquired by the TMS is of doubtful utility for the objectives of this project.

SIGNIFICANCE

Artificial target simulation is essential when there are few experimental images. However, our ability to adequately capture the spectral and spatial variations of a real scene is not yet developed. This type of target simulation will have increasing importance when the models work well enough to simulate the complete range of target and atmospheric conditions.

FUTURE EMPHASIS

Efforts should be made to generate synthetic scenes, and acquire sets of digital aircraft imagery and associated ground and atmospheric observations, for the purpose of testing various MLA sensor options and OLOS mission scenarios. Financial support needs to be identified for both software development and data acquisition.

PUBLICATIONS

Forman, M.L. "The Use of Thematic Mapper Simulator Calibration Data for Assessment of Data Quality", submitted for TM publication, December, 1980.

C. SIMULATING SENSOR PERFORMANCE FROM FIELD SPECTRA

by

B.L. Markham, J.L. Barker and C.C. Schnetzler

OBJECTIVE

The purpose of this study was to develop and evaluate a procedure and a computer capability for comparing the performance of current Landsat Multispectral Scanner (MSS) and the expected 1982 Landsat Thematic Mapper (TM) sensor using ground-acquired reflectance spectra.

Two specific applications of this tool were to:

     a.   Examine the feasibility of simulating MSS data from TM data in order to provide continuity of service.

     b.   Illustrate the potential value of bands that are narrower than TM bands.

BACKGROUND

There is a general need to be able to use laboratory, field and aircraft spectra to simulate the expected performance of proposed new sensors. The Thematic Mapper to be carried on Landsat-D incorporates a number of engineering improvements over the Multispectral Scanners on earlier Landsats: These changes include additional spectral bands and increased spectral and radiometric resolution. These improvements are designed to increase the usefulness of the data for monitoring Earth resources. This study is designed to provide a tool for quantifying the increased utility resultant from these changes.

Continuity of MSS data may prove important during the transition to new TM sensors. There is currently a relatively large body of users that have become accustomed to using Landsat MSS-type data. They are familiar with the MSS response to various ground features and have systems and procedures designed to work with MSS data that provide adequate information for their needs. Most advanced sensors as envisioned for operational land observing systems will have finer spatial and radiometric resolutions and different as well as narrower spectral bands (TM bandwidths or narrower). Without simulation of MSS data from the advanced sensor data, the user's procedures and systems would have to be extensively revised or redeveloped to use the new data. In addition, at the time of the launch of such an operational system there will be nearly 20 years of MSS-type data on record. Historical comparisons will be enhanced if the advanced sensor data can be modified to look like MSS data. A comparision of the sensor options in terms of their amenability to MSS simulation is therefore necessary.

In the past, the band width of sensors on satellite scanners has been limited by the signal-to-noise ratio of the detectors. With the increased dwell time of multi-linear arrays proposed for use in missions in the 1990's, it will be possible to achieve band widths of 10 nanometers, or less. There are several potential reasons to narrow spectral bands:

a. Increase discrimination and identification of target objects as a result of greater target-to-background contrast.

b. Locate spectral regions with reduced atmospheric interference.

c. Locate spectral regions with increased atmospheric contributions in order to make atmospheric corrections.

d. Place bands in regions of flat target response to reduce target-dependent stripping between detectors with slightly different spectral responses.

One illustrative example to quantify the first of these potential advantages is to simulate the increased sensitivity of infrared/red ratios using different band widths. This ratio is commonly used to identify living vegetation in Landsat images.

ACCOMPLISHMENTS

Algorithms have been developed and implemented on an HP-3000 mini-computer. The resulting program accesses field reflectance spectra stored in an on-line data base and generates simulated MSS/TM sensor outputs. The field reflectance measurements collected in narrow spectral bandwidths between 0.4 and 2.5 um with a Barnes spectro-radiometer are converted to radiances and passed through a simulated atmosphere (Turner and Spencer, 1972) for one of three haze conditions and one of three sun angle conditions. These 'at-satellite' radiances are integrated across the band passes of the TM and MSS channels. Integrations can be performed either using an assumed square wave response or using a spectral weighting function corresponding to actual or predicted sensor performance characteristics.

Simulated MSS or TM data can be output as radiances or linearly quantified digital counts. Quantization noise can be used to simulate sensor noise to allow comparison of radiometric sensitivity differences between the sensors.

In the first example of such a simulation, Barnes spectral reflectometer spectra of corn and soybeans, taken throughout the 1978 growing season on 6 plots at Beltsville Agricultural Research Center, BARC, were used to simulate the four MSS bands and the six reflective TM bands. Results are given in Table 11C-1 for recommended simulations of MSS from TM bands.

Figure 11C-1 illustrates that for MSS bands 4, 5 and 7, more than 99.5% of the MSS variance can be simulated using single TM bands. With simulations of this accuracy, it is likely that any significant vegetative information directly derivable from these three MSS bands will also be derivable from MSS bands simulated from TM data.

Figure 11C-2 illustrates the correlation between observed MSS6 and predicted MSS6, using 3 TM bands and using 2 TM bands. The recommended two band combination will probably be less sensitive to potential atmospheric interference. It is possible that some vegetative information derivable from MSS6 will not be derivable from a TM simulator of MSS6.

Table 11C-1

MSS Simulation From TM Bands For Agriculture

MSS BAND SIMULATED	TM BAND(S) USED	AMOUNT OF VARIANCE ACCOUNTED FOR	RECOMMENDED SIMULATIONS OF MSS FROM TM
4	2	99.96%	Yes
5	3	99.92%	Yes
6	4	86.20%	No
6	3,4	97.01%	Yes
6	1,2,4	99.16%	No
7	4	99.56%	Yes

The conclusion is that MSS bands can indeed be radiometrically simulated to better than 1% in the variance from TM bands. Recommended bands for this simulation are given in Table 11C-1. Potentially, this might be important if an on-board MSS simulator were considered to replace a real MSS sensor on the new TM missions.

A second simulation study examined the possible value of narrower spectral bands. 1979 spectra of bare soil and full canopy covered soybeans were used to simulate MSS, TM and 15 nanometer narrow bands in the red and near infrared positions of the spectrum. After normalization of all simulated radiances to unity for zero crop cover, the relative sensitivity at various crop covers was found by ratioing TM and MSS bands. The narrower TM3 was 6% more sensitive than MSS 5 at 100% cover. TM4 was 4% more sensitive than MSS 7. Figure 11C-3 illustrates the reason for the increased contrast in the red chlorophyll absorption region and the resulting improved sensitivity of TM3 to MSS5 and the even greater improvement of RED 15 to MSS5. It also illustrates a slightly less significant increase in sensitivity for TM4 and MSS7 and for IR15 to MSS7; this lower sensitivity is due to the broader peak in the near infrared region than in the red region.

SIGNIFICANCE

This program provides a method and capability to compare MSS and TM sensor performance for monitoring earth resources targets in terms of their spectral and radiometric characteristics. Relatively simple modifications of the program allow simulation of sensors with other bandwidths in the 0.4-2.5 μm region, as was done for the Landsat

11-16

Solid-State Sensor System Study (LS^3).

This capability to simulate at-satellite radiance from spectra
compliments the simulations done with fixed band scanners from
aircraft. It allows one to address questions of band numbers,
location, width and signal-to-noise before examining spatial
questions. This will be important in the trade-off studies
that will come with the definition and fabrication of an operational
land observing system for the 1990's.

FUTURE EMPHASIS

It is anticipated that this program will receive continued used with
the Barnes spectroradiometer studies. Potential modifications of the
program include options to add guassian 'white' noise and signal
dependent noise to better simulate sensor noise characteristics.
It may also be necessary to add water vapor and carbon dioxide
absorption terms into the atmospheric model.

REFERENCES

Turner, R.E. and M.M. Spencer, 1972. "Atmospheric Model for Correction
    of Spacecraft Data". In proceedings of the International Symposium
    on Remote Sensing of Environment, held at Ann Arbor, MI pp. 895-933.

Figure 11C-1

SIMULATION OF MSS BANDS BY TM BAND SUBSTITUTION
TM & MSS BANDS SIMULATED FROM FIELD ACQUIRED REFLECTANCE SPECTRUM
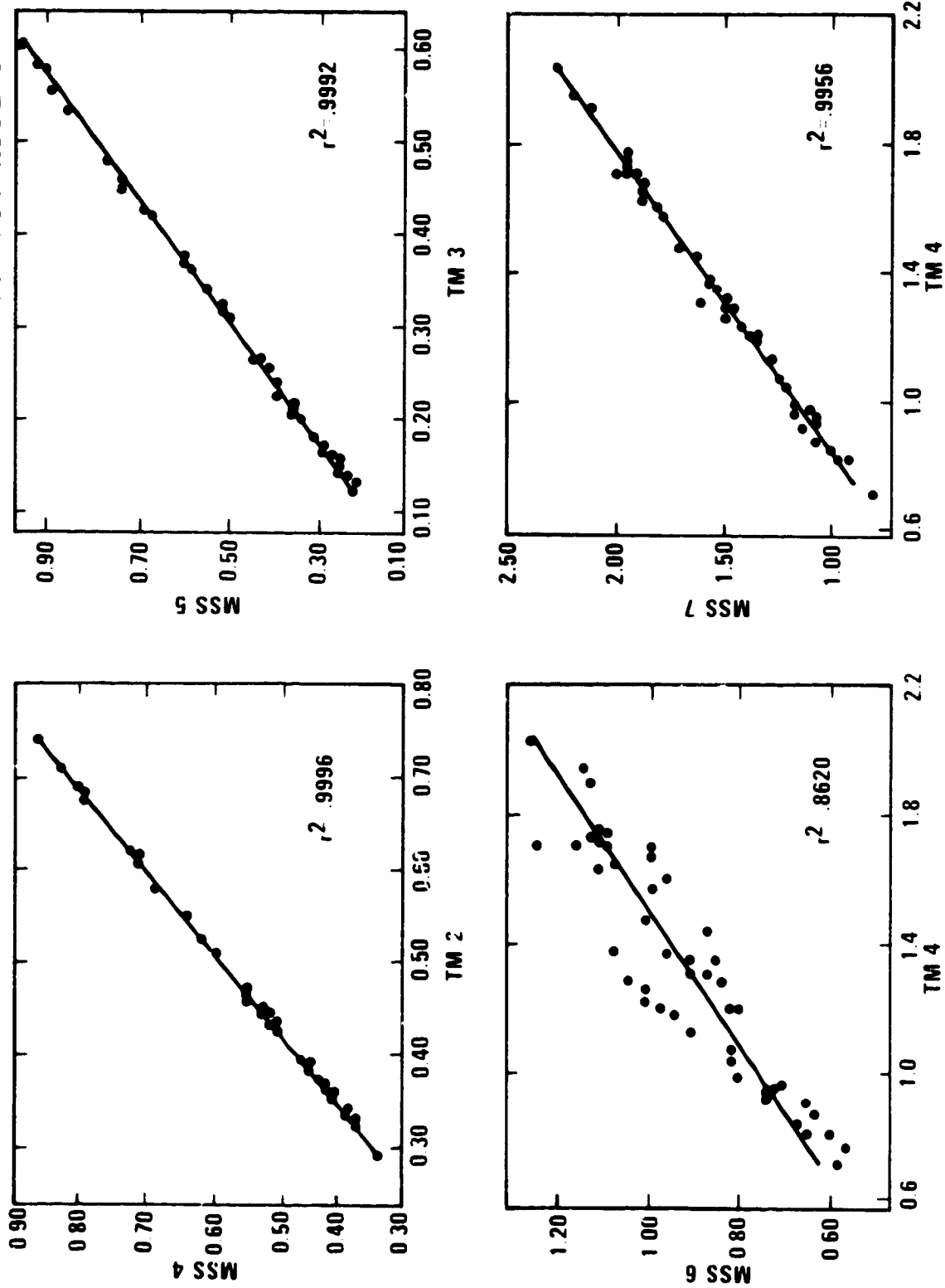
Figure 11C-2

TM BAND COMBINATIONS FOR MSS6 SIMULATION

DATA FROM FIELD-ACQUIRED SOIL/CROP REFLECTANCE SPECTRA

- BEST COMBINATION OF 3 BANDS FOR CONSTANT ATMOSPHERIC CONDITIONS
  TM4, TM2, TM1

- SIMULATION FROM SPECTRALLY CLOSEST BANDS: TM4, TM3

- SIMULATION POTENTIALLY LEAST AFFECTED BY ATMOSPHERE

$r^2 = .9916$

$r^2 = .9701$
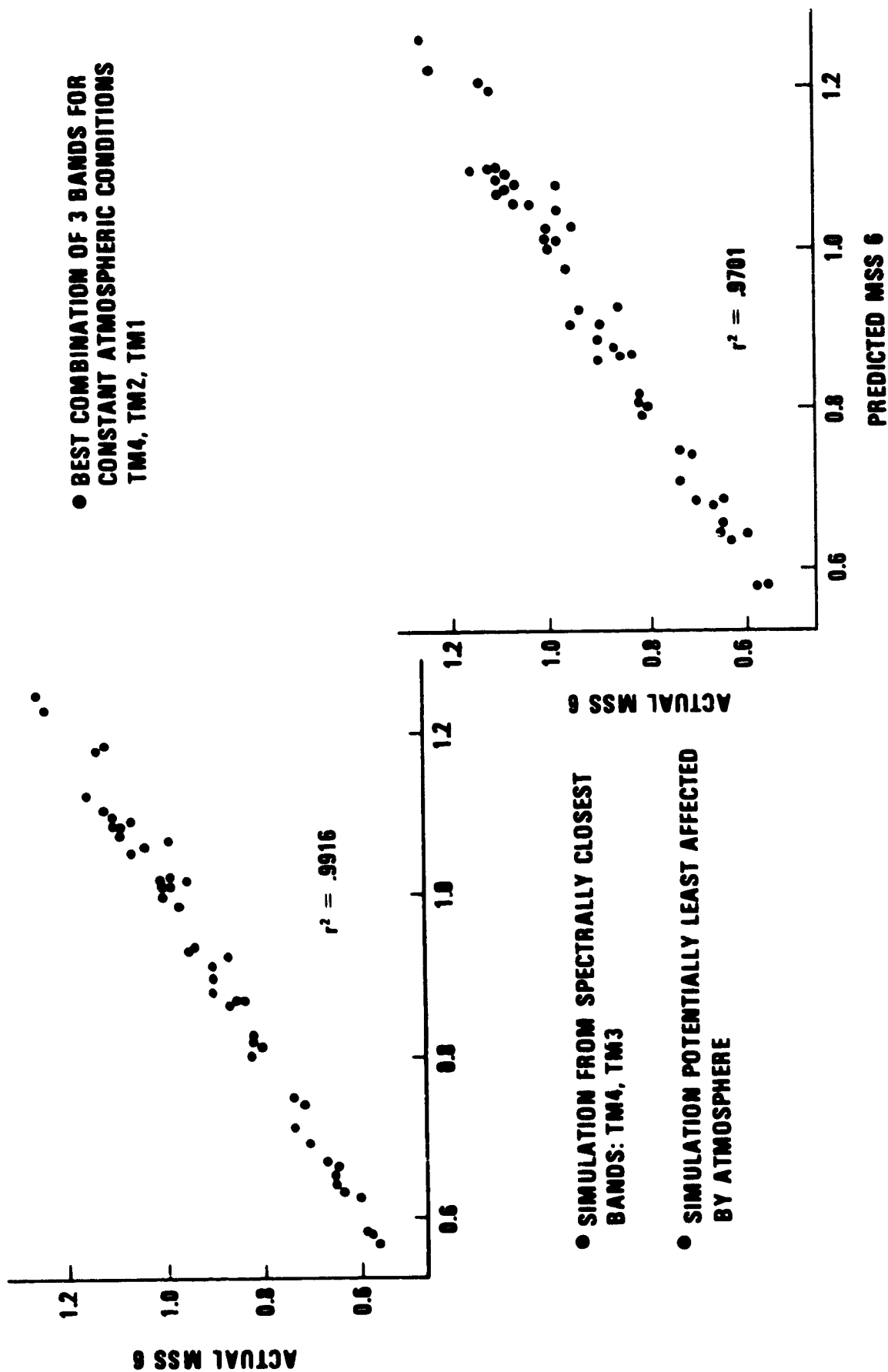
SENSITIVITY IMPROVEMENT

● PROPER PLACEMENT OF NARROW BANDS
   PERMITS MAXIMUM TARGET - BACKGROUND CONTRAST
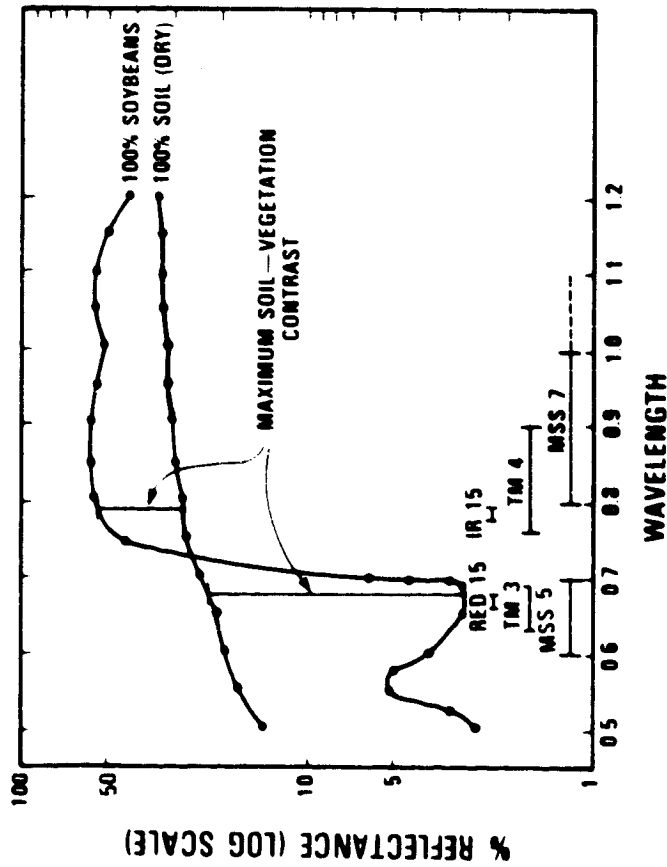
● NARROW BANDS PROVIDE MAXIMUM
   SENSITIVITY
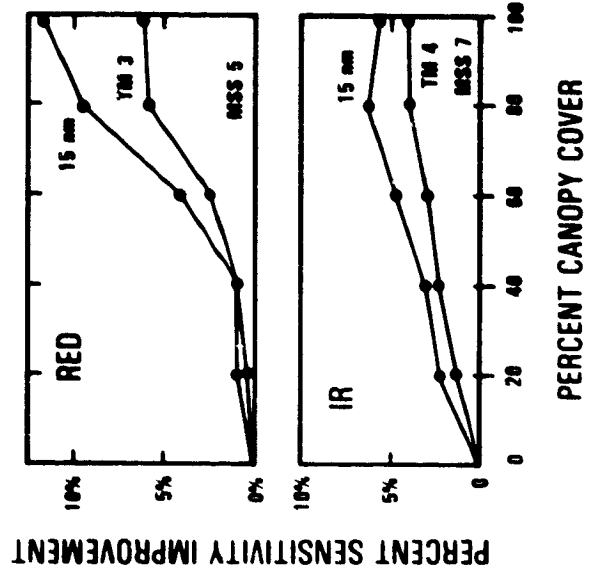
ACRONYMS AND ABBREVIATIONS

AgRISTARS	Agriculture and Resources Inventory Surveys Through Aerospace Remote Sensing
AGU	American Geophysical Union
ALTKAL	Linear Filter for Altimeter Data
AMI	Agricultural Management Information
AOIPS	Atmospheric and Oceanographic Image Processing System
APL	Applied Physics Laboratory
APT	Applications Pilot Test
ARIES	Astronomical Radio Interferometric Earth Survey
ASVT	Applications Systems Verification Test
ATS	Attitude Transfer System
BARC	Beltsville Agriculture Research Center
BIH	Bureau de l'Heure
BRDF	Bidirectional Reflectance Distribution Function
CDIST	Category Distribution Program
CLRS	Compact Laser Ranging System
COCORP	Consortium for Continental Reflection Profiling
CPU	Central Processing Unit
CRREL	Cold Regions Research and Engineering Laboratory
CV	Coefficient of Variation
DEM	Digital Elevation Model
ECOOE	East Coast Onshore-Offshore Experiment
EPA	Environmental Protection Agency
ERT	Effective Radiant Temperature
ESAD	Earth Survey Applications Division
ESMR	Electrically Scanning Microwave Radiometer
FOV	Field of View
GEM	Goddard Earth Model
GEODYN	Geodynamics Orbit Determination and Parameter Estimation Program
GHz	GigaHertz
GIFOV	Ground-Instantaneous-Field-of-View
GM	Gravitational Mass of the Earth
GPS	Global Positioning System
GRAVSAT	Dedicated Gravity Field Satellite
GSFC	Goddard Space Flight Center
ha	Hectare
HMS	Highly Mobile System (Laser)
IDIMS	Interactive Digital Image Manipulation System
IFOV	Instantaneous Field of View
I/O	Input/Output
IR	Infrared
IR15	Simulated 15 nm Band in NIR from 775 to 790 nm
ITI	Information Theory Inference
IUGG	International Union of Geodesy and Geophysics
JPL	Jet Propulsion Laboratory
kg	Kilogram
km	Kilometer
LACIE	Joint NASA/USDA/NOAA Large Area Crop Inventory Experiment
LAGEOS	Laser Geodynamics Satellite
LAI	Leaf Area Index
LANDSAT	Satellites Containing MSS and RBV Sensors for Observations of Land

LAPR	Linear Array Pushbroom Radiometer
LS3	Landsat Solid-State Sensor System Study
MAGSAT	Magnetic Field Satellite
MERIT	Monitoring of Earth Rotation and Intercomparison of Techniques
MLA	Multispectral Linear Array
Moho	Mohorovcic Discontinuity
MPP	Massively Parallel Processor
M^2S	Modular Multispectral Scanner
MSS	Multispectral Scanner
ND	Normalized Difference
nm	nanometer
NOAA	National Oceanic and Atmospheric Administration
NOSS	National Ocean Satellite System
NSWC	Naval Surface Weapons Center
OLOS	Operational Land Observing System
ORION	4m Highly Mobile VLBI System
OSTA	Office of Space and Terrestrial Applications
OVRO	Owens Valley Radio Observatory
PCA	Point of Closest Approach
POGO	Polar Orbiting Geophysical Observatory
PRISMS	Plan of Research for Integrated Soil Moisture Studies
RBV	Return Beam Vidicon
RRI	Renewable Resources Inventory
RVI	Ratio Vegetation Index
SAR	Synthetic Aperature Radar
SLR	Satellite Laser Ranging
SMMR	Scanning Multifrequency Microwave Radiometer
SSARR	Streamflow Synthesis and Reservoir Regulation
SWIR	Short Wave Infrared
TIR	Thermal Infrared Region
TLRS	Transportable Laser Ranging System
TM	Thematic Mapper
TMS	Thematic Mapper Simulator
TVA	Tennessee Valley Authority
TVDS	Transportable VLBI Data System
TVI	Transformed Vegetation Index
um	same as um = micron or micrometer = 10^{-6} m
USDA	U.S. Department of Agriculture
USDC	U.S. Department of Commerce
USDI	U.S. Department of Interior
USGA	U.S. Geological Survey
UT	Universal Time
VIS	Visible Region of the Electromagnetic Spectrum from 350 to 760 nm
VLBI	Very Long Baseline Interferometer
um	micron or micrometer = 10^{-6} m

END
DATE
FILMED

JUL 27 1981